GEOLOGICA ULTRAIECTINA

Mededelingen van de
Faculteit Geowetenschappen
Universiteit Utrecht

No. 289

EBSD analysis of heterogeneous microstructures in experimentally deformed calcite: development of core and mantle subgrains, grain boundary bulges and recrystallised grains

Siska Lisa Albertine Valcke

Promotors:	Prof. dr. S.H. White
	Prof. dr. C.J. Spiers
Co-promotors:	Dr. M.R. Drury
	Dr. J.H.P. De Bresser
	Dr. G.M. Pennock

Members of the dissertation committee:

Dr. K. Kunze (ETH Zurich)
Prof. dr. E.H. Rutter (University of Manchester)
Prof. dr. J. Tullis (Brown University)
Prof. dr. J. Wheeler (University of Liverpool)
Prof. dr. J.C. White (University of New Brunswick)

The research was carried out at:

Department of Earth Sciences
Faculty of Geosciences
Utrecht University
Budapestlaan 4
3584CD Utrecht
The Netherlands

The work was funded by ‘de Nederlandse Organisatie voor Wetenschappelijk Onderzoek (NWO) – Aard en Levenswetenschappen (ALW)’

ISBN/EAN: 978-90-5744-155-4

Cover illustration: EBSD image showing typical microstuctures in Carrara marble: a deformed grain containing core and mantle subgrains, surrounded by recrystallised grains.

EBSD analysis of heterogeneous microstructures in experimentally deformed calcite: development of core and mantle subgrains, grain boundary bulges and recrystallised grains

EBSD analyse van heterogene microstructuren
in experimenteel gedeformeerd calciet:
de ontwikkeling van kern- en mantel-subkorrels,
korrelgrens-uitstulpingen en gerekristalliseerde korrels

(met een samenvatting in het Nederlands)

Proefschrift

ter verkrijging van de graad van doctor aan de Universiteit Utrecht op gezag van de rector magnificus, prof.dr. J.C. Stoof, ingevolge het besluit van het college voor promoties in het openbaar te verdedigen op woensdag 28 mei 2008 des ochtends te 12.45 uur

door

Siska Lisa Albertine Valcke

geboren op *28 maart 1979*
te Kortijk, België

Promotoren:	Prof. dr. S.H. White
	Prof. dr. C.J. Spiers
Co-promotoren:	Dr. M.R. Drury
	Dr. J.H.P. De Bresser
	Dr. G.M. Pennock

Dit proefschrift werd mede mogelijk gemaakt met financiële steun van de Nederlandse Organisatie voor Wetenschappelijk Onderzoek (NWO) – Aard en Levenswetenschappen (ALW)

“La science ne sert qu’à vérifier les découvertes de l’instinct”

[Jean Cocteau]

“A relaxed mind is a creative mind”

[anonymous]

Table of contents

Summary / Samenvatting

Summary

Geodynamic, large scale tectonic processes such as mountain building, subduction and rifting are to a large extent controlled by high temperature plastic deformation of crystalline solids. During plastic deformation by motion of lattice dislocations (linear defects), internal substructures develop within the crystals and dynamic recrystallisation may take place. Deformed grains have a substructure that consists of free dislocations and a polygonal network of subgrain walls comprised of dislocation arrays, while recrystallised grains are free of such substructure. It is well known from experiments on rocks and minerals that elements of the microstructure such as subgrains and recrystallised grains are potentially useful as indicators of past deformation conditions and mechanisms in the Earth. Furthermore, subgrains can influence the formation of recrystallised grains, of which the size and texture play an important role in the flow strength of the Earth's materials. Evidently then, a good understanding of the origin and mechanical significance of grain and subgrain microstructures is required to (i) develop relations that provide reliable estimates of palaeo-stress in naturally deformed rocks, (ii) to understand and quantitatively model recrystallisation processes and their effect on microstructure in zones of active Earth deformation. In other words, a thorough understanding of the development of subgrains and recrystallised grains in relation to deformation conditions is important because many physical properties of rocks are strongly influenced by the evolving microstructure. The general aims of this study are (i) to establish state-of-the-art methods that allow a quantitative description of microstructures in geological materials that often show complex, heterogeneous microstructures and (ii) to analyse deformation mechanisms and the relationship between various elements of the microstructure and deformation conditions, such that microstructural elements in geological materials can be used as indicators of (palaeo-) deformation processes and conditions. The material of this study consists of samples of experimentally deformed calcite, which is an important rock forming material often involved in major crustal deformation zones and has complex heterogeneous microstructures consisting of recrystallised and deformed grains, the latter containing mantle and core subgrains.

In Chapter 1, the geological context and motivation of this study are outlined. It is shown that despite many studies on deformation mechanisms, microstructures and piezometry, the different, sometimes contrasting outcome of these studies requires further research. As such, a framework for the present work is established, focusing particularly on calcite, but with attention for the general relevance for geological materials.

In Chapter 2, processing methods are investigated to obtain subgrain sizes in function of misorientation angle using electron backscattered diffraction (EBSD) data. Two methods have been compared: the linear intercept hierarchy (LI-MH), which measures domain sizes based on linear intercepts between boundaries larger than a given misorientation angle and the domain hierarchy (DH) method, which measures domain sizes based on the area of domains surrounded by boundaries larger than a given misorientation angle. The LI-MH method appears to be better than the DH method to measure (sub)grain sizes as a function of their misorientation angle when no separation is made between recrystallised and deformed grains nor between core and mantle subgrains.

In Chapter 3, a method is suggested to reduce the low angle misorientation noise and the effect of charging on size measurements. Furthermore, a method based on the average internal misorientation within a (sub)grain is demonstrated to distinguish between the different types of grains (recrystallised and deformed) and subgrains (core and mantle subgrains) and to measure their sizes separately.

In Chapter 4, we investigate the influence of strain and deformation conditions (stress and temperature) on recrystallised grains, grain boundary bulges and deformed grains. We show that, within the high temperature creep regime, the overall character of microstructures can vary depending on deformation conditions. In heterogeneous samples showing core mantle microstructures, the bulges and recrystallised grains are independent of strain. The recrystallised grain and bulge size show an inverse stress dependency, which can be affected by temperature (especially at high stress). The bulge size – stress dependency is suggested to be related to pinning of grain boundaries by sub-boundaries, and/or differences in driving forces for migration. The recrystallised grain size – stress dependency is related to the stress dependency of the bulges, because the recrystallised grains nucleate at grain boundary bulges. The deformed grain size decreases with strain, due to ongoing recrystallisation and rotation of core subgrains with strain. The core subgrain rotation and therefore the deformed grain size reduction is slowed down at high temperatures. These findings provide new input for modeling and applying recrystallised grain size –stress piezometers: particularly the influence of temperature and the origin of recrystallised grains at grain boundary bulges should be taken into account for heterogeneous core – mantle microstructures as seen in high temperature deformed calcite.

In Chapter 5, we investigate the development of core and mantle subgrains with increasing natural strain (0.15-0.90) during minor weakening behaviour. It is found that the mantle subgrain size has already become

dynamically stable at low strain (0.15). It is suggested that this is related to a balance between formation and 'growth' processes (subgrain boundary migration and subgrain coalescence). In contrast, the core subgrain size decreases with increasing strain and is linked to the deformed grain size. The microstructural changes that accompany minor weakening towards steady state are an increasing amount of recrystallised grains, the increase in mantle fraction per grain and the simultaneous reduction of deformed grains and core subgrains until the sizes of the grains and subgrains have become similar. At this point (natural strains > 3) a true mechanical steady state is predicted. Increasing temperature tends to slow down the grain size reduction and the evolution towards a microstructure of uniform grain and subgrain size.

In Chapter 6, we investigate the influence of stress and temperature on core and mantle subgrains. A mechanistic model based on slip system activation and stress intensification at grain boundaries in polycrystalline materials is proposed to explain the development of core mantle substructures. The core subgrains originally are formed by single slip and are not only dependent on stress, but also on grain size, strain and temperature. The low angle mantle subgrains are formed by slip on more than one slip system. They have a low stress sensitivity, which is probably related to cross-slip as a deformation mechanism and/or geometrically necessary dislocations accumulating in the mantle. In contrast, high angle mantle subgrains mainly consist of 'bulge subgrains' that are relatively more stress sensitive due to their origin by bulge rotation. These findings provide new insights that are useful for modeling subgrain size – stress relationships for materials with heterogeneous core – mantle microstructures.

In Chapter 7, a synthesis of the foregoing chapters is given and special attention is paid to which microstructures are the most useful for palaeopiezometric purposes. The relation between recrystallised grains and stress has been calibrated in this study for a specific type of microstructure, namely, a heterogeneous microstructure of calcite in which deformed grains have grain boundary bulges and contain core and mantle subgrains. In this type of microstructure the recrystallised grains were mainly formed by grain boundary bulging and subgrain rotation, and they are located at old grain boundaries. The stress sensitivity of recrystallised grains, $p = 0.6$, is lower than in recrystallised grain size piezometers from previous studies on Carrara marble ($p \sim 1$). This may be related to the different way in which the microstructures are treated: for example, whether or not rotation and migration recrystallised grains were separated or whether or not heterogeneous microstructures were combined with homogeneous microstructures. This suggests that recrystallised grains can have different stress sensitivities, depending on the details of the recrystallisation mechanism in relation to the microstructure. The bulge size is a potential palaeostress indicator that can serve as an alternative to the recrystallised grain size. The bulge size is not dependent on strain and its temperature dependency is small and more clearly defined than that of the recrystallised grain size. While a grain boundary migration component can affect the average recrystallised grain size such that it significantly deviates from the general subgrain size – stress relation, the bulge size appears not to be affected by pervasive migration. Due to its low stress sensitivity ($m = 0.11$), the low angle mantle subgrain size is not very useful as a palaeostress indicator, because small errors in size measurements can lead to large errors in stress estimations. In contrast, high angle mantle subgrains are more sensitive to stress ($m = 0.43$), so they are more accurate as palaeostress indicators. Because core subgrains are not only dependent on stress, but also on deformed grain size, temperature and strain, they are not straightforward to use as an indicator of (palaeo-)stress.

Samenvatting

Grootschalige tectonische processen zoals gebergtevorming, subductie en het opbreken van continenten worden in belangrijke mate gecontroleerd door hoge temperatuur plastische vervorming (vloei) van kristallijne gesteenten diep in de aarde. Tijdens plastische vervorming ontwikkelen zich interne substructuren in de kristallen als gevolg van het ontstaan en de verplaatsing van lijndefecten (dislocaties) in de kristalroosters. Gerelateerd daaraan kunnen vervormde korrels vervangen worden door nieuwe korrels, een proces dat dynamische rekristallisatie wordt genoemd. De substructuur van vervormde korrels bestaat gewoonlijk uit vrije dislocaties zowel als een polygonaal netwerk van subkorrel-grenzen opgebouwd uit geordende dislocaties. Gerekristalliseerde korrels vertonen nauwelijks een substructuur. Experimenten hebben aangetoond dat microstructurele elementen zoals subkorrels en gerekristalliseerde korrels in gesteenten en mineralen kunnen dienen als indicatoren voor de vroegere vervormingscondities en -mechanismen tijdens deformatie diep in de aarde. Bovendien kunnen subkorrels het ontstaan en de groei van gerekristalliseerde korrels beïnvloeden; deze nieuwe korrels spelen op hun beurt een belangrijke rol in de vloeisterkte van gesteenten. Het is daarom belangrijk om de oorsprong en mechanische betekenis van subkorrel-microstructuren goed te begrijpen zodat (i) relaties geformuleerd kunnen worden die betrouwbare bepalingen mogelijk maken van paleo-spanningen in natuurlijk vervormde gesteenten (paleo“stress”/paleopiezometrie) en (ii) rekristallisatie processen en hun effect op de microstructuur in actieve vervormingszones in de aarde beter begrepen en daardoor kwantitatief gemodelleerd kunnen worden. Met andere woorden, een grondig inzicht in de ontwikkeling van subkorrels en gerekristalliseerde korrels in relatie tot vervormingscondities is belangrijk omdat veel fysische eigenschappen van gesteenten sterk beïnvloed worden door hun microstructurele ontwikkeling. Om een dergelijk inzicht te verkrijgen is allereerst een methode nodig om betrouwbaar metingen te doen van substructuren en gerekristalliseerde korrels in plastisch vervormde gesteenten. De algemene doelstellingen van deze studie zijn daarom:

(1) het ontwikkelen van innovatieve methodes, gebruik makend van diffractie van teruggekaatste electronen (electron backscattered diffraction, EBSD) in een scanning electronen microscoop (SEM), om de complexe microstructuren in gesteenten te kwantificeren;

(2) het gebruik maken van deze nieuwe methoden om vervormingsmechanismen en hun relatie met verschillende microstructurele elementen te analyseren, zodat microstructuren in gesteenten gebruikt kunnen worden als betrouwbare indicatoren voor (paleo-)vervormingsprocessen en -condities.

Het materiaal in deze studie is experimenteel vervormd polykristallijn calciet (marmer), een gesteente dat veel voorkomt in grootschalige vervormingszones in de aardkorst. Vervormd calciet vertoont vaak heterogene microstructuren die bestaan uit vervormde zowel als gerekristalliseerde korrels. Een belangrijk aspect van de vervormde korrels is hun veelal complexe substructuur, waarbij onderscheid gemaakt kan worden tussen de substructuur in de kerngedeelten van de korrels en daaromheen een mantelsubstructuur met zijn eigen karakteristieke elementen.

In hoofdstuk 1 wordt de geologische context en de motivatie voor deze studie uiteengezet. Aan de hand van een literatuurstudie wordt aangetoond dat er nog steeds veel onenigheid bestaat omtrent het gebruik van microstructuren voor (paleo-)piezometrie, en dat verder onderzoek vereist is. In hoofdstukken 2 en 3 worden bestaande EBSD methoden onderzocht en nieuwe methoden ontwikkeld om (sub)korrel-structuren in complexe, heterogene microstructuren betrouwbaar te kwantificeren. In hoofdstuk 4 wordt de invloed van de mate van vervorming (“strain”) en de vervormingscondities op gerekristalliseerde korrels, korrelgrensuitstulpingen en vervormde korrels onderzocht. In hoofdstuk 5 wordt de ontwikkeling bestudeerd van kern- en mantel-subkorrels als functie van hun misoriëntatie (kristaloriëntatie t.o.v. naburige subkorrels) tijdens toenemende mate van vervorming. In hoofdstuk 6 wordt de invloed van spanning en temperatuur op kern- en mantel-subkorrels onderzocht. Hoofdstuk 7 geeft een samenvatting van de bevindingen in de voorgaande hoofdstukken, alsmede suggesties voor toekomstig onderzoek.

In deze studie is de relatie tussen gerekristalliseerde korrels en opgelegde spanning gekalibreerd voor een welbepaald type (calciet) microstructuur, namelijk voor een heterogene microstructuur waarbij in de vervormde korrels kern- en mantelsubkorrels voorkomen, en waarin de korrelgrenzen van vervormde korrels uitstulpingen vertonen. In dit type microstructuur worden gerekristalliseerde korrels voornamelijk gevormd door nucleatie achter korrelgrensuitstulpingen. De grootte en de spanning-gevoeligheid van de gerekristalliseerde korrels zijn daarom vergelijkbaar met die van de korrelgrensuitstulpingen. Het blijkt dat, onafhankelijk van de mate van vervorming, de groottes van de gerekristalliseerde korrels en die van korrelgrensuitstulpingen bij toenemende spanning afnemen. Bij relatief hoge waardes van de spanning heeft de temperatuur een niet te verwaarlozen invloed op de grootte van gerekristalliseerde korrels die groeien door korrelgrensmigratie, terwijl de korrelgrensuitstulpingen veel minder gevoelig zijn voor temperatuur. Om deze reden is de grootte van korrelgrensuitstulpingen

mogelijk een goed alternatief voor gerekristalliseerde korrelgrootte als indicator voor (paleo-)spanning. De spanning-gevoeligheid van de gerekristalliseerde calciet korrels zoals gevonden in deze studie is lager dan geobserveerd in eerdere studies. Dit is mogelijk gerelateerd aan verschillen tussen de diverse studies in termen van actieve rekristallisatie mechanismen. De kern-subkorrels worden in eerste instantie gevormd door glij van dislocaties op enkelvoudige slipvlakken in het kristalrooster, en hun grootte is niet alleen afhankelijk van de opgelegde spanning, maar ook van de grootte van de vervormde korrels, de mate van vervorming en de temperatuur. De mantel-subkorrels met een geringe misoriëntatie ontstaan voornamelijk door de activiteit van meerdere slip-systemen. Ze zijn onafhankelijk van de mate van vervorming, hebben geen noemenswaardige temperatuursafhankelijkheid en vertonen slechts een lage gevoeligheid voor de spanning. Daarentegen zijn de mantel-subkorrels met een hoge misoriëntatie voornamelijk gevormd door rotatie van de korrelgrensuitstulpingen, zodat deze mantel-subkorrels met een hoge misoriëntatie dezelfde spanning-gevoeligheid vertonen als de korrelgrens-uitstulpingen. De subkorrels met grote misoriëntaties zijn derhalve geschikter voor het bepalen van (paleo-)spanning dan sub-korrels met geringe misorientaties. Deze bevindingen zijn van belang voor het modelleren van de relatie tussen de spanning en de groottes van sub-korrels en gerekristalliseerde korrels, in het bijzonder in materialen met heterogene kern- en mantel-substructuren.

1

Introduction: context and aims of study

1.1 Broad geological context and motivation

Geodynamic processes such as mountain building and subduction are to a large extent controlled by high temperature plastic deformation of crystalline solids. During plastic deformation by motion of lattice dislocations, internal substructures develop within the crystals and dynamic recrystallisation may take place. Deformed grains have a substructure that consists of free dislocations (linear defects) and a polygonal network of subgrain walls, comprised of dislocation arrays, while recrystallised grains are free of such substructure. It is well known from experiments on rocks and minerals that elements of the microstructure such as subgrains and recrystallised grains are potentially useful as indicators of past deformation conditions and mechanisms in the Earth (White, 1975; Twiss, 1977; White, 1979b; Pfiffner & Ramsay, 1982; Kenkmann & Dresen, 2002). Furthermore, subgrains can influence the formation of recrystallised grains, of which the size and texture play an important role in the flow strength of the Earth's materials. Evidently then, a good understanding of the origin and mechanical significance of grain and subgrain microstructures is required to (i) develop piezometric relations that provide reliable estimates of palaeo-stress in naturally deformed rocks, (ii) to understand and quantitatively model recrystallisation processes and their effect on microstructure in zones of active Earth deformation. In other words, a thorough understanding of the development of subgrains and recrystallized grains in relation to deformation conditions is important because many physical properties of rocks are strongly influenced by the evolving microstructure.

The general aims of this study are (i) to establish state-of-the-art methods that allow a quantitative description of microstructures in geological materials that often show complex, heterogeneous microstructures and (ii) to analyse deformation mechanisms and the relationship between various elements of the microstructure and deformation conditions, such that microstructural elements in geological materials can be used as indicators of (palaeo-) deformation processes and conditions. In the last few years, new methods of fast automatic crystal orientation mapping have been developed and continuously improved, especially electron backscattered diffraction (EBSD) in the scanning electron microscope (SEM). The basic methods involved are not new (Lloyd & Ferguson, 1986), but the advent of automatic analysis and analysis speed currently available, allow fast collection of large data sets and a complete quantitative description of the deformation induced substructure (Trimby *et al.*, 2002). EBSD techniques of crystal orientation mapping have been used recently to investigate the microstructures of deformed rocks and metals (Kunze *et al.*, 1994; Fliervoet *et al.*, 1999; Prior, 1999; Heidelbach *et al.*, 2000; Trimby *et al.*, 2000) and this study investigates the application of these techniques for the purpose of measuring grain and subgrain sizes. The material of this study consists of samples of experimentally deformed calcite, which is an important rock forming material often involved in major crustal deformation zones and has complex heterogeneous microstructures consisting of recrystallised and deformed grains, the latter containing mantle and core subgrains. Our findings will also be more generally relevant for rock types having similar heterogeneous core mantle microstructures.

1.2 Palaeopiezometry: problems

1.2.1 General

Palaeopiezometers are calibrated, quantitative relationships that can be used to estimate palaeostress conditions from microstructures. These relations are often based on empirical data sets obtained from experimental deformation studies, underpinned by microphysical models. Previous studies have shown that several microstructures can be used for palaeopiezometry, namely, dislocation density, subgrain size and syntectonically recrystallised grain size (see reviews by Takeuchi & Argon, 1976; Mercier *et al.*, 1977; Twiss, 1977; White, 1979a; Poirier, 1985; Raj & Pharr, 1986; Orlova, 1996). In this study the focus is on subgrain as well as recrystallised grain sizes and their applicability for palaeopiezometric purposes. The equation for the relation between stress and recrystallised grain size as well as subgrain size has a general form:

$$\frac{d}{b} = K\left(\frac{\mu}{\sigma}\right)^{C}, \tag{1.1}$$

in which d is the size of grains or subgrains, b, is the length of the Burgers vector, μ, the shear modulus, σ, the flow stress, and K and C are parameters that are related to the type of microstructure measured, i.e., recrystallised grain or subgrain size (Takeuchi & Argon, 1976; Twiss, 1977; Raj & Pharr, 1986). To make a distinction between the theoretical models on recrystallised grains versus subgrains, K in Eq. 1.1 is termed K_X for recrystallised grains and K_{SG} for subgrains. The stress exponent or stress sensitivity C is termed p for recrystallised grains and m for subgrains.

1.2.2 Theoretical models

Below we briefly review the most well known microphysical models that provide theories that could explain the empirical observations of relationships between subgrain/grain size and stress.

Subgrains

Twiss (1977) has modeled the subgrain size – stress relation based on the assumption that the subgrain formation is an energetically favorable process and a stable subgrain size is formed at equilibrium. As a consequence, the total strain energy of dislocations, ordered in a subgrain boundary, can be assumed to be less than or equal to the total energy of a steady state density of dislocations within the enclosed volume. In the model of Twiss (1977), the subgrain size – stress sensitivity, *m*, is a constant and has a value of 1 (Table 1.1). The assumptions of the Twiss model have been questioned by Edward et al. (1982) and Poirier (1985), because the equilibrium situation does not apply to a steady state condition in which subgrain formation and evolution is a dynamic process with continuous generation and annihilation of boundaries.

article	*p*	*m*
Twiss (1977)	1.3-1.5	1
Derby and Ashby (1987)	*n*/2	-
Shimizu (1998)	1.3	-
Edward et al. (1982)	-	*n*/4
Orlova (2001)	-	1
Raj (2002)	-	1

Table 1.1: Summary of the stress sensitivity of recrystallised grains (p) and subgrains (m) predicted by several theoretical models.

In contrast to the Twiss model, the model of Edward et al. (1982) is dynamic, i.e., subgrains can form and annihilate within a dynamic balance, in relation to the creep process. The model is based on the fact that the total change in geometrically necessary dislocation length ($\dot{L}$) equals the rate of arrival of geometrically necessary dislocation length at subgrain walls ($\dot{L}^+$) minus the rate of annihilation of geometrically necessary dislocation length in subgrain walls ($\dot{L}^-$) (Fig. 1.1). If there is no further subgrain rotation, there is no change in total dislocation length, i.e., $\dot{L}$= 0. In this case, there is a dynamic balance between $\dot{L}^+$ and $\dot{L}^-$. The influence of stress comes in through $\dot{L}^+$, which is dependent on the creep rate, chosen by Edward et al. (1982) to be controlled by the dislocation climb rate (Fig. 1.1). The subgrain size factor comes in through $\dot{L}^-$: the dislocation climb distance is determined by the subgrain size because the dislocations at maximum can climb over the length of the subgrain walls to the nodes of the subgrain walls where they may annihilate by meeting dislocations of opposite sign (Fig. 1.1). The resultant stress sensitivity, *m*, of the subgrain size is (Table 1.1):

$$m = \frac{n}{4} \ , \tag{1.2}$$

with *n* being the stress exponent of the power creep

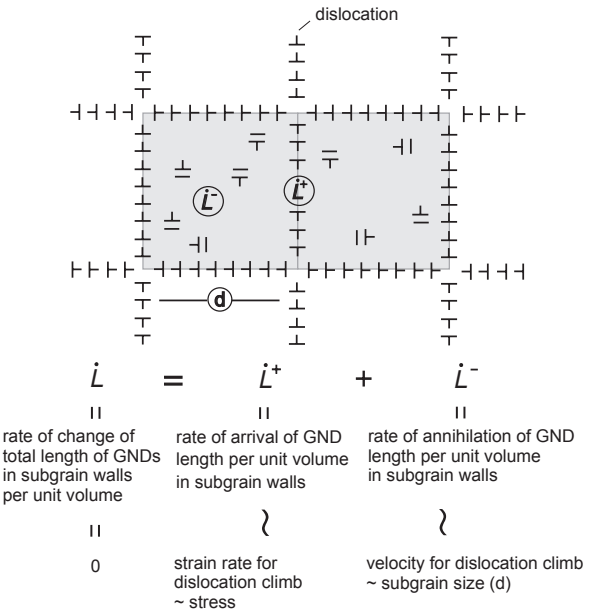

Fig. 1.1: Simplified figure to illustrate the Edward model; modified after Edward et al. (1982). The two grey squares are two subgrains, having subgrain boundaries consisting of parallel sets of geometrically necessary dislocations (GNDs); within the subgrains, free dislocations are shown that move towards the subgrain boundaries.

law in which the strain rate, $\dot{\varepsilon}$, is related to stress, σ, as follows:

$$\dot{\varepsilon} = R\sigma^n \ , \tag{1.3}$$

with *R* being dependent on temperature and material properties (Weertman, 1955; Poirier, 1985).

Orlová (2001), Raj (2002) and Orlová and Dobes (2004) modeled the subgrain size versus stress relation using a composite model of dislocation structure. This means that hard and soft regions are considered, consisting of the subgrain boundaries and subgrain interiors respectively. These regions both have internal stresses and the sum of these stresses, when volume averaged for the relative fraction of hard and soft regions, equals the total flow stress. The model of Raj (2002) makes similar assumptions as Twiss (1977) and combines the same basic equations to come to a subgrain size – stress dependency. However, the model of Raj (2002) additionally is linked with a model for creep and therefore does not separate the subgrain forming processes from the deformation processes. The two basic equations in the Raj model (1) link subgrain size (*d*) to dislocation density (ρ) (e.g., Holt, 1970):

$$d = P\rho^{\frac{1}{2}} \ , \tag{1.4}$$

where *P* is a geometrical constant and (2) link the mobile dislocation density, ρ, with stress, σ (Honeycombe, 1968; Kohlstedt & Weathers, 1980; Weertman & Weertman, 1983; Poirier, 1985):

$$\sigma = \alpha \mu b \rho^{q} \quad , \tag{1.5}$$

where α is a constant, μ is the shear modulus, b, the Burgers vector and q, the stress sensitivity of the dislocation density. In most studies, q equals 0.5, a value which is also used in the model of Raj, such that combining these two equations results in a subgrain size – stress sensitivity, m, that is linked to the sensitivity of dislocation density to stress, with the value of m being 1. Equation 1.5 is a basic assumption often used in microphysical models for flow laws (e.g., Weertman, 1968) and palaeopiezometers (e.g., Twiss, 1977), but the theoretical basis and value of α (~1, e.g., Kohlstedt & Weathers, 1980) and of q (~0.5, e.g., Honeycombe, 1968) are still subject of much debate (e.g., White, 1979a; e.g., De Bresser, 1996) and α is often treated as a fitting parameter rather than a universal parameter with a profound theoretical basis.

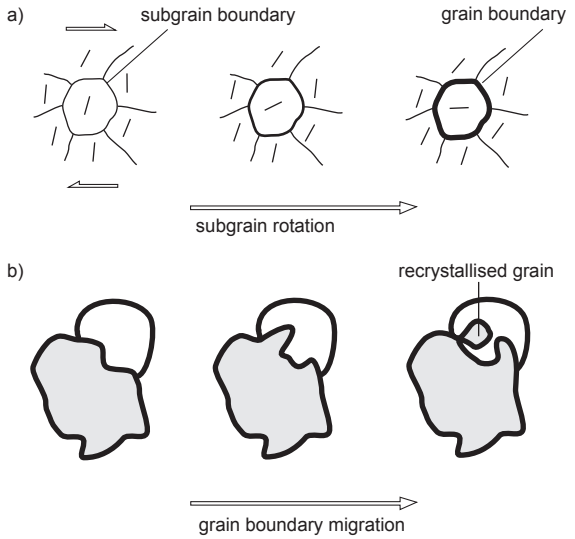

Fig. 1.2: Simplified diagrams that show examples of how two mechanisms of dynamic recrystallisation can lead to recrystallised grains (after Passchier & Trouw, 1996). a) Subgrain rotation recrystallisation (SGR). The subgrain rotates such that the orientation differences between subgrains become larger and the misorientation angle of the subgrain boundary (thin line) becomes higher until the misorientation becomes so high that the subgrain boundary becomes a grain boundary. The bars indicate lattice orientation. b) Grain boundary migration recrystallisation (GBM). A grain boundary bulges into the grain with the highest dislocation density (white grain) and the bulge eventually develops into an individual grain with low dislocation density (grey grains).

Recrystallised grains

Two end-member mechanisms of recrystallisation can be distinguished (Guillopé & Poirier, 1979; Urai *et al.*, 1986; Drury & Urai, 1990): (1) subgrain rotation recrystallisation (SGR) and (2) grain boundary migration recrystallisation (GBM). The first mechanism, SGR, involves the progressive misorientation of subgrain boundaries with strain, such that the grains divide into subgrains that eventually become so misoriented that they need to be regarded as individual grains (Hobbs, 1968; Poirier, 1985) (Fig. 1.2a). The second mechanism, GBM, involves the migration of grain boundaries resulting in grain dissection, grain coalescence or the development of new grains from grain boundary bulges (Means, 1989) (Fig. 1.2b). This process is driven by boundary surface energies and/or the strain energy difference between relatively strain free and deformed regions (Poirier, 1985).

Few quantitative microphysical models exist to underpin the above mechanisms of recrystallisation, their interaction or the observed relation between recrystallised grain size and flow stress. An overview of the models can be found in De Bresser et al. (2001) and Kellermann Slotemaker (2006). Probably the most widely quoted model is that of Twiss (1977) who considered the relation between grain size and stress to be universal, with the stress sensitivity of the recrystallised grains, p, 1.3-1.5 (Table 1.1). The model is based on the assumption that a unique recrystallised grain size exists at which the total energy of dislocations ordered in a grain boundary is equal to the stored energy of free dislocations in the enclosed volume. The Twiss model has been questioned because it incorrectly applies equilibrium thermodynamics to a dynamic, non-equilibrium process (Edward *et al.*, 1982; Poirier, 1985; Derby, 1990), as grains are cyclically formed and disappear in the course of dynamic recrystallisation (Sellars, 1978). No explicit distinction was made by Twiss between rotation and migration mechanisms. In contrast, the models of Derby and Ashby (1987) and Shimizu (1998) take into account the type of recrystallisation mechanism forming the grains. In both models, a dynamically stable recrystallised grain size is achieved by a competition between grain nucleation at mean rate, $\dot{N}$, and grain growth at mean rate, $\dot{R}$. At steady state, the recrystallised grain size, d_x, is then expressed as:

$$d_x = \left(\frac{\dot{R}}{\dot{N}} \right)^{z} \quad , \tag{1.6}$$

with values for z being dependent on the details of the theoretical considerations behind the model (Derby & Ashby, 1987; Derby, 1990; Shimizu, 1998). To obtain a relation between the size, d_x, and stress, σ, Shimizu (1998) and Derby and Ashby (1987) expressed $\dot{N}$ and $\dot{R}$ as functions of σ, resulting in relationships given by equation 1.1. Derby and Ashby (1987) assumed grain boundary migration, while Shimizu (1998) assumed subgrain rotation recrystallisation as the main recrystallisation mechanism. This resulted in different values for the stress sensitivity: p in the Derby and Ashby model equals n/2, n being the power law stress exponent (see

Eqn. 1.3) and p in the Shimizu model is a material independent constant (p = 1.3) (Table 1.1). Despite the differences, both models suggest a dependency of the recrystallised grain size – stress relation on the creep and recrystallisation mechanisms and also a slight temperature dependence of the parameter K_X. De Bresser et al. (1998; 2001) also predicted a temperature dependency of K_X by advancing the hypothesis that dynamic recrystallisation results in a balance between grain size reduction and grain growth processes, set up in the vicinity of the boundary between the grain size insensitive (GSI) and grain size sensitive (GSS) creep fields. Kellermann Slotemaker (2006) developed a model that describes the large strain transient evolution of the microstructure of a polycrystalline material with a distributed grain size that evolves towards a dynamic recrystallised steady state including processes of nucleation and growth. The model predicts that high strain is needed to reach a steady state recrystallized grain size. Hence, a stress-recrystallized grain size relationship of the type of eq. 1.1 might not be established in an unique form until such high strains have been reached.

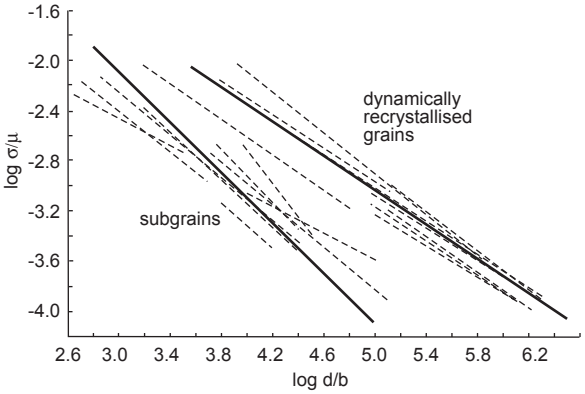

Fig. 1.3: Normalised plot of experimentally determined stress (σ/μ; σ = stress; μ = shear modulus) versus subgrain size and recrystallised grain size (d/b; d = size; b = burgers vector) (redrawn from Twiss, 1977). Dashed lines are unweighted linear regressions to individual data sets (for references of these data, see Twiss, 1977). Each solid line is a best fit to the respective group of data for subgrains and recrystallised grains. The slope of the solid line is taken to be the mean of the slopes of the data sets in each group (see Twiss, 1977).

1.2.3 Experimental studies versus theory

Numerous studies on experimentally deformed materials have demonstrated the existence of a systematic relationship between stress and recrystallised grain size (Mercier *et al.*, 1977; Post Jr., 1977; Guillopé & Poirier, 1979; Ross *et al.*, 1980; Schmid *et al.*, 1980; Karato & Ogawa, 1982; Van der Wal *et al.*, 1993; Stipp & Tullis, 2003) or stress and subgrain size (Streb & Reppich, 1973; Young & Sherby, 1973; Takeuchi & Argon, 1976; White, 1979a; Schmid *et al.*, 1980; Raj & Pharr, 1986; Orlova & Podstranská, 1998). Twiss (1977) has made a compilation of data of recrystallised grain sizes as well as subgrain sizes in relation to stress and has made empirical best fits for each material (Fig. 1.3). Then, based on his theoretical equation, Twiss (1977) fitted a universal linear relation to all data, with constant stress sensitivity (Fig. 1.3). However, it has been noted that the recrystallised grain size - stress sensitivity, p, considerably varies between experimental studies, with values for

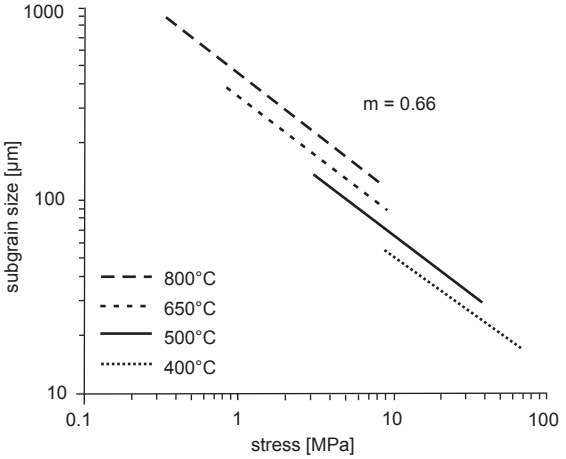

Fig. 1.4: Subgrain size data plotted versus flow stress for LiF from data from Streb and Reppich (1973) redrawn from De Bresser et al. (2001).

p between 0.6 and 2 (e.g., De Bresser *et al.*, 2001). Also the subgrain size - stress sensitivity is variable, seen on the graph of Twiss (1977) and in the compilation of literature data from Raj and Pharr (1986) and De Bresser et al. (2001), in which m varies between 0 and 2. Therefore, the application of a simple equation to the recrystallised grain size as well as subgrain size data with only stress as the main independent variable and constant stress sensitivity should be questioned.

It is now realized that additional factors next to stress can play a role. For the recrystallised grains, these additional factors have been predicted by models and they are temperature (De Bresser *et al.*, 2001), type of deformation/recrystallisation mechanism (Guillopé & Poirier,

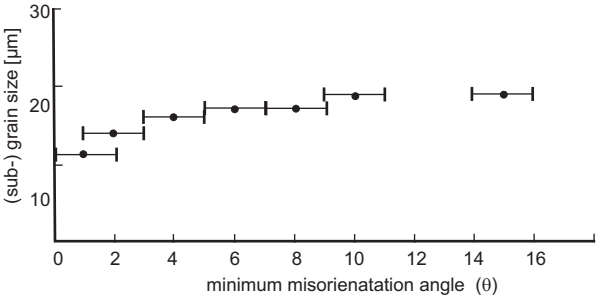

Fig. 1.5: Average subgrain size plotted against minimum misorientation angle (θ) for a quartz mylonite (redrawn from Trimby et al., 1998).

1979; Derby & Ashby, 1987; De Bresser *et al.*, 2001) and strain (Kellermann Slotemaker, 2006) (see paragraph 1.2.2). For subgrains, the additional factors mainly were put forward by experimental studies and they are temperature (Streb & Reppich, 1973; Young & Sherby, 1973; Orlova & Podstranská, 1998), strain (Takeuchi & Argon, 1976), misorientation angle (White, 1976; Kuhlmann-Wilsdorf, 1989; Trimby *et al.*, 1998) and grain size (Pennock *et al.*, 2005). For example, a temperature effect on the subgrain size is seen in a graph of Streb and Reppich (1973), on which isolines of constant temperature can be distinguished that have a lower slope than a best fit taking all data together (Fig. 1.4). A relation between subgrain size and misorientation angle, i.e., the minimum angle of mismatch between two lattice regions that have a different orientation, is demonstrated for example for quartz: the subgrains show a 'hierarchy' for their size, which increases with misorientation angle (White, 1976; Trimby *et al.*, 1998) (Fig. 1.5).

Another important discrepancy lies in the general applicability of steady state. Theoretical models assume steady state in a dynamically stable microstructure, while many geological materials deformed in nature or the laboratory, have heterogeneous microstructures that evolve during hardening and weakening stages before the development of a dynamically stable average microstructure at high strains. For example, microstructures can consist of recrystallised grains and deformed grains, the latter containing large core and small mantle subgrains, which continuously evolve with increasing strain. Also, the experimental materials used for the empirical relationships often have not reached a true mechanical and microstructural steady state.

In order to explain the discrepancies between theory and experiment, more quantitative data as well as conceptual interpretations are needed regarding the effects of strain, temperature, grain size and misorientation on the recrystallised grain size and subgrain size. This can provide input for adjusting or redefining microphysical models, which currently only assume a stress dependency and a constant value of the stress sensitivities, p and m. Therefore in this study, experimentally deformed Carrara marble showing gradual microstructural modification with increasing strain as well as heterogeneous microstructures, has been investigated to better understand how the different microstructural elements develop during ongoing deformation and to validate the applicability of piezometers on rocks exhibiting transient microstructures. Also the effects of temperature and grain size on the microstructures have been explicitly considered. Specifically the relation between subgrain size and misorientation angle and its consequences on the subgrain size – stress relation have not received much attention previously and therefore an important aim in this study is to develop new EBSD methods for the quantification of subgrain sizes in relation to the misorientation angle.

1.3 Material: experimentally deformed Carrara marble

1.3.1 Why Carrara marble?

Calcite is an important rock forming mineral, being the principal constituent of carbonate rocks such as limestone and marble (metamorphosed carbonate rocks). Carbonates accumulate mainly in marine sedimentary basins and they often are subsequently deformed during orogenic processes. In a sedimentary sequence of mainly sandstones, siltstones and limestones, the latter are usually the weakest and deform the most. Therefore, even though volumetrically calcite might not be so important as other rock forming minerals, calcite rocks are often involved in lithosphere scale shear zones because deformation tends to concentrate in these mechanically weaker rocks (e.g., Busch & van der Pluijm, 1995; e.g., Bestmann *et al.*, 2000; Molli *et al.*, 2000; Ulrich *et al.*, 2002; Ebert *et al.*, 2007). The microstructures of highly deformed limestone, i.e., marble, therefore can be considerably different from microstructures in the less deformed surrounding rocks. If the marbles take up most of the deformation, i.e., in shear zones, their microstructures are often the only observable features that can be used to infer the conditions and mechanisms that were active during deformation.

In order to reliably interpret natural microstructures in calcite rocks, criteria and constraints are needed regarding the significance of microstructures in relation to deformation conditions (for calcite see, e.g., De Bresser, 1989; Van der Pluijm, 1991; Bestmann *et al.*, 2000;

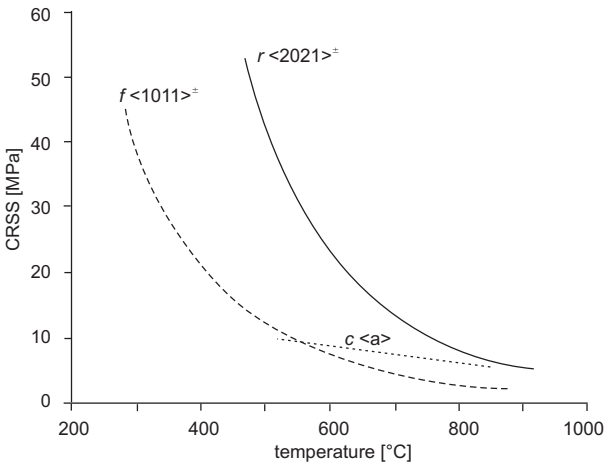

Fig. 1.6: Best-fit lines of the CRSS data for r-slip, f-slip and c-slip as a function of temperature (redrawn from De Bresser et al., 1997).

Oesterling, 2004). Rock deformation experiments are of particular help here, since these allow control of extrinsic conditions and the associated microstructures can be studied after the experiments.

Calcite is one of the best studied materials in rock deformation and experiments on polycrystalline calcite aggregates, such as marble, date back to the early days of experimental rock deformation studies (Griggs, 1936). Since these early studies, the mechanical behaviour of marbles has been explored by numerous studies, which demonstrated that different marbles at a wide range of conditions dominantly deform by plastic flow accompanied by dynamic recrystallisation, in particular at temperatures above ~600°C (Heard & Raleigh, 1972; Rutter, 1974; Schmid *et al.*, 1977; Schmid *et al.*, 1980; Rutter, 1995; Covey-Crump, 1998; Pieri *et al.*, 2001; Barnhoorn *et al.*, 2004). Carrara marble forms an ideal material for focusing on more specific subjects such as palaeopiezometry using the EBSD technique because of the following reasons: 1) Carrara marble has a rather homogeneous starting microstructure with no initial lattice preferred orientation, hence, all deformation microstructures in the deformed samples are linked solely to the experimental conditions (Ter Heege *et al.*, 2002); 2) it is a coarse grained, pure calcite material, that has been shown to deform, under normal laboratory conditions, in the (grain size insensitive) dislocation creep field. In addition, it is known to develop subgrains and recrystallised grains at high temperatures (e.g., Schmid *et al.*, 1980; Rutter, 1995; De Bresser, 2002); 3) there is a good knowledge of the rheology so that the experiments can be well designed particularly for our purposes; 4) calcite is a material that has clear backscattered diffraction patterns and can be relatively easily investigated using automatic EBSD.

1.3.2 Properties of Carrara marble

The mineral calcite ($CaCO_3$) has trigonal crystal symmetry with point group $\bar{3}m$ and space group $R\bar{3}c$. The lattice parameters of the calcite unit cell (hexagonal system) are $a = b = 4.99$ Å, $c = 17.06$ Å, $\alpha = \beta = 90°$ and $\gamma = 120°$. The crystal structure can be described as a face-centered rhombohedron containing four $CaCO_3$ molecules (Deer *et al.*, 1962; Phillips, 1962). The classical work of Turner et al. (1954) and Griggs et al. (1960) has shown that there are three important systems in calcite, namely, *e*-twinning on $e\,\{\bar{1}018\}\langle 40\bar{4}1\rangle^{+}$ (three systems), slip on $r\,\{\bar{1}014\}\langle 40\bar{4}1\rangle^{\pm}$ (three systems) and slip on $f\,\{\bar{1}012\}\langle 40\bar{4}1\rangle^{\pm}$ (six systems). More recent studies have revealed the existence of additional subsidiary glide systems, such as $f\,\{\bar{1}012\}\langle 10\bar{1}1\rangle^{\pm}$ and c $\{0001\}\langle \bar{1}2\bar{1}1\rangle$ (cf., De Bresser & Spiers, 1997). The critical resolved shear stress (CRSS), which is the shear stress resolved on the slip plane in the slip direction needed to produce significant plastic deformation, is different for each slip system and is dependent on temperature (Fig. 1.6).

The marble investigated in this study originates from a block of Carrara marble ('Lorano Bianco' type) that has been selected as a laboratory standard for deformation experiments on marble. The structural elements, chemical composition and material properties of the marble are well characterized and the structure, stratigraphy and tectonic setting of the source of the block in the area near Carrara in the Apuane Alps in Italy have been well documented (Molli *et al.*, 2000; Pieri *et al.*, 2001). The marble consists of ~99 % calcite with a few grains of muscovite, quartz, dolomite and graphite. The marble has undergone static annealing, such that no significant deformation microstructure exists prior to the deformation experiments. However, there is a weak shape preferred orientation (Ter Heege *et al.*, 2002).

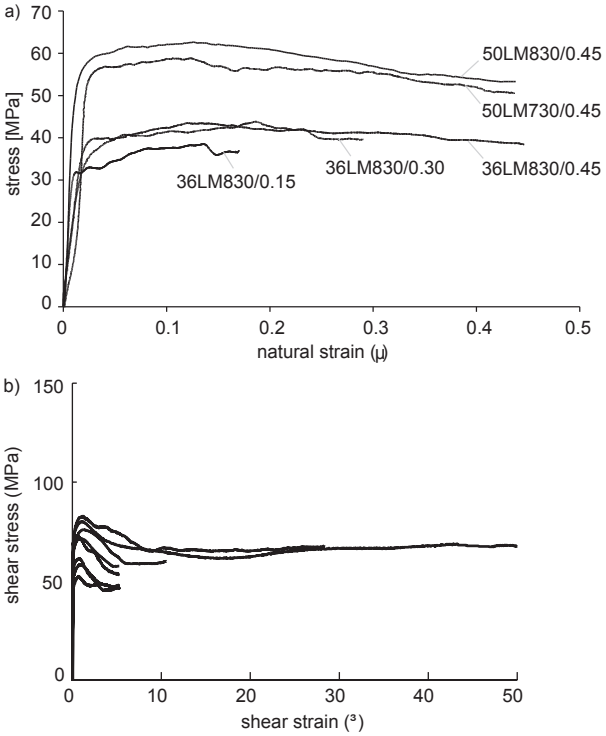

Fig. 1.7: Stress-strain curves showing the mechanical behaviour of experimentally deformed Carrara marble. a) Compression tests from Ter Heege et al. (2002). The samples are named as in their study: the first number is the stress, LM stands for Lorano Marble, the second number is the temperature and the third number is the natural strain. b) Torsion tests from Barnhoorn et al. (2004).

1.3.3 Mechanical behaviour Carrara marble: previous studies

Most of the experimental studies on Carrara marble were done applying a uniaxial deformation geometry (mostly in compression, a few in extension) (Rutter, 1974; Schmid *et al.*, 1980; Rutter, 1995; Covey-Crump, 1998; Molli *et al.*, 2000; Turner, 2001; Ter Heege *et al.*,

2002; De Bresser *et al.*, 2005). The natural strains, ε, reached in axial compression are not higher than 1 and the stress – strain curves show that after a peak has been reached, the material slowly continues to weaken and true steady state conditions are not reached (Fig. 1.7a) (Ter Heege *et al.*, 2002). Recently, high strain torsion experiments on Carrara marble have shown that weakening continued until shear strains, γ, of 5 and afterwards, stresses remained approximately constant up to very large strains (γ=50) (Pieri *et al.*, 2001; Barnhoorn *et al.*, 2004). In other words, a steady state situation appears to be reached only after γ=5 (Fig. 1.7b). Notwithstanding the limited strain reached, axial compression tests have

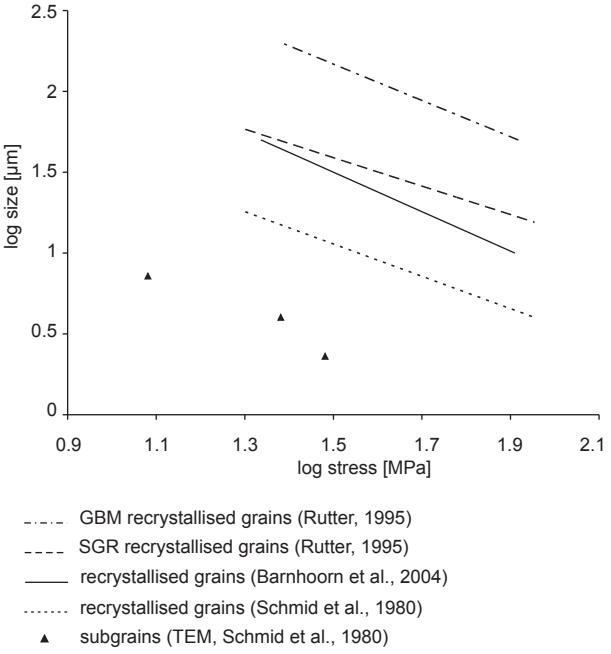

Fig. 1.8: Log-log plot of differential stress versus recrystallised grain sizes comparing piezometers for Carrara marble from Schmid et al. (1980), Rutter (1995) and Barnhoorn et al. (2004). Shear stresses of the torsion tests of Barnhoorn et al (2004) were multiplied by √3 for conversion to equivalent stresses.

often been used to make inferences on recrystallised grain size, subgrain size and rheological behaviour of calcite rocks, which might not be fully justified. Therefore, this study specifically focuses on the evolution of the microstructure during the post peak stress deformation phase in which minor weakening continues to occur, in order to better understand the underlying mechanisms responsible for microstructures in natural rocks that also may not be in true steady state.

1.3.4 Palaeopiezometry on Carrara marble: previous studies

Already a substantial amount of data has been published on microstructures in calcite as a function of deformation conditions, particularly in experimentally deformed Carrara marble (Schmid *et al.*, 1980; Rutter, 1995; Ter Heege *et al.*, 2002; Barnhoorn *et al.*, 2004). All studies have focused only on recrystallised grains, except the one of Schmid et al. (1980), who considered subgrains to a limited extent. These studies showed that the recrystallised grain size is inversely proportional to stress. The reported stress sensitivity, *p*, of the recrystallised grains is similar in all studies (~1), but the curve is

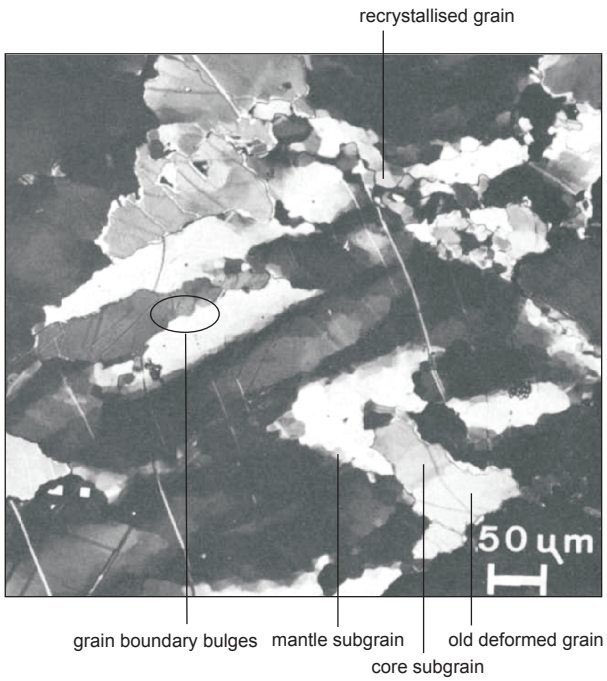

Fig. 1.9: Light microscopy micrograph from Schmid et al. (1980) showing heterogeneous microstructures in calcite. The sample was deformed at 900°C, at a flow stress of 30 MPa and to a natural strain of 0.30.

displaced to different values (Fig. 1.8). The grains recrystallised by GBM (Rutter, 1995) are significantly larger than the ones recrystallised by SGR (Schmid, 1980; Rutter, 1995), so the type of recrystallisation mechanism clearly can have an influence on the recrystallised grain size – stress relation. Furthermore, the SGR grain size measured by Rutter (1995) is slightly larger than the sizes measured by Schmid et al. (1980) and Barnhoorn et al. (2004). As these studies have used light microscopy, the differences in size could be due to differences in resolution related to a variation in thicknesses of the thin sections, to a different way of determining the average value, or to a difference in the criteria for manually selecting the grains belonging to specific recrystallisation mechanisms. Schmid et al. (1980), Rutter (1995) and Barnhoorn (2004) have not considered a possible effect of strain or temperature on the grain size. In contrast, Ter Heege et al. (2002) have reported an influence of strain and temperature on the grain size. However, these effects of strain and temperature are difficult to interpret because

Ter Heege et al. (2002) have considered the sizes of all grains together, deformed as well as recrystallised, while the other studies selected only recrystallised grains.

Schmid et al. (1980) studied subgrains and recognized that also on the level of the subgrains the microstructure in deformed calcite is heterogeneous (Fig. 1.9). There are two types, namely core and mantle subgrains. Schmid et al. (1980) only made a qualitative remark on the core subgrains, namely that they are larger than the mantle subgrains and do not appear to be related to stress. They measured 50 mantle subgrains in one sample and as these appeared similar in size to the recrystallised grains, they suggested that the piezometric relation for recrystallised grains might also be applied to mantle subgrains. However, limited transmission electron microscope (TEM) measurements made by Schmid et al. (1980) suggest that subgrains exist which are much smaller than the recrystallised grains (Fig. 1.8). This difference in subgrain size could be related to a difference in misorientation angle (Trimby et al. 1998), which could not be resolved using light microscopy. Schmid et al. (1980) also recognized the presence of grain boundary bulges (Fig. 1.9), which they suggested play a role in dynamic recrystallisation. However, these were not further investigated even though grain boundary bulges may be essential microstructures that should be taken into account as they are involved in the formation of the small recrystallised grains at grain boundaries (Drury *et al.*, 1985; Drury & Urai, 1990) and these recrystallised grains might not solely be the result of subgrain rotation as Schmid et al (1980) suggested.

The comparison of these different studies on Carrara marble has raised a few specific issues that are dealt with in the present study. 1) How can the different elements of the microstructure (recrystallised and deformed grains, mantle and core subgrains) be separated objectively from the quantitative data obtained using the EBSD technique? 2) Is there a relation between misorientation angle and subgrain size and if so, how does this affect the stress – subgrain size relation? 3) What are the recrystallisation mechanisms in calcite, do the grain boundary bulges play a role and how do these affect the recrystallised grain size - stress relation? 4) How does subgrain development play a role in recrystallisation? 5) How and why are the different microstructural elements related to stress, as well as strain, temperature and deformed grain size?

1.4 Methodology

1.4.1 Experiments

Previous experimental studies on palaeopiezometry used tests at various but constant strain rate and temperature, resulting in a range of flow stresses. Consequently, for calibrating a palaeopiezometer, they combine data at low temperature and high stress with data at high temperature and low stress. However, if temperature plays a role as suggested by experimental studies (e.g., Streb & Reppich, 1973 - see paragraph 1.2.3) and models (e.g., De Bresser *et al.*, 2001 - see paragraph 1.2.2), tests should be done at constant stress and varying temperature to verify these suggestions. This has not been done so far. Furthermore, many materials are in transient stages showing minor mechanical weakening and a microstructure that continues to evolve with strain (Takeuchi & Argon, 1976; Ter Heege *et al.*, 2002; Kellermann Slotemaker, 2006 - see paragraph 1.2.3). Therefore, experiments should be designed such that the role of strain can be investigated.

We use a unique series of experimentally deformed calcite samples of Ter Heege et al. (2002) plus additional new samples deformed in this study, designed such that systematic analysis of stress, temperature and strain is possible. The samples have been deformed in axial compression by constant displacement rate tests in a constant volume, internally heated argon gas medium apparatus (Ter Heege *et al.*, 2002) under a confining pressure of 300 MPa, to natural strains of 0.15-0.90 at strain rates of 3.0×10^{-6} to 4.9×10^{-4} s^{-1} and temperatures of 700-990 °C (0.5-0.7 T_m where T_m is the incongruent melting temperature of calcite in the system $CaO\text{-}CO_2$ at 100 MPa pressure – see Wyllie & Tuttle (1960)). Measured flow stresses range between 15-90 MPa (Ter Heege *et al.*, 2002 and this study). After the experiments, the samples have been rapidly cooled (ca. 70 °C/min) to limit post-deformation annealing. Further experimental details can be found in Ter Heege et al. (2002).

1.4.2 EBSD and TEM

Previously, the determination of subgrain sizes was difficult and required time consuming transmission electron microscopy (TEM) or decoration techniques. Therefore, most studies have concentrated on the recrystallised grain size, which can easily be measured using light microscopy (e.g., Schmid *et al.*, 1980; e.g., Rutter, 1995). However, the relatively recent technique of EBSD provides statistically meaningful data on the subgrain size in metals and geological materials and importantly, misorientation angles can be quantified (Trimby *et al.*, 1998; Prior, 1999; Schwartz *et al.*, 2000; Lloyd, 2004).

EBSD, used in a scanning electron microscope (SEM), allows the automated collection of absolute three dimensional crystallographic orientations in rock specimens (e.g., Kunze *et al.*, 1994; Trimby *et al.*, 1998; Wheeler *et al.*, 2001; Bestmann & Prior, 2003; Pennock & Drury, 2005). Recent reviews on the possibilities and limitations of EBSD, are given by Humphreys (2001) and Schwartz

et al. (2000). From grid based EBSD analyses, orientation maps are constructed and misorientations between each point can be calculated. This allows identification of boundaries with different misorientation angles and measurement of subgrain sizes as a function of the misorientation angles of the subgrain boundaries (e.g., boundary hierarchy of Trimby *et al.*, 1998). Also, EBSD can be used to identify recrystallised and deformed grains. Additionally, TEM has been used to obtain qualitative information on the smallest microstructures, such as dislocations and subgrains on the nanoscale.

1.5 Research questions and structure of the thesis

The broad aim of this study is to establish novel methods using EBSD that (1) allow making a quantitative description of heterogeneous microstructures as a function of the misorientation angle and (2) help to interpret deformation/recrystallisation mechanisms on the basis of microstructures and to define and understand the relationship between specific elements of the microstructure (recrystallised grains, deformed grains, core and mantle subgrains) and deformation conditions (stress, strain and temperature). The study concentrates on calcite material (Carrara marble) but the results are of relevance for rock material in general. The review of models and data in the previous sections have put forward problems (paragraph 1.2.3 and 1.3.4) and raised research questions that specifically are addressed in the individual chapters of this thesis. The chapters have been written for publication and consequently there may be some repetition, especially concerning methodology and material.

Chapter 2 (method):

As EBSD has not previously been applied for purpose of quantifying the different elements of heterogeneous microstructures as a function of the misorientation angle, the appropriate procedures to measure the microstructures still should be explored, which is done in Chapters 2 and 3. The main research question in Chapter 2 is how to measure the subgrain size in relation to the misorientation angle (i.e., the boundary hierarchy) for the microstructure taken as a whole (i.e., without separating the various microstructural elements).

Chapter 3 (method):

While in Chapter 2 the complete microstructure is considered, in Chapter 3 the main aim is to develop a reliable and objective method using EBSD to separate the various microstructural elements (i.e., recrystallised grains, core and mantle subgrain etc). Furthermore, in this chapter it is investigated what the best filtering method is to reduce the low angle erroneous misorientations (noise) in the EBSD analyses and what the errors on the measurements are due to noise and charging.

Chapter 4 (grain boundary bulges, recrystallised and deformed grains):

In Chapter 4, the focus is on the recrystallised grains, grain boundary bulges and deformed grains. The main research questions are as follows:

1) What are the quantitative relationships between the sizes of the carefully separated recrystallised grains, grain boundary bulges and deformed grains and (a) the deformation conditions (stress and temperature) and (b) the state of strain in the material?

2) What are the relationships between the different elements of the heterogeneous microstructure; e.g., between recrystallised grains and grain boundary bulges?

3) How are the grain boundary bulges, recrystallised grains and deformed grains formed and can this explain the observed relationships between their average sizes and deformation conditions?

4) Is the widely accepted and applied piezometric relationship between recrystallised grain size and stress valid for all types of microstructures and deformation conditions?

Chapters 5 (subgrains - strain):

The focus in chapter 5 is on the microstructural evolution of the subgrains with strain. The specific research questions are:

1) Does a systematic relationship exist between strain and the sizes of core and mantle subgrains and what are the processes responsible for this?

2) Does a systematic relationship exist between misorientation angle and the sizes of core and mantle subgrains and what are the processes responsible for this?

4) How is the development of the various microstructural elements with strain related to the changes of flow stress with strain (i.e., to what extent does the microstructural evolution reflect the minor weakening behaviour towards steady state)?

5) Considering their evolution with strain, which subgrains are the most suitable for palaeopiezometry: core or mantle subgrains?

Chapter 6 (subgrains – stress/temperature):

While in chapter 5 the focus is on the influence of strain on the subgrains, in chapter 6 the influence of stress and temperature on the subgrains is investigated. The specific research questions are:

1) What is the influence of stress and temperature on the core and mantle subgrain size and does this influence change with misorientation angle?

2) What is the origin of the core-mantle sub-structure?

3) What is the cause of the observed relation between the subgrain size at various misorientation angles and stress/temperature? More specifically, how can the variable subgrain size – stress sensitivity be explained?

4) Considering the relation between the subgrain size at various misorientation angles and stress and temperature, which subgrains (core/mantle; low/high misorientation angles) are the most useful for palaeopiezometry?

Finally, in Chapter 7 a synthesis is given of the answers found to the research questions in chapters 2-6 and suggestions for future research are made.

2

Electron backscattered diffraction as a tool to quantify subgrains in deformed calcite

This chapter has been published as:
Valcke, S. L. A., Pennock, G. M., Drury, M. R. & De Bresser, J. H. P. 2006. Electron backscattered diffraction as a tool to quantify subgrains in deformed calcite. Journal of Microscopy 224, 264-276

Abstract

This paper investigates processing methods to obtain subgrain sizes from electron backscattered diffraction (EBSD) data using samples of experimentally deformed calcite ($CaCO_3$) polycrystals. The domain boundary hierarchy (*DH*) method, based on area measurements of domaiNs enclosed by boundaries larger than a given misorientation angle, has been applied to these calcite samples and was found to be limited by: (1) topological problems, (2) under sampling of large grains and (3) artifacts caused by non-indexing. We tested two alternative methods that may reduce the problems: (1) the measured linear intercept hierarchy (*LI-MH*) method, based on measurements of linear intercept between boundaries having larger misorientations than a given minimum angle and (2) the calculated linear intercept hierarchy (*LI-CH*) method, based on the total length of boundaries having misorientations larger than a given minimum angle. The *LI-MH* method was found to produce results more representative for the microstructure than the *LI-CH* method because the *LI-CH* method has a significant uncertainty related to the grid based nature of the measurements. Preliminary results on calcite suggest that the *LI-MH* is related, in a complex way, to deformation conditions such as stress, strain and temperature as well as to the characteristics of subgrain rotation and grain boundary migration processes.

2.1 Introduction

The characterization and measurement of sub-structural features such as subgrain size, dislocation density and subgrain boundary misorientations are of great interest to geologists, as substructures are potential indicators of deformation mechanisms and conditions in the Earth (e.g., Twiss, 1977; White, 1979; Schmid *et al.*, 1980; Pfiffner & Ramsay, 1982; Poirier, 1985; Trimby *et al.*, 1998; Wheeler *et al.*, 2001; Kenkmann & Dresen, 2002; Pennock & Drury, 2005). In particular, the subgrain size may be used to estimate palaeostress in naturally deformed rocks (Twiss, 1977; White, 1979; Twiss, 1986). Furthermore, subgrains play a key role in recrystallisation processes, as new grains can develop from progressive rotation of subgrains (White, 1977; Shimizu, 1998). Conventional geological studies describe substructures by using average values for the subgrain size and dislocation density, measured using light microscopy and transmission electron microscopy (TEM) (e.g., Schmid *et al.*, 1980; Van der Wal, 1993). However, it has been shown that a hierarchy of subgrain sizes exists depending on the misorientation angle of the subgrain boundaries (e.g., White, 1973; Trimby *et al.*, 1998). The subgrain sizes can be presented using a hierarchy graph of misorientation angles versus the size of the domains that these misorientations enclose. Also, the frequency distribution of the misorientation angles, or the density of subgrain boundaries of specific misorientations, can be used to detect physical processes such as subgrain rotation or boundary migration that may have contributed to the microstructural development in deformed rocks (Fliervoet *et al.*, 1999; Wheeler *et al.*, 2001). This contribution concentrates on defining subgrain size parameters that could be used for estimating stress magnitudes prevalent in natural rocks in the geological past. Earth scientists use the term palaeopiezometry to refer to the relation between microstructural parameters and stress in the past (palaeostress). Existing subgrain palaeopiezometers are based on the assumption that subgrain size is only a function of stress (Twiss, 1977). However, recent experimental studies suggest that parameters such as temperature (Orlova & Podstranská, 1998), grain size (De Bresser, 1996) and water content (Van der Wal, 1993) also influence the substructure and therefore need to be included in the palaeopiezometric relations. In order to quantitatively assess the influence of parameters other than stress, extensive subgrain size data are needed using samples of different deformation conditions. The motivation for using EBSD to quantify new subgrain size parameters is that this method allows fast automated analyses of many samples to get statistically meaningful data sets, which was previously difficult using TEM or light microscopy.

EBSD, used in a scanning electron microscope (SEM), allows the automated collection of absolute 3D crystallographic orientations in rock specimens (e.g., Kunze *et al.*, 1994; Trimby *et al.*, 1998; Wheeler *et al.*, 2001; Bestmann & Prior, 2003; Pennock & Drury, 2005). Recent reviews on the possibilities and limitations of EBSD, are given by Humphreys (2001) and Schwartz *et al.* (2000). From grid based EBSD analyses, orientation maps are constructed and misorientations between each point can be calculated. This allows identification of boundaries with different misorientation angles and measurement of subgrain sizes as a function of the misorientation angles of the subgrain boundaries (e.g., boundary hierarchy of Trimby *et al.*, 1998). The aim of the present study is to examine three methods to extract boundary hierarchy data from EBSD maps:

(1) the domain hierarchy (*DH*) method (area based),

(2) the measured linear intercept hierarchy (*LI-MH*) method (measurements along intercept lines),

(3) the calculated linear intercept hierarchy (*LI-CH*) method (based on total boundary length).

The three methods are applied to the same set of boundaries in deformed calcite samples in order to deduce the most appropriate technique to quantify the hi-

sample	final grain size [μm]					size of low angle subgrains [μm]		size of medium angle subgrains [μm]		size of high angle subgrains [μm]	
	light microscopy		*DH*	*LI-MH*	*LI-CH*	*LI-MH*	*LI-CH*	*LI-MH*	*LI-CH*	*LI-MH*	*LI-CH*
	median	mean	θ>15°	θ>15°	θ>15°	θ>1°	θ>1°	θ>3°	θ>3°	θ>5°	θ>5°
36LM830/0.15	58	85	70.4	77.1	62.5	21.3	17.4	53.7	45.3	69.2	56.2
36LM830/0.30	52	80	33.0	64.4	51.1	11.2	8.7	27.9	22.9	43.1	35.5
36LM830/0.45	45	62	23.0	37.2	30.7	8.8	7.2	16.8	14.3	24.3	20.7
50LM830/0.45	41	50	31.1	37.2	32.1	10.9	9.1	22.7	19.6	29.6	26.2
50LM730/0.45	27	39	18.7	37.9	32.3	8.8	7.3	17.8	15.2	24.9	21.9

Table 2.1: Final grain size values using light microscopy, DH (including border grains, excluding badly indexed grains), LI-MH (excluding badly indexed grains) and LI-CH methods, and the low, medium and high angle subgrain size values, using LI-MH and LI-CH methods, for five calcite samples. The final grain sizes measured using light microscopy (Ter Heege et al., 2002) are equivalent circular diameter (ECD) size data. In the label, e.g., '36LM830/0.30', the first integers are the final differential stress in MPa, LM stands for Lorano marble, the following integer is the temperature in °C and the last integer is the final natural strain.

erarchy in our samples. The data of selected deformed calcite samples serve as an illustration of the advantages, disadvantages and potential of the methods.

2.2 Material and methodological details

Calcite ($CaCO_3$) has a trigonal crystal symmetry. The polycrystalline calcite samples included in this study come from experimentally deformed Carrara (Lorano) marble, uniaxially compressed for a range of stress, strain and temperature conditions, at a confining pressure of 300 MPa and a strain rate between $3x10^{-6}$ and $3x10^{-4}$ s^{-1}. Details can be found in Ter Heege *et al.* (2002). The deformed samples were cut and sliced parallel to the maximum compression direction to make polished blocks for EBSD. Care was taken to keep the sections flat parallel to the SEM specimen holder to avoid errors in size measurements (Humphreys, 1999). To achieve good quality EBSD patterns, it was important to polish the specimen surface so that all surface damage and relief was removed. Standard metallographic techniques were used to polish the specimen to 1 μm finish using Al_2O_3. Colloidal silica (0.05 μm) (Fynn & Powell, 1979) was used for the last polishing stage, which is a chemical-mechanical treatment of the surface. The final polishing stage only needed to be applied for ~15 minutes to obtain an adequately polished surface. Longer polishing times tended to produce deep scratches caused by grain pull out. Highly deformed calcite (natural strains of 0.45) was more difficult to adequately polish than undeformed calcite. This is possibly related to the dense boundary network of highly strained, fine grained calcite, which leads to more topography and/or easier grain pull out. The samples were coated with a thin carbon layer to prevent charging during EBSD mapping. Samples containing cracks or holes due to grain pull out were first coated with a thin gold layer. The gold layer was subsequently removed by wiping the surface, leaving only pores and cracks partially filled with the gold.

EBSD data were collected and analysed using HKL Channel 5 software on a Philips XL30SFEG SEM with a Nordlys 2 CCD camera. SEM conditions that typically yielded high indexing success rates (>90%) for calcite were a beam of 20 kV, a beam current of 2 nA and a working distance of 15 mm for a 70° tilted sample. The signal was strong enough to reliably index patterns with a speed of 0.1 s per grid point. Forescattered electron images showed that the majority of the subgrains were larger than a few microns, so that a mapping step size of 1 μm was sufficient to representatively sample the subgrains and simultaneously acquire relatively large maps (1000 x 1000 μm) that included small grains (~100 grains or more) as well as large grains (~10 grains or more). While spatial resolution of EBSD maps was sufficient to map the smallest subgrains, angular resolution limits the subgrain misorientation angles that can be used to investigate microstructures. Random misorientations not associated with structure are called 'noise'. In calcite, angles smaller than ~1° typically contain a lot of noise so that subgrain boundaries <1° are difficult to discriminate from noise. Low angle noise ~1° could be reduced sufficiently using the method of Cao *et al*. (2003).

Misindexing occurred in EBSD mapped microstructures of calcite when the automated indexing could not distinguish between similar patterns with different orientations. Usually, the misindexing gave a twin relationship solution, displayed in EBSD maps as high angle boundaries (Fig. 2.1b - Appendix A). These boundaries often had angle/axis disorientations (minimum angle misorientations) of 78° or 104° about <20-21>, which is consistent with *e*- and *r*-twins respectively. Deformation *e*-twins also occurred in calcite (Fig. 2.1a - appendix A). Both high angle twin boundaries and misindexed points were ignored in (sub-)grain size analysis.

Details of the samples and deformation conditions

are given in Table 2.1. These samples were selected to show the typical range of microstructures found in deformed calcite. EBSD maps showing the boundary microstructures of the samples are shown in Fig. 2.1 (Appendix A). The low strain sample 36LM830/0.15 (deformed at 36MPa flow stress, at 830°C, to a natural strain of 0.15) shows predominantly large original, relict grains (Fig. 2.1a - Appendix A). The subgrain boundaries are mainly concentrated along the grain boundaries; the cores of the grains are relatively undeformed, with only a few long, straight, low angle subgrain boundaries. Sample 36LM830/0.30 (higher strain, same temperature) also contains relict grains, but the grains show a more dense subgrain boundary network and small new grains occur along the boundaries of the large grains (Fig. 2.1b Appendix A). The higher stress, higher strain sample 50LM830/0.45 has well sub-structured relict grains, but also a significant area fraction of non-substructured recrystallised grains (Fig. 2.1c - Appendix A). These recrystallised grains are relatively large and randomly distributed. In contrast, in the lower temperature sample 50LM730/0.45, many small recrystallised grains occur along old grain boundaries. The subgrain structure extends to the core of the grains, but is more dense at the grain boundaries (core-mantle substructure).

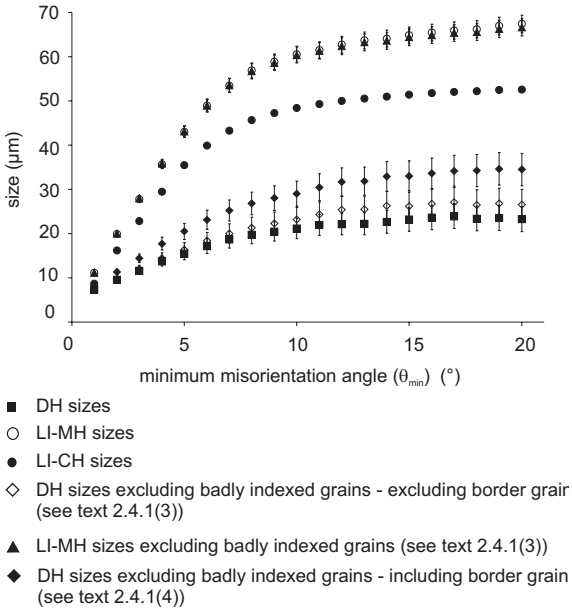

Figure 2.2: Comparison of three hierarchy graphs for sample 36LM830/0.30 (after noise reduction): domain hierarchy (DH), measured linear intercept hierarchy (LI-MH) and calculated linear intercept hierarchy (LI-CH) methods. The error bars of the DH and LI-MH method are standard errors. Errors on LI-CH are discussed in paragraph 2.4.2.

2.3 EBSD processing methods for obtaining subgrain size data

2.3.1 *DH* method

A boundary hierarchy shows the size of 'domains' (grains, subgrains) completely surrounded by boundaries that are larger than a minimum misorientation angle. In the *DH* method of Trimby *et al.* (1998) the domain size for a given minimum misorientation angle, θ_{min}, is given in terms of the average equivalent circular diameter (ECD) of the area of all domains completely enclosed by boundaries larger than θ_{min}. A domain boundary hierarchy graph (θ_{min} versus domain size) typically has a near linear relationship between θ_{min} and domain size at low misorientation angles, followed by an asymptotic approach to a plateau at higher angles in which the size of the domains no longer significantly changes with increasing misorientation (Fig. 2.2). In other words, subgrains (θ_{min} < 10~15°) show a hierarchy of sizes, while grains (θ_{min} > 10°~15°) do not show this hierarchy and their size no longer significantly increases with increasing misorientation angle. Consequently, the grain size can be deduced from *DH* data at high grain angles. For calcite, there are currently no data on the minimum misorientation angle to define a grain boundary. Therefore, we arbitrarily take the domain size for boundaries larger than 15° to represent the grain size (Table 2.1). According to Rossi & Sellars (1997) about 450 grains should be measured for a representative estimate of the average grain size. However, due to the restricted sampling area (1000 x 1000 µm), only ten to a few tens of large grains (~100-400 µm) were measured, while the small grains are sampled adequately (on average >450 grains). This means that calculated average grain sizes might be biased towards the small grains in the *DH* method.

2.3.2 *LI-MH* method

In the *LI-MH* method (where *M* stands for 'measured'), the domain size presented for a given minimum misorientation angle θ_{min}, is the arithmetic mean of all intercept lengths measured between boundaries with misorientation angles larger than θ_{min}. The intercept lines along which the intercepts were measured were taken parallel and perpendicular to the compression axis, so that the measurements relate to the short and long axes of the average strain ellipse of the deformed grains (Underwood, 1970). The average of the parallel and perpendicular intercepts was taken for the *LI-MH* sizes. The spacing of intercept lines is usually chosen such that the spacing is not smaller than the size of the domains. Because determining the subgrain size was the main objective of this study, we took a narrow spacing of 20 µm between the measurement lines, which is larger than the average subgrain size, but produces enough measurements to obtain statistically meaningful averages for the subgrain size. This had the consequence that some grains, which were much larger than subgrains, were sampled more

than once. Furthermore, because the high angle grains have a broad grain size distribution, this sampling effect was stronger for the large grains than for the small grains. Therefore, the *LI-MH* method does not give an unbiased sampling of the complete size range of grains but gives a good sampling of subgrain sizes. Changing the spacing of the intercept lines is expected to influence the *LI-MH* values because the sampling of the large versus small grains changes (Exner, 1972). However, for our EBSD map data, the effect of changing the spacing of the intercept lines was found to be rather small (Table 2.2). This is because the maximum area analysed is too small to allow a spacing of intercept lines larger than the largest grains and at the same time sample enough grains to have statistically representative data. For example, a spacing of more than 350 µm (~largest grain size) on a surface of 1000 x 1000 µm results in only two lines for intercept measurements. Taking a smaller spacing, i.e., more than two lines on 1000 x 1000 µm maps, results in a bias towards the large grains, an effect which does not change significantly when taking smaller line spacings (Table 2.2). Therefore, within the limitations of the spacing of intercept lines for our EBSD maps, a spacing of 20 µm was considered to be a reasonable choice.

θ_{min}	***LI-MH* size [µm] for different number (spacing) of horizontal lines**				
	200 (5µm)	50 (20µm)	20 (50µm)	10 (100µm)	4 (250µm)
1°	10.18	10.16	10.19	10.41	9.93
3°	25.58	25.61	25.47	25.02	26.37
10°	58.32	58.03	59.15	57.46	59.07

Table 2.2: The influence of the different spacings of intercept lines on the LI-MH size measurements is shown for sample 36LM830/0.30.

The shape of the *LI-MH* curve shows a near constant slope at relatively low misorientation angles, followed by a change in slope at higher misorientation angles, asymptotically approaching a plateau (Fig. 2.2). This is similar to the shape of the *DH* curve, although the *LI-MH* curve is shifted to larger size values (Fig. 2.2). Similar to the *DH* method, the grain size can be deduced from the *LI-MH* data by taking the *LI-MH* size for θ_{min}>15°.

2.3.3 *LI-CH* method

The *LI-CH* method (where *C* stands for 'calculated') is similar to the method of Wheeler *et al*. (2003), in which the boundary density is used as a parameter for subgrain structure. Here, we use the boundary density (length/unit area) [µm^{-1}] to calculate a 'size' (length) [µm].

In a square grid EBSD map, the boundary length $B(\theta')$ [µm], for a given misorientation θ', is given by

$$B(\theta') = \mathrm{f}(\theta') \times \textit{step size} \quad , \tag{2.1}$$

where $\mathrm{f}(\theta')$ is the number of misorientation measurments between adjactent pixels larger than θ'. This boundary length $B(\theta')$ has a bias due to grid ased measurements, which will be discussed in paragraph 2.4.2. The boundary length, $B(\theta')$ is related to the boundary length per unit area, L_a [µm^{-1}]:

$$L_a(\theta') = \frac{B(\theta')}{(\textit{mapped area})} \quad , \tag{2.2}$$

and to the total area per unit volume, S_v [µm^{-1}] (Underwood, 1970):

$$S_v(\theta') = \frac{4}{\pi} L_a \quad , \tag{2.3}$$

S_v can be described in terms of the mean linear intercept length, *LI-C* [µm] (Gifkins, 1970):

$$L - C(\theta') = \frac{2}{S_v(\theta')} \quad , \tag{2.4}$$

Combining these equations, we have:

$$L - C(\theta') = \frac{\pi}{2} \frac{(\textit{mapped area})}{B(\theta')} \quad , \tag{2.5}$$

The hierarchy values (*LI-CH*) are derived in a similar manner, but for boundaries with a misorientation >θ_{min}:

$$\textit{LI-CH}(\theta_{min}) = \frac{\pi}{2} \frac{(\textit{mapped area})}{B(\theta_{min})} \quad , \tag{2.6}$$

The shape of the *LI-CH* is similar to the *LI-MH* and the *DH* graphs (Fig. 2.2). However, the sizes of the *LI-CH* are less than the *LI-MH* values and much larger than the *DH* values.

2.4 Discussion of processing methods

As pointed out by Wheeler *et al.* (2003) 'There are advantages and disadvantages to all the various methods of quantifying microstructure. It is a matter of scientific judgement which of these will be the most appropriate in any particular study.' In what follows we will compare the three methods described above to find out which is the most appropriate method for our purposes, i.e., quantifying microstructures in geological materials that show a heterogeneous microstructure, such as the rock material calcite.

2.4.1 *DH* versus *LI-MH* methods

The hierarchy analyses of our EBSD maps of calcite show significant differences. The *LI-MH* values are consistently larger than the *DH* values (Fig. 2.2 and Table 2.1). Furthermore, the grain size deduced from the *LI-MH* method is similar to the grain size measured using light microscopy, while the *DH* method gives a much lower

value for the grain size (Table 2.1). Below we discuss reasons why these differences might arise and which of these reasons might apply for our specific data sets.

(1) When the *DH* and *LI-MH* methods are applied to the same microstructure, a stereological relationship exists relating the results of both methods:

$$DH(\theta_{min}) = k(LI\text{-}MH(\theta_{min})) \quad , \qquad (2.7)$$

in which k is a constant ranging from 1.2 to 2.2 depending on the shape of the grains (Underwood, 1970; Han & Kim, 1995). According to Eqn. (2.7), the *LI-MH* values should be smaller than the *DH* values. However, our data show that *LI-MH* is significantly larger than *DH* for all misorientation angles. A possible reason for this discrepancy is that the given values of k only apply to aggregates of grains of equal size, while the samples in this study have a relatively broad grain size distribution. For wider grain size distributions, the values of k may be ≤ 1 (Han & Kim, 1995) (see also point (5)).

(2) In the *DH* method the area (ECD) of domains is defined on the basis of closed boundaries that completely surround the domains with a minimum misorientation angle. However, the boundaries of subgrains often do not have constant misorientation angles along the whole boundary. If only one pixel segment of a given boundary has a lower misorientation than the considered minimum domain angle, θ_{min}, then the boundary no longer forms a closed domain and the measured domain size ($>\theta_{min}$) increases dramatically, whereas the structure does not change significantly (Wheeler *et al.*, 2003). This problem becomes important if many subgrain boundaries have misorientations near the angular resolution limit. In our case, 0.5° misorientations form a large amount of noise, even after noise reduction. Therefore, for quantifying subgrain sizes, selecting misorientation angles larger than 1° is better. However, many subgrains are then no longer detected by the *DH* method because parts of the subgrain boundary are frequently lower than 1°. This is illustrated by comparing two maps, one with domains defined by boundaries >0.5° and one by boundaries >1° (Fig. 2.3 - Appendix A). The maps show that even though the geometry of the subgrain boundary network for θ_{min} >1° does not significantly change compared to the network for θ_{min} >0.5°, the *DH* method detects fewer subgrains for θ_{min} >1° than for θ_{min} >0.5°, particularly in the core of the grains. In contrast, the *LI-MH* method does not require closed loops and measures from boundary to boundary along the intercept line. Therefore *LI-MH* does not have the problem associated with low angle subgrains that have 'discontinuous' boundaries and the *LI-MH* method detects more subgrains for θ_{min} >1° than the *DH* method (Fig. 2.3 - Appendix A). This should result in lower *LI-MH* size values for the low angles compared to the *DH* values as for example, for θ_{min} >1°, the *DH* includes large apparently 'un-substructured' areas, while the *LI-MH* measures the smaller substructure (Fig. 2.3 - Appendix A). However, Fig. 2.2 shows that the *LI-MH* values for the low angles are larger than the *DH* values, opposite to what can be expected on the basis of the above discussion. Clearly, *LI-MH* method captures the microstructure more accurately than *DH*, but the difference in size values cannot be explained by the non-closure of domains in EBSD maps.

(3) The method of noise reduction (Cao *et al.*, 2003) can reduce most noise for misorientations ~1°, but some artificial domains and single pixel boundaries remain (e.g., Fig. 2.3 - Appendix A, isolated pixel size boundaries). Both the *DH* and the *LI-MH* method are affected by the presence of noise, but in different ways. The *DH* method measures only the remaining artificial pixel sized, fully enclosed domains, while the *LI-MH* method is affected by both closed and open (i.e., not closed) noise boundaries when these are sampled by an intercept line. However, this low angle noise affects only the lowest angle (0.5°-1°) subgrain size measurements, and therefore does not explain the large difference in *DH* and *LI-MH* size for the medium and high angle subgrains and the grains. Furthermore, noise reduces the low angle size measurements. Consequently, the *LI-MH* measurements, which are additionally influenced by open isolated noise boundaries, should be smaller than the *DH* measurements. This is, again, opposite to what we observe.

(4) Non-indexed pixels occur when EBSD patterns are difficult to index. In many non-geological materials, non-indexed solution pixels are often restricted to grain boundaries and can be removed easily by extrapolation, which only causes minor errors in the grain size determination (Humphreys, 2001). However, in geological materials the number of non-indexed pixels can be quite significant due to pre-existing porosity or polishing artifacts. Up to 5% non-indexed pixels typically remain after moderate extrapolation, often concentrated in patches along grain boundaries or inside grains (Fig. 2.4 - Appendix A). These non-indexed pixels create a problem in determining sizes, which can be dealt with in a better way using the *LI-MH* method than using the *DH* method. In the area based *DH* method, the border between an indexed solution and a non-indexed solution is considered as a boundary. Consequently, patches of non-indexed pixels along pores or within badly indexed grains cause small, artificial grains to be defined, which lowers the average domain size (Fig. 2.4a - Appendix A). This is evidenced by the difference between the *DH* graph of an EBSD map that includes badly indexed grains and the

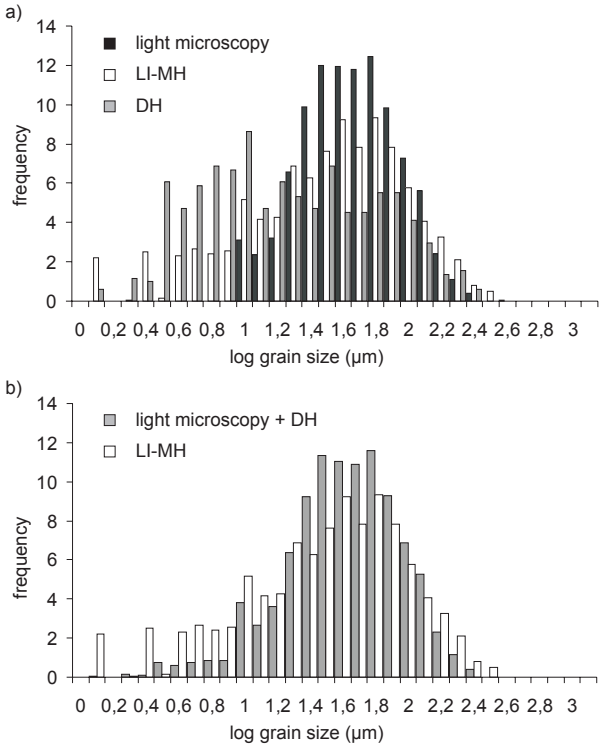

Figure 2.5: Comparison of logarithmic grain size distributions obtained using light microscopy (ECD; Ter Heege et al., 2002), DH and LI-MH methods. The LI-MH data have been multiplied by the stereology correction factor k = 1.224 of Eqn. 2.7, which is a first order approach assuming spherical grains with a uniform distribution (Underwood, 1970).

DH graph of the same map that excludes badly indexed grains (Fig. 2.2). In the *LI-MH* method, the part of the linear intercept line running through a patch of non-indexed pixels is divided in two halves and added to the linear intercepts lengths on each side of the non-indexed patch (Fig. 2.4b - Appendix A). If the non-indexed patch is along a border, half of the patch intercept length is added to the linear intercept length of the grain on one side while the other half to the grain on the other side (Fig. 2.4b-B - Appendix A). If the non-indexed patch is inside a grain, then the patch is fully included in the intercept length of that grain (Fig. 2.4b-A - Appendix A). In this way, the sizes of badly indexed grains are still detected reasonably well with the *LI-MH* method, which is evidenced by the good correspondence between the *LI-MH* measurements of a map that includes badly indexed grains and the *LI-MH* measurements of the same map, but excluding the badly indexed grains (Fig. 2.2). As non-indexing lowers the *DH* values, non-indexing is one of the reasons that *DH* values are lower than *LI-MH* values. However, on the scale of a 1000 x 1000 µm map, the effect is small and mainly affects the higher misorientation angles (Fig. 2.2).

(5) A hierarchy method is cumulative and measures the sizes of all domains with boundaries that have misorientations *larger* than a given angle. As long as all grains in the aggregate are sufficiently substructured, hierarchy measurements for low angles result in good estimates of the average subgrain size. However, if many high angle grains without substructure are present, as is the case in our heterogeneous calcite, then the sizes of these grains strongly affect the hierarchy domain sizes for all misorientation angles and hence affect the values of the average subgrain size. Therefore, an appropriate sampling of the high angle grains is needed, which means that a statistically representative number of grains should be measured. For example, the effect of the number of high angle grains (θ_{min} >15°) sampled using the *DH* method can be seen when comparing two *DH* graphs; one including border grains and one excluding border grains (Fig. 2.2). Including border grains, i.e., sampling a higher number of large grains, results in higher *DH* values for all misorientation angles. The *LI-MH* method, however, excludes intercept measurements along the border (red lines in Fig. 2.4 - Appendix A), although border grains are still sampled if the intercept line is situated in the non-bordering part of the grain. Although increasing the number of grains sampled in the *DH* method by including the border grains increases the *DH* domain size values, the *DH*-values were still less than the *LI-MH* values (Fig. 2.2). This can be explained by the fact that there is a difference in the sampling of the grains (θ_{min} >15°). The *DH* method has a bias towards small grains (average grain size is underestimated, see paragraph 2.3.1), while the *LI-MH* method has a bias towards large grains (average grain size is overestimated, see paragraph 2.3.2). Therefore, the grain size distribution has an effect on the difference between the *DH* and *LI-MH* values, which agrees with Han and Kim (1995) (see also (1)). To shed further light on this, we compared the grain size frequency distributions of the *DH*, the *LI-MH* and the light microscopy methods (Fig. 2.5a). The *DH* and light microscopy methods are both based on the measurement of grain areas. However, their frequency distributions are somewhat different (Fig. 2.5a). On the one hand, the light microscopy distribution lacks data on the smallest grains, because no measurements on grains smaller than 5 µm were made (Ter Heege *et al.*, 2002), while the EBSD method allowed grains to be measured down to 2 µm. On the other hand, the *DH* distribution shows low frequencies at large grain sizes, because it misses out large grains. Strikingly, the combined light microscopy and *DH* measurements show a reasonable sampling of the whole range of grain sizes (Fig. 2.5b). Moreover, the *LI-MH* frequency distribution is similar to this combined light microscopy and *DH* distribution (Fig. 2.5b). This suggests that in our samples, the *LI-MH* method gives a reasonable representation of the distribution of the small as well as the large size intervals, while the *DH* method undersamples the large grains and the light microscopy

is likely to miss out some of the very small grains (Fig. 2.5b).

Points (1) to (5) above demonstrate that the main reason for the difference between the *DH* and the *LI-MH* values is related to the different ways in which large and small grains are sampled in both methods. If an accurate grain size (e.g., θ_{min}>15°) is required, larger areas should be mapped using EBSD or measured using light microscopy. However, for our purposes, i.e., subgrain characteristics of geological materials, the *LI-MH* method works well, particularly for EBSD maps that have:

(1) an angular resolution limit (e.g., 1°), so that many low angle subgrains cannot be measured by the *DH* method because they do not form closed loops;

(2) a broad grain size distribution, in which the large grains cannot easily be sampled in a statistically representative way owing to restrictions on the map size;

(3) more than 5% non-indexed pixels, related to holes, scratches or specific grain orientations.

We note that these conclusions are made for averages that are not area weighted. We found that for area weighted averages the *LI-MH* and *DH* methods still differ significantly.

Methods similar to the *DH* and *LI-MH* have been applied previously by Cao *et al.* (2003). They found that a modified *DH* method was more representative for the microstructure than the *LI-MH* method and that the *DH* measurements resulted in larger average values than the *LI-MH* measurements. This is in contrast to our study. However, the conclusions of Cao *et al*. were based on the low angle range of the hierarchy; at higher angles both *DH* and *LI-MH* methods approached each other. For the low angles, their lower *LI-MH* results were explained by noise problems which lower the *LI-MH* values (see point 3 above). Based on these observations and the type of samples used by Cao *et al.*, we infer that the *DH* works better for relatively homogeneously well structured metals having a small grain size, in which a sufficient amount of grains can be sampled and in which large non-substructured grains do not have a large influence. For example, deformed NaCl with homogeneously distributed subgrains and very few non-substructured grains (Pennock *et al.*, 2005), show *DH*, *LI-MH* and light microscopy values that are similar to each other. The above discussion shows that the applicability of hierarchy methods is very dependent on the heterogeneity of microstructure and the quality of maps.

2.4.2 *LI-MH* versus *LI-CH* methods

We now compare the *LI-MH* and the *LI-CH* method for quantifying the substructure of calcite. As we concluded that the *LI-MH* is more appropriate for our purposes than the *DH* for calcite (see paragraph 2.4.1), no comparison will be made between the *LI-CH* and *DH* methods. The *LI-CH* has a similar hierarchy shape as the *LI-MH* graph, but the values are smaller (Table 2.1 and Fig. 2.2). Paragraph 2.3.3 shows how we have determined the linear intercept lengths using the *LI-CH* method. We have called this a *calculated* intercept length to clearly distinguish it from the conventional *measured* intercept (*LI-MH*) method (paragraph 2.3.2). The observed lower values of *LI-CH* values compared to *LI-MH* values are probably caused by errors relating to square grid based measurements. Boundaries in EBSD maps are built up of vertical and horizontal segments equal to the step size (step size of 1 μm: pixel size of 1 μm). For the *LI-MH* method, which measures intercept lengths from boundary to boundary, the error due to square grid measurements ('grid error') has a maximum value of 0.5 μm (step size/2) at each side of the intercept measurement, so the total maximum error is 1 μm per measurement. For boundary length measurements, on which the *LI-CH* is based, the grid error is larger (Russ & Dehoff, 1999). As stated above a boundary will appear on the EBSD map as vertical and horizontal segments, while in reality, the boundary is a continuous curve. The boundary length of these vertical and horizontal segments, $B(\theta_{min})$ will be different from the true boundary length, B_T. This difference, or the grid error is dependent on two factors (Fig. 2.6):

(1) The grid spacing (pixel size) determines how well the true boundary can be approached and if B_T is larger or smaller than $B(\theta_{min})$. If the true boundary segment cannot be split into vertical and horizontal segments, then $B_T \geq B(\theta_{min})$ (positive grid error) (Fig. 2.6a). If the considered true boundary segment can be split between vertical and horizontal segments, then $B_T < B(\theta_{min})$ (negative grid error) (Fig. 2.6b).

(2) For a step size much smaller than the curvature of the boundary (1 μm step in this study), the boundary can be split into a series of straight segments. In this case, $B(\theta_{min})$ is larger than B_T (negative grid error, Fig. 2.6b) and the small angle α between the true boundary (B_T) and the grid segments ($B(\theta_{min})$) determines the amount of the grid error. For $\alpha = 0°$, $B_T = B(\theta_{min})$ and the error is zero. For $\alpha = 45°$, the *LI-CH* value based on $B(\theta_{min})$ as the total boundary length (Eqn. 2.6), is a factor of $0.5\sqrt{2}$ smaller than the *LI-CH* value based on B_T (Fig. 2.6b), which implies a negative grid error of 29%. We calculated that for random boundary orientations ($\alpha = 0°$ to 45°), the total negative grid error is 20%. In general, for

a small step size, the *LI-CH* values based on $B(\theta_{min})$, will be smaller than the ones based on B_T (Eqn. 2.6). The difference observed between the *LI-CH* and *LI-MH* values is 12% to 23% with an average of 17% (based on data in Table 2.1). Thus, this difference could be well explained by the grid error of the *LI-CH* method, which lowers the *LI-CH* values with respect to the *LI-MH* values. Still, despite these differences, the *LI-CH* method remains useful to measure sizes of misorientation intervals, $[\theta_1\text{-}\theta_2]$, rather than taking cumulative angle ranges ($>\theta_{min}$) as in the hierarchy methods. In this way, high angle grains can be excluded from the low angle subgrain size measurements. Furthermore the *LI-CH* could be of interest if the applied software only allows the measurement of horizontal and vertical intercept lines and while the microstructure has a complex anisotropy. In this case, the *LI-MH* method would bias the measurements, while the *LI-CH* method would sample the anisotropic microstructure better. It should be emphasized that using the *LI-CH* method for misorientation intervals will only work for a well developed and connected substructure network. For the heterogeneous samples used in this study, which contain a significant proportion of non-substructured area, normalising a low frequency of subgrain boundary misorientations for the whole analysis area to obtain the *LI-CH* values, resulted in subgrain sizes that are larger than the average grain size and no longer correlated in a straightforward manner with the microstructure.

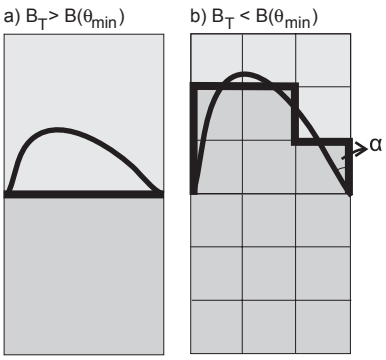

Figure 2.6: Schematic diagram to illustrate grid errors using the *LI-CH* method (section 4.2). A true boundary (B_T) is shown (thin black line). The pixel size in a) is larger than in b). The grey shades of the pixels relate to the crystal orientation. Boundaries, $B(\theta_{min})$, are drawn between pixels having different orientations (thick black line). In a) B_T is longer than $B(\theta_{min})$, in b) B_T is smaller than $B(\theta_{min})$ and the difference (grid error) is dependent on α, the angle between B_T and $B(\theta_{min})$.

2.4.3 Significance of linear intercept hierarchy

In the linear intercept hierarchy (*LI-MH*) subgrain sizes for a particular minimum misorientation can be considered, which is of direct relevance for palaeopiezometry. Alternatively, the hierarchy can be considered as a comprehensive visualisation for all misorientation angles. Trimby *et al.* (1998) have suggested a model to explain the shape of the hierarchy graph. Their model shows a simple linear size hierarchy in samples in which deformation mechanisms such as subgrain rotation, recovery and/or grain boundary migration were active (see black line on Fig. 2.7). However, true linear trends for low angle size hierarchies appear to be rare in reality (Fig. 2.2, see also Trimby *et al*, 1998, Fig. 2.7a and 12b). We infer that the curved nature of the hierarchy graphs is the consequence of the gradual transition from subgrain to grain structure. For a relatively low frequency of high subgrain misorientation angles (θ_{min} ~ 5-10°), the subgrain structure will be close to the grain structure and therefore the *LI-MH* values at these high angles will be close to the grain size. Consequently, at high subgrain misorientation angles the slope gradually decreases and approaches zero when a grain misorientation is approached and the grain size no longer changes significantly with misorientation angle. *LI-MH* graphs that extend to high angle boundaries of grains appear to approach asymptotically to a maximum value. They can be fitted empirically to the exponential relationship (Wheeler J., pers. comm.):

$$\text{LI-MH}(\theta_{min}) = a\left[1 - \exp\left(-\frac{\theta_{min}}{b}\right)\right] , \qquad (2.8)$$

in which the *LI-MH* size [μm] is a function of θ_{min} and *a* [μm] and *b* [°] are variable factors dependent on the shape of the curve. The factor *a* represents the domain size to which the curve asymptotically approaches and therefore is related to the average grain size. The factor *b* is a measure of the shape of the curve for the subgrain angles at which the domain size is still significantly dependent on misorientation angle. Applying a non-linear regression best fit analysis, we determined values for *a* and *b* for the studied samples. The *a* and *b* values are found to vary systematically with deformation conditions (Table 2.3 and Fig. 2.8). Factor *a* decreases with increasing strain.

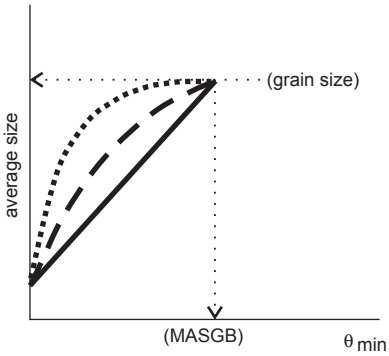

Figure 2.7: Schematic diagram with hypothetical hierarchy curves. The black line is the hypothetical shape suggested by Trimby et al. (1998) for materials that undergo subgrain rotation, grain boundary migration and recovery. The dotted and dashed lines are hypothetical shapes for hierarchies in calcite materials. MASGB is the maximum angle to define a subgrain boundary (see text 2.4.3).

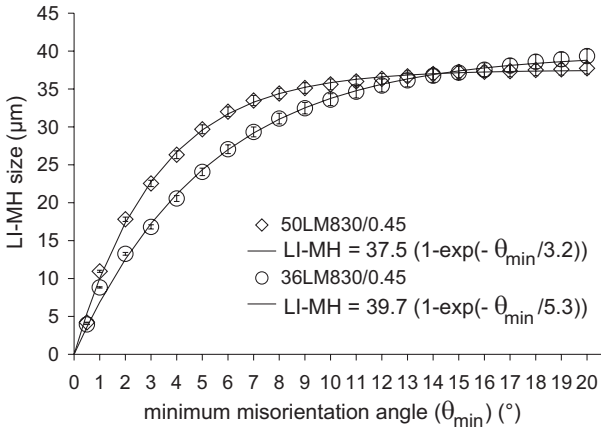

Figure 2.8: Comparison of the LI-MH hierarchy for two calcite samples, deformed at the same temperature (830°C) and to the same natural strain (0.45), but at different flow stresses (50 and 36 MPa). The exponential best fit is shown.

Factor *b* increases with increasing strain, decreases with increasing temperature and decreases with increasing stress. This can be explained by the fact that the shape of the curve is related to the size, as well as to the frequency, of subgrains and misorientation angles. Therefore *b* is dependent on the specific deformation mechanisms that build up or annihilate subgrain boundaries, such as subgrain rotation, grain boundary migration and recovery. It is observed in our samples that these three mechanisms have played a role in the development of the microstructure (Fig. 2.1 - Appendix A and Ter Heege *et al.*, 2002). For a low frequency of high angle subgrain boundaries (θ_{min} ~ 5-10°) or a poorly-developed network of subgrains (e.g., core-mantle structures as in our calcite samples, Fig. 2.1 - Appendix A), the size of many large non-substructured cores and high angle grains is included in the linear intercept measurements so that the *LI-MH* of these boundaries quickly approaches the grain size, resulting in a steep slope and a low *b* value (see dotted line on Fig. 2.7). In contrast to this type of microstructures, for a high frequency of high angle subgrain boundaries (θ_{min} ~ 5-10°) and a relatively well connected network, only few non-substructured cores or grains will be included in the linear intercept measurements, so that the *LI-MH* size for these boundaries is significantly smaller than the grain size. This results in a low slope and a high *b* value (see dashed line on Fig. 2.7). In summary, the curved shape of the hierarchy graph, quantified using *b*, is not only dependent on the existing *size* hierarchy of subgrains, but also on the relative frequency of low angle versus high angle misorientations and strained versus strain free area. These findings correlate well with the exponential decay of the misorientation angle frequency distribution, described by Wheeler *et al*. (2003). These authors also explain the exponential shape of the frequency distribution in terms of a combination of subgrain rotation and grain boundary migration.

It has been stated above that a hierarchy including high angle misorientations consists of a part that represents the subgrains and a part that represents the grains. The critical subgrain misorientation angle, θ_C, that separates a subgrain boundary from a grain boundary, varies depending on how a subgrain boundary is defined (de Meer *et al.*, 2002). Different definitions can be found based on structural characteristics, such as the type of dislocations (White, 1977) or properties of the boundary, such as mobility (Lloyd & Freeman, 1994). Furthermore, some studies have suggested that θ_C is different for different minerals, e.g., 15° to 22° for olivine (Poirier & Nicolas, 1975; Heinemann *et al.*, 2005) and 10° for quartz (White, 1977). For calcite such a critical subgrain angle is not known. Because the domain size approaches a near constant value with increasing misorientation angle, the hierarchy could be used to define a maximum angle of subgrain boundary development (MASGB) above which the domain size is determined by the grain boundaries. The MASGB is the angle at which the slope (~ derivative of Eqn. 2.6) of the hierarchy becomes lower than the standard error of the measurements (~1 µm). It should be emphasized that the MASGB is an empirically derived maximum subgrain angle, based on the idea that the domain size is observed to be invariant at higher misorientation angles. The MASGB varies from 8° to 13° (Table 2.3) according to the specific deformation conditions, so cannot be regarded as the maximum critical subgrain angle for calcite in general. The variation of the MASGB could be related to the subgrain boundary mobility being dependent on deformation conditions, e.g., temperature (Humphreys & Hatherly, 1995). For example, a low MASGB may be related to (1) little subgrain rotation activity, which causes few high angle subgrain boundaries to develop (at low strain) or (2) grain boundary migration (at high temperature) and/or to recrystallisation (at high stress) both consuming high angle subgrain boundaries.

2.4.4 Heterogeneity

In this paragraph, we consider the significance of the *LI-MH* values for a given minimum misorientation, θ_{min}. Each point on the *LI-MH* graph is the average size of all linear intercepts between boundaries larger than θ_{min}. This average is a combination of different types of subgrains: 1) small mantle subgrains, 2) larger core subgrains and 3) long, straight subgrain boundaries that run from the border to the centre of grains (e.g., Fig. 2.1a and 2.1b - Appendix A). Any information on the specific characteristics of the sub-structure is lost when taking an average. It is possible that mantle subgrains show a different relation with deformation conditions than core subgrains or long, straight subgrain boundaries. Furthermore, non-substructured (strain free or recrystallised) areas, significant in sample 36LM830/0.15 and

50LM830/0.45 (Fig. 2.1a and 2.1c - Appendix A), are included in the average when relating the *LI-MH* data to deformation conditions.

Intercept distribution curves, for example, of the >1° subgrain sizes, are unimodal and skewed towards small values due to the very high frequency of small subgrains versus relatively few large, core subgrains and straight subgrain boundary spacings (Fig. 2.9a - Appendix A). The *LI-MH* (>1°) is therefore closer to the value of the small, mantle subgrains, although this value can be slightly modified towards higher values because of the presence of larger core subgrains, straight subgrain boundary spacings and recrystallised grains. This is illustrated by comparing the *LI-MH* (>1°), measured automatically along 50 horizontal and vertical lines, with manual measurements on EBSD maps (Fig. 2.9b - Appendix A). Manual means that the user distinguishes between mantle and core subgrains. On average 50 to 100 grains are measured for both mantle and core subgrains. The automatically measured *LI-MH* size (>1°) differs only by a few microns from the manually measured mantle subgrain size, but the *LI-MH* size (>1°) is ten to a few tens of microns smaller than the core subgrain size or the straight boundary spacing. Therefore, the *LI-MH* sizes appear to be generally representative for the sizes of the mantle subgrains. However, the difference between the manually measured mantle subgrain size and the automatically measured *LI-MH* size (>1°) on one sample is of the same order as the variation between the *LI-MH* sizes (>1°) of different samples (~a few microns) (Table 2.1). So in order to relate the subgrain sizes to deformation conditions, separate measurements of the three different types of subgrains are required.

2.5 Conclusion

In this paper we have investigated methods to extract subgrain size data from EBSD maps of deformed polycrystalline calcite samples. The microstructures are heterogeneous having (1) well-substructured areas as well as non-substructured areas, (2) small mantle subgrains as well as large core subgrains and (3) large relict grains, up to two orders of magnitude larger than subgrains, as well as small recrystallised grains. In this kind of material it is not straightforward to extract subgrain size values that are easy to interpret. Moreover, EBSD data of geological materials, such as calcite, are subject to a significant amount of non-indexing, and a poor angular resolution limit, both creating difficulties and errors in the measurement of low angle subgrains. We have compared three hierarchy methods to quantify sizes in relation to misorientation angles: (1) the domain boundary hierarchy (*DH*) method (Trimby *et al.*, 1998), which measures domain sizes based on the area of domains surrounded by boundaries larger than a given misorientation angle; (2) the measured linear intercept hierarchy (*LI-MH*) method, which measures domain sizes based on linear intercepts between boundaries larger than a given misorientation angle and (3) the calculated linear intercept hierarchy (*LI-CH*) method, which calculates domain sizes based on the total length of boundaries larger than a given misorientation angle. We have found that the *LI-MH* method is the best method to characterize these heterogeneous calcite samples. The advantages of this method compared to the *DH* method are that (1) *LI-MH* measures subgrain boundaries that are not fully closed owing to the angular resolution limit of EBSD in our samples; (2) *LI-MH* is not significantly affected by noise and non-indexing, after appropriate noise reduction has been applied; and (3) *LI-MH* provides a reasonable sampling of domain sizes for analyses in which the mapped area is small with respect to the grain size (for practical EBSD reasons).

sample	*a* [µm]	*b* [°]	MASGB [°]
36LM830/0.15	75.8	2.5	9
36LM830/0.30	58.8	4.9	13
36LM830/0.45	39.7	5.3	11
50LM830/0.45	37.5	3.2	8
50LM730/0.45	39.8	5.0	11

Table 2.3: The maximum angle of subgrain boundaries (MASGB) and factors a and b of Eqn. (2.8) for five calcite samples.

The *LI-CH* is an alternative, new method, which could be useful for measuring the size of subgrains for misorientation intervals rather than cumulative misorientation angles, and for samples having a well developed substructure for all misorientation angles. Care should be taken as this method is particularly sensitive to errors caused by measuring on grid based maps.

The *LI-MH* curve of the domain size versus misorientation angle can be described by an exponential equation of the type: $LI\text{-}MH(\theta) = a\,[1 - \exp(\theta/b)]$. The factor a can be used as a measure of the grain size, while the factor b is dependent on the existing size hierarchy of subgrains and on the relative frequency of low angle versus high angle misorientations and strained versus strain free area. We also define the maximum angle of subgrain boundaries (MASGB) as the minimum angle for which the derivative of the hierarchy equation is below the standard error of the domain size measurements (~1 µm). The factors a, b and the MASGB are related to the relative amount of subgrain rotation, grain boundary migration and recrystallisation, which suggests that these parameters could be used as indicators of deformation conditions. The single *LI-MH* values for a specific minimum misorientation angle are averages of the sizes of three different types of subgrains: mantle subgrains, core subgrains and subgrain bands extending through the whole grain. This average lies close to the mantle subgrain size because of the high frequency of these mantle

subgrains in our material.

Acknowledgements

This manuscript has largely benefited from the useful comments of J. Wheeler and an anonymous reviewer. This study forms part of a project funded by the NWO council. Electron microscopy was conducted at Electron Microscopy Utrecht (EMU). The authors would like to thank J.H. Ter Heege for providing the calcite samples.

3

Measuring and distinguishing heterogeneous microstructures in deformed calcite using electron backscattered diffraction

Part of this chapter has been published as:
Valcke, S. L. A., Drury, M. R., De Bresser, J. H. P. & Pennock, G. M. 2007. Quantifying heterogeneous microstructures: core and mantle subgrains in deformed calcite. Materials Science Forum 550, 307-312.

Abstract

Rocks deformed at high temperature develop a microstructure that is related to the deformation conditions. In order to infer palaeo-deformation conditions from microstructures in natural rocks, calibrated relationships are needed between specific microstructures and stress, strain or temperature. A first step in establishing these relationships is finding methods to accurately quantify the microstructures. We have chosen to use electron backscattered diffraction (EBSD) because this method provides statistically significant datasets with quantitative information on the subgrain size and the subgrain misorientation. However, EBSD has angular and spatial resolution limits related to low angle misorientation noise and charging. Also, apart from these inherent problems with EBSD, there are issues related to the microstructure itself as it is heterogeneous in high temperature deformed calcite and therefore not straightforward to measure. The microstructure consists of recrystallised and deformed grains and the latter contain small subgrains at grain boundaries (mantle subgrains) and relatively large subgrains in the core of grains (core subgrains). These different microstructural parameters may be related in different ways to deformation conditions and therefore it is important to study them separately. In this chapter, a method is suggested to reduce the low angle misorientation noise and the effect of charging on size measurements is discussed. Furthermore, a method is demonstrated to distinguish between the different types of grains and subgrains and to measure their sizes separately.

3.1 Introduction

In rocks deforming at high temperature by crystal plastic mechanisms, a substructure of subgrain walls and dislocations develops in the crystals (Poirier, 1985). Various elements of the substructure are useful as indicators of deformation mechanisms and conditions in the Earth (Mercier *et al.*, 1977; Post Jr., 1977; Twiss, 1977; White, 1979; Poirier, 1985; Kenkmann & Dresen, 2002). In particular, the sizes of recrystallised grains and subgrains depend on stress. Therefore, they could be used as an indicator of the stress in the geological past ('palaeostress') if a calibrated size-stress relationship ('palaeopiezometer') is available for the relevant rock type. To measure grain and subgrain sizes, several techniques are available, such as light microscopy, decoration techniques, transmission electron microscopy (TEM) and electron backscattered diffraction (EBSD). EBSD appears to be the best option as it allows fast automated analysis such that statistically meaningful datasets for many samples can be obtained, which is more time consuming and difficult using TEM or light microscopy (Valcke et al., 2006). However, despite the advantages of EBSD, it remains important to reassess the method for each material type because the spatial and angular resolution can vary depending on the microscope conditions and materials (Humphreys, 1999; Prior, 1999; Humphreys *et al.*, 2001). In this chapter, spatial and angular resolution, orientation filter processing and errors will be discussed particularly for measuring sizes of grain and subgrains in marble.

Carrara marble (calcite) was chosen as the study material because it is relatively easy and reliable to deform, such that a large dataset can be generated in order to calibrate relationships between microstructure and deformation conditions. The deformed calcite samples in this study show a heterogeneous microstructure, containing recrystallised and deformed grains, and core and mantle subgrains. Schmid et al. (1980) also observed this microstructural heterogeneity in Carrara marble, but they did not measure each structure. They measured the recrystallised grain size using light microscopy and found that the recrystallised grain size is inversely proportional to stress. They suggested that the piezometric relation for recrystallised grains also can be applied to (mantle) subgrains, as these seem to be similar in size as the recrystallised grains. However, they did not quantify this similarity between mantle subgrains and recrystallised grains and their limited transmission electron microscope (TEM) measurements suggest that subgrains exist which are much smaller than the recrystallised grains. Furthermore, Schmid et al. (1980) noticed that the core subgrains are highly variable in size and do not show an obvious dependence on stress, but this was not quantified. These issues indicate that a better quantification and understanding of the relationship between the different types of microstructures and deformation conditions must be obtained before size-stress relations for calcite can be reliably applied to nature. In this chapter, we therefore aim to develop a method using EBSD to separate the recrystallised grains from the deformed grains and within the latter, the core from mantle subgrains and consequently to accurately quantify their size.

3.2 Materials and method

The marble investigated in this study comes from a block of Carrara marble ('Lorano Bianco' type) that is selected as a laboratory standard for deformation experiments on marble (Ter Heege *et al.*, 2002). The samples were deformed by uniaxial compression to natural

sample	*a* [µm]	*b* [°]	MASGB [°]
36LM830/0.15	75.8	2.5	9
36LM830/0.30	58.8	4.9	13
36LM830/0.45	39.7	5.3	11
50LM830/0.45	37.5	3.2	8
50LM730/0.45	39.8	5.0	11

Table 3.1: Deformation conditions for the samples used in this study as an illustration of the technique.

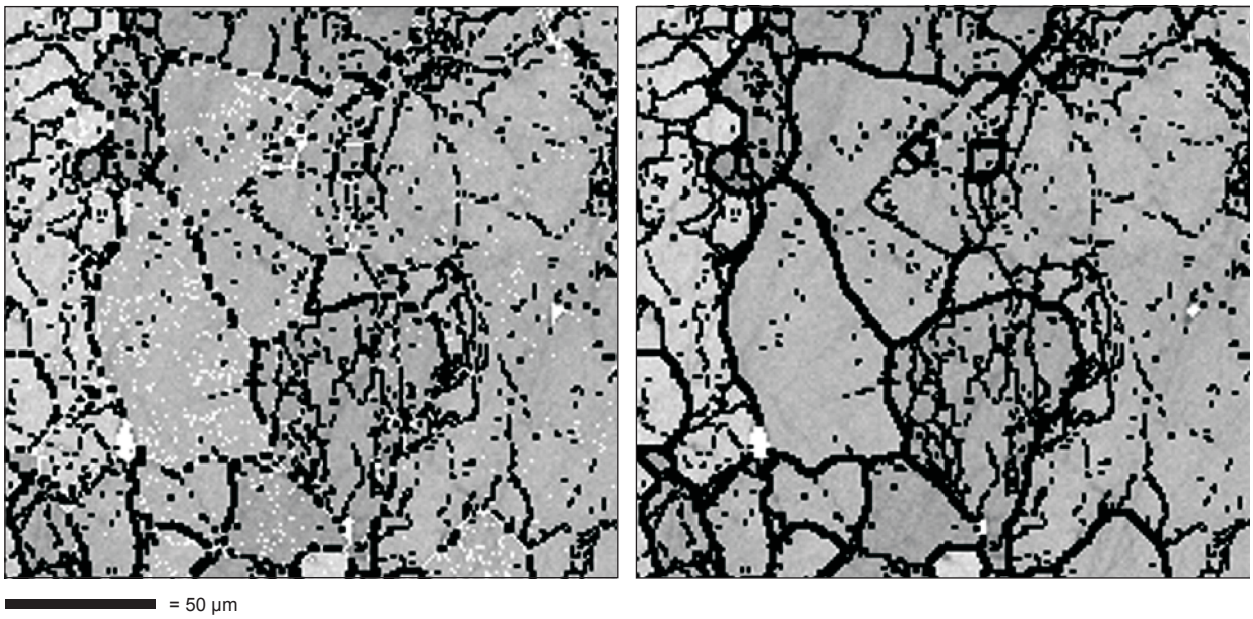

Fig. 3.1: Detail of an EBSD map (1 µm step) of 25LM900/0.45, before (left image) and after (right image) applying an automatic extrapolation routine for removing non-indexed and misindexed pixels. The grey scale corresponds to the EBSD pattern quality (lighter grey is better quality), the thick black lines are boundaries >10° and the thin black lines are boundaries >1°. Non-indexed pixels are indicated in white.

strains of 0.15-0.45 at final strain rates of 3.0 x 10^{-6} to 4.9 x 10^{-4}, temperatures of 700-990°C, which resulted in flow stresses from 15-85 MPa. The few samples of this dataset considered in this chapter only serve as an illustration of the technique (Table 3.1) and experimental details are given more extensively in chapters 4, 5 and 6 (See also Ter Heege *et al.*, 2002).

The deformed samples were sectioned parallel to the maximum compression direction to make polished blocks for EBSD (Valcke *et al.*, 2006 and Chapter 2). EBSD data have been collected and analysed using Channel 5 software (Oxford Instruments HKL Technology) with service pack 9, on a FEI XL30SFEG scanning electron microscope (SEM) with a Nordlys 2 CCD camera (Oxford Instruments HKL Technology). From grid based EBSD analyses, orientation maps were constructed and misorientations between each pixel were calculated

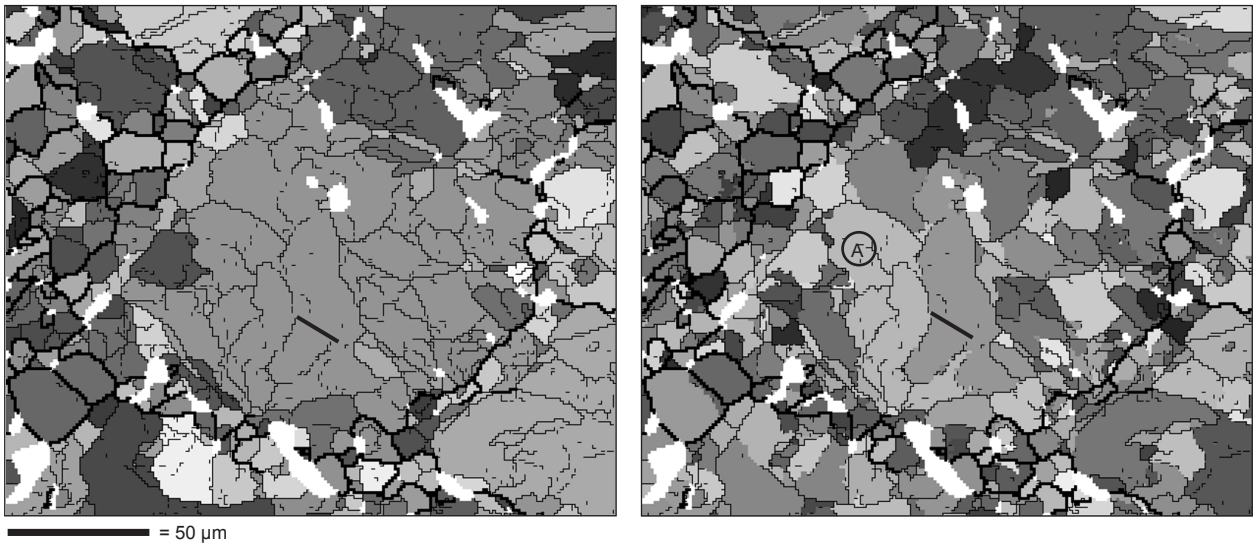

Fig. 3.2: Detail of an EBSD map (1 µm step) of 36LM830/0.45, showing the same area but with different domain detection conditions. The thick black lines are grain boundaries >10°; the thin black lines are subgrain boundaries >1°. The domains are randomly coloured in gray scale, i.e., each domain has a different grey colour, so it can be seen which entities are detected as separate domains. (a) Domain detection for θ_{min}=1° and no closure of boundaries. (b) Domain detection for θ_{min}=1° and θ_c=0.5°. In (b) more and smaller domains are detected (for example, see arrow). The subgrain indicated by 'A' contains subgrain boundaries inside.

(e.g., Schwartz *et al.*, 2000). This allowed identification of boundaries with different misorientation angles and measurement of subgrain sizes as a function of the misorientation angle of the subgrain boundaries. Maps of 1µm step size for a grid of 1000 x 1000 appeared to be a good compromise to obtain a reasonable variation of grain orientations (~ 100 grains) within a feasible time span of automated analysis (~36 hours) (Valcke *et al.*, 2006). The percentage of successfully indexed points was typically larger than 90%, and this was improved to > 97% with commercial software that replaces these non-indexed points using the orientation of (at least 6) neighbouring pixels. Isolated, individual misindexed pixels (i.e., spikes) were also similarly replaced. In Figure 3.1 an example of an EBSD map is shown before and after the extrapolation routine. After the extrapolation routine, there are fewer non-indexed single pixels and the boundaries are better connected (Fig. 3.1).

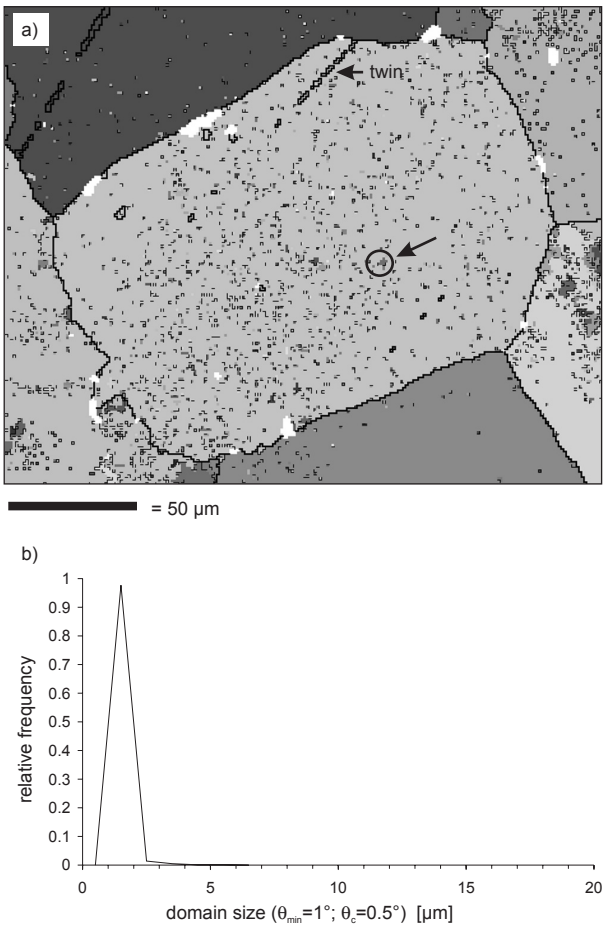

Fig. 3.3: EBSD analysis (1 µm step) of a grain in undeformed starting material. Non-indexed and misindexed pixels have been removed but no orientation filtering has been applied. Domain detection has been applied for θ_{min} = 1° and θ_c = 0.5°. a) EBSD map: the thick black lines are grain boundaries >10°; the thin black lines are subgrain boundaries >1°. The domains are randomly coloured in grey scale. Pixel size domains (see for example, arrow) are detected as artificial subgrains due to low misorientation noise. Twins occur as high angle grain boundaries, but they are not detected as grains. b) Domain size distribution for the area shown in a). The peak at small sizes is related to the angular resolution limit (≤ 1°) of the EBSD technique and the frequency of the subgrain misorientations (2°- 10°) is very low.

To detect and measure grains and subgrains automatically, the domain boundary method was used. This method is based on determining domains (grains, subgrains) surrounded by boundaries having misorientations larger than a minimum misorientation angle θ_{min} (Trimby *et al.*, 1998). The size of a domain is then represented by means of the equivalent circular diameter (ECD) of the domain area. To measure subgrain sizes, the domain boundary method is chosen rather than the linear intercept boundary method (Valcke *et al.*, 2006), because of two reasons:

(1) Recently, commercial software has become available, which makes it possible to include a lower closure angle (called θ_c) in the domain boundary method. Boundaries larger than θ_{min} are first detected and then 'closed' along misorientation angles smaller than θ_{min}, but larger than θ_c (and $\theta_c < \theta_{min}$). Previously, some domains were not detected when small sections of the boundary were below θ_{min} and therefore did not form an entirely 'closed' domain (Fig. 3.2a) (Wheeler *et al.*, 2003; Valcke *et al.*, 2006 and chapter 2). Now, using θ_c, many more subgrains are surrounded by closed boundary loops and can be detected as domains (Fig. 3.2b);

(2) In this study, we are specifically interested in measuring small subgrains with low misorientation angles, in contrast to measuring domain hierarchies extending to high angle boundaries, for which a linear intercept method would be more appropriate (Valcke *et al.*, 2006).

3.3 Angular resolution

3.3.1 Methods to improve angular resolution

Angular resolution limits the lowest subgrain misorientation angles that can be resolved. The angular resolution is determined by the amount of low angle random misorientations near the detection limit of the microscope, which are not associated with structure. These low angle misorientations are called 'noise'. In calcite, angles smaller than ~1° typically contain a lot of noise so that real subgrain boundaries <1° are difficult to discriminate from this noise. To detect low angle subgrain boundaries, θ_{min} is taken >1° (~ resolution), but to close the boundaries, θ_c is <1°. In practice, we set θ_c = 0.5° for areas containing a lot of noise, e.g., the mantle near grain boundaries, and θ_c = 0° in areas with less noise, e.g., the core of grains (see paragraph 3.5.2). Therefore, it is important to reduce the very low angle noise <1° as much as possible without introducing artefacts. Methods to reduce these artificial low angle misorientations in EBSD mapped data are called orientation filter methods.

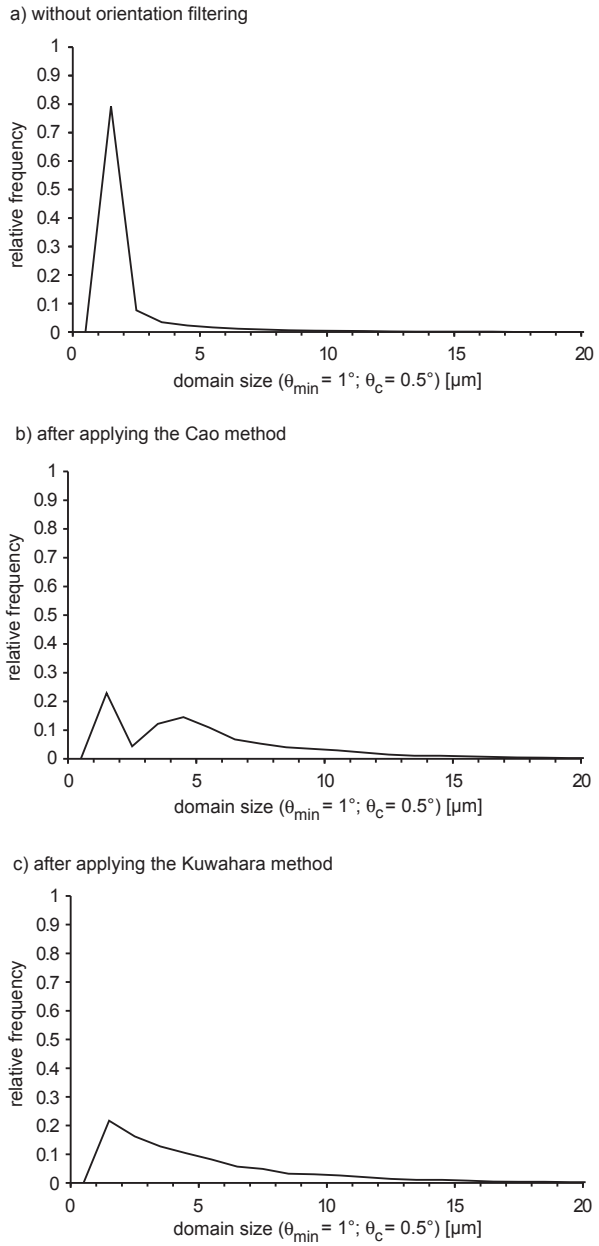

Fig. 3.4: a) Unimodal, skewed size distribution showing the relative frequency versus domain size (θ_{min}=1°; θ_c=0.5°) in sample 36LM830/0.45 before applying a filtering method. b) Bimodal size distribution for domains (θ_{min}=1°; θ_c=0.5°) in the same sample as in a), but after applying the noise reduction method of Cao et al. (2003). The peak at very small sizes is related to remaining noise after applying the filtering method, while the distribution at higher sizes is of the subgrain sizes. c) Size distribution for domains (θ_{min}=1°; θ_c=0.5°) after applying the Kuwahara method in the same sample as in a).

Currently, the most commonly used filter methods are a Cao et al. (2003) type method, or a type of orientation averaging such as the method of Humphreys et al. (2001), which is based on the Kuwahara filter (Kuwahara & Eiho, 1976). Below, both filter methods are explained and a comparison of both methods is made.

The method of Cao et al. (2003), henceforth called the Cao method, is based on the observation that many of the low angle misorientations, which arise from orientation noise in the data, form artificial boundaries that have a length of only a few pixels (where a pixel is equivalent to the map step size) and these short boundaries can surround pixel sized domains. Cao et al. (2003) selected a subset of all domains with areas smaller than 4 pixels, to subsequently include them into their larger neighbouring cells. In this study, we chose to exclude all domains (clusters) smaller than 7 pixels, which are domains with an equivalent circular diameter smaller than 3 µm. The choice of excluding low angle domains with an area smaller than 7 pixels rather than 4 pixels as suggested by Cao et al. (2003), was made because a lot of low angle (~1°) isolated misorientations, not related to orientation differences in the substructure, still remained after removing only clusters smaller than 4 pixels. The fact that domains smaller than 7 pixels (i.e., < 3 µm) are related to noise rather than real orientation differences, is confirmed by an EBSD analysis of undeformed material, in which only a few or no subgrains are expected. However, in practice, the EBSD map shows many isolated, pixel size low angle misorientations and the domain size distribution shows a significant peak at 1-2µm, which decreases around 3µm (Fig. 3.3). This indicates that noise related domains typically have sizes smaller than 3µm.

In Figure 3.4a, the domain size distribution for very low misorientation angles is shown (θ_{min} = 1°; θ_c = 0.5°) for a deformed sample without applying an orientation filter. The distribution is skewed towards very small sizes and is similar to the distribution of the undeformed material (Fig. 3.3b), except that the tail of the distribution in the deformed material ends at higher size values. This is the result of the combined effect of noise and the existence of real subgrains, which mostly have larger sizes than 3 µm.

The details of the Cao method are as follows: first, domains are detected for θ_{min} = 1° and θ_c = 0°, then domains smaller than 3µm are replaced with a non-indexed value, or 'zero solution'. Subsequently, an automated extrapolation routine is applied to fill in the zero solution pixels with a neighbouring orientation. Then the subgrains are measured for θ_{min} = 1° and θ_c = 0.5°. Figure 3.4b shows the low angle distribution after filtering using the Cao method. Although the automated extrapolation routine can have created some new artificial misorientations, the noise peak is significantly reduced, resulting in a bimodal distribution with a much reduced low angle noise peak at ~2 µm and a clearly distinguishable, second peak showing the distribution of subgrains >3 µm (compare Fig. 3.4a and 3.4b). The domains <3 µm that remain after orientation filtering, are ignored by setting a minimum size of 3µm when determining the average

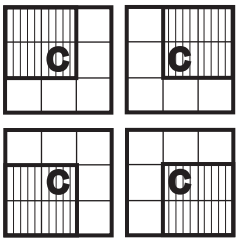

Fig. 3.5: Example of a filter window, showing four sub-blocks around a central pixel: the misorientation of the central pixel is calculated using every pixel in the 4 sub-blocks (see text, 3.3.1)

size for the (sub-) grains. This has the consequence that the resolution of the 1µm step maps is now 3µm instead of 1µm.

The orientation averaging method of Humphreys et al. (2001) is a modification of the Kuwahara filter (Kuwahara & Eiho, 1976), which smoothes the data whilst preserving boundaries. This filter improves the angular accuracy at the expense of the spatial resolution. The filter size (n x n) determines the height and width of the averaging filter window (Fig. 3.5). This window is divided into four sub-blocks, where the orientation of the central pixel is calculated using every pixel in the sub-blocks. The central pixel is given the value of the mean orientation of the sub-block that has the lowest overall internal misorientation. For a filter size of 3x3 (used in Figs. 3.5-3.7), the orientation error is reduced, and the spatial resolution decreases by a factor of ~3. Thus, the angular resolution becomes 0.3° instead of 1°, while the spatial resolution becomes 3µm instead of 1µm. Pixels with misorientations to the central pixel that are higher than the smoothing angle (~1° in the examples used here), are not allowed to contribute during the filter operation. The noise peak is significantly reduced after applying the Kuwahara filter (compare Fig. 3.4a and 3.4c). The noise peak has a similar height as after applying the Cao method, which means that a similar amount of noise is removed using both filters (compare Fig. 3.4b and 3.4c). The Kuwahara filter method only works if there is a homogeneous distribution of local orientations and there are no orientation gradients (see below).

3.3.2 Influence of filtering on the microstructure

In some of our samples, grains with very few subgrain boundaries show orientation gradients. An orientation gradient is a gradual change in orientation within the grain. Such a gradual change is seen by diffuse changes of grey shade in a concentric pattern in forescatter images (Fig. 3.6a) or on EBSD maps, by concentrations of low angle isolated ‘boundaries’, having a length of only a few pixels (~1µm), so not forming a real continuous

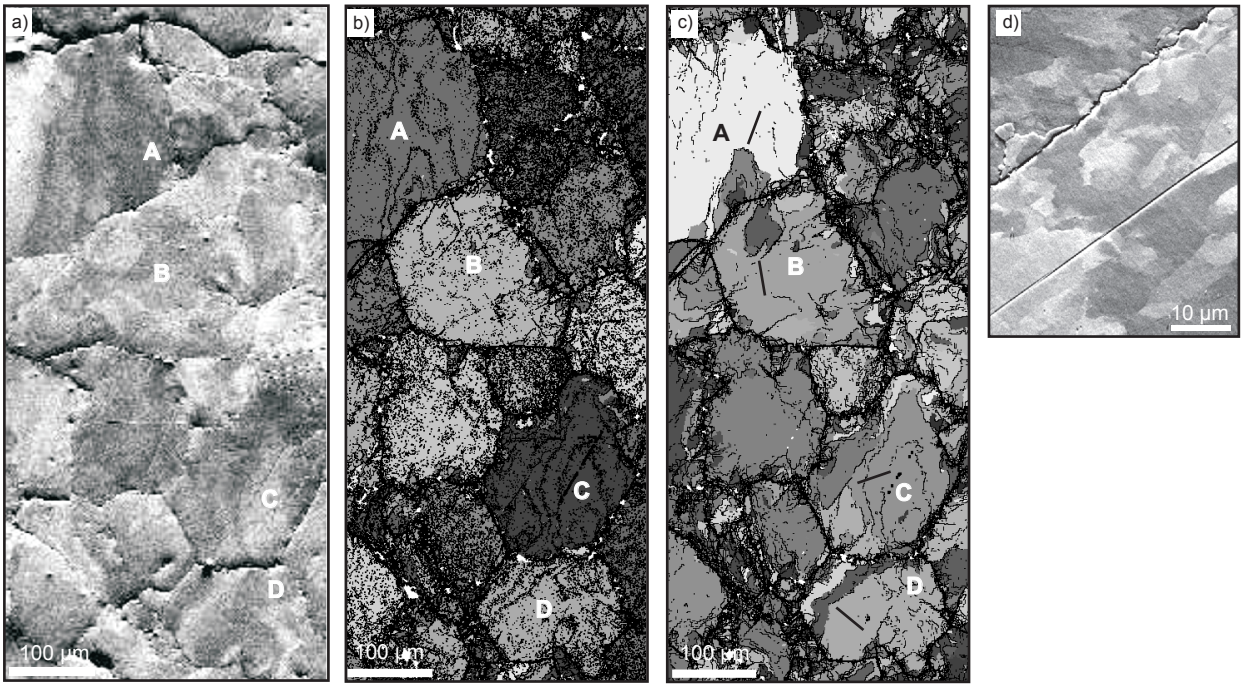

Fig. 3.6: Images to illustrate the Cao and Kuwahara filter methods. a), b) and c) are images from sample 85LM730/0.15, while d) is from sample 36LM830/0.45. Grains A, B, C and D in images a), b) and c) show an orientation gradient. a) Forescatter (FS) image showing orientation contrast in grey shades of the area analysed by EBSD in b) and c). b) and c) are EBSD maps that have been processed using the Cao method and the Kuwahara filter respectively. Misorientation boundaries >0.5° are indicated in thin black lines, misorientations >10° in thick black lines. The different shades of grey indicate individual domains that have been detected (θ_{min}=1°; θ_c=0°). The Kuwahara method creates distinct subgrains in the grains that contain orientation gradients (see arrows), while the Cao method leaves diffuse misorientation gradients, but does not create subgrain boundaries. d) FS image showing the typical appearance of subgrains (grey shade).

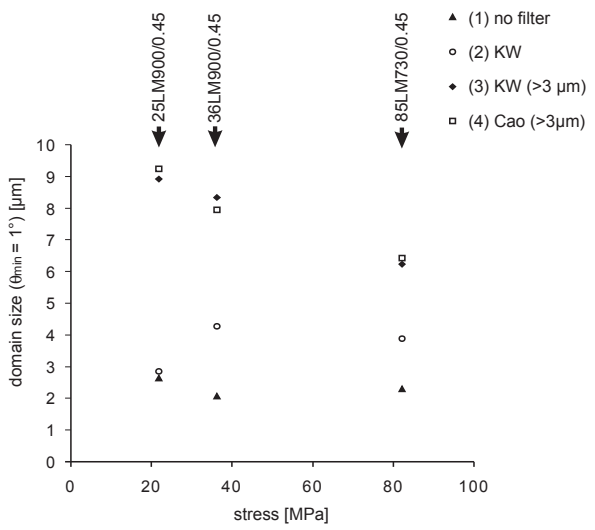

Fig. 3.7: Graph showing the average domain size (θ_{min} = 1°) as a function of stress for three samples (25LM900/0.45, 36LM900/0.45, 85LM730/0.45) after different processing: (1) only non-indexed and mis-indexed pixels have been removed but no orientation filtering was applied, (2) the Kuwahara (KW) filter method was applied, (3) the Kuwahara filter was applied and domains < 3 µm were removed and (4) the Cao method was applied (domains >3 µm).

boundary that encloses a subgrain (Fig. 3.6b). In light microscopy, undulose extinction shows that these gradients are a real microstructure as a result of bending of the grain rather than a polishing artifact. This structure occurs in very low strain samples and also in the starting material. In contrast to orientation gradients with gradual changes in orientation, subgrain boundaries have more abrupt, sharp changes in orientation, seen by the grey shades on forescatter images (Fig. 3.6d). Subgrain boundaries do not appear as concentric boundaries but rather as a network of distinct changes in grey scale.

Filtering methods can modify the diffuse boundary structure of orientation gradients into sharp boundaries and consequently they could be misinterpreted as subgrains. The size of such artifact subgrains would depend on the magnitude of the orientation gradient and the parameters of the filter. When applying the Kuwahara filter method, the number of isolated, short, low angle misorientation boundaries reduces significantly, but the dense concentrations of pixel size boundaries related to orientation gradients can become sharply defined low angle continuous boundaries. Consequently, detecting low angle domains (θ_{min} = 1° and θ_c = 0°) results in artificial, concentric subgrains that arise from a gradient in orientation when EBSD maps are processed using the Kuwahara filter to improve the angular resolution (Fig 3.6c). The Cao method does not alter orientation gradients into artificial subgrain boundaries; the orientation gradients are still visible by the dense zones of short, low angle boundaries, but they are not recognized as closed boundaries surrounding domains (Fig. 3.6b). As this study is concerned with measuring subgrain sizes, the Cao method is chosen as the appropriate filter for reducing the pixel size, low angle misorientation domains related to noise without introducing artifacts related to orientation gradients.

3.3.3 Influence of filtering on the subgrain size

Because the reason for measuring (sub)grain sizes in deformed calcite is to study the effect of deformation conditions such as stress on the subgrain size (see chapters 4, 5 and 6), the filtering methods are compared for their effect on the relationship between subgrain size and stress (Fig. 3.7) (25 MPa, 36 MPa and 85 MPa). Without filtering, the data are dominated by noise, which hinders reliable size measurements. For example, the average domain sizes measured on the three unfiltered maps are all similar, ~ 2 µm (Fig. 3.7), which reflects the contribution of noise that has a peak value at 2 µm. Because of this, possible differences with stress from sample to sample cannot be resolved. Subsequently, the maps have been filtered using the Kuwahara method and the Cao method. Because in the Cao method all sizes below 3 µm are ignored and because the Kuwahara filter reduced the spatial resolution from 1 to 3 µm (see above), it was necessary to exclude the sizes smaller than 3µm for the Kuwahara filtered data. The Kuwahara filter method and the Cao method result in average sizes that are similar and systematically decrease with increasing stress (Fig. 3.7). It is reassuring that both filtering methods result in very similar sizes per sample and it confirms that both filtering methods succeed in removing noise related pixel size domains such that possible trends with stress are no longer concealed by noise. Even though the filtering methods result in similar average sizes, we have applied the Cao method rather than the Kuwahara filter because the latter is unreliable as it creates subgrains related to orientation gradients (paragraph 3.3.2). In summary, the minimum misorientation angles that can be resolved without introducing too much noise, after using a filtering method, are ~1°. The filtering methods limit the smallest sizes that can be measured to 3 µm. Because filtering techniques have a dramatic effect on the domain size, it is essential that data sets are processed in the same way when determining trends.

3.4 Spatial resolution and errors

Above, the angular resolution was improved by using the Cao method. However, this method limits the spatial resolution, i.e., the smallest size that can be measured, to 3 µm. The spatial resolution is also influenced by spatial errors, i.e., errors related to size measurements on grids. These types of errors are discussed in this paragraph. The

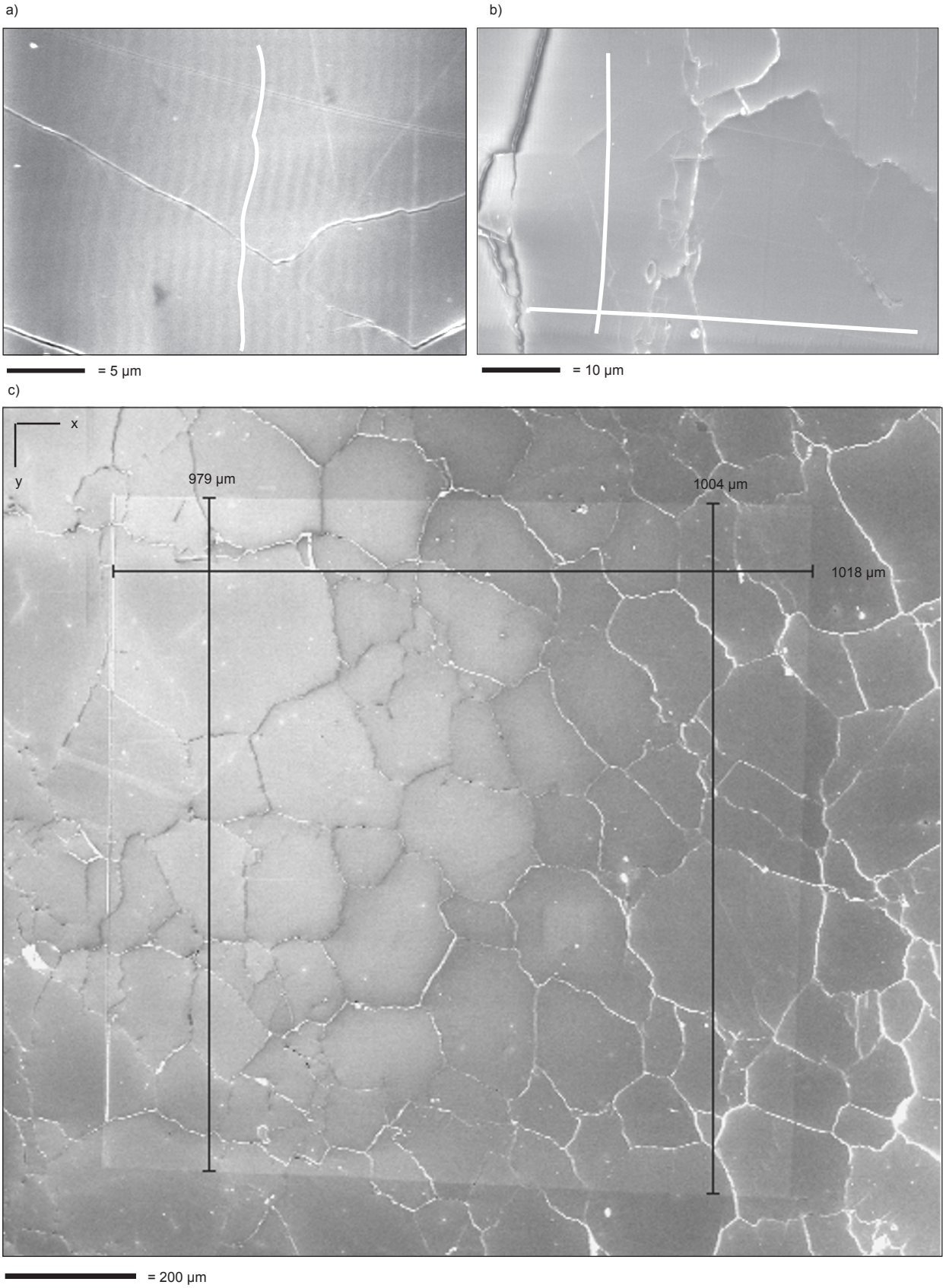

Fig. 3.8: SEM images showing examples of the beam drift (deflection) problem due to a slow charge build up in sample 85LM730/0.45 (untilted). In a) the mapped scanning lines are irregular, for clarity one of the lines is indicated in white. In b) the bending of the horizontal lines causes an increase in the lengths in the Y-direction (see also white line). In c) the total x and y-lengths of a 1000 x 1000 µm map are measured. The grid is not orthogonal and not exactly 1000 x 1000 µm, due to the drift caused by charge build up during mapping. The x-axis is horizontal and y-axis vertical on all images.

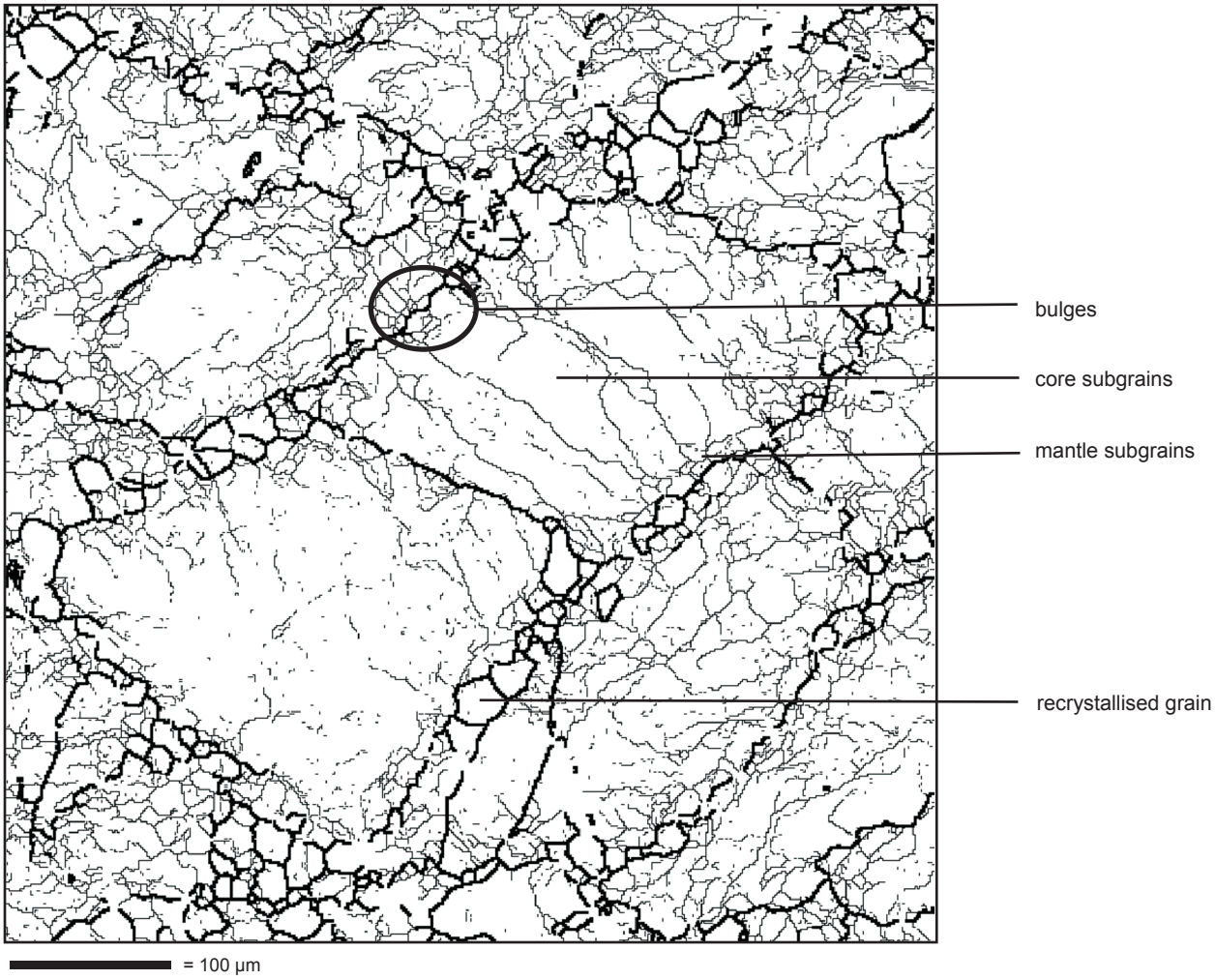

Fig. 3.9: Detail of EBSD map on 36LM830/0.45 to illustrate the heterogeneity of the microstructure. Misorientations >10° are shown in thick black lines, misorientations >1° in thin black lines. The different microstructures are indicated on the figure.

main source of errors in the accuracy of the grid is a slow charge accumulation on the specimen surface, causing a deflection of the beam (Fig. 3.8a & b). Charge accumulation on a poor conductor, such as polycrystalline calcite, cannot be totally avoided. This is mainly because a thicker carbon coating, which would reduce the charging, dramatically reduces the quality of EBSD patterns and therefore was not applied. The charge build up is gradual and causes a small beam deflection. This charging effect is not visible when doing manual measurements, as the image of the sample and the diffraction patterns appear stable. The drift caused by charging only becomes obvious by measuring the effective size of the scanned map on the sample in an untilted 'flat' position. In the untilted configuration, the scanned area is visible from the small amount of beam damage and contamination that occurs at each grid point on the sample surface and in this position accurate measurements of the scanned area can be made (Fig. 3.8). The scanned area should be 1000x1000 µm, but the length in the X-direction was often around 1050 µm and in the Y-direction the map length varies on different samples from 950 to 1000 µm (related to charging) (Fig. 3.8c). The non-orthogonal shape of the scanned area is thought to be related to the local deflections of the beam, as evidenced by the wavy grid lines. The variations are different for each individual mapped area and are sometimes localized. Another cause of small errors in the map size is the configuration of EBSD measurements, which require a sample surface tilt at 70°. This results in a foreshortened image, which is corrected by applying an electronic tilt correction that stretches the image. This tilt correction has introduced additional errors due to calibration problems with the software.

Because of both sources of errors, i.e., localized charging and calibration errors, the measurements cannot be corrected with a single correction factor. However, the error can be estimated for the whole map length by comparing the map length entered for the automated analysis (1000 µm) with the effectively measured length (950-1050 µm), i.e., 5 % difference. So a maximum error of 5% on the size measurements should be taken into

account.

3.5 Separation of heterogeneous microstructures

EBSD maps show that the microstructure in calcite is very heterogeneous (Fig. 3.9): there are grains showing no substructure, grains containing subgrains and there are small subgrains at grain boundaries, sometimes forming part of a grain boundary bulge, while there are large subgrains in the grain interiors. All these different microstructures possibly have different relationships with the deformation conditions. For example, it is reported that recrystallised grain sizes have an inverse relationship with stress (e.g., Twiss, 1977), while the deformed, relict grain sizes are related rather to strain than to stress (Chapter 4). Schmid *et al.* (1980) have suggested that subgrains near grain boundaries have similar sizes as the recrystallised grains and are dependent on stress, while subgrains in the grain interiors are not obviously related to stress. Because of these varying relations between stress and microstructures, it is necessary to separate the microstructures before determining their average sizes. Methods to separate recrystallised grains, deformed grains, mantle subgrains, core subgrains and bulges are described below.

3.5.1 Recrystallised and deformed grains

The samples in this study have dynamically recrystallised during deformation. In deformed materials, grains might have a complex (multi-cycle) history, being recrystallised and consequently deformed again, but we focus on the structure developed in the last stage of deformation. Henceforth, grains without any subgrains are defined as recrystallised grains, while grains containing subgrains are considered as deformed grains, even though they might already have undergone recrystallisation in an earlier stage. In this paragraph, a method is given how to separate the recrystallised from the deformed grains. The domain method, used to detect individual domains surrounded by boundaries, involves a *minimum* misorientation angle (θ_{min}) to define e.g., subgrains. This has the disadvantage that high angle (>10°) recrystallised grains are included in the subgrain data when determining the subgrain size by setting e.g., θ_{min} = 1° (Valcke *et al.*, 2006). To avoid this, we have set up a method to distinguish between recrystallised and deformed grains, allowing measurement of subgrain sizes exclusively in deformed grains. The parameter used to distinguish between the recrystallised and the deformed grain fraction is the average misorientation within a grain (AMG). This is a parameter in the Channel 5 software (Oxford Instruments HKL Technology), which is the average of misorientations between *randomly chosen* pixels (1000 pairs) within a grain. This is similar to the method used by McCabe and Teter (2006), except that they defined the grain average misorientation as being the average of misorientations between *neighbouring* pixels within a grain. Both methods can be used because the averages are linearly related to each other (Fig. 3.10). Ideally, a recrystallised grain without subgrains has no internal misorientation and therefore has an AMG value of zero. However, some random low angle misorientation noise remains even after orientation filtering, so that in reality the AMG for a recrystallised grain is rarely zero. Still, the AMG of a recrystallised grain will be typically smaller than ~1° and therefore the cut off AMG that distinguishes a recrystallised grain from a deformed grain is chosen to be 1°. Grains were first determined by defining domains having θ_{min} = 10° and θ_c = 0.5°. From these grains the AMG is determined and recrystallised grains are separated by setting the AMG < 1° (see Fig. 3.11 - Appendix A).

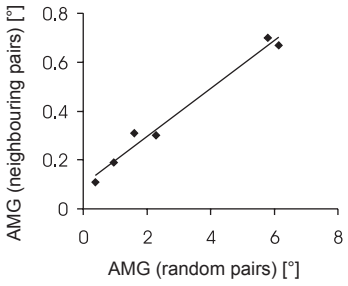

Fig. 3.10: Graph showing the average misorientation within a grain (AMG) determined between randomly chosen pairs of pixels (this study) and the average misorientation within a grain (AMG) determined between neighbouring pixels (McCabe & Teter, 2006) for six grains in sample 36LM830/0.45. The averages are linearly related to each other.

3.5.2 Core and mantle subgrains

Mantle subgrains are small subgrains that concentrate around the grain boundaries, forming a necklace around the core (Fig. 3.9). Core subgrains occur more in the centre of the grains and are usually larger than the mantle subgrains (Fig. 3.9). Even though there is a size difference between the mantle and core subgrains, this is not reflected in a bimodal size distribution. Rather, the size distribution is skewed towards the small subgrain sizes as there are many more mantle subgrains than core subgrains. This means that it is hard to separate core and mantle subgrains based on their size differences. Core subgrains with boundaries above 1° typically contain internal subgrain boundaries having misorientations of 1° or lower (Fig. 3.2b and Fig. 3.9), while the small mantle subgrains (>1°) do not have lower angle misorientations inside. This difference in internal substructure of mantle versus core subgrains is a useful quantitative criterion to distinguish core from mantle subgrains. The average misorientation within a subgrain (AMS) can be used as a

parameter to describe the internal structure of a subgrain, similar to the AMG for grains. Because small, low angle mantle subgrains are free of substructure (comparable to recrystallised grains), the AMS of the mantle subgrains is typically below ~1°. In contrast, core subgrains often contain substructure, and the AMS is above ~1°. Consequently, mantle and core subgrains can be distinguished by their AMS.

So the method to define the core and mantle subsets is as follows. Firstly, all recrystallised grains are removed and a subset is created of only deformed grains (see paragraph 3.5.1). Secondly, domains are defined with θ_{min} = 1° and a closing angle, θ_c = 0.5°. Then, a separation of these domains is made based on the AMS: ≤ 1° for mantle subgrains and > 1° for core subgrains. The resulting subsets of mantle and core subgrains correlate well with the microstructure: subgrains with AMS ≤ 1° are typically small and concentrate around boundaries and therefore they are a good representation of mantle subgrains (Fig. 3.11 - Appendix A). Now having two subsets of mantle and core subgrains, their average size is measured separately as follows. For the lowest misorientation mantle subgrains, θ_{min}=1° and θ_c=0.5° are used for domain detection, as these domains seem to be the smallest entities that can be defined without introducing a significant amount of noise. Namely, because grain boundaries typically are zones that contain a lot of noise (Humphreys, 2001), θ_c could not be set lower than 0.5° for mantle subgrains. On the other hand, to measure the lowest misorientation core subgrains, domain detection was made setting θ_{min}= 1° and θ_c to 0°, rather than 0.5°, because the core of grains contained much less noise than the mantle and setting θ_c to 0° did not introduce many noise related domains. Using a different θ_c for core and mantle is justified as long as comparisons of subgrain sizes in different samples are made separately for the core and mantle. In other words core subgrain sizes cannot directly be compared with mantle subgrain sizes because they have been measured using different data processing.

3.5.3 Bulges

Bulges are in fact not a separate microstructure, they form part of a deformed grain and often a subgrain boundary closes off the bulge (Fig. 3.9). However, we are interested in measuring the size of bulges separately, as on the one hand, certain bulges are associated with mantle subgrains and on the other hand, bulges are often the precursors of recrystallised grains (see Chapter 4). Therefore, to understand the development of mantle subgrains and recrystallised grains and their relationship with stress, it is useful to investigate the size of the bulges.

Grain boundary bulges represent a deviation from an otherwise straight or slightly curved grain boundary (Tungatt & Humphreys, 1984; Drury *et al.*, 1985). Measuring the bulge size is done by fitting circles into the bulges (Fig. 3.12a - Appendix A). More specifically, three points on the curved grain boundary are fixed and a circle is drawn through these three points using an image analysis software program (Scandium software, Soft Imaging System, Germany). Then the area of this circle is calculated and this area divided by two, which is the half circle that fits the bulge. From this area, the equivalent circular diameter (ECD) is calculated, so that the bulge size measurements can be compared with the sizes of other microstructural entities, also expressed by an ECD. The transition from a bulge to a lobate grain boundary was made when the indent was larger than the diameter of the fitted circle (Fig. 3.12b - Appendix A). Large deviations in the grain boundary trace, creating lobate grain boundaries, were not included in the bulge measurements. When the indent was no more than a few microns, it was not considered as a bulge, because the spatial resolution of the EBSD maps is 3 μm (Fig. 3.12b - Appendix A). An example of the measurement of bulge sizes is given in Figure 3.12c.

3.6 Conclusions

This study has explored the application of electron backscattered diffraction (EBSD) to measure the sizes of microstructures in experimentally deformed Carrara marble. It was found that the angular resolution of the EBSD analyses can be improved using the Cao method (Cao *et al.*, 2003), which excludes small domains (< 3 μm) resulting from random low angle misorientations not related to the microstructure. Automated EBSD analysis of large 1000 x 1000 grids of 1 μm step size, suffers from a slow charge accumulation that causes minor electron beam deflections. The errors on size measurements as a consequence of this charge build up are maximum 5 %.

Experimentally deformed calcite (Carrara marble) has a heterogeneous microstructure consisting of recrystallised grains, deformed grains, and within the latter, core and mantle subgrains. In this study, recrystallised grains are defined as grains that are free of subgrains at the end of deformation. In practice, this means that their average internal misorientation (AMG) is below 1°, which can be used as a criterion to separate the recrystallised grains from the deformed grains, the latter having an AMG above 1°. The mantle subgrains are defined as small subgrains near the grain boundary that are free of internal lower angle subgrains. In other words, the average internal misorientation of a subgrain (AMS) in the mantle is below 1°. Based on this, they can be separated from the core subgrains that have their AMS above 1°. Bulge sizes are quantified on the basis of circles fitted to the bulge.

4

Influence of deformation conditions on the development of heterogeneous recrystallisation microstructures in experimentally deformed Carrara marble

Abstract

Recrystallised grains are potentially useful as indicators of palaeostress in naturally deformed rocks, provided well calibrated relationships exist between recrystallised grains and stress (palaeopiezometers). Rocks can exhibit microstructures that are heterogeneous, i.e., containing recrystallised and deformed grains and core and mantle subgrains. Previous studies on palaeopiezometers rarely take into account different types of heterogeneous microstructures, even though the observed differences of microstructures, depending on deformation conditions, might indicate that different recrystallisation mechanisms were active. This would suggest that different relations between recrystallised grain size and stress exist. Also the effects of temperature and strain are often ignored in palaeopiezometers, while theoretical models have suggested that these parameters could play a role. This study uses electron backscattered diffraction (EBSD) to accurately quantify the heterogeneous microstructures in experimentally deformed Carrara marble (flow stress 15-85 MPa; temperature 700-990 °C and natural strain 0.15-0.90). The sizes of bulges, recrystallised grains and deformed grains are measured separately and their changes with stress, strain and temperature are investigated. We show that, within the high temperature creep regime, the overall character of microstructures can vary depending on deformation conditions. In heterogeneous samples showing core-mantle microstructures, the bulges and recrystallised grains are independent of strain. The recrystallised grain and bulge size show an inverse stress dependency, which can be affected by temperature (especially at high stress). The bulge size – stress dependency is suggested to be related to pinning of grain boundaries by subgrain boundaries and/or differences in driving forces for migration. The recrystallised grain size – stress dependency is related to the stress dependency of the bulges, because the recrystallised grains nucleate at grain boundary bulges. The deformed grain size decreases with strain, due to ongoing recrystallisation and rotation of core subgrains with strain. The core subgrain rotation and therefore the deformed grain size reduction is slowed down at high temperatures.

4.1 Introduction

4.1.1 General

The deformation of coarse grained calcite rocks under high temperatures (more than half of the melting temperature) generally results in dynamic recrystallisation and grain size reduction. These processes may already be active at natural strains below 0.15. The microstructure that develops is usually heterogeneous, consisting of recrystallised and deformed grains, containing subgrains. The characteristics of the heterogeneous microstructure are the result of the specific conditions of deformation, e.g., stress and temperature, the amount of strain the material has undergone and the properties of the material, such as its anisotropy, second phase content etc. A good quantitative description of the various elements making up the microstructure can provide a useful tool to unravel the deformation and recrystallisation processes that were active in natural rocks, leading to estimates of the imposed (palaeo-) deformation conditions (e.g., Twiss, 1977; White, 1977; Christie *et al.*, 1980; Kohlstedt & Weathers, 1980; Ross *et al.*, 1980; Etheridge & Wilkie, 1981; Van der Wal *et al.*, 1993; Rutter, 1995; Ulrich *et al.*, 2006; Austin & Evans, 2007). In order to define reliable (palaeo-) deformation indicators, one should not only consider the common heterogeneous nature of the microstructures of rocks, but also take into full account the fact that deformation and recrystallisation processes can change with deformation conditions (e.g., Schmid *et al.*, 1980; Hirth & Tullis, 1992; Van der Wal *et al.*, 1993; Rutter, 1995; De Bresser *et al.*, 1998; Shimizu, 1998; Stipp *et al.*, 2002; Ter Heege *et al.*, 2002; Humphreys & Hatherly, 2004). The latter aspect has not received much attention in previous work. Chapters 5 and 6 concentrate on subgrains in a heterogeneous microstructure, while here we focus on the characteristics of the recrystallised grains and the deformed grains. The ultimate goal is to formulate improved, reliable indicators of deformation conditions, in particular palaeopiezometers for calcite.

4.1.2 Definition of the various microstructural elements and recrystallisation mechanisms

Dynamic recrystallization is one of the processes by which a crystalline aggregate can lower its free energy during deformation (Urai *et al.*, 1986). Several definitions of the term have been proposed in the geological literature, differing in the inclusion of certain processes in the definition. Current use of the term can be best described as requiring the establishment of an array of grain boundaries in new material positions, in other words dynamic recrystallisation involves the formation and/or migration of grain boundaries (Vernon, 1981; Means, 1983; Urai *et al.*, 1986). Following this definition, recrystallised grains have new grain boundaries and/or contain strain free volumes with no lattice distortion. This general definition needs to be refined if one wants to objectively measure recrystallised grains (Humphreys & Hatherly, 2004 and Chapter 3). For the purpose of measuring recrystallised grains using EBSD, we considered a recrystallised grain as a grain containing no subgrains, while a deformed grain has an internal subgrain structure (Chapter 3). This is consistent with the definition metallurgists use for conventional dynamic recrystallisation, which involves the formation of new dislocation free grains in the deformed structure, which grow at the expense of old deformed grains (Doherty *et al.*, 1997). It

should be clarified that these definitions of recrystallised and deformed grains elucidate nothing about the process or history of recrystallisation of the grains. For instance, after deformation, a grain with no internal microstructure, could be a recrystallised grain or an old grain that was in a 'hard' orientation, such that it was difficult to deform and form subgrains. Likewise, a grain containing subgrains, so defined as a deformed grain, may have undergone several cycles of recrystallisation and subsequent deformation.

There are two basic types of dynamic recrystallisation mechanisms: 1) (subgrain) rotation (SGR), which involves the formation of new grain boundaries and 2) grain boundary migration, which involves the migration of existing grain boundaries (White, 1977; Haessner & Hoffmann, 1978; Drury & Urai, 1990). The first mechanism, SGR involves the progressive increase in misorientation of subgrain boundaries with strain, such that the grains divide into subgrains that eventually are so misoriented that they become individual grains (Hobbs, 1968; Poirier, 1985). This type of recrystallisation has been described in many geological materials: quartz (White, 1973), calcite (Schmid *et al.*, 1980; Rutter, 1995), NaCl (Guillopé & Poirier, 1979), $NaNO_3$ (Tungatt & Humphreys, 1981) and olivine (Poirier & Nicolas, 1975). The second mechanism, grain boundary migration recrystallisation (GBM), involves the migration of grain boundaries resulting in grain dissection, grain coalescence or the development of new grains from grain boundary bulges (Means, 1989). This process is driven by boundary surface energies and/or by the strain energy difference between relatively strain free and deformed regions (Poirier, 1985). Examples of GBM in geological materials include quartz (Jessel, 1987; Hirth & Tullis, 1992), NaCl (Guillopé & Poirier, 1979) and calcite (Rutter, 1995). It is very common in rocks for the two basic recrystallisation mechanisms to occur simultaneously, with one of the two being dominant (Drury & Urai, 1990; Hirth & Tullis, 1992). One recrystallisation mechanism that is often quoted to be a combination of the two basic mechanisms (SGR and GBM) is bulging recrystallisation (BLG) (Bailey & Hirsch, 1962; Drury *et al.*, 1985). In many cases of bulging recrystallisation, subgrain rotation occurs first, then a high angle grain boundary structure is built up and when the mobility of this boundary, proportional to the misorientation angle, is high enough, the boundary can move, i.e., migrate, and a new grain is formed (Drury *et al.*, 1985; Poirier, 1985). Alternatively, migration may occur first driven by strain energy differences and a bulge is formed before subgrain rotation separates the bulge from the old grain (Means, 1981; Tungatt & Humphreys, 1984; Urai *et al.*, 1986). Bulging recrystallisation has been well described for quartz (Hirth & Tullis, 1992; Stipp *et al.*, 2002) and feldspar (Tullis & Yund, 1985). Grain boundary bulges will be studied here as they are interesting microstructures that form the transitional link between subgrains and recrystallised grains.

In coarse grained materials such as Carrara marble, dynamic recrystallisation leads to reduction of the initial grain size by formation of new, small recrystallised grains at the expense of old grains (Schmid *et al.*, 1980; De Bresser *et al.*, 2001; Ulrich *et al.*, 2006). However, grain size reduction does not only happen by the creation of new, strain free grains, but can also occur due to subdivision of the old grains into smaller grains that are not strain free. This may happen by large core subgrains of which the boundaries, cross-cutting deformed grains, increase in misorientation (Fig. 4.1). Because these large core subgrains still contain smaller subgrains, the resulting 'new' grains, have a substructure, whereas subgrain rotation recrystallisation of individual subgrains creates new, strain free grains.

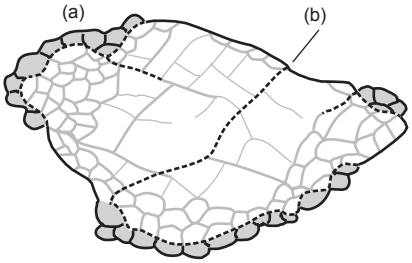

Fig. 4.1: schematic figure to illustrate the reduction of deformed grain size by (a) recrystallisation (formation of strain free grains) and (b) increase in misorientation of core subgrain boundaries to become grain boundaries. The thin grey lines are low angle subgrain boundaries, the thick grey lines high angle subgrain boundaries (<10°), the black full lines are original parts of old grain boundaries (>10°), while the dashed black lines are new grain boundaries (>10°).

4.1.3 The relationship between grain size and stress

Experimental work on various materials, metals as well as rocks, has demonstrated that high temperature creep generally results in grain size reduction by dynamic recrystallisation, with the average recrystallised grain size (d_X) being related to the flow stress (σ) by a relation of the type:

$$\frac{d_X}{b} = K_X \left(\frac{\mu}{\sigma} \right)^p \quad , \tag{4.1}$$

in which b is the Burgers vector, μ, the shear modulus. The parameters K_X and p (stress sensitivity) are variable, e.g., p, typically has values in the range 0.7-1.4 (Takeuchi & Argon, 1976; Mercier *et al.*, 1977; Twiss, 1977; Schmid *et al.*, 1980; Drury *et al.*, 1985; Van der Wal *et al.*, 1993; Stipp & Tullis, 2003). The existence of

such a relationship creates potential for using the recrystallised grain size for estimating the palaeostress of naturally deformed rocks (Weathers *et al.*, 1979; Avé Lallement, 1985; Hacker *et al.*, 1990; Stipp *et al.*, 2002). The empirically derived relationships can only be extrapolated to natural conditions in a meaningful way if they are underpinned by microphysical models that explain the relation between stress and recrystallised grain size and also the observed variations in the parameters, K_X and p. The most widely quoted theoretical model in the geological literature is the one of Twiss (1977), which is based on an equilibrium thermodynamic approach: it assumes that a unique recrystallised grain size exists at which the total strain energy of dislocations ordered in a grain boundary is equal to the stored energy of the dislocations in the enclosed volume. This model has been questioned because it incorrectly applies equilibrium thermodynamics to a dynamic, non-equilibrium process (Edward *et al.*, 1982; Poirier, 1985; Derby, 1990). In the models of Derby and Ashby (1987) and Shimizu (1998) a steady state average grain size is achieved by a dynamic balance between grain nucleation and grain growth events. The main differences between these two models are that (1) the stress sensitivity, p, in the Derby and Ashby model equals $n/2$, n being the creep law exponent, while p in the Shimizu model is a material independent constant and (2) the Derby and Ashby model assumes grain boundary bulging, while the Shimizu model assumes subgrain rotation as the main recrystallisation mechanism. Despite these differences, both models suggest a dependency of the recrystallised grain size – stress relation on the creep and recrystallisation mechanisms and also a slight temperature dependence of the parameter K_X. De Bresser et al. (1998; 2001) predicted similar results by advancing the hypothesis that dynamic recrystallisation results in a balance between grain size reduction and grain growth processes set up in the vicinity of the boundary between the grain size insensitive (GSI) and grain size sensitive (GSS) creep fields. Kellermann Slotemaker (2006) developed a model that describes the transient evolution of a polycrystalline material with a distributed grain size towards a dynamic recrystallised steady state including processes of nucleation and growth. The model predicts that the recrystallised grain size is not only dependent on stress but also on temperature and strain and with increasing strain, the recrystallised grain size – stress relationship evolves to the subgrain size – stress relationship. These theoretical models have raised new elements that can have an effect on the recrystallised grain – stress size relationship, namely, strain, temperature and recrystallisation mechanisms.

Our study material is experimentally deformed calcite. Considerable data on microstructures versus deformation conditions have been published for experimentally deformed calcite (Schmid *et al.*, 1980; Rutter, 1995; Ter Heege *et al.*, 2002). The reported relationship between stress and recrystallised grain size is similar in all studies, but there is controversy on the effect of temperature and strain. Schmid et al. (1980) and Rutter (1995) do not recognise an effect of temperature or strain on the recrystallised grain size. In contrast, Ter Heege et al. (2002) has reported an influence of strain and temperature on the grain size, but the observed trends are difficult to interpret because Ter Heege et al. (2002) considered the sizes of both deformed as well as recrystallised grains together.

4.1.4 Specific questions

The heterogeneity of microstructures consisting of subgrains, grain boundary bulges, recrystallised and deformed grains, and the existence of different recrystallisation mechanisms, such as grain boundary migration, subgrain rotation and bulging recrystallisation, are rarely taken into account when palaeopiezometric relationships are calibrated or applied. Moreover, the effect of temperature and strain on the recrystallised grain size - stress relation, predicted by theoretical models, should be verified experimentally. The general aim in this chapter is to investigate these issues in experimentally deformed calcite, in particular concentrating on bulges, recrystallised and deformed grains (subgrains are considered in Chapters 5 and 6). Even though deformed grains are not used for palaeopiezometry, they will be considered here, because their evolution with deformation gives extra information on the mechanisms involved in transforming original grains to recrystallised grains. The following specific questions will be addressed:

1) What are the quantitative relationships between the sizes of the different microstructural elements and the deformation conditions (strain, stress and temperature)? (paragraph 4.3)

2) What are the relationships between the different elements of the heterogeneous microstructure; for example, between recrystallised grains and grain boundary bulges? (paragraph 4.4.1)

3) How are the microstructural elements (recrystallised grains, grain boundary bulges, deformed grains) formed and can this explain the observed relationships between their average sizes and deformation conditions? (paragraphs 4.4.2 - 4.4.4)

4) Is the palaeopiezometric relationship between recrystallised grain size and stress valid for all types of microstructures and deformation conditions in Carrara marble? (paragraph 4.4.5)

The approach in this study is to use large automated

EBSD maps containing a few hundreds of grains for describing the microstructures and measuring the average size of the various microstructural elements at different deformation conditions.

4.2 Material and approach

4.2.1 Carrara marble

The samples in this study come from a block of 'undeformed' Carrara marble (Lorano Bianco type). This material is fully recrystallised, with an average grain size of 84 μm (measured using the same technique as for the deformed material – see below) and a very weak shape preferred orientation, meaning, the grains have an aspect ratio of 1.30 with the long axis of the grains at an angle of ~20° with respect to the sample axis (Ter Heege *et al.*, 2002). The marble consists of ~99 % calcite with a few grains of muscovite, quartz, dolomite and graphite (Pieri *et al.*, 2001). These second phase grains have not been observed on the EBSD scale (1 μm) in the samples used in this study. Cylindrical samples have been deformed in axial compression under a confining pressure of 300 MPa, to natural strains of 0.15-0.90 at strain rates of 3.0 x 10^{-6} to 4.9 x 10^{-4} s^{-1} and temperatures of 700-990 °C (0.5-0.7 T_m where T_m is the incongruent melting temperature of calcite in the system CaO-CO_2 at 100 MPa pressure – see Wyllie & Tuttle (1960)). Measured flow stresses range between 15-90 MPa (Ter Heege *et al.*, 2002 and this study) (Table 4.1). After the experiments, the samples have been rapidly cooled (ca. 70 °C/min) to limit post-deformation annealing. The stress strain curves in Carrara marble show a broad peak starting at a natural strain of ~ 0.10 and minor weakening (= ($\sigma_{\phi inal}$ – σ_{peak})/σ_{peak})*100%) up to 10% in the low temperature samples and up to 20% in the high temperature samples

sample name	peak stress [MPa]	final stress [MPa]	natural strain	temperature [°C]	deformed GS [μm]	N_D	recrystallised GS [μm]	N_X	bulge size [μm]
15LM950/0.45	24.9	14.6	0.45	962	84.7	57	37.2	80	-
25LM900/0.45	25.4	21.8	0.42	906	35.5	545	13.8	325	13.2
25LM950/0.45	24.8	24.8	0.45	950	61.3	60	10.0	44	10.4
25LM990/0.45	25.0	28.1	0.45	992	45.7	93	14.8	79	11.3
36LM830/0.15	38.5	36.7	0.17	829	69.4	77	11.5	50	10.4
36LM830/0.30	43.9	39.6	0.29	830	35.8	218	7.4	211	8.9
36LM830/0.45a	43.4	38.7	0.45	835	26.4	508	9.0	546	10.9
36LM830/0.45b	43.4	38.7	0.45	835	36.2	283	10.3	247	10.2
36LM900/0.15	37.4	34.1	0.16	903	68.3	83	8.3	61	9.7
36LM900/0.30a	35.6	32.9	0.27	901	58.4	65	7.0	38	10.1
36LM900/0.30b	35.6	32.9	0.27	901	46.8	49	14.8	56	10.4
36LM900/0.45	39.9	36.3	0.40	898	29.6	164	10.7	146	9.9
36LM900/0.90	33.9	26.2	0.90	902	21.7	854	9.6	672	10.1
36LM950/0.15	36.7	35.2	0.16	960	65.0	76	9.4	49	9.9
36LM950/0.30	38.5	32.5	0.30	957	56.2	62	13.7	71	9.7
36LM950/0.45	42.6	31.6	0.46	949	42.6	202	9.9	151	8.7
50LM730/0.45	58.5	52.1	0.44	731	22.0	607	7.7	604	8.9
50LM780/0.45a	55.6	47.3	0.43	776	34.4	333	11.6	277	8.0
50LM780/0.45b	55.6	47.3	0.43	776	36.2	387	11.0	328	8.1
50LM830/0.45	62.6	53.3	0.44	830	33.3	318	11.3	207	7.6
50LM900/0.45	56.2	44.4	0.40	900	39.9	173	29.8	134	-
65LM700/0.45	73.5	65	0.43	689	21.6	720	7.5	678	7.9
85LM730/0.15	88.8	89.3	0.15	735	77.9	71	5.2	75	7.6
85LM730/0.30	91.4	88.5	0.28	735	43.1	175	5.1	169	7.2
85LM730/0.45	88.7	82.1	0.42	735	22.8	308	5.8	419	6.9

Table 4.1: list of samples used in this study with the deformation conditions and the average sizes of the deformed grains, recrystallised grains and bulges. ND is the number of deformed grains measured and NX the number of recrystallised grains. The errors on the size measurements is 5% (see Chapter 3). The average bulge size is based on ~100 bulges per sample and is not measured in samples 15LM950/0.45 and 50LM900/0.45 because the deformed grains in these samples do not show bulges. On samples indicated with a and b, two EBSD analyses have been performed in order to compare the variation within one sample.

(Fig. 4.2). Further experimental details can be found in Ter Heege et al. (2002). The labeling of the samples in Table 4.1 contains the values of the final stresses and when the stress mentioned in the text is not specified, it is the final stress.

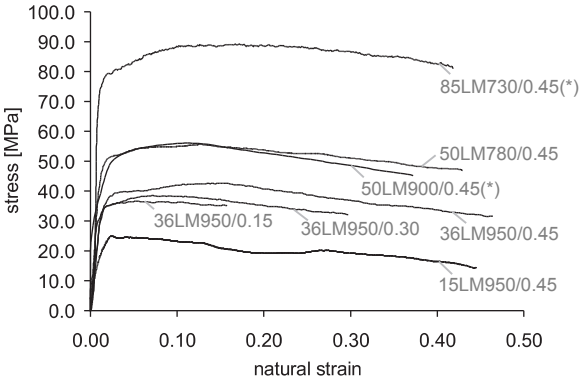

Fig. 4.2: Stress-strain curves of a selection of the samples in this study. The samples with an asterisk are from this study and the others are from Ter Heege et al. (2002), who have shown that the flow stress at a given strain can be reproduced within ~10%.

4.2.2 Measuring sizes using EBSD

Schmid et al. (1980) and Rutter (1995) have measured the size of recrystallised grains in calcite using light microscopy and defining recrystallised grains as grains being free of subgrains. However, subgrains cannot always be clearly identified in light microscopy (see Chapter 2) and therefore this technique does not result in reliable recognition of recrystallised grains. We have used electron backscattered diffraction (EBSD), which is a more accurate technique for recognizing subgrains because low angle boundary misorientations can be visualized and quantified.

The deformed samples were sectioned parallel to the maximum compression direction to make polished blocks for EBSD (see Chapter 2 and Valcke et al. (2006) for more details on the sample preparation). EBSD data have been collected and analysed using HKL Channel 5 software on a FEI XL30SFEG scanning electron microscope (SEM) with a Nordlys 2 CCD camera. Automated maps of 1μm step size for a grid of 1000 x 1000 were made, in which each pixel contains the 3D orientation information of the crystal (see Chapter 3 for more details on the measurement procedure). The angle of orientation difference between two pixels is called the misorientation angle. To detect and measure grains and subgrains automatically, the domain boundary method was used. This method is based on determining domains (grains, subgrains) having boundaries with misorientations larger than a minimum misorientation angle θ_{min} (Trimby *et al.*, 1998 and Chapter 3). Grains have been defined as having boundaries with misorientations above 10° (Chapter 2 and Valcke et al., 2006). After detecting grain boundaries larger than 10°, the boundaries that do not form closed domains are connected along parts that have misorientations lower than 10° down to a minimum closure angle, θ_c, of 0.5°. This means that microstructures defined as grains, have misorientation angles predominantly above 10°, but can also locally have lower misorientations (only a few pixels). The size of a domain is then represented by the equivalent circular diameter (ECD) of the domain area. Recrystallised grains have been separated from deformed grains based on their average internal misorientation, a method that is explained in Chapter 3. Bulges are the areas of a deformed grain just behind a grain boundary bulge and they are measured by fitting circles to the grain boundary bulges (Fig. 4.3, see Chapter 3 for a detailed description). The different terms associated with grain boundary bulges are shown on Fig. 4.3c.

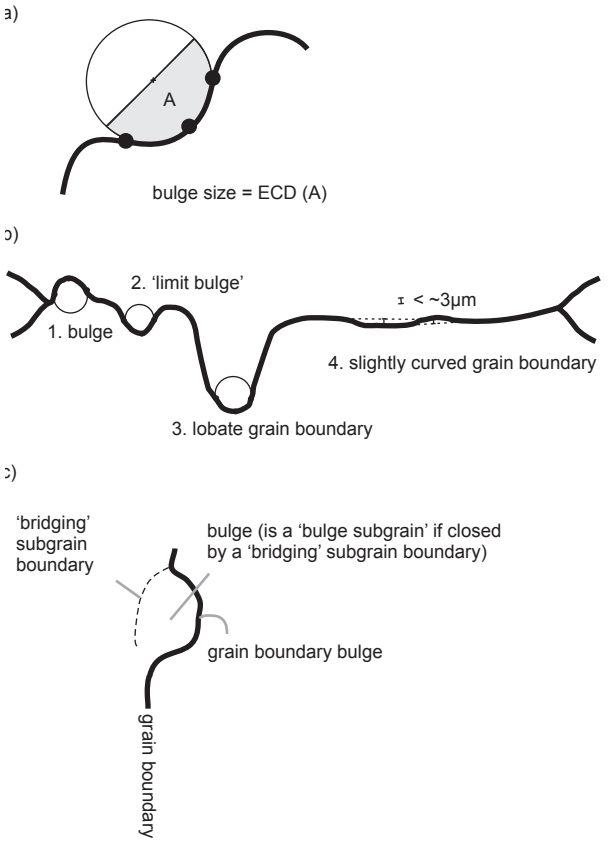

Fig. 4.3: a) Figure to illustrate how grain boundary bulge are measured (taken from Chapter 3): three points on the curved grain boundary are fixed and a circle is drawn through these three points using an image analysis software program (Scandium software). Then the area of this circle is calculated and this area divided by two, which is the half circle that fits the bulge. From this area, the equivalent circular diameter (ECD) is calculated. b) Schematic figure to illustrate how grain boundary bulges are distinguished from lobate grain boundaries (when the indent is larger than the fitted circle) and slightly curved grain boundaries (when the deviation from a straight boundary is only a few microns (~resolution limit)). c) Schematic figure to illustrate the terms 'grain boundary bulge', 'bulge', 'bulge subgrain' and 'bridging subgrain boundary'. The grain boundary is indicated in black and the subgrain boundary in the dashed black line.

4.3 Results

4.3.1 Qualitative description of the microstructures

An EBSD map of the undeformed starting material (not heated) is shown in Figure 4.4. The grains do not show a clear shape preferred orientation and they are fairly equiaxed. Many grains show straight e-twin boundaries. A few grain boundaries show bulges, but most of the boundaries are fairly straight to slightly curved (see Fig. 4.3 for a definition of bulges and curved boundaries). The isolated, low angle misorientation boundaries (>1°) that have a length of only a few pixels are artificial boundaries not related to real microstructures (see Chapter 3) (Fig. 4.4). There are no clear low angle boundaries that show a subgrain like structure.

In Figure 4.5, maps are shown from selected, representative samples to illustrate the typical microstructures (deformed grains, recrystallised grains and bulges). Almost all samples have at least a few grains that show a core-mantle substructure, i.e., small mantle subgrains at the grain boundaries and larger core subgrains in the grain interiors (Fig. 4.5a-f - Appendix A). The boundaries between two deformed grains often show bulges (e.g., green circles in Fig. 4.5a & d - Appendix A), while the boundaries between a deformed and a recrystallised grain or between two recrystallised grains are generally straight or only slightly wavy (e.g., green circles in Fig. 4.5e & f - Appendix A). Compared to the starting material (Fig. 4.4), more grain boundary bulges occur in the deformed material, in which every boundary between two deformed grains shows bulges (Fig. 4.5 apart from 4.5f - Appendix A). At low strains, the boundaries between deformed grains, including the grain boundary bulges, have relatively high misorientation angles (>30° : black lines on Fig. 4.5 - Appendix A). At higher strains, many recrystallised grain boundaries have the same high angles as the grain boundaries of the deformed grains around which they are located (>30° : black lines on Fig. 4.5 - Appendix A), although sometimes part of the recrystallised grain boundary has lower angles (10°-30° : red lines on Fig. 4.5 - Appendix A) (e.g., frame on Fig. 4.5b and blue circle on Fig. 4.5c - Appendix A). The sample deformed at the lowest stress (15 MPa) does not show a core-mantle substructure nor grain boundary bulges (Fig. 4.6 - Appendix A).

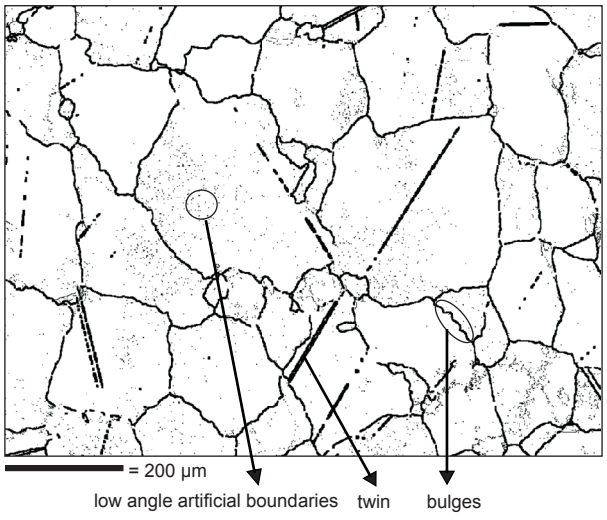

Fig. 4.4: EBSD map of the undeformed starting material. Grain boundaries >10° are indicated in thick black lines and low misorientation angle boundaries >1° are indicated in thin black lines.

Below, the microstructures are described qualitatively and sets of two samples are compared to investigate trends with strain, stress and temperature.

Trends with increasing strain at constant stress (~36 MPa) and temperature range (900 °C) (compare Figs. 4.5a and b):

Deformed grains become more substructured: at low strain (0.15), grains show some straight subgrain boundaries cross-cutting the grains and very few mantle subgrains, while at high strain (0.90), the mantle is well developed and there is a dense core subgrain boundary microstructure. Furthermore, at high strain, the deformed grains are more flattened. The grain boundaries already show bulges at low strain, of which the size does not significantly change with strain. At low strain there are only a few recrystallised grains at the old grain boundaries (0.15), while at high strain (0.90) the recrystallised grains start to cover the entire length of the old grain boundary and form a necklace. At this point, the irregular character of the grain boundary directly in contact with the recrystallised grains is due to the shape of the recrystallised grains rather than to bulges of an old grain boundary between two deformed grains (see e.g., the frame on Fig. 4.5b - Appendix A).

Trends with increasing stress at constant strain and temperature (e.g., compare Figs. 4.5c and d):

At high stress (85 MPa) the grains are less subdivided in the core compared to lower stress (50 MPa). The deformed grains do not significantly change in shape, but the grain boundary bulges become smaller with increasing stress (e.g., compare orange circles on Figs. 4.5c & d). Also the recrystallised grain size decreases with stress.

Trends with increasing temperature at constant stress and strain (compare Figs. 4.5c, e and f):

With increasing temperature, the recrystallised grain

size increases. Furthermore, the shape of the deformed grains becomes increasingly irregular: at low temperature (730 °C), the deformed grains are polygonal with near straight boundaries (apart from the small bulges), while at higher temperature (≥ 780 °C) the grains are far more lobate. With increasing temperature, the deformed grains have less substructure and the core-mantle structure and bulges are less clearly developed. The 50MPa – 900°C sample even does not show bulges of the type described in Fig. 4.3. Furthermore, at low temperatures, the recrystallised grains are concentrated along the grain boundaries like a necklace, while at high temperatures, this necklace type structure is less common (780 °C) to non-existent (900 °C).

Because the bulges between deformed grains occur less at high strain (0.45-0.90) due to the ubiquitous presence of recrystallised grains along the grain boundaries (see above), we focus on low strain samples, in which bulges are more easy to observe, to further characterize them. Figure 4.7 shows three samples deformed to a natural strain of 0.15 at nominally 36 MPa and different temperatures (Fig. 4.7a-c - Appendix A) and one sample deformed to a strain of 0.30 at 85 MPa (Fig. 4.7d - Appendix A). In all samples, the bulges often occur where straight subgrain boundaries, sometimes extending to the core, intersect with grain boundaries and the angle between such a straight subgrain boundary and the grain boundary is often high, between 45° and 90° (green circles on Fig. 4.7 - Appendix A). In a few cases, the bulge seems to show less substructure than the surrounding part of the grain (red circles on Fig. 4.7b and d - Appendix A). At low strain, the bulges are usually open, i.e., with no 'bridging' subgrain boundary behind the grain boundary bulge (blue circles on Fig. 4.7a - Appendix A), or the bulges are isolated by a 'bridging' subgrain boundary (>1°) and they are in fact 'bulge subgrains' (orange circle on Fig. 4.7a - Appendix A). At high strain, almost all bulges are closed by higher angle 'bridging' subgrain boundaries (>5°) (Fig. 4.8 - Appendix A).

The overall core-mantle structure development within the deformed grains differs between the samples: in the higher temperature, low stress samples (e.g., Fig. 4.7a-c - Appendix A) some grains virtually have no mantle and only show some straight subgrain boundaries, and other grains have a broad mantle and the difference between core and mantle is small. In contrast, in the low temperature – high stress sample (85 MPa, 730 °C – Fig. 4.7d - Appendix A) all grains have a well developed mantle and only minor core subdivision.

4.3.2 Recrystallised grain size as a function of strain, temperature and stress

In Figure 4.9a, the recrystallised grain size at a given stress (36 MPa) is plotted as a function of strain for constant temperature series. At the same temperature, the recrystallised grain size does not systematically change with strain. However, within one sample, there appears to be more variation in size at low strain than at high strain (compare the average size on two maps within the same sample: 36LM900/0.30a & b and 36LM830/0.45a & b; see arrows on the graphs in Fig. 4.9).

In Figure 4.9b, the recrystallised grain size at a strain of 0.45 is plotted as a function of temperature for constant stress series. At low stress (23 MPa and 36 MPa), the recrystallised grain size does not systematically change with temperature, but at higher stress (50 MPa), the recrystallised grain size increases with increasing temperature. The increase in size is the most obvious for the 50 MPa; 900 °C sample, which could be an exceptional outlier. However, it is seen from microstructures on the EBSD maps that there are effectively already larger recrystallised grains at 780 °C compared to 730 °C (Fig. 4.5c and e - Appendix A). This is not immediately reflected in the average size because many small recrystallised grains keep the average relatively low.

Even though the recrystallised grain size does not change systematically with either strain or temperature, the number of recrystallised grains (measured on similar sized area of map) does change (Fig. 4.9c-d): at constant stress and temperature, the number of recrystallised grains increases with increasing strain, and at constant stress and strain, the number of recrystallised grains decreases with increasing temperature.

For constant temperature and strain, there is a decrease in recrystallised grain size with increasing peak as well as final stress, regardless of temperature. There are two samples that somewhat deviate from the trend, namely 15LM950/0.45 and 50LM900/0.45 (see arrows on Fig. 4.9e). These particular samples show significantly different microstructures than the other samples (compare Figs. 4.5f and Fig. 4.6 with Figs. 4.5a-e - Appendix A).

4.3.3 Bulge size as a function of strain, temperature and stress

The bulge size at a given stress (36 MPa) is plotted as a function of strain in Figure 4.10a for constant temperature series. At the same temperature, there is no systematic change of the bulge size with strain, nor is there any significant variation in bulge size within one sample (see arrows on the graphs in Fig. 4.10).

In Figure 4.10b the bulge size is plotted as a function of temperature at a strain of 0.45 for constant stress series. At the same stress, the bulge size slightly decreases

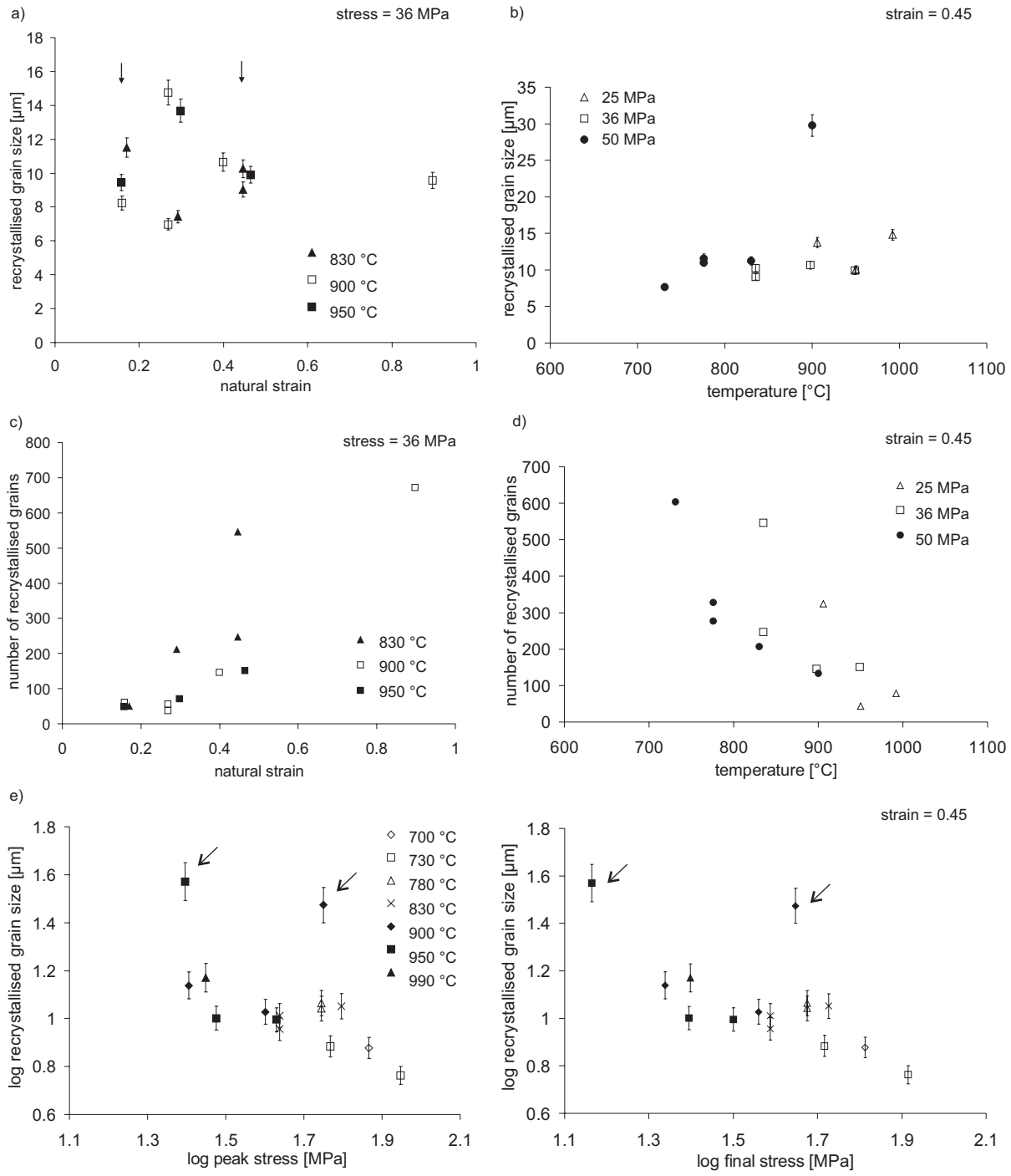

Fig. 4.9: Graphs illustrating the relationship between recrystallised grain size and deformation conditions: strain (a) temperature (b) and stress (e). (c) and (d) show the relation between the number of recrystallised grains and strain (c) and temperature (d). The arrows in (a) point out two measurements, made on two different EBSD maps of the same sample. The arrows in (e) show two datapoints that deviate from the trend.

with increasing temperature.

The bulge size is plotted as a function of peak and final stress (Fig. 4.10c). There are no clear temperature isolines, but because of the small effect of temperature seen in Figure 4.10b, two linear trends can be distinguished for low (< ~900 °C) and high (> ~900 °C) temperatures (Fig. 4.9c), both showing that the bulge size decreases with increasing stress.

4.3.4 Deformed grain size as a function of strain, stress and temperature

Figure 4.11a shows a plot of the deformed grain size at a given stress (36 MPa) as a function of strain for constant temperature series. The deformed grain size

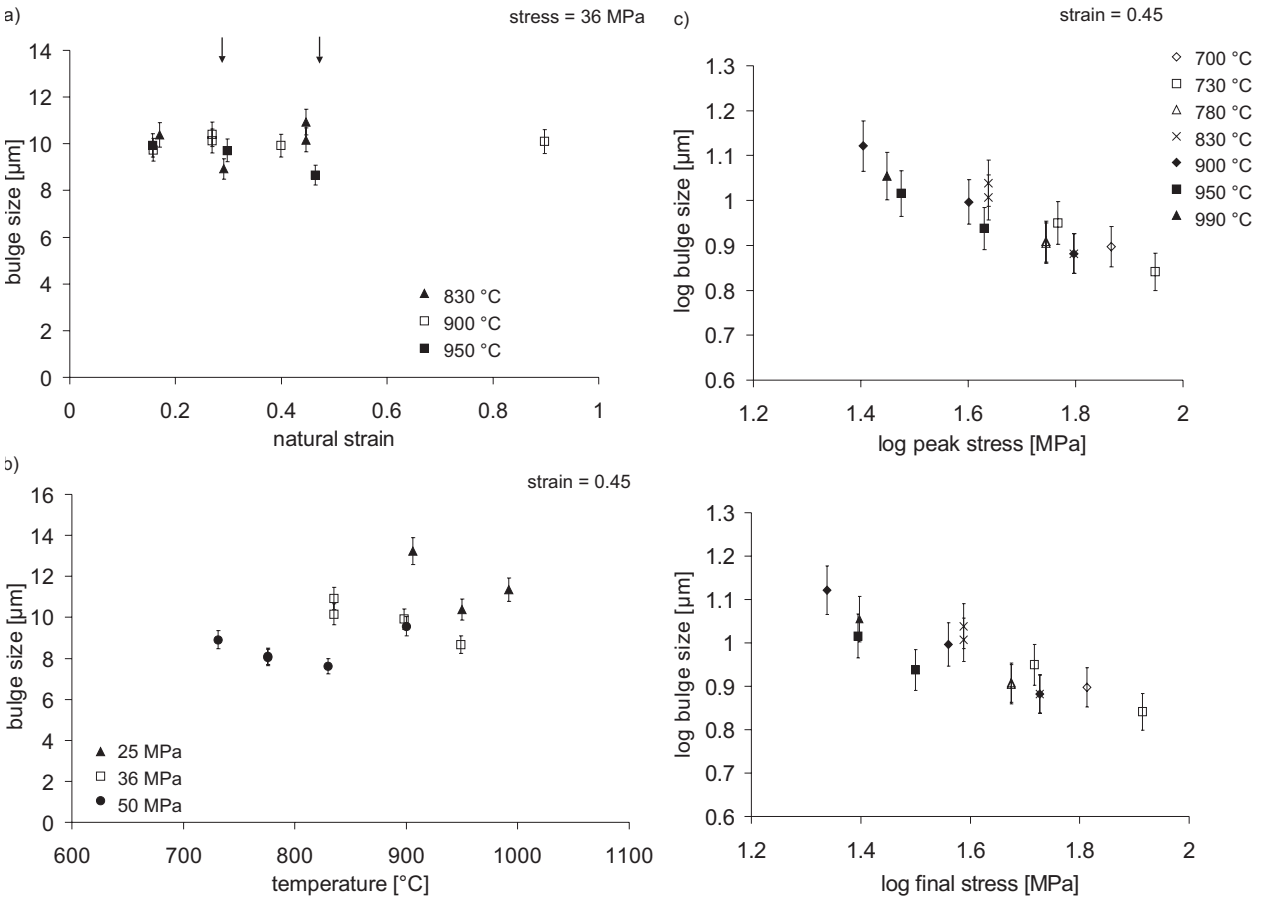

Fig. 4.10: The relationship between bulges and deformation conditions: strain (a), temperature (b) stress (c). The arrows in (a) point out two measurements, made on two different EBSD maps of the same sample.

decreases with increasing strain for each temperature series. De Bresser et al. (2005) have shown that in axisymmetric compression, as applied here, there is an apparent grain size reduction of 20 % at a natural strain of 0.45 in 2D sections, due to movement of material out of the plane section. The deformed grain size in our study at 0.45 strain is ~30 µm, which is a reduction of more than 60% of the initial grain size (84 µm) and therefore this is not only an apparent reduction due to uniaxial compression. Note that within one sample there can be substantial variation in deformed grain size (see samples 36LM900/0.30a&b and 36LM830/0.45a&b, marked by arrows on Fig. 4.11a).

In Figure 4.11b, the deformed grain size is plotted as a function of temperature at a strain of 0.45 for constant stress series. At high temperatures, the deformed grain size is larger, i.e., less reduced with respect to the initial grain size, than at low temperatures.

As the deformed grain size decreases with increasing strain, the size is plotted as a function of peak and final stress (Fig. 4.11c). At the same temperature and strain, there is no systematic change of the deformed grain size with stress.

4.4 Discussion

4.4.1 Relationship between different microstructures

In samples with deformed grains having a core-mantle structure, the recrystallised grains surrounding the deformed grains often have relatively high misorientation angles (>30°) for at least a part of their boundary. This part can be interpreted as an original bulge of a deformed grain (see green circles in Fig. 4.12 - Appendix A). The other part of the recrystallised grain boundary often has lower misorientations (10°-30°) and probably originated after an increase in misorientation from a ‘bridging’ subgrain boundary that isolated the original bulge (Fig. 4.12 - Appendix A). In Figure 4.13, the recrystallised grain size is plotted against three microstructural parameters: the bulge size, the mantle and the core subgrain sizes (taken from Chapter 6). The bulge size compares well with the recrystallised grain size, but not with the mantle nor core subgrain size (Fig. 4.13).

Some grain boundary bulges can be open, i.e., there is no ‘bridging’ subgrain boundary present that is >1° and connects the high angle grain boundary parts of the

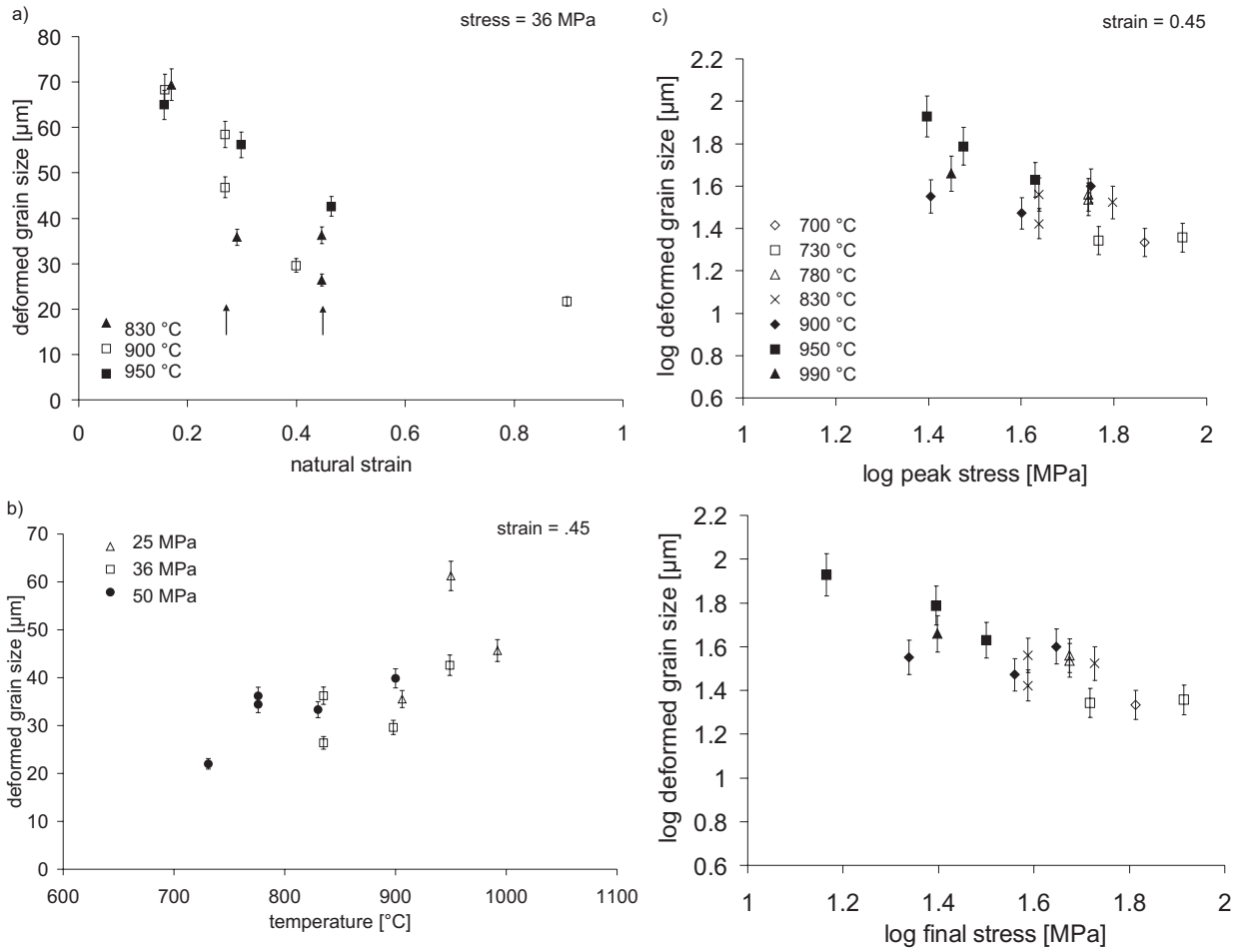

Fig. 4.11: The relationship between deformed grains and deformation conditions: strain (a), temperature (b) stress (c). The arrows in (a) point out two measurements, made on two different EBSD maps of the same sample.

bulge (e.g., Fig. 4.7a - Appendix A), while others have 'bridging' subgrain boundaries (Fig. 4.8 & 4.12 – blue circles - Appendix A). In the former case a bulge is in fact a bulge subgrain (Fig. 4.3c). The bulge subgrains often have boundaries with higher misorientation angles (>3°-5°) than the surrounding mantle subgrains, which do not form part of a bulge and often have boundaries with misorientations below 3° (Fig. 4.8 & 4.12 - Appendix A). This suggests that recrystallised grains that form by an increase in subgrain misorientation, will preferentially nucleate at bulges rather than at subgrains elsewhere in the deformed grains where subgrain misorientation angles are lower.

Most of the long, straight parts of deformed grain boundaries and also of recrystallised grain boundaries have high misorientation angles (>30°), but occasionally they have lower misorientations (10°-30°) (Fig. 4.14a & b - Appendix A). The recrystallised grain boundaries can be parallel with or form a continuous trace with the core subgrain boundaries (>5°) (Fig. 4.14 - Appendix A). In the higher temperature samples there are recrystallised grains with boundaries that are parallel to core subgrain boundaries (Fig. 4.14b - Appendix A). This parallel geometry of core subgrain boundaries and grain boundaries shows that they are related to one another; more specifically, a low angle grain boundary can have resulted from the progressive core subgrain rotation with increasing strain.

4.4.2 Formation of bulges and their stress and temperature dependence

In order to explain the dependency of the bulge size on stress and temperature (paragraph 4.3.3), we speculate on how the bulges were formed. A few bulges preexisted before deformation took place (Fig. 4.4), these are likely to remain during deformation and possibly migrate further, but they are not the precursor of all bulges as many more have formed during deformation (Fig. 4.5 - Appendix A). The formation of a grain boundary bulge requires the grain boundary to be mobile and a driving force for migration to be present. The kinetics of the driving process were first analysed by Bailey and Hirsh (1962). If two deformed grains have stored energies of E_1 and E_2 and $E_1 < E_2$, then the driving force is provided

by the energy difference $\Delta E = E_2 - E_1$ [J/m^3]. If the bulge is a spherical cap of radius R, with a specific boundary energy, γ_b, then the condition for a bulge to grow is:

$$R > \frac{2\gamma_b}{\Delta E} \quad . \tag{4.2}$$

In Carrara marble deformed in the temperature range of this study (700-990 °C) grain boundaries are mobile (Rutter, 1995; McCaig *et al.*, 2007). For deformed materials with heterogeneous microstructures, the main driving force for migration has been suggested to be due to a difference in stored energy on the opposite sides of the grain boundary. This could be either a difference in subgrain boundary structure (e.g., subgrain size) or a difference in dislocation density (Bailey & Hirsch, 1962; Drury *et al.*, 1985; Derby & Ashby, 1987; Humphreys & Hatherly, 2004). As many bulges were found associated with subgrain boundaries (Figs. 4.5, 4.7, 4.12), a heterogeneity in subgrain boundary spacing is thought to be the most important driving force in our samples. 'Bridging' subgrain boundaries (Fig. 4.3c), only occasionally have been seen at low strain (0.15) (Fig. 4.5a - Appendix A), while they commonly are present at higher strains (0.30-0.45) (Figs. 4.5b & 4.7). This suggests that subgrain boundaries at high angles to the grain boundary existed already at the very beginning of the bulge formation and possibly pin the grain boundary bulge (Figs. 4.5 and 4.7), while the 'bridging' subgrain boundaries only appeared later. Based on this, we propose the following conceptual model (Fig. 4.15 - Appendix A):

(1) At the onset of deformation, (straight) subgrain boundaries are formed at high angles to the grain boundary (Fig. 4.15a-b - Appendix A). Because these boundaries do not form at regular spacing and because locally some mantle subgrains might have formed (see e.g., Fig. 4.7a-c - Appendix A), this results in a heterogeneous substructure.

(2) This heterogeneity of subgrain boundary spacing provides the driving force for the grain boundary to migrate and form a bulge. The bulge can be pinned at the point where a subgrain boundary connects at high angles with a grain boundary (Fig. 4.15b - Appendix A). However, such a pinning boundary is not always observed on the EBSD maps, either because it has angles lower than the resolution limit of EBSD (<1°) or simply because a bulge is not always pinned by a pre-existing subgrain boundary (Fig. 4.15a - Appendix A). Occasional bulges even exist in the starting material before deformation takes place and these are not associated with subgrain boundaries (Fig. 4.4). It should be noted that second phases/particles could also cause the pinning and nucleation of bulges (Smith, 1948; Humphreys & Hatherly, 2004). However, no second phase grains associated with bulges have been observed in this study.

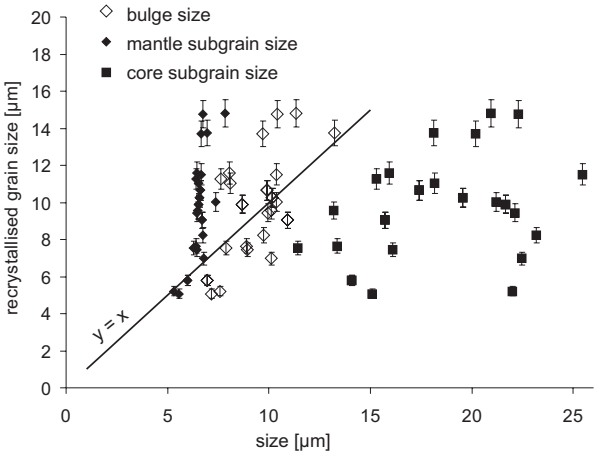

Fig. 4.13: The relation between the recrystallised grain size and three different microstructural parameters: the bulge size, the core or mantle subgrain size (see legend). The line on the graph shows the condition for which x = y in order to indicate the microstructural parameter which best approaches the recrystallised grain size.

(3) Once the bulges have formed, they become less mobile, stop migrating and instead, start rotating because of the following: (i) the driving force for migration has decreased as the strain energy differences became smaller after the low strain bulge has consumed part of the high strain region and when the inward pointing migration force due to the surface energy of the grain boundary bulge has opposed the outward pointing migration force (Bate & Hutchinson, 1997), (ii) the grain boundary has become irregular, and under continued deformation, shear forces or sliding along the grain boundary will induce rotation of the bulges; and/or (iii) the bulge is surrounded by material with a different orientation and under continued deformation, geometrically necessary dislocations will form and arrange into a 'bridging' subgrain boundary to accommodate these orientation differences. Under continued rotation, the 'bridging' subgrain boundary will increase its misorientation and eventually connect both ends of the bulge (Fig. 4.15c - Appendix A).

The proposed model is similar to the model of Beck (1954; see also Smallman, 1985) except that in our hypothesis, the bulge forms prior to the 'bridging' subgrain boundary, while in the Beck model, the 'bridging' subgrain boundary was already there as part of the subgrain at which the bulge nucleates.

Starting from this model, possible reasons for the stress and temperature dependency of the bulge size can be discussed. The bulge size is likely to be influenced by two processes, namely (1) the pinning of the grain boundary by subgrain boundaries and (2) the amount (distance) of migration of the bulge.

(1) If the bulge is pinned, then its size will be determined by the spacing of the pinning subgrain boundaries in the low strain, migrating grain, so the larger subgrain spacing of the two sides of the boundary (Fig. 4.15b - Appendix A). If this subgrain boundary spacing is stress dependent, then the bulge size will have a similar stress dependency. This subgrain boundary spacing at the grain boundaries is expected to be similar to the mantle subgrain size, also measured at grain boundaries. Unfortunately, this causes a measurement problem because the average subgrain boundary spacing relevant for the bulge size is localised on one side of the grain boundary and therefore cannot be measured directly using automatic methods.

(2) If the grain boundary bulge is not pinned, then the bulge size will be determined by the amount of migration, which is directly proportional to the mobility of the grain boundary and the driving force (see Eqn. 4.2). The grain boundary mobility is higher at higher temperatures. The main driving force during deformation is formed by strain energy differences, which increase with difference in subgrain structure between grains (Poirier, 1985). The subgrain structure difference between grains is the highest in the low stress – high temperature samples (paragraph 4.3.1 and Fig. 4.7a-c - Appendix A). Therefore the grain boundary bulges are likely to migrate faster and hence, the bulges will become larger in the low stress – high temperature samples compared to the high stress – high temperature samples. In addition to a possible stress dependent pinning of bulges at subgrain boundaries (see above), bulge mobility could be an alternative explanation for the observed stress dependency of the bulge size. Even though the main driving force during deformation is related to strain energy differences, surface energy also plays a role (Atkinson, 1988): while the strain energy difference results in bulge growth, the surface energy contribution may result in bulge shrinkage. These two competitive processes of growth and shrinkage are thermally activated and if their activation energies differ, there will be a temperature dependency of the bulge size. In the case of the bulges described here, the difference in activation energy is such that with increasing temperature, the bulge size decreases (Fig. 4.10b). This is comparable with the findings for recrystallised grains of De Bresser et al. (1998).

4.4.3 Formation of recrystallised grains and their stress and temperature dependence

We will now try to explain the stress and temperature dependency of the recrystallised grains on the basis of a conceptual model for the formation of the recrystallised grains (Fig. 4.15d-g - Appendix A).

Because the subgrain misorientation angles are the highest at the grain boundaries, where recrystallised grains mainly occur (Fig. 4.8 - Appendix A), and this misorientation tends to increase with strain (Chapter 5), the recrystallised grains most likely nucleate after an increase in misorientation of a subgrain boundary (SGR). This subgrain boundary can be part of (i) a bulge; (ii) a mantle subgrain (not at a grain boundary bulge) or (iii) a core subgrain. These three cases are all a form of subgrain rotation recrystallisation, although in the first case, a migration process to form the bulge has preceded the rotation and this combined process of migration and rotation is called bulging recrystallisation (BLG). Recrystallisation solely by migration (GBM) is not observed in our samples, but once recrystallised grains have nucleated, they can migrate and grow. Consequently, the recrystallised grain size is the result of a complex combination of mechanisms and different nucleation sites (bulges and subgrains). While it is not straightforward to determine the sole recrystallisation mechanisms for one grain, the general appearance of all recrystallised grains in a sample can give an indication of which recrystallisation mechanism was the most dominant. In our samples, three types of microstructures are observed: (i) a homogeneous microstructure with homogeneously distributed subgrains (rather than a core-mantle structure) and recrystallised grains that have similar sizes as the subgrains (sample 15LM950/0.45 – Fig. 4.6 - Appendix A); (ii) a heterogeneous microstructure with core and mantle subgrains, grain boundary bulges and recrystallised grains that are mainly concentrated as a necklace around the old grain boundaries (Figs. 4.5a-e and 4.7) and (iii) a largely recovered microstructure with only few subgrains, no bulges and large recrystallised grains (sample 50LM900/0.45 – Fig. 4.5f - Appendix A). There are only two samples in this study representing microstructure types (i) and (iii) and therefore we will mainly focus on unraveling the recrystallisation mechanisms for type (ii), although we will also consider how the averages of the recrystallised grain size in the samples with microstructure (i) and (iii) compare with the averages in type (ii).

The fact that the average recrystallised grain size is similar to the average bulge size, while it differs from the average mantle and core subgrain size (Fig. 4.13), suggests that most recrystallised grains mainly nucleated at bulges (Fig. 4.15d - Appendix A) (Beck, 1954; Bailey & Hirsch, 1962; Drury *et al.*, 1985; Humphreys & Hatherly, 2004) and in most cases there was no drastic amount of subsequent migration (schematized in Fig. 4.15e-f - Appendix A).

Because the recrystallised grains nucleate from the bulges, the recrystallised grain size decreases in a similar way as the bulge size with increasing stress (compare Figs. 4.9e & 4.10c). However, the recrystallised grain

size does not show the small, but systematic temperature dependency shown by the bulge size: the former slightly decreases with increasing temperature at constant stress (Fig. 4.10b), while the recrystallised grain size is not systematically dependent on temperature (Fig. 4.9e). Even though there might be some migration and growth of the recrystallised grains in most higher temperature samples, this does not affect the recrystallised grain size averages such that they deviate in a systematic way from their general trend with stress (Fig. 4.9c). However, at high stress, the amount of migration appears to affect the average recrystallised grain size, which becomes larger with increasing temperature (Fig. 4.5d-e and Fig. 4.9b - Appendix A). In the sample deformed at simultaneously high stress and high temperature, migration has become so dominant, that bulges can no longer be distinguished and the microstructure is of type (iii). The pervasive growth of recrystallised grains at high temperature and high stresses, is probably related to the fact that an increased stress lowers the activation temperature for migration to take place (Guillopé & Poirier, 1979; Poirier, 1985). Consequently, while a temperature of 900 °C at low stresses is not high enough to activate significant migration, in the high stress samples, pervasive migration already occurs at temperatures lower than 900°C and the average recrystallised grain size increases with temperature (Fig. 4.9b). The average recrystallised grain size in sample 15LM950/0.45, which has a type (i) microstructure, is larger than that suggested by the trend of recrystallised size with stress for samples of type (ii). Based on this one sample, it is not clear which mechanism is operative, but it is clear that bulging recrystallisation does not play a dominant role in this sample.

Strain does not systematically affect the recrystallised grain size, but the overall microstructure changes with increasing strain and this is likely to affect the formation of the recrystallised grains: the number of recrystallised grains increases with strain (Fig. 4.9c) and the new grains start to form a necklace around the old grain (Fig. 4.16 – detail of Fig. 4.5b - Appendix A). Consequently, the deformed grain is surrounded by volumes of low internal strain. Therefore the driving force for the grain boundary to bulge into the higher strain region of a neighbouring deformed grain is lost and bulges no longer can form by migration (Sellars, 1978). At this point, reduction of strain during ongoing deformation is no longer fulfilled by bulge recrystallisation. To reduce strain energy, the recrystallised grains could grow at the expense of the highly deformed mantle regions. However, this is not observed, probably because ongoing deformation immediately produces dislocations in the recrystallised grains, such that the strain differences between the recrystallised grains and the mantle regions of the deformed grains quickly re-equilibrate and the recrystallised grains do not grow. Alternatively, ongoing deformation can be taken up by rotation, which is indeed observed by the increase of subgrain misorientations with increasing strain (Chapter 5). At strains of 0.45 and especially at 0.90, it is observed that the sites of subgrain rotation are less often the bulges, but rather the volumes in between recrystallised grains. The boundary of the deformed grain is now no longer irregular due to the presence of bulges, but rather due to the arrangement of recrystallised grains around the deformed grain boundary (Fig. 4.15g - Appendix A). These irregularities form ideal sites for rotation, the subsequent formation of a ‘bridging’ subgrain boundary and after an increase in misorientation of this subgrain boundary, for the nucleation of recrystallised grains. Because these irregularities, formed by a first generation of recrystallised grains, have a wavelength similar to the size of these first recrystallised grains, the new generation of recrystallised grains will have similar sizes (Fig. 4.15g - Appendix A). This is probably why the recrystallised grain size does not tend to change with increasing strain as long as nucleation is mainly concentrated at the grain boundaries of old grains. Ponge and Gottstein (1998) also have observed a switch from bulging recrystallisation to another dominant recrystallisation mechanism after the first generation of recrystallised grains has formed a necklace around the grain boundary. However, in their case the second recrystallisation mechanism has been suggested to be twinning, while in this study it seems to be subgrain rotation at sites between the recrystallised grains.

4.4.4 Size reduction of deformed grains and their strain and temperature dependence

In our samples the recrystallised grains initially develop in the grain boundary region through bulging recrystallisation (paragraph 4.4.3). This results in a reduction in size of the old, deformed grains. The microstructures also show that core subgrain boundaries locally attain high misorientations, turning into grain boundaries and that boundaries of grains can be parallel to core subgrain boundaries (Fig. 4.14b - Appendix A). Therefore, deformed grains are occasionally divided into two or more smaller grains by an increase in misorientation, i.e. by core subgrain rotation. Because after the subdivision, the ‘new’ grains still contain subgrains, they are regarded as deformed grains in this study (see paragraph 4.1.2). From the above, it follows that any reduction in size of the deformed grains may be related in a systematic way to the development of recrystallised grains at the grain boundaries of deformed grains and to a lesser extent, the development of subgrains in the core of the grains. Considering this, an explanation can be given for the effect of strain and temperature on the deformed grain size.

Subgrain misorientation angles increase progressively with strain (Pennock *et al.*, 2005 and Fig. 5.4a-c in Chapter 5 - Appendix A) and therefore the subdivi-

sion of deformed grains by core subgrain boundaries mainly happens at higher strains. Also, at high strains more recrystallised grains have formed around old grain boundaries (compare Figs. 4.4a-b). Because recrystallisation and grain subdivision both become more pervasive with strain, the resulting deformed grain size will decrease with strain, as is shown in paragraph 4.3.4 (Fig. 4.11a). Temperature lowers the frequency of core subgrain boundaries and misorientation does not build up so quickly at high temperatures (see Chapter 5), such that grain size reduction by core subgrain rotation is slower at high temperatures. A more elaborate discussion on the relationship between deformed grains and core subgrains is given in Chapter 5, where this relationship is also quantified.

4.4.5 Piezometry

In this study it is found that the recrystallised grain size is not systematically dependent on strain within the range of 0.15-0.90. This is consistent with the study on Carrara marble of Barnhoorn et al. (2004), who found that the recrystallised grain size does not change up to very high shear strains ($\gamma \sim 50$). Therefore the recrystallised grain size is a useful indicator of palaeostress. Nevertheless, although strain does not have a systematic influence on the recrystallised grain size, the average sizes are more variable at low strains (Fig. 4.9a), which could be due to the fact that there are few recrystallised grains at low strain and changes in the average size show statistical scatter. However, given the observed scatter, there is no indication that the relation would be substantially different if low strain data would be included. For this reason it is acceptable to calibrate a stress – subgrain size relation in this study for the data at 0.45-0.90 strain and to compare it with the piezometers of Schmid et al. (1980) (maximum natural strain 0.15) and Rutter (up to 60% shortening and 500% extension). The stress – strain curves of the samples in this study show that stress decreases with increasing strain (Fig. 4.2), while the recrystallised grain size does not change with strain (Fig. 4.9a). This suggests that the recrystallised grain size does not immediately re-equilibrate with a decreasing stress during ongoing deformation. This is consistent with the suggestion made in paragraph 4.4.3, namely that the recrystallised grain size is determined at the onset of deformation, i.e., around peak stress levels, by the bulge size and thereafter by the size of the older generation of recrystallised grains. Therefore, a palaeopiezometer should be calibrated using peak stress values. In Fig. 4.17, a linear best fit is applied to the recrystallised grain size data versus peak stress in logarithmic space for the samples with microstructure type (ii). Only the lowest temperature sample (50LM730/0.45) of the 50 MPa sample series is included in the best fit because this sample still shows a clear type (ii) microstructure, while the higher temperature samples at this stress show more migration, which affects the average recrystallised grain size, especially at 900°C (Figs. 4.5c, e-f and 4.9b). The resulting equation for recrystallised grain size versus peak stress is:

$$\log d_x = -\ 0.6\,(\pm\ 0.1) \log \sigma_{peak} + 1.9\,(\pm\ 0.2), \qquad (4.3)$$

in which d_X is the recrystallised grain size and σ the peak stress. In order to compare with literature data, this equation is rewritten in the form of Eqn. (4.1):

$$\frac{d_x}{b} = 10^{2.5 \pm 0.2} \left(\frac{\mu}{\sigma_{peak}} \right)^{0.6 \pm 0.1}, \qquad (4.4)$$

in which b is the Burgers vector for calcite ($6.37\ 10^{-4}$ μm (De Bresser, 1996)) and μ is the shear modulus for Carrara marble ($2.5\ 10^{4}$ MPa at 700°C (De Bresser, 1996)). Applying a best fit using the final stress instead of peak stress, results in the values for K_X and p that are very similar within error. So the equation in this study can be compared with the literature, in which final stress is used. For applications to natural samples, it should be considered that in some cases, when weakening or hardening has occurred during deformation, this cannot be resolved by the recrystallised grain size as they do not quickly re-establish their size during small stress changes (also seen by White *et al.*, 1985 for magnesium; Barnhoorn *et al.*, 2004 for Carrara marble). This means that recrystallised grains are useful as indicators of palaeostress as they are likely to represent the stress when they were first formed and not for example, stress related to exhumation.

It is seen that the 15LM950/045 and the 50LM900/0.45 samples have size averages that deviate the most from the best fit. On the other hand, the 50MPa samples at lower temperatures, which also showed some temperature dependency due to migration, still have averages that lie quite close to the best fit. This can be explained by the fact that these samples still have a significant number of bulges and bulge recrystallised grains compared to the 50LM900/0.45 sample, in which grain boundary migration has swept away the bulge microstructure.

We will now compare the best fit equation deduced above (Eqn. 4.4), with the palaeopiezometers calibrated by Schmid et al. (1980) and Rutter (1995) for Carrara marble, deformed at similar conditions as in our study. The average recrystallised grain sizes are similar to the ones of Schmid et al. (1980), while they are significantly smaller than the ones of Rutter (1995) (Fig. 4.17). This could be related to a different resolution of the measurement techniques or to a different way of determining the average value. Rutter (1995) used light microscopy, which has a lower resolution than EBSD, such that many

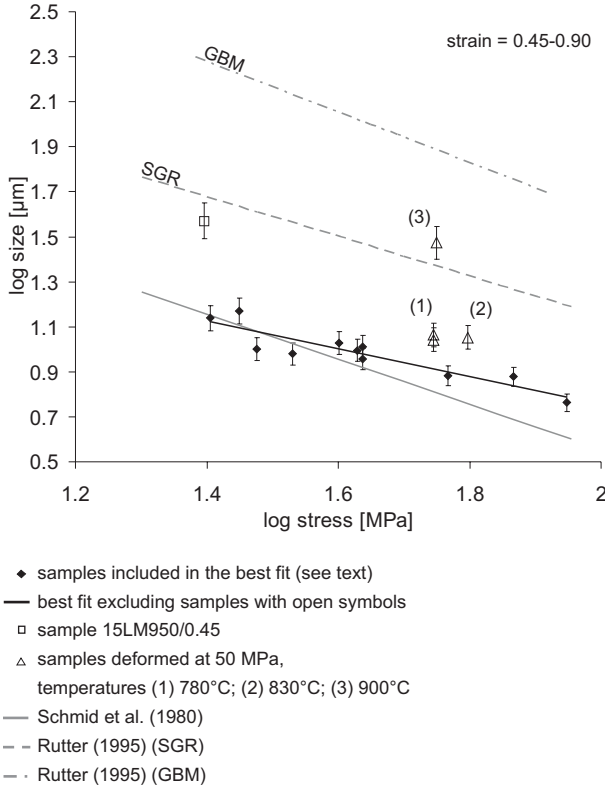

Fig. 4.17: Graph in logarithmic space showing the linear best fit to the recrystallised grain size data (excluding the samples 50LM780/0.45, 50LM830/0.45, 50LM900/0.45 and 15LM950/0.45 – see text, 4.4.5), in order to compare with the data of Schmid et al. (1980) and Rutter (1995) (see legend).

small grains are missed out, which are included in the current EBSD measurements. Also, Rutter (1995) used a linear intercept method, which is biased towards larger sizes (see Chapter 2). Therefore, it is important in palaeopiezometry to compare only data measured in the same way. The stress sensitivity of the recrystallised grain size to stress, p, equals 0.88 or 1.01 ± 0.05 for subgrain rotation recrystallised grains (Schmid *et al.*, 1980; Rutter, 1995) and p equals 1.10 for migration recrystallised grains (Rutter, 1995 - no error given). The recrystallised grain sizes in our samples (p = 0.6 ± 0.01) are not so sensitive to stress compared to values quoted in the literature. It is shown in this study that the recrystallisation in Carrara marble is complex and a recrystallised grain is the result of a combination of different mechanisms such as bulging, subgrain rotation and migration. This is probably the reason why our data are not simply related to the data of Schmid et al (1980) and Rutter (1995), who made separate piezometers for subgrain rotation and migration recrystallisation. Ter Heege et al. (2002) came to a similar conclusion based on light microscopy analyses on the same samples as in this study: they noted that recrystallised grains can have undergone several cycles of recrystallisation and therefore it is problematic to calibrate piezometers for each recrystallisation mechanism separately, evaluated for each measured grain. We suggest that it is possibly more reproducible to calibrate and use piezometers based on recrystallised grain size averages in samples that show similar overall recrystallised microstructures, such as type (i), (ii) and (iii), each of these microstructures being the result of a different combination of recrystallisation mechanisms. The fact that the stress sensitivity of the recrystallised grains, here deduced for only one type of microstructure (ii), is lower than in palaeopiezometers calibrated by combining different types of microstructures, suggests that recrystallised grains effectively can have different stress sensitivities, depending on which recrystallisation mechanism is dominant in a particular type of microstructure. In the case of bulging recrystallisation, as described in this study being the main mechanism, the bulge size should be considered as playing an important role in determining the recrystallised grain size rather than, e.g., the subgrain size in SGR dominated recrystallisation. The role of bulge recrystallisation can form the basis of a critical review of microphysical models that underpin empirically derived piezometers, questioning even some of the basic assumptions of earlier models.

Schmid et al. (1980) suggest that the mantle subgrain size equals the recrystallised grain size, directly related to the inferred mechanism of recrystallisation, i.e. recrystallisation by the progressively increasing misorientation of the subgrain boundary, without growing in size. However, in the samples with a core-mantle structure, the mantle subgrains measured using EBSD are significantly smaller than the recrystallised grains (Fig. 4.13). The reason for this is that the recrystallised grains are mainly formed from subgrains associated with bulges rather than from the other mantle subgrains. The latter mantle subgrains may be related differently to stress because stress intensification may play a role at grain boundaries (e.g., White, 1979 and Chapter 6). This means that for the mantle subgrains, the piezometric relationship for recrystallised grains of Schmid et al. (1980) cannot be applied.

The bulge size could be an interesting alternative palaeostress indicator in addition to the recrystallised grain size. Namely, the bulge size is not dependent on strain and its temperature dependency is small and more clearly defined than that of the recrystallised grain size (compare Figs. 4.9b and 4.10b). While a grain boundary migration component affects the average recrystallised grain size, it does not seem to have the same effect on the bulge size. For example, the samples 50LM780/0.45 and 50LM830/0.45 have average recrystallised grain sizes that are somewhat larger than expected from the trend with stress (Fig. 4.17 – open triangle symbols), while the bulge size is not affected by the migration in these high stress – high temperature samples and follows the trend with stress (Fig. 4.10c). Therefore, as long as the migra-

tion of recrystallised grains does not wipe out all bulges, the bulge size will be a good indicator of palaeostress. However, the small, systematic temperature dependence of the bulges, probably related to surface energy (see paragraph 4.4.2), should be accounted for when deducing a microphysical model for the bulge size – stress relation. No attempt is made to apply an empirical best fit to the bulge size data in this study because there is currently no equation, based on a microphysical model on bulge formation, to support the choice of the best fit.

4.5 Conclusions

Carrara marble, deformed in axial compression at medium to high flow stresses (15-85 MPa), temperatures between 730-990 °C and to maximum natural strains of 0.90, shows a heterogeneous microstructure consisting of recrystallised grains and deformed grains, the latter having grain boundary bulges and containing core and mantle subgrains. We have separated these various microstructures and evaluated the recrystallised grains, grain boundary bulges and deformed grains in terms of their formation and relation with deformation conditions.

Three different types of microstructures were distinguished: (i) a homogeneous microstructure with homogeneously distributed subgrains and recrystallised grains that have similar sizes as the subgrains (final stress below 20 MPa); (ii) a heterogeneous microstructure with core and mantle subgrains, grain boundary bulges and recrystallised grains that are mainly located as a necklace around the old grain boundaries (final stress above 20 MPa) and (iii) a largely recovered microstructure with only few subgrains, no bulges and large recrystallised grains (simultaneously high stress and high temperatures: ~50 MPa; 900°C).

It is found that the bulge and recrystallised grain sizes both are independent of strain and reduce in a similar way with increasing stress. The bulge size decreases slightly with increasing temperature. In contrast, the recrystallised grain size does not vary with temperature at low stresses (below 50 MPa), while it increases with temperature at high stress (50MPa).

The bulges are interpreted as being formed by limited migration of an existing grain boundary. Subsequently the bulges start rotating and subgrains are formed associated with the bulges. If rotation of the ‘bulge subgrains’ continues, this results in the formation of recrystallised grains (bulging recrystallisation). As recrystallisation proceeds, a necklace of recrystallised grains forms around deformed grains. Once the necklace is complete, subsequent new recrystallised grains nucleate by the formation and subsequent rotation of subgrains at the grain boundary irregularities in between the previously formed recrystallised grains. This is a process of subgrain rotation recrystallisation rather than bulging recrystallisation.

The stress dependency of the first generation of recrystallised grains is directly related to the size of the grain boundary bulges. We suggest that the bulge size and its stress dependency in turn are related to the subgrain boundary spacing where the bulges are pinned, and in case of no pinning, the bulge size is solely dependent on the amount of local grain boundary migration at the bulges. The local migration at the bulge is likely to be driven by differences in subgrain boundary density on the opposite sides of a grain boundary and, to a minor extent, by the surface energy of a bulged grain boundary. Because the latter is dependent on temperature, this might explain the slight temperature dependency of the bulge size. The temperature dependency of the recrystallised grain size at high stresses is proposed to be related to enhanced pervasive migration at high temperatures of recrystallised grains after their nucleation.

With increasing strain, the deformed grain size reduces with respect to the starting grain size because of continued recrystallisation and to a minor extent, due to rotation of core subgrains. High temperatures delay this process and therefore the deformed grain size reduces less quickly at high temperatures.

As the recrystallised grain size is independent of strain and it does not show a temperature dependency as long as no pervasive migration takes place (at simultaneously high stress and temperature), it is a straightforward indicator of (palaeo)stress. However, due to the complexity of recrystallisation mechanisms and the resulting different types of microstructures in calcite, it is not easy to compare the piezometer calibrated in this study with these reported in the literature. Therefore, we suggest that piezometers should be calibrated and applied for a single type of overall microstructure. In this respect, microphysical models should be critically reconsidered. For heterogeneous microstructures with grain boundary bulges, the bulge sizes could be a useful alternative indicator of palaeostress, because they are less affected by growth due to migration than the recrystallised grain size at the same conditions.

5

Influence of strain on the development of subgrains in experimentally deformed Carrara marble

Abstract

Substructures are useful to gain information on the (palaeo-) deformation conditions of naturally deformed rocks. Current models on the relation between substructure and stress assume that the microstructure is dynamically stable at constant external stress and temperature conditions. However, in nature, rocks are often in transitional stages to readjust to a change in external deformation conditions and therefore it is interesting to determine how a microstructures evolves before it has reached a dynamically stable microstructure. This study investigates the development of the subgrain microstructure with strain during minor weakening in four series of Carrara marble samples, axially deformed to different strains (0.15-0.90) at constant strain rate. Electron backscattered diffraction has been used to quantify the different elements of the microstructure, which is heterogeneous with recrystallised and deformed grains, the latter consisting of mantle and core subgrains. It is found that the mantle subgrain size has already become dynamically stable at low strain (0.15). It is suggested that this is related to a balance between formation and 'growth' processes (subgrain boundary migration and subgrain coalescence). Because mantle subgrains are already dynamically stable at low strains, they can be simple indicators of (palaeo-) stresses. In contrast, the core subgrain size decreases with increasing strain and is linked to the deformed grain size. Therefore the core subgrains are not straightforward to use for palaeopiezometry. The microstructural changes that accompany minor weakening prior to the onset of steady state are an increasing amount of recrystallised grains, the increase in mantle fraction per grain and the simultaneous reduction of deformed grains and core subgrains until the sizes of the grains and subgrains have become similar. An increasing temperature tends to slow down the grain size reduction and the evolution towards a microstructure of uniform grain and subgrain size.

5.1 Introduction

Microstructures in deformed rocks are related to deformation conditions. Piezometers are calibrated relationships between flow stress and microstructural parameters (for example, grain or subgrain size), which can be applied to quantitatively constrain the conditions during deformation (Twiss, 1977; Edward *et al.*, 1982; Orlova, 1996; Orlová & Dobes, 2004). In nature, deformation conditions change continuously and therefore many rocks are in a transitional stage, having heterogeneous, unstable microstructures, rather than in a steady state stage with dynamically stable microstructures (Carreras *et al.*, 1977; Means, 1981). Consequently, different deformation stages from a rock's history can best be traced in heterogeneous microstructures, rather than in dynamically stable microstructures. However, theoretical models for explaining piezometric relations assume that at constant external conditions, a dynamically stable microstucture develops resulting in mechanical steady state implicitly assuming no influence of strain. Empirical piezometers obtained in metals are established for high strain, normally steady state deformation experiments (e.g., Takeuchi & Argon, 1976), while most piezometers obtained in minerals are derived for relatively low strain experiments (e.g., Schmid et al., 1980). So the main emphasis in this study is on the influence of strain on heterogeneous microstructures to better understand how they develop before a steady state is reached and to validate the applicability of piezometers on rocks exhibiting microstructures that are not dynamically stable.

In Chapter 4, it has been shown that the recrystallised grain size could be a useful indicator of palaeostress, but that temperature might complicate the relation between recrystallised grain size and stress because of thermally activated grain boundary migration, especially at simultaneously high stress and temperatures. In contrast to recrystallised grain boundaries, subgrain boundaries have relatively low misorientation angles and because of their different structure and properties they are considered to be less mobile and less prone to migration than high angle grain boundaries (Duyster & Stöckhert, 2001). This suggests that boundary migration might not play such a significant role in determining the subgrain size and consequently temperature is less likely to affect the subgrain size than the recrystallised grain size. Also, subgrains already reach a dynamically stable size at very low strains (<0.15) (White, 1976). Therefore, the more stable subgrains are potentially more reliable as a palaeostress indicator than the recrystallised grain size.

There is a large variation in the average size of subgrains depending on a) their location (near the boundary or in the core of the grains), b) their origin (e.g., Means & Ree, 1988) or c) their misorientation (e.g., White, 1973; Kuhlmann-Wilsdorf, 1989; Trimby *et al.*, 1998). For example, White (1976) noted that only the 'large' subgrains appear to remain constant with increasing strain. It is, however, unclear what these 'large' subgrains are, since their boundary misorientation or characteristics were not specified. Therefore, different types of subgrains should be investigated separately to determine how they each are related to deformation conditions.

Rock deformation experiments to different finite strains under constant stress (or strain rate) and temperature conditions can be used to study microstructures as a function of increasing finite strain (for calcite see e.g., Ter Heege *et al.*, 2002; Barnhoorn *et al.*, 2004). In the present study, experimentally deformed sample sets of calcite (Carrara marble) are used and the microstruc-

series	sample name	σ [MPa]	natural strain	T [°C]	d_g[µm]	N_g	dx_p[µm]	N_X	$dm_{(1°-2°)}$ [µm]	$N_{m(1°-2°)}$	M (1°-2°)	$dm_{(2°-3°)}$ [µm]	$N_{m(2°-3°)}$	M (2°-3°)	$dm_{(3°-4°)}$ [µm]	$N_{m(3°-4°)}$	M (3°-4°)	$dm_{(>5°)}$ [µm]	$N_{m(>5°)}$	M (>5°)	$dc_{(>1°)}$ [µm]	$N_{c(>1°)}$	$dc_{(>2°)}$ [µm]	$N_{c(>2°)}$	$dc_{(>3°)}$ [µm]	$N_{c(>3°)}$	$dc_{(>5°)}$ [µm]	$N_{c(>5°)}$
1	**36LM830/0.15**	36.7	0.17	829	69.4	77	11.5	50	6.7	1825	0.092	8.0	551	0.041	8.1	237	0.020	7.5	71	0.004	9.4	2144	25.5	401	30.5	285	43.9	154
	36LM830/0.30	39.6	0.29	830	35.8	218	7.4	211	6.5	5534	0.261	6.9	1951	0.098	6.9	912	0.043	6.5	342	0.015	9.6	3445	16.1	1326	17.5	1115	21.5	643
	36LM830/0.45a	38.7	0.45	835	26.4	508	9.0	546	6.7	6505	0.333	7.6	2660	0.167	7.7	1448	0.089	7.4	651	0.041	9.5	3717	15.7	1802	16.9	1676	19.8	1143
	36LM830/0.45b	38.7	0.45	835	36.2	283	10.3	247	6.6	3740	0.178	7.6	1208	0.078	7.8	628	0.044	7.5	262	0.017	10.2	2996	19.6	971	21.7	785	26.8	515
2	**36LM900/0.15**	34.1	0.16	903	68.3	83	8.3	61	6.8	2534	0.133	7.5	818	0.051	7.3	387	0.020	7.2	114	0.006	9.9	2717	23.2	580	26.7	442	36.6	233
	36LM900/0.30a	32.9	0.27	901	58.4	65	7.0	38	6.8	1990	0.102	7.1	620	0.031	7.8	283	0.041	7.4	91	0.005	9.4	2393	22.5	427	25.7	301	33.4	167
	36LM900/0.30b	32.9	0.27	901	46.8	49	14.8	56	6.7	1836	0.100	7.7	630	0.044	7.5	294	0.022	7.3	99	0.006	10.1	2060	22.3	379	25.2	285	31.2	133
	36LM900/0.45	36.3	0.40	898	29.6	164	10.7	146	6.6	3514	0.207	7.2	1216	0.085	7.2	636	0.049	7.2	228	0.015	9.2	2155	17.4	747	18.2	686	21.5	400
	36LM900/0.90	26.2	0.90	902	21.7	854	9.6	672	6.5	9700	0.473	7.3	4207	0.253	7.2	2249	0.132	7.1	1005	0.058	8.6	3573	13.2	2567	14.6	2459	17.0	1747
3	**36LM950/0.15**	35.2	0.16	960	65.0	76	9.4	49	6.4	2051	0.113	7.1	656	0.052	6.8	287	0.010	6.2	75	0.003	9.6	2344	22.1	457	26.4	322	38.2	168
	36LM950/0.30	32.5	0.30	957	56.2	62	13.7	71	6.7	2076	0.116	7.2	689	0.047	7.6	305	0.023	7.0	97	0.005	10.7	2251	20.2	468	22.4	360	30.1	180
	36LM950/0.45	31.6	0.46	949	42.6	202	9.9	151	6.5	2517	0.129	7.1	868	0.054	7.3	409	0.032	6.8	137	0.007	10.4	2254	21.7	637	25.3	484	30.9	339
4	**85LM730/0.15**	89.3	0.15	735	77.9	71	5.2	75	5.3	2060	0.061	5.6	535	0.020	5.9	239	0.010	5.2	76	0.002	8.1	2465	22.0	418	29.4	266	44.3	143
	85LM730/0.30	88.5	0.28	735	43.1	43.1	5.1	169	5.6	4792	0.143	5.9	1778	0.061	5.7	891	0.031	5.4	404	0.009	8.8	3993	15.1	1260	17.3	965	21.9	256
	85LM730/0.45	82.1	0.42	735	22.8	308	5.8	419	6.0	5818	0.208	6.3	2225	0.083	6.0	1320	0.042	5.5	729	0.020	9.1	3697	14.1	1501	15.0	1279	16.8	878

Table 5.1: List of samples used in this study with the deformation conditions and the average sizes (mean) of the deformed grains (dg), recrystallised grains (dX) and mantle subgrains (dm) and core subgrains (dc). The subgrains are measured for specific misorientation angle ranges. The error on the size measurements is 5%. N is the number of each microstructural element measured for calculating the mean. M is the mantle fraction for specific misorientation intervals (see text, 5.3). On samples indicated with a and b, two EBSD analyses have been performed in order to compare the variation within one sample.

tures are analysed using electron backscattered diffraction (EBSD). The influence of strain is investigated on the average mantle and core subgrain size. Furthermore, the relation between subgrain size and misorientation angle, i.e., the domain hierarchy (Trimby *et al.*, 1998) is studied. From the evolution of the subgrain size with strain and with misorientation angle, inferences regarding which processes determine the subgrain size are made. Based on this, it is suggested how microstructures are related to the mechanical behaviour. Finally, it is proposed which subgrains are the most suitable for palaeopiezometry.

5.2 Material

The calcite rock samples used in this study come from a set of experimentally deformed, cylindrical samples of Carrara marble (Lorano type), uniaxially compressed at a confining pressure of 300 MPa. The samples were deformed to natural strains of 0.15-0.90 at strain rates between $3x10^{-6}$ and $3x10^{-4}$ s^{-1} and temperatures of 830 - 950°C (i.e., 0.5-0.7 T_m where T_m is the incongruent melting temperature of calcite in the system $CaO\text{-}CO_2$ at 100 MPa pressure – see Wyllie & Tuttle (1960)), which resulted in flow stresses between 36 MPa and 85 MPa (Ter Heege *et al.*, 2002 and this study). Four sample series were made: a) deformed to a natural strain of 0.15, 0.30 and 0.45 at nominally 36 MPa at 830 °C (series 1), 900 °C (series 2) and 950 °C (series 3), with one test to a strain of 0.90 at 900 °C; and b) deformed to a natural strain of 0.15, 0.30 and 0.45 at nominally 85 MPa and 730 °C (series 4) (Table 5.1). The samples were cooled rapidly after the experiments (70 °C/min) to limit annealing. Stress strain curves for selected samples are given in Figure 5.1 and they represent the flow behaviour of all samples. The curves show a broad peak stress (σ_{peak}), followed by minor weakening continuing up to the maximum strains reached. The strain levels of the samples in this study (0.15, 0.30, 0.45 & 0.90) correspond to this post peak, minor weakening stage. For the samples considered in this chapter, the weakening ($= (\sigma_{final} - \sigma_{peak})/\sigma_{peak})*100\%$) is typically 10-15% for strains up to 0.45. All stresses mentioned in this chapter are final stresses unless specified otherwise. More details on the experiments can be found in Ter Heege *et al.* (2002). The deformed samples were sectioned parallel to the maximum compression direction to make polished blocks for EBSD (Valcke *et al.*, 2006;

Chapter 2).

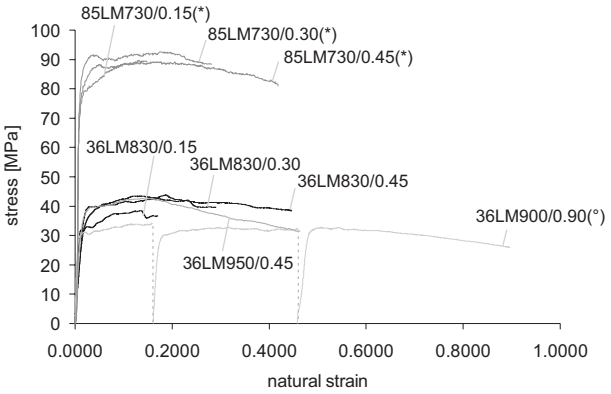

Fig. 5.1: Stress strain curves of a selection of the samples in this study. The samples with an asterisk are from this study and the others are from Ter Heege et al. (2002). They have shown that the flow stress at a given strain can be reproduced within ~10%. The sample deformed to a natural strain of 0.90 indicated with (°) is a three step experiment (see Ter Heege et al., 2002).

5.3 Method

EBSD data were collected and analysed using HKL Channel 5 software on a FEI XL30SFEG scanning electron microscope (SEM) with a Nordlys 2 CCD camera. Using automated EBSD, 1000 x 1000 grid maps were constructed with a step size of 1µm. More details on sample preparation, data collection and processing can be found in Chapters 2 & 3.

The material used in this study shows heterogeneous microstructures, containing recrystallised grains, deformed grains, and within the latter core and mantle subgrains (Fig. 5.1). In order to measure different elements of the microstructure separately, recrystallised grains were defined as domains having no internal subgrains, and deformed grains as domains having subgrains inside them (Valcke *et al.*, 2007 and Chapter 3). These definitions describe the final state of grains after deformation ceased: due to the dynamic nature of the recrystallisation process the 'deformed' grains could already have undergone a cycle of recrystallisation and subsequent deformation, or alternatively a 'recrystallised' grain could be an original grain which has not been deformed at all. The grains and subgrains were measured using the domain detection tool of the Channel 5 software (Oxford Instruments HKL Technology) with service pack 9. Deformed and recrystallised grains were separated based on the average misorientation within the grain (AMG: <1° for recrystallised grains) and mantle and core subgrains have been separated based on the average misorientation within the subgrain (AMS: ≤1° for mantle subgrains) (Valcke *et al.*, 2007 and Chapter 3). For grains, the minimum misorientation angle to define a domain, θ_{min}, is 10° and the closure angle, i.e., the lowest angle to close the domain, θ_c, is 0.5° (Chapter 3). For subgrains, θ_{min} is ≥ 1° and because mantle subgrains are often partly enclosed by a grain boundary, their maximum misorientation can be larger than 10°. For the core, θ_c = 0°, while for the mantle, θ_c = 0.5° because of low angle misorientation noise (Chapter 3). A problem that still remains with this method is that the domain detection is cumulative, i.e., domain detection is based on a minimum misorientation angle rather than an interval of angles. This means that low and high angle misorientations cannot be separated and high angle subgrains can be included in the low angle subgrain data sets because subgrain boundaries have varying misorientation angles, (see also Chapter 2). In order to circumvent this problem, subsets were made for the mantle subgrains that exclude higher angle subgrains. For example, a subset is made of mantle subgrains having boundaries with at least a part of the boundary above 1° (θ_{min}=1°; θ_c=0.5°) and from this subset, mantle subgrains having their entire boundary above 2° (θ_{min}=2°; no θ_c) are excluded. Such a subset will be called mantle subgrains (1°-2°). Note that subgrains of this subset (1°-2°) can still have parts of their boundary showing misorientations larger than 2°, but the subgrain will never be entirely surrounded by a boundary with misorientation above 2°. Also, they can have parts of the boundary between 0.5° and 1°, because θ_c=0.5°, but the boundary will never be completely below 1°. Although this might appear as a complex way of defining subsets, following this approach is necessary to account for the possible differences between low angle and high angle subgrains. We were able to do this type of 'angular interval' measurements because each mantle subgrain is defined as an entity which is not further subdivided, at least not by subgrain boundaries above the resolution limit of EBSD (~1°, Chapter 3) (Fig. 5.2). Four misorientation angle intervals were sampled: (1°-2°), (2°-3°), (3°-4°) and (>5°). We have combined all high angle mantle subgrains >5° into one subset because the frequency of these high angle mantle subgrains is so low that any further subdivision

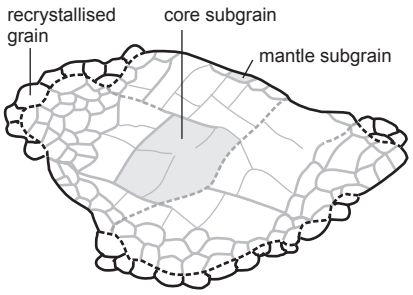

Fig. 5.2: Schematic figure to illustrate the heterogeneous microstructure with recrystallised grains and deformed grains consisting of core and mantle subgrains. The thin grey lines are low angle subgrain boundaries, the thick grey lines high angle subgrain boundaries (<10°), the black full lines are grain boundaries (>10°). A core and mantle subgrain as they would be defined as described in paragraph 5.3 are indicated in grey.

would result in average values that are statistically not meaningful (less than 20 measurements).

For core subgrains it is more complicated to make subsets that have a limited range of misorientation angles because the AMS for core subgrains is defined as >1° and therefore the higher angle core subgrains are subdivided by lower angle subgrains (Fig. 5.2). For example, low angle core subgrains >1° are always found inside higher angle core subgrains >2°, so that excluding core subgrains >2° from the subset containing core subgrains >1°, would result in an empty subset. This precludes considering misorientation angle intervals for the core subgrains, while this problem does not occur for the mantle subgrains because of the way the mantle subgrains are defined (AMS ≤1°). So for core subgrains, cumulative data ranges >1°, >2°, >3° and >5° are considered.

The mantle fraction per grain (M) is another parameter, which we have used to describe subgrain development. It is an estimate of the total area of mantle subgrains, A_m, with respect to the total area of the deformed grains, A_g, on a 1000x1000 μm EBSD map:

$$M = \frac{A_m}{A_g} \quad , \tag{5.1}$$

Transmission electron microscopy (TEM) was used as a qualitative and descriptive tool to visualize the subgrain structure at scales smaller than the EBSD resolution. TEM samples were prepared on copper grids and were thinned using an argon ion beam thinner (Gatan PIPS, beam 5 kV; angle 4-6°). The electron microscope used is a Tecnai 20 FEG, with a voltage of 200 kV and a current of 4400 μA. A double tilt holder was used to visualize the smallest subgrains and misorientations down to 0.1° (Huang & Jensen, 2000; Kumar *et al.*, 2001). Bright field images of subgrains and dislocations were made using two beam conditions (McLaren, 1991). Misorientation angles have been worked out by collecting diffraction patterns along the crystal zone axes and their accompanying tilt axes α and β of the sample orientation. Limited measurements of this type were done and the misorientation between subgrains was often found to be around 1°, rather than much smaller than 1°. A full systematic study of the misorientation angle distribution was not done as statistics would be too poor to provide useful, complementary data to the large EBSD dataset (Humphreys, 2001). In many of the imaged subgrain boundaries, individual dislocations could be clearly distinguished and the diffraction patterns on both sides of the boundary did not shift more than a few degrees, which allowed the boundaries to be recognised as subgrain boundaries and not grain boundaries.

5.4 Results: qualitative description of microstructure development with strain

An EBSD map of the undeformed starting material (not heated) is shown in Figure 5.3. The grains do not show a clear shape preferred orientation and they are fairly equiaxed. Many grains show straight e-twin boundaries. A few grain boundaries show bulges. The isolated, low angle misorientation boundaries (>1°) that have a length of only a few pixels are artificial boundaries not related to real microstructures (see Chapter 3). There are no clear low angle boundaries that show a subgrain like structure.

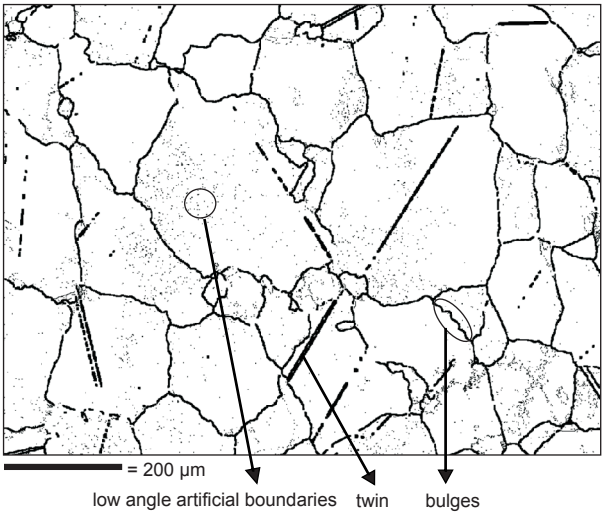

Fig. 5.3: EBSD map of the undeformed starting material. Grain boundaries >10° are indicated in thick black lines and low misorientation angle boundaries >1° are indicated in thin black lines. (Shown also as Fig. 4.4).

Figure 5.4 shows the evolution of grains and subgrains as a function of strain for the four series at nominally constant stress and temperature. The selected maps in Figure 5.4 show representative microstructures and much larger areas (1000 x 1000 μm) were used to get quantitative data (paragraph 5.5). Firstly, we qualitatively describe the typical subgrain structure and then we consider the effect of deformation conditions, specifically strain. In most grains, core and mantle subgrains can be seen, although the amount of mantle subgrains and core subgrains can vary significantly between samples and also between individual grains. The smaller mantle subgrains at grain boundaries are generally equiaxed, while the larger core subgrains have elongate, straight boundaries. These boundaries often start near triple junctions and run straight to the grain centres, having directions at 20-70° (average of all angles = 50°) to the compression axis. The directions of the straight core subgrain bounda-

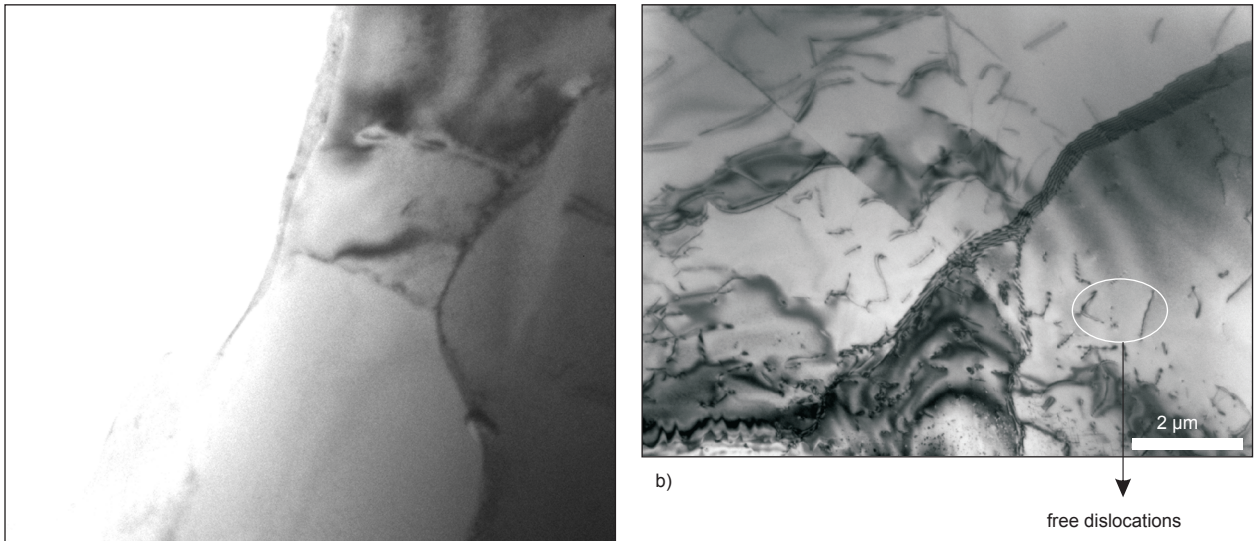

Fig. 5.5: Two beam bright field TEM images of sample 36LM900/0.30. All boundaries on the images are subgrain boundaries, a) is in a mantle region and shows cusp like shapes of the boundaries (see arrows); b) is in a core region and shows the dislocation density variations in subgrains and the wavy character of subgrain boundaries. The TEM conditions are given in paragraph 5.3.

ries are sometimes (sub)parallel to the directions of the grain boundaries. At higher strain, the core subgrain boundaries tend to have higher angles to the compression axis, compare for example, the 0.15 samples with the 0.90 sample (Fig. 5.4 - Appendix A).

In broad terms, strain has a similar effect on microstructures of all series (independent of stress and temperature). Namely, the size of the deformed grains decreases, the number of mantle subgrains increases and the grain centres increasingly become subdivided into core subgrains. The misorientation angle of the mantle subgrains and also occasionally of the straight core subgrain boundaries increases with increasing strain. At high strains (0.45-0.90), especially at low temperatures (730°-830 °C), the core subgrains are increasingly subdivided such that the straight boundaries structure is less obvious and the core subgrains have sizes that resemble those of the mantle.

When looking at the maps in more detail, there are, however, important differences in the microstructure development with strain for the individual series. Temperature (compare the series 1-3, 36 MPa) has an effect on how fast the mantle and core subgrains are formed with strain. At low temperature (830°C) a dense substructure with a high number of mantle and core subgrains, has already been formed at a strain of 0.30 (Fig. 5.4a-b - Appendix A), while at higher temperature (900°C) a strain of at least 0.45 is needed for the grains to become subdivided. Even then, large deformed grains remain present that only show a pattern of isolated, elongate subgrain boundaries cross-cutting the grains and no well developed mantle (Fig. 5.4d-g - Appendix A). Only at a strain of 0.90 does the microstructure become more homogeneous with core subgrains that approach the mantle subgrain size. For even higher temperatures (950°C), the microstructure does not change significantly with increasing strain: the amount of mantle subgrains per grain remains similar and the core subgrains do not develop progressively (Fig. 5.4h-j - Appendix A).

In Figure 5.5, TEM images are shown from sample 36LM900/0.45, demonstrating the character of the subgrain boundaries. The most striking microstructural feature is that the subgrain boundaries from the mantle (Fig. 5.5a) as well as from the core (Fig. 5.5b) show a wavy shape, even sometimes a cusp like structure (Fig. 5.5a). Another observation is that within one subgrain the dislocation density can vary: there seem to be more dislocations closer to the subgrain boundaries (Fig. 5.5b).

5.5 Results: quantitative description of the mantle subgrain evolution

5.5.1 Variation of mantle subgrain size with misorientation

The average size of the mantle subgrains is given in Fig. 5.6 as a function of the misorientation angle for samples at a constant strain of 0.45 (see also Table 5.1). For all samples, the differences in size with misorientation are not very pronounced. For the low stress samples (36 MPa), there is an increase in size from the lowest angle subgrains (1°-2°) to the high angle subgrains (>2°). For the high stress sample, there is no obvious hierarchy in size.

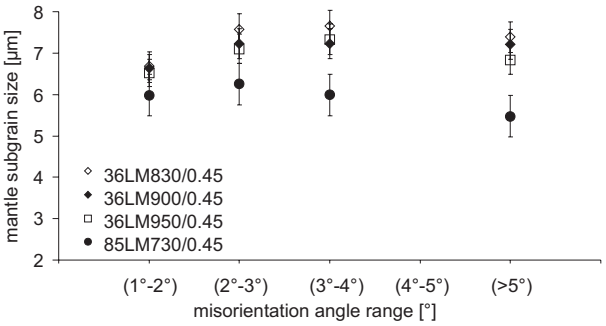

Fig. 5.6: Graph showing the variation of the mantle subgrain size with misorientation for samples at the same strain (0.45) (see legend).

5.5.2 Development of mantle subgrain sizes with strain

The mantle subgrain size versus strain is shown only for one misorientation interval (1°-2°) because misorientation does not have a pronounced effect on the size (paragraph 5.5.1). First, the results for the 36 MPa series (1, 2, 3) are described (Table 5.1 and Fig. 5.7). Different EBSD mapped data from different areas of the same sample (36LM830/0.45a,b and 36LM900/0.30a,b) do not show a significant difference in the average value of the mantle subgrain size (Table 5.1). This demonstrates that for the average mantle subgrain size, the samples can be considered as relatively homogeneous. Comparing samples deformed to the same strain (for example, to 0.3, see Fig. 5.7), no effect of temperature emerges. Taking then all data at 36 MPa together, no systematic effect of strain is observed. Going on to the data at 85 MPa, the mantle subgrain size tends to increase with strain (Fig. 5.7).

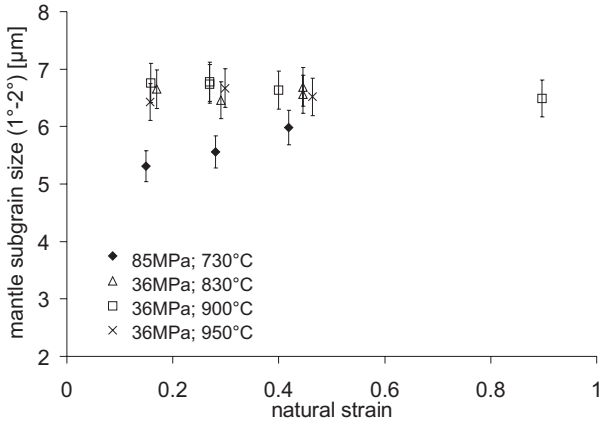

Fig. 5.7: Graph of the mantle subgrain size versus strain at the same misorientation interval (1°-2°) and different temperature and stress conditions (see legend).

5.5.3 Development of the mantle fraction per grain with strain

Both *M* and the number of mantle subgrains increase with strain, while the size of the mantle subgrains remains fairly stable (Table 5.1). This shows that *M* is related to the number of mantle subgrains rather than to the mantle subgrain size. The mantle fraction per grain is shown versus strain for one misorientation interval (1°-2°) in Figure 5.8. For the highest temperature series (>950°C), there is no influence of strain on the typically small mantle fraction per grain. For temperatures below 950°C, the mantle fraction per grain for subgrains (1°-2°) systematically increases with strain. The variations of *M* for two maps on the same sample (36LM830/0.45a,b) show that there is also an effect of the deformed grain size on *M*: in 36LM830/0.45a, *M* is larger than in 36LM830/0.45b, because in the sample (a) the average grain size is smaller (there are more small grains) in which the mantle fraction

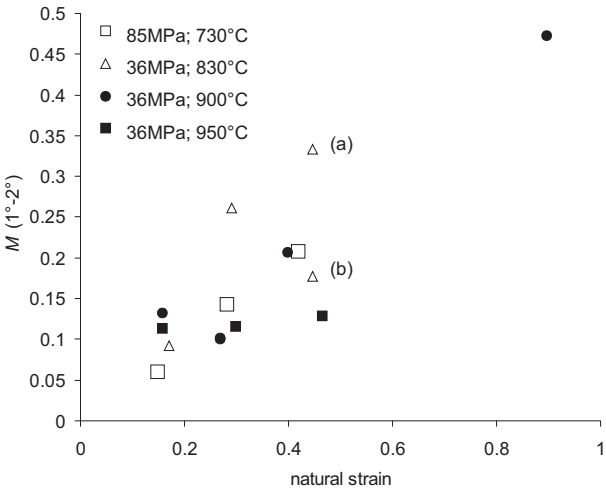

Fig. 5.8: Graph of the mantle fraction per grain (M) for misorientation interval (1°-2°) versus strain for different temperature and stress (see legend). The deformed grain size measured in 36LM830/0.45(a) is smaller than in 36LM830/0.45(b) (Table 5.1).

is larger (Table 5.1) (see also paragraph 5.4). So, while the mantle subgrain size is fairly homogeneous and does not change with strain, the number of mantle subgrains

differs from grain to grain and depends on deformation conditions.

5.6 Results: quantitative description of the core subgrain evolution with strain

5.6.1 Variation of core subgrain size with misorientation

The average size of the core subgrains is given in Fig. 5.9 as a function of the misorientation angle for samples at a constant strain of 0.45 (see also Table 5.1). The average core subgrain size increases with increasing misorientation angle and high misorientation core subgrains have sizes that are close to the deformed grain size (>10°). The slope of the hierarchy is dependent on the deformed grain size: the increase in core subgrain size is steeper for the larger grain sizes.

5.6.2 Development of average core subgrain size with strain

The influence of strain on the core subgrain size is considered for low (>1°), medium (>3°) and high (>5°) subgrain misorientation angles, because the misorientation has a significant effect on the core subgrain size, as shown in the previous paragraph (Fig. 5.10 - Appendix A and Table 5.1). The average low angle core subgrain size (>1°) does not show an obvious change with strain, while the average size of the core subgrains (>2° or higher), decreases systematically with increasing strain, except for the high temperature series 3 (950°C), which shows no significant change in core subgrain size with strain (see the crosses on Fig. 5.10 - Appendix A). The core subgrain sizes for the high stress series are somewhat smaller than for the 36 MPa series, but the trend with strain remains the same.

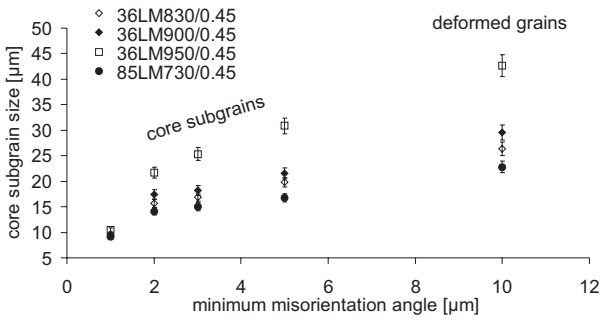

Fig. 5.9: Graph showing the variation of the core subgrain size with misorientation angle for samples at the same strain (0.45) (see legend). The size of deformed grains (misorientation >10°) has been indicated as a comparison.

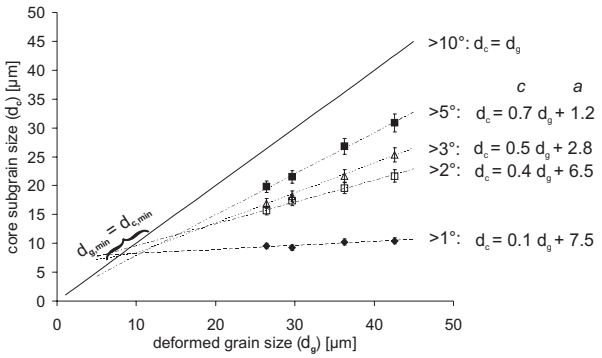

Fig. 5.11: Graph showing the relation between core subgrain size (dc) and deformed grain size (dg) for different misorientation angles. The equations of the best fits with the values for parameters c and a (Eqn. 5.4 – see text, 5.6.3) are shown on the figure. The best fits intersect roughly at the same point where dc = dg.

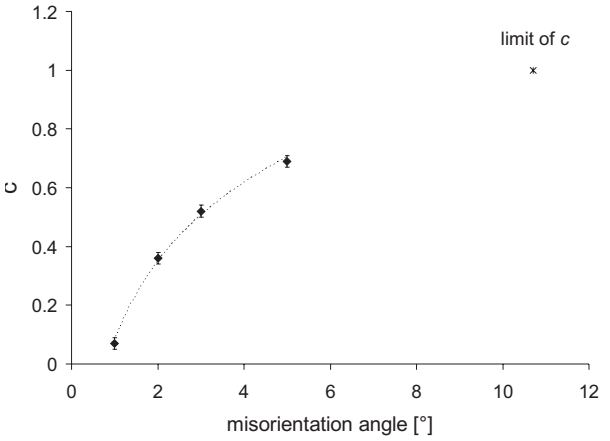

Fig. 5.12: Graph of the parameter c of Eqn. 5.4 versus misorientation angle. A non linear fit has been applied. The limit of c is 1, which is reached at misorientation angle 10.7° (see text, 5.6.3).

5.6.2 Relation of core subgrain size with deformed grain size

In Chapter 4, it was shown qualitatively that the core subgrains appear to be related to the deformed grains, deduced from the geometry of their boundaries being related to the geometry of the grain boundaries: core subgrain boundaries nucleate at the grain boundaries and sometimes their trace is (sub)parallel to the grain boundaries (Fig. 4.14 in Chapter 4, see also Fig. 5.4b, e, f - Appendix A). In this paragraph we will quantitatively examine the relation between the core subgrain size and the grain size. In order to have enough variation in grain size, average values from different samples have been taken, at the same strain and stress, but at different temperatures (Fig. 5.11). The core subgrain size increases with increasing grain size. For each misorientation, the relation between average core subgrain size, d_c, and average deformed grain size, d_g, can be described by linear relation (Fig. 5.11):

$$d_c = d_g + a \quad , \tag{5.4}$$

where c and a are empirical parameters. Two interesting characteristics can be seen from the linear best fits. Firstly, c increases with increasing misorientation from 0.1 at 1° to 0.7 at 5° (Fig. 5.11). Secondly, the best fit lines for different misorientations appear to intersect the line at roughly the point where $d_c = d_g$ (Fig. 5.11). Given the fact that d_c can never be larger than d_g, the minimum possible core subgrain size equals the minimum grain size and the intersection point is therefore where $d_{c,min} = d_{g,min}$. This intersection point can be calculated for the lines for each misorientation: $d_{c,min}$ appears to be similar within error for each misorientation, namely ~8 µm (Fig. 5.11). Based on the above, Eq. 5.4 can be rewritten:

$$d_c = d_{c,\min} + c\,(\theta)\,(d_{g,\min} - d_g) \quad , \tag{5.5}$$

The slope, c, can be described by a non-linear relation with the misorientation (Fig. 5.12). The limit of c is 1, which is reached at misorientation angles as high as grain boundary misorientations, such that only grain sizes are measured. The misorientation for which c = 1, is 10.7°, which corresponds very well with the maximum misorientation angles for a subgrain boundary that were suggested for calcite to range between 8° and 13° by Valcke et al. (2006) (Chapter 2).

The influence of grain size on the subgrain size is also seen by considering the variations of the core subgrain size on two maps of the same sample, 36LM830/0.45a & b. The core subgrain size is the largest in the map with the largest deformed grain size (Table 5.1).

5.7 Discussion

We first interpret the significance of the observed change in subgrain size with misorientation angle and the evolution of the mantle and core subgrain size with strain (paragraph 5.7.1 & 5.7.2). Secondly, the influence of temperature on the evolution of the subgrains with strain is discussed (paragraph 5.7.3). Thirdly, a link is made between the microstructural signature and the mechanical behaviour during minor weakening before a steady state is reached (paragraph 5.7.4). Lastly, considering the evolution with strain of the subgrains, suggestions will be made on which subgrain type is the best to use as an indicator of palaeostress (paragraph 5.7.5).

5.7.1 Significance of the changes in mantle subgrain size with misorientation angle and strain

The changes in mantle subgrain size with misorientation (Fig. 5.6) and strain (Fig. 5.7) are summarised schematically for their evolution with strain and misorientation (Fig. 5.13a & b). In this diagram, distinction is made between the low stress (36 MPa) – high temperature (830 – 950 °C) series 1-3 and the high stress (85 MPa) – low temperature (730 °C) series 4. At low stress, the size increases with misorientation and does not change with strain, while at high stress, the size is independent of the misorientation angle and slightly increases with strain. Combining the evolution of subgrain size and misorientation with strain, a visualisation of how the microstructure evolves is made in a simplified diagram for low stress – high temperature (Fig. 5.13c) and high stress – low temperature (Fig 5.13d).

At low stress, a hierarchy of the subgrain sizes exists (Fig. 5.13a). The mantle subgrains in this study are defined as containing no internal subgrains. Therefore this hierarchy is the result of a microstructure with small low angle subgrains next to larger high angle subgrains (Fig. 5.13c). This differs to the hierarchy of subgrain microstructure described by Trimby et al. (1998), in which the large high angle subgrains contain smaller, low angle subgrains (compare Figs. 5.14a and 5.14b). At high stress, for a given strain, the size does not change with increasing misorientation (Fig. 5.13a). This type of microstructure can be interpreted as the reflection of a uniform mantle microstructure (Fig. 5.13d).

With ongoing deformation, formation of new subgrains and/or a reduction in subgrain size and a flattening of the mantle subgrains could be expected due to an increase in strain. In contrast, over the range of stresses investigated, the subgrains remain unchanged or slightly increase in size (Fig. 5.13b) and they maintain approximately an equiaxed shape with increasing strain (Fig. 5.3). This suggests that 'growth' mechanisms have been active in maintaining the constant size and shape of mantle subgrains. In what follows, two possible mechanisms are described.

(1) Subgrain coalescence. This is a process of two subgrains rotating until they have a similar orientation. The low angle boundary between these subgrains decreases in misorientation until the boundary disappears and the two subgrains coalesce, causing an increased misorientation of the outer boundaries. The theory of subgrain coalescence has been developed in the context of static annealing (Hu, 1962; Li, 1962), though the topic is controversial because it requires very high homologous temperatures (0.9 T_m) for rotation to take place (Humphreys & Hatherly, 2004). Coalescence is rarely considered during deformation (Godfrey & Hughes, 2000). However, in our deformed samples, microstructures that imply subgrain rotation are commonly observed (see also Chapter 4) and therefore extremely high temperatures are clearly not required. Subgrain coalescence is favoured in regions of very dense subgrain wall spacings (Godfrey & Hugh-

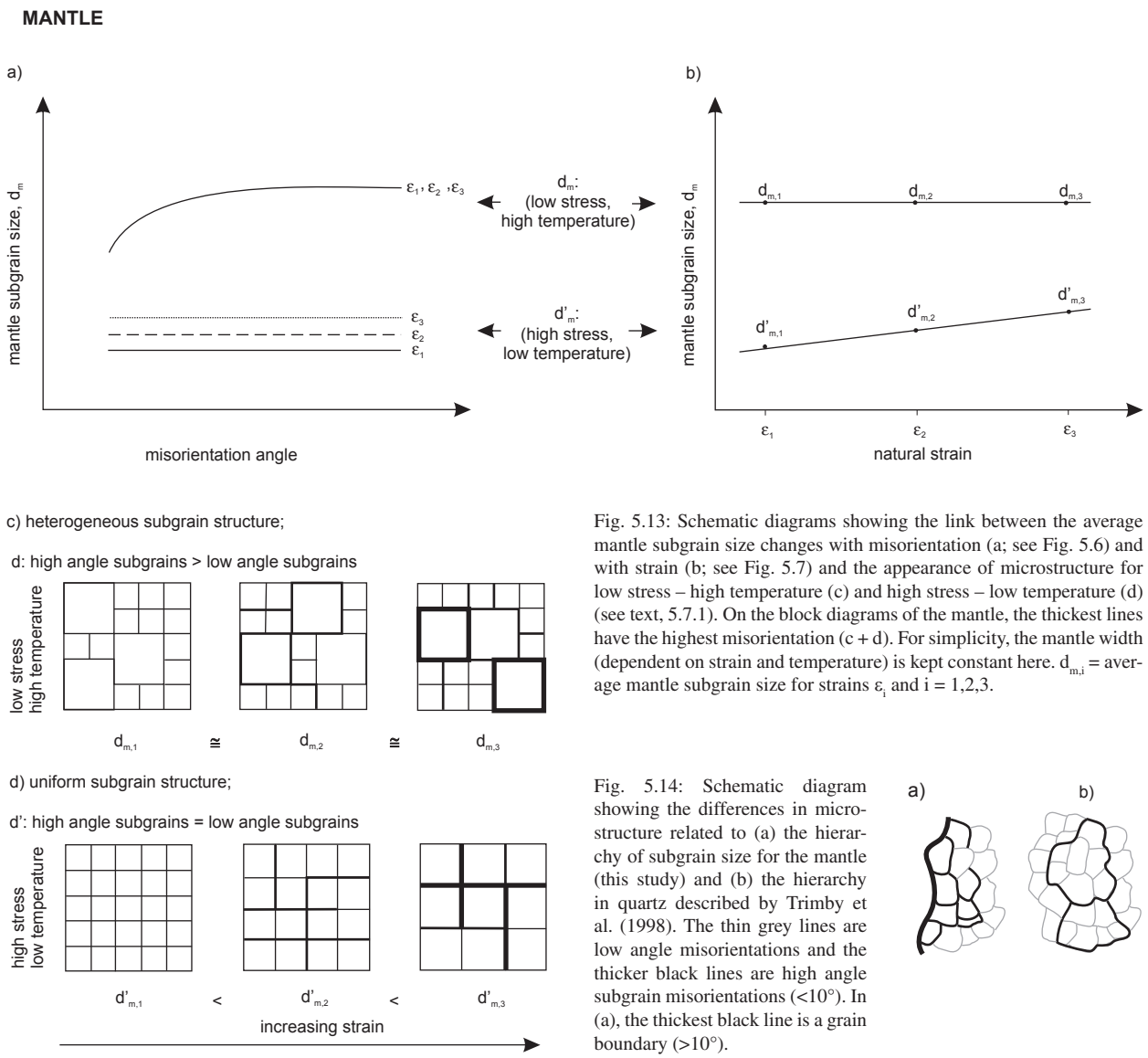

Fig. 5.13: Schematic diagrams showing the link between the average mantle subgrain size changes with misorientation (a; see Fig. 5.6) and with strain (b; see Fig. 5.7) and the appearance of microstructure for low stress – high temperature (c) and high stress – low temperature (d) (see text, 5.7.1). On the block diagrams of the mantle, the thickest lines have the highest misorientation (c + d). For simplicity, the mantle width (dependent on strain and temperature) is kept constant here. $d_{m,i}$ = average mantle subgrain size for strains ε_i and i = 1,2,3.

Fig. 5.14: Schematic diagram showing the differences in microstructure related to (a) the hierarchy of subgrain size for the mantle (this study) and (b) the hierarchy in quartz described by Trimby et al. (1998). The thin grey lines are low angle misorientations and the thicker black lines are high angle subgrain misorientations (<10°). In (a), the thickest black line is a grain boundary (>10°).

es, 2000). In our case, mantle subgrains with a relatively high amount of subgrain rotation and a dense subgrain structure compared to the core, form an ideal region for subgrain coalescence to take place.

(2) Subgrain boundary migration. It is known that the subgrain boundary energy increases with misorientation (Read, 1953; Humphreys & Hatherly, 2004). If temperatures are high enough and there are local driving forces for migration to take place, for example, in the presence of an orientation gradient, a migrating boundary will consume lower angle boundaries and accumulate the misorientation (Huang *et al.*, 2000). Consequently, this higher angle boundary surrounds a larger, strain free subgrain. Local driving forces can arise from the energy and orientation differences of adjacent boundaries and/or by differences in internal dislocation density of different subgrains. Subgrain boundary migration is mainly observed during static annealing (e.g., Ray *et al.*, 1975; Berger *et al.*, 1983), but is also occasionally observed during deformation (Means & Ree, 1988). Migration of boundaries is usually evidenced by bulging, wavy boundaries which occur when segments of the boundary are locally migrating faster than the rest of the boundary. However, mantle subgrain boundaries are short and are less likely to encounter significant velocity differences over very short lengths. This results in slightly curved subgrain boundaries rather than in distinct bulges of the subgrain boundaries.

While evidence of subgrain coalescence is virtually impossible to observe in a final microstructure, our calcite samples do show evidence for subgrain boundary migration. Namely, the mantle subgrain boundaries are mostly curved and can even locally show some cusp like, wavy shape (Fig. 5.5). Also, there are differences in dislocation density (Fig. 5.5). This implies a difference in strain energies between subgrains, which can provide a driving force for subgrain boundaries to migrate. In general, (subgrain) boundaries are more mobile

at higher temperatures and therefore subgrain boundary migration might occur faster and be more prominent in the low stress – high temperature samples (Exell & Warrington, 1972; Humphreys & Hatherly, 2004). On one hand, the higher mobility of subgrain boundaries at low stress – high temperatures might be the cause of the heterogeneous, hierarchical mantle subgrain structure (Fig. 5.13c), while at high stress – low temperatures, the low subgrain boundary mobility could be the cause of the sustained uniform subgrain structure (Fig. 5.13d). On the other hand, subgrain coalescence and limited subgrain growth with strain (Fig. 5.13d) might occur more easily in the high stress – low temperature samples because the mantle subgrain boundary density, which enhances subgrain coalescence, is higher in these samples compared to the low stress samples.

5.7.2 Significance of the changes in core subgrain size with misorientation angle and strain

The changes of the core subgrain size with misorientation, strain (for misorientations >2°) and grain size are summarised schematically in Fig. 5.15. The subgrain size shows a hierarchical behaviour (Fig. 5.15a): it increases with increasing misorientation angle until it reaches an upper limit size at misorientation angles (>10°) used to define a grain boundary. The hierarchy for the core subgrain sizes reflects that the large high angle subgrains contain smaller low angle subgrains, similar to the microstructure that corresponds to a hierarchy in the study of Trimby et al. (1998) (Fig. 5.14b and 5.15b).

The development of the core subgrains is closely linked to the size and shape of the grains, as core subgrains preferentially develop from grain boundaries and triple junctions and they are more densely spaced near grain corners (Fig. 5.4 and 5.15b - Appendix A). Because the core subgrain size is directly related to the deformed grain size (Eqn. 5.5, Fig. 5.15c), it is expected that the core subgrains are dependent on deformation conditions in a similar way as the deformed grains. Indeed, except for the lowest angle subgrains (>1°), both the deformed grain size and the core subgrain size decrease with increasing strain, especially for the low temperatures (see also paragraph 5.7.3) (Fig. 5.15d). The reason why the lowest angle, small core subgrains seem not to be dependent on strain is possibly because the formation of new low angle core subgrains might be balanced by 'growth' processes such that the low angle core subgrain size does not decrease with strain, similar to the mantle subgrains.

In what follows we discuss the meaning of the slope, c, in Eqn. 5.5. The size d_c in this equation is an average value and when, for example, $c = 0.5$, it does not mean

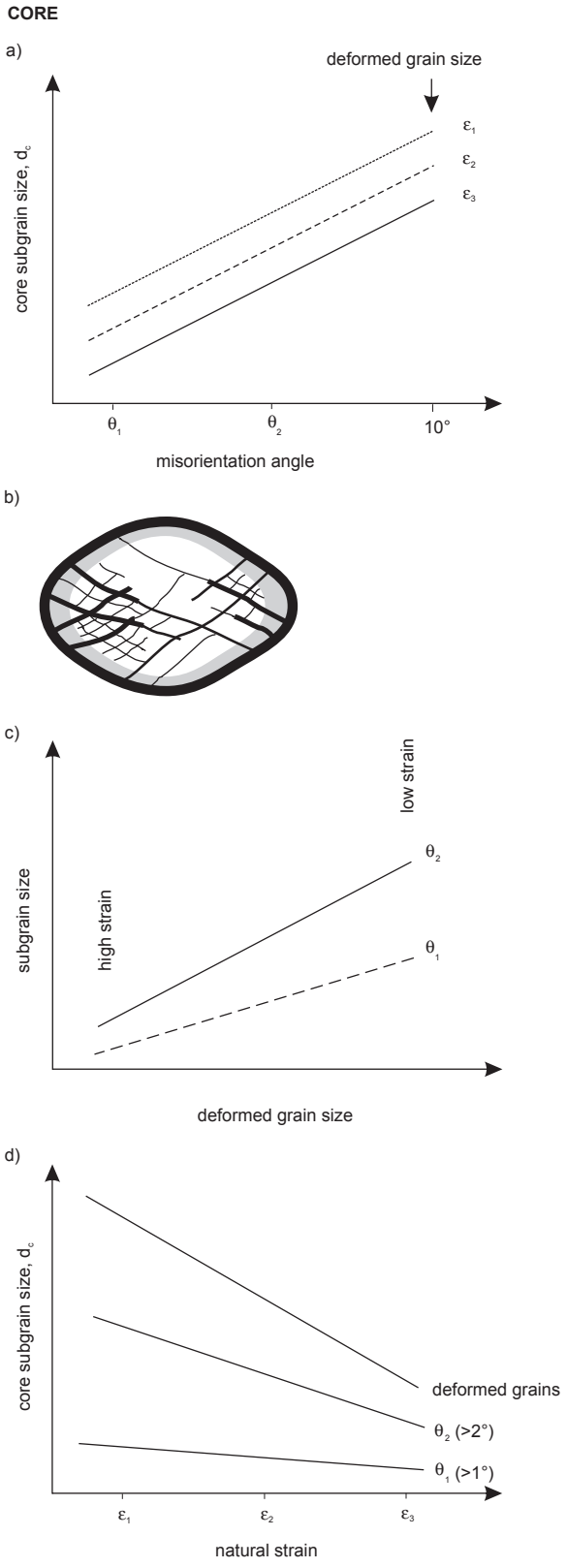

Fig. 5.15: Schematic diagrams showing the link between the average core subgrain size changes with misorientation (a, see Fig. 5.9) and appearance of the microstructure (b). The thickness of the black lines in (b) increases with misorientation, which is the highest at the grain boundaries. The mantle is indicated in grey. Schematic diagrams showing the evolution of the average core subgrain size (c) with strain (see Fig. 5.10) and (d) grain size (see Fig. 5.11).

that the deformed grain is divided by two equal sized subgrains (Fig. 5.16). Rather, the boundary subdividing the grain can be at any location within the grain; still, the average subgrain size will be half of the grain size. In other words, *c* does not really describe the geometry of the grain subdivision and the individual core subgrain sizes, but rather relates to the frequency or total length of the core subgrain boundaries within a grain: the larger *c*, the lower the amount of subgrain boundaries. Because the core subgrain boundary frequency decreases with increasing misorientation angle, *c* increases with misorientation angle. So in summary, the slope *c* of the linear relation (Eq. 5.5) shows that the core subgrain size is a fraction of the grain size and this fraction is dependent on the misorientation angle.

5.7.3 Microstructural development during minor weakening

The stress strain curves of the experimentally deformed Carrara marble samples, show that the material weakens at natural strains above 0.1 (Fig. 5.1) (Ter Heege *et al.*, 2002). High strain torsion tests on Carrara marble, done by Barnhoorn et al. (2004), have shown that it requires natural strains of about 3 before a true steady state is reached and the flow stress no longer changes with strain. There is much debate about which processes might be responsible for mechanical weakening leading to steady state behaviour during high temperature creep (e.g., Takeuchi & Argon, 1976; Means, 1981; Ter Heege *et al.*, 2002; Nabarro, 2006). A first step is to unravel which microstructures correspond to each type of mechanical behaviour. The experimental samples in this study all come from the minor weakening stage (0.15-0.9) where the material slowly weakens after having reached a peak. The formation of small recrystallised grains has been suggested to be a cause of minor weakening in Carrara marble owing to the increased contribution of grain size sensitive mechanisms (Ter Heege *et al.*, 2002) or to softening in subgrain free recrystallised grains. Below we discuss in detail which microstructural changes accompany this minor weakening.

The torsion experiments of Barnhoorn et al. (2004) show that in Carrara marble, steady state is attained when the material is fully recrystallised. In our Carrara marble samples, the microstructure for true steady state is predicted by extrapolating the observed microstructures at low strains to high strains. This is done using a conceptual model of the samples deformed at 36 MPa and 900 °C to different strains (Fig. 5.17c). Below the graph, simplified diagrams are made of the evolution of the microstructure towards a steady state. The main feature appearing from the graph is that the grain and subgrain sizes tend to develop towards a similar value at high strains. The deformed grain size reduces faster than the core subgrain size such that at high strains the grain size will become similar to the core subgrain size. Simultaneously, the mantle fraction per grain increases and the core subgrain size reduces, such that the subgrain structure becomes more homogeneous (Fig. 5.17c). It appears that the core subgrain size does not reduce to similar values as mantle subgrain size until the central region of the deformed grain has reduced significantly. In other words, the large grains never really contain a homogeneous subgrain structure until they have reduced in size so much that they are not much larger than the subgrains and they only contain a few subgrains, i.e., the core mantle subdivision disappears (Fig. 5.17c). From the graphs of the core subgrain size versus deformed grain size (Fig. 5.11) it was deduced that the deformed grain size decreases with strain to become similar to the subgrain size at values around ~8 μm (paragraph 5.6.3). This lies in the range of the recrystallised grain size in this study and also in the study of Barnhoorn et al. (2004). So when the deformed grain size has reduced to become similar to the core subgrain size, there is no longer a size difference between 'old' and recrystallised grains. In deformed microstructures where deformed grains and recrystallised grains have the similar small sizes, dynamic recrystallisation models suggest that subgrains develop in those grains that have slightly grown by migration, in order to subdivide these slightly larger grains and as such maintain a dynamically stable grain size (Kellermann Slotemaker, 2006).

The several stages of grain size reduction and recrystallisation with strain can actually be found in a single sample as different grains show different stages of subgrain development. For example, in the 0.90 strain sample there are small grains that approach a more homogeneous substructure with little differentiation between

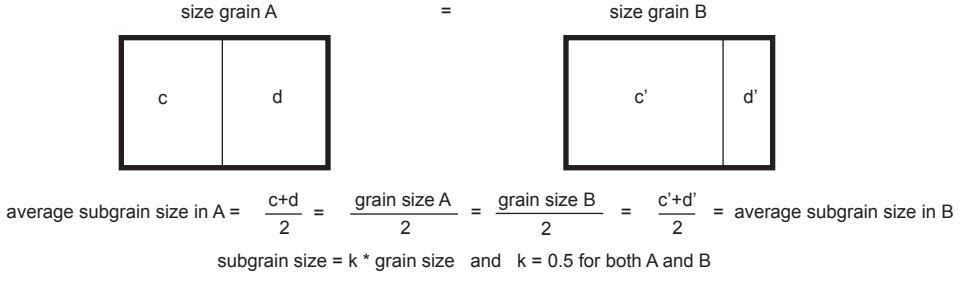

Fig. 5.16: Schematic diagram to explain that the parameter c does not describe the individual core subgrain sizes or geometry, but rather relates to the frequency of core subgrain boundaries within a grain.

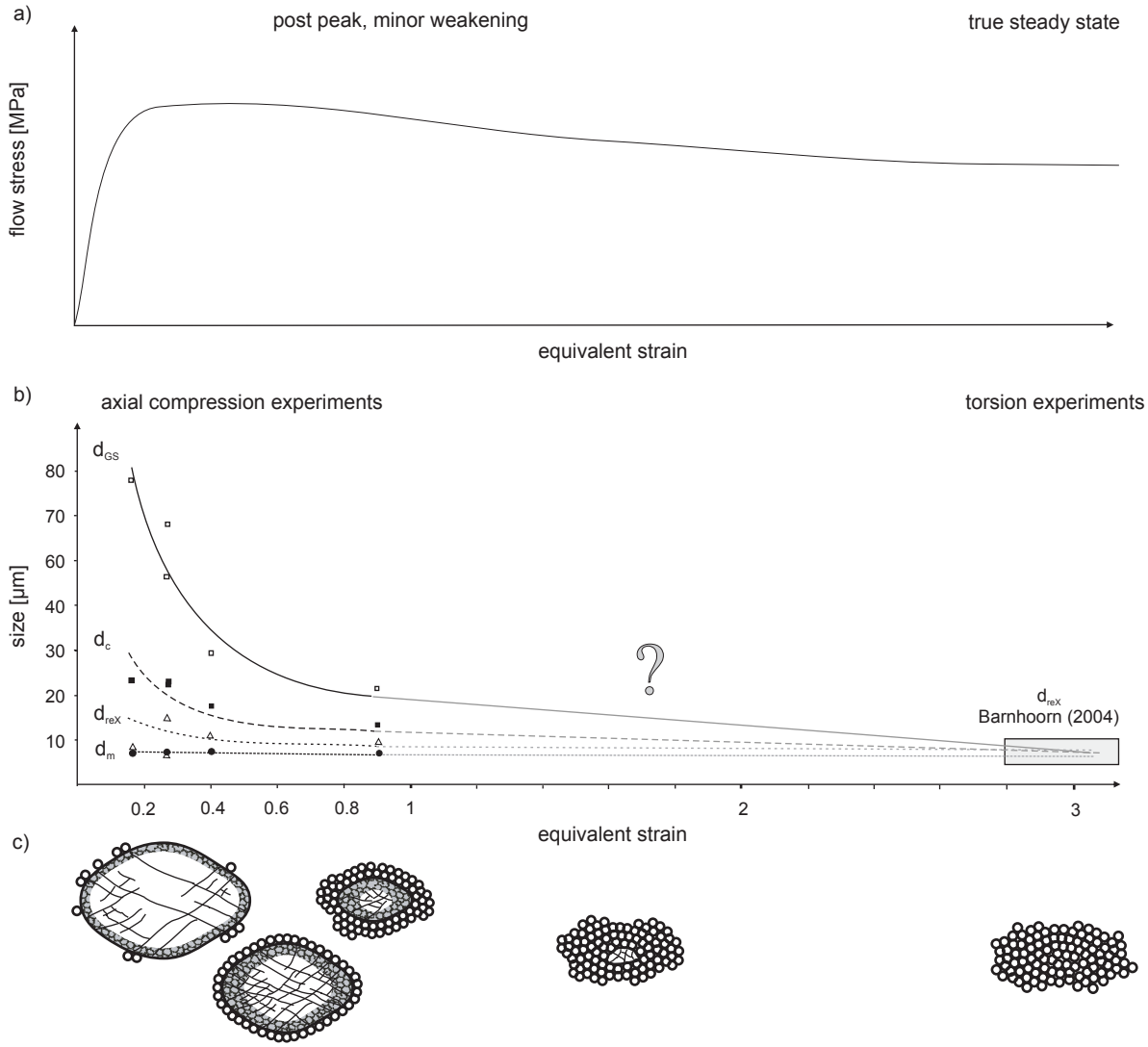

Fig. 5.17: Hypothetical diagram to show the link between the mechanical behaviour in calcite up to high natural strains (a) and the microstructures (b). (c) shows schematic diagrams of the microstructure evolving with strain: one deformed grain is drawn, surrounded by small, recrystallised grains. The thickest black lines are the grain boundaries and the thin ones are subgrain boundaries. The mantle is indicated in grey.

core and mantle, while there are other larger grains that still show a clear core mantle substructure (Fig. 5.4g - Appendix A).

It is uncertain if the torsion experiments of Barnhoorn et al. (2004) can be readily compared to the axial compression tests of this study, but it is encouraging that in axial compression as well as torsion, the old grains initially develop core mantle structures and recrystallise to sizes which are similar in both compression and torsion tests (Fig. 5.17b). The minor weakening part of the microstructural evolution as seen in our experiments compared to the high strain final microstructures of Barnhoorn et al. (2004), suggests that natural (equivalent) strains > 3 are needed to reach a 'recrystallised' microstructure (this is, when deformed and recrystallised grains have similar sizes) and a mechanical steady state.

5.7.4 Effect of temperature on the subgrain development with strain

Temperature has no significant effect on the evolution of the subgrain size of the mantle (Fig. 5.7). However, it does appear to influence the evolution of the mantle fraction per grain, *M*, and also the core subgrain size. At low temperatures, *M* clearly increases and the core subgrain size decreases with strain, while at the highest temperatures (950°C), *M* hardly increases with strain and the core subgrain size only slightly decreases with strain (Figs. 5.8 & 5.9). This means that the core subgrain size is not strongly developed at high temperature. We speculate that this is a consequence of the fact that temperature tends to increase the (subgrain) boundary mobility (Poirier, 1985) and more annihilation of the subgrain boundaries might take place at high temperatures. Alternatively, at homologous temperatures, T/T_m, above 0.3, disloca-

tions are more mobile with increased temperature (Evans *et al.*, 1967) and they might annihilate more rapidly (e.g., Karato & Ogawa, 1982). Therefore, at constant stress, an increased temperature could result in a lower dislocation density and consequently in fewer subgrain boundaries because dislocation density and subgrain boundary spacing are proportionally related (Holt, 1970). This suggests that high temperatures slow down the spread of the small mantle subgrains towards the grain interiors and the reduction of the core subgrain size. Consequently, a steady state situation might be reached at higher strains for high temperatures compared to low temperatures.

5.7.5 Which subgrains can be used for palaeopiezometry?

Models for palaeopiezometers assume a state of dynamically stable, homogeneous microstructures at given external conditions. They hardly ever describe the evolution towards this state (except Kellermann Slotemaker, 2006), meaning that it is not clear how fast a microstructure develops towards a dynamically balanced microstructure and it is not known how stress or temperature might influence this development. In this study the evolution of the microstructures with strain is investigated under different external conditions (stress and temperature) and it is shown that a dynamically balanced microstructure that no longer changes with strain, is reached only at very high natural strains (> 3). Moreover, samples deformed at high temperatures might reach this state later than samples deformed at low temperatures. This shows that dynamically stable conditions are not always met in experimental studies and also not in natural rocks (White, 1979; Trimby *et al.*, 1998). However, this does not exclude the use of palaeopiezometers as long as it is known how the size evolves with strain in the non-steady state situations. Even though the microstructure as a whole might not be homogeneous, there can be elements of the microstructure that quickly reach a dynamically stable size that no longer changes with strain. These are the most interesting microstructures to use in palaeopiezometry, because the relation between stress and size is not further complicated by an effect of strain.

In this chapter it has been shown that in heterogeneous microstructures such as in deformed Carrara marble, a balance between subgrain formation and 'growth' processes results in a dynamically stable mantle subgrain size at low strain (0.15), except for some minor growth of the subgrains in high stress samples. This suggests that mantle subgrains could be a reliable indicator of palaeostress, as long as the following aspects are taken into consideration:

(1) In this study, subgrains are considered in a material that shows a heterogeneous microstructure consisting of grains with core mantle substructures. This results in a palaeopiezometric relation that only can be used for mantle subgrains in heterogeneous microstructures. As soon as the structure is more homogeneous in terms of subgrain structure, for example, at low stresses (< 15 MPa, see Chapter 4) or at high natural strains >1 (see paragraph 5.7.3) the subgrain size – stress relation might be different. Therefore, when estimating palaeostresses in natural rocks, care should be taken that the same type of subgrains are measured as the ones on which the palaeopiezometer is based. This requires measurements using EBSD.

(2) At low stresses, a small hierarchy exists for the mantle subgrain size, meaning, the size increases slightly with misorientation. Consequently, when estimating palaeostresses, subgrains should be measured using EBSD and the same misorientations have to be considered as the ones for which the palaeopiezometer has been defined. In Chapter 6 it is shown that mantle subgrains have a different stress sensitivity depending on their misorientation angle and that high angle mantle subgrains are more useful for piezometric purposes due to their higher stress sensitivity compared to low angle mantle subgrains (see Chapter 6).

(3) The mantle subgrains considered in this study are from samples that show a minor weakening behaviour. This means that the flow stress is still slightly decreasing with increasing strain. Because the subgrain size increases with decreasing stress (Chapter 6), this can cause the mantle subgrain size to readjust following the small stress change. However, the stress decrease during weakening is small (final stress is 10-15% of the peak stress) such that the corresponding changes in subgrain size predicted from the stress – subgrain size relation (Chapter 6) are within error and even smaller than the slight increase in subgrain size with strain seen at high stress (85 MPa).

(4) The mantle subgrain size is in many cases smaller than the recrystallised grain size, especially at low stresses and higher temperatures, such that subgrain palaeopiezometers suggesting the mantle subgrain size to be equal to the recrystallised grain size are not valid (Schmid et al., 1980).

5.8 Conclusions

A set of experimentally deformed samples of Carrara marble was used to investigate the influence of strain on the development of the subgrain microstructure. It was found that within the deformation conditions studied (flow stress: 36 – 85 MPa; temperature: 730 – 950 °C; natural strain: 0.15 – 0.90), the microstructure is heterogeneous consisting of recrystallised and deformed grains

and, within the latter, core and mantle subgrains. Using electron backscattered diffraction (EBSD), these microstructures could be separated by applying the method described by Valcke et al. (2007 and Chapter 3).

At the same strain, the average mantle subgrain size shows a weak hierarchy of sizes with misorientation angle at low stress and shows no hierarchy at high stress. At strains of 0.15 to 0.90, the mantle subgrain size does not show much change, consistent with the limited decrease in stress. The maintenance of the dynamically stable size is attained by a balance between subgrain formation and 'growth' processes (such as subgrain coalescence and subgrain boundary migration).

At the same strain, the average core subgrain size increases with increasing misorientation until it reaches an upper limit size at misorientation angles (>10°) used to define a grain boundary. The core subgrain size decreases with strain at least up to strains of 0.90, which is related to a simultaneous reduction in the deformed grain size. Therefore the core subgrains are not straightforward to use for palaeopiezometry.

The mantle subgrain size is potentially useful as an indicator of palaeostress, because this microstructural element is invariant with strain, while core subgrains are not. However, to estimate palaeostresses in natural rocks using subgrains, only those piezometers should be used that have been calibrated for the same type of subgrains and the same misorientation.

The microstructural changes that accompany minor weakening towards steady state are an increasing amount of recrystallised grains, the increase in mantle fraction per grain and the simultaneous reduction of deformed grains and core subgrains until the sizes of the grains and subgrains have become similar. By comparison of the new results to previous data of Carrara marble deformed to high strains, it is inferred that when recrystallised grains are similar in size to deformed grains and in the latter the subgrains no longer show a core mantle substructure, a true mechanical steady state will be reached where the stress no longer changes with increasing strain. An increasing temperature tends to slow down the grain size reduction and the evolution towards a microstructure of uniform grain and subgrain size.

6

Influence of stress and temperature on the development of subgrains in experimentally deformed Carrara marble

Abstract

In deformed rocks, the average subgrain size is linked to deformation conditions and therefore could be a useful indicator for (palaeo) stress conditions. However, previous studies have shown that the subgrain size – stress sensitivity can vary depending not only on the material or deformation conditions, but also on the type of subgrains. This study uses electron backscattered diffraction to quantitatively investigate the subgrain structure in experimentally deformed Carrara marble (stress 20 – 85 MPa; temperature 700 – 990 °C; natural strain 0.45) and the relation between the subgrain size and deformation conditions. Carrara marble shows recrystallised and deformed grains that have heterogeneous core-mantle substructures. A mechanistic model based on slip system activation and stress intensification at grain boundaries in polycrystalline materials is proposed to explain the development of core-mantle substructures. The core subgrains originally are formed by easy slip and are not only dependent on stress, but also on grain size, strain and temperature. Because of this complex combination of parameters influencing the core subgrain size, these subgrains are not straightforward as indicators of palaeostress. The low angle mantle subgrains are formed by slip on more than one slip system. They have a low stress sensitivity, which is probably related to cross-slip as a deformation mechanism and/or geometrically necessary dislocations accumulating in the mantle. Due to their low stress sensitivity, low angle mantle subgrains are not strong indicators of palaeostress. In contrast, high angle mantle subgrains mainly occur mainly in grain boundary bulges and these subgrains are relatively more stress sensitive, such that they are more useful as indicators of palaeostress.

6.1 Introduction

The subgrain size in metals and rocks is related to the stress during steady state deformation (e.g., Bird *et al.*, 1966; Weertman, 1968; Takeuchi & Argon, 1976; Ross *et al.*, 1980; Poirier, 1985; Raj & Pharr, 1986). Therefore the subgrain size is potentially useful as an indicator of palaeostress in naturally deformed rocks with preserved deformation microstructures (e.g., Twiss, 1977; White, 1979; Pfiffner & Ramsay, 1982; Kenkmann & Dresen, 2002). In order to reliably estimate the palaeostress for a subgrain size measured in a natural rock, the empirical relationships between subgrain size and stress calibrated in laboratory experiments need to be underpinned by microphysical models, such that extrapolation to natural conditions can be done with confidence. Several theories have been suggested for the relation between subgrain size and steady state stress (Poirier, 1974; Twiss, 1977; Edward *et al.*, 1982; Orlova, 1996; Raj, 2002). The approaches in these theories are different (e.g., static versus dynamic models) and there is no consensus on a theory that succeeds in explaining all established empirical relationships or observations in natural rocks (e.g., Mercier *et al.*, 1977; White, 1979; Etheridge & Wilkie, 1981; e.g., Edward *et al.*, 1982; Poirier, 1985; Twiss, 1986). In particular, there are three assumptions in these models that have not been proven to be universally applicable.

(1) The first assumption is that stress is the only major factor influencing the subgrain size. However, several studies suggest that other parameters, such as temperature (e.g., Streb & Reppich, 1973; e.g., Orlova & Podstranská, 1998) and subgrain misorientation (e.g., White, 1973; Trimby *et al.*, 1998) can influence the subgrain size. Furthermore, amongst others, Ashby (1970) and De Bresser (1996) have suggested that in polycrystals, the grain size influences the dislocation density. Therefore, the grain size could also play an important role in the subgrain formation because the subgrain size is linked to the dislocation density (Holt, 1970).

(2) Secondly, many models assume a universal stress (σ) sensitivity of the subgrain size (d) of the type $d \sim \sigma^{-1}$, while empirical stress-subgrain size relationships show substantial variation: they all show that the subgrain size is inversely related to stress, but the sensitivities to stress vary between 0 and 2 (Edward *et al.*, 1982; Raj & Pharr, 1986; Twiss, 1986).

(3) The third assumption is that the subgrain size is dynamically stable and spatially homogeneous. However, many geological materials show a heterogeneous distribution of subgrains as well as evidence that the microstructure reflects a transient rather than a dynamically stable deformation stage. Also, the experimental materials used to calibrate the empirical relationships often have not reached a true mechanical and microstructural steady state. For example, the experimentally deformed Carrara marble in this study shows heterogeneous core-mantle substructures. While the mantle subgrain size is already relatively stable at low strain, the core subgrain size continues to decrease at least until natural strains of 0.90 (Chapter 5). Schmid et al. (1980) remark that the core subgrain sizes in Carrara marble do not show a stress dependency, while the mantle subgrain sizes are related to stress similar to the recrystallised grains. Alternatively, White (1979) suggests that core subgrain sizes are related to the bulk stress while mantle subgrains are related to local stresses. Both studies show that different subgrain types exist and that they might have different stress dependencies (cf., Means & Ree, 1988; Raj & Pharr, 1989), but the relations between stress and different subgrain types have not been quantified.

In the present study detailed and quantitative information on the different types of subgrains in experimentally

name	σ_{peak} [MPa]	σ_{final} [MPa]	ε	T [°C]	d_g [µm]	N_g	d_x [µm]	N_x	bulge size [µm] (~100 bulges)	d_m (1°-2°) [µm]	N_m (1°-2°)	M	d_m (2°-3°) [µm]	N_m (2°-3°)	d_m (3°-4°) [µm]	N_m (3°-4°)	d_m (>5°) [µm]	N_m (>5°)	d_c (>1°) [µm]	N_c (>1°)	d_c (>2°) [µm]	N_c (>2°)	d_c (>3°) [µm]	N_c (>3°)	d_c (>5°) [µm]	N_c (>5°)
25LM900/0.45	25.4	21.8	0.424	906	35.5	*545*	13.8	*325*	13.2	7.0	*4419*	0.27	8.4	*1262*	8.5	*568*	9.8	*204*	9.9	*3821*	18.1	*1498*	21.8	*1114*	27.4	*722*
25LM950/0.45	29.9	24.8	0.446	950	61.3	*60*	10.0	*44*	10.4	7.4	*1261*	0.06	8.4	*413*	8.8	*219*	8.4	*46*	11.3	*1746*	21.2	*519*	25.7	*321*	30.4	*170*
25LM990/0.45	28.1	25	0.386	992	45.7	*93*	14.8	*79*	11.3	7.9	*1722*	0.13	9.8	*632*	10.4	*325*	10.6	*129*	10.7	*1804*	21.0	*568*	23.4	*402*	28.6	*230*
36LM730/0.45a	43.4	38.7	0.446	835	26.4	*508*	9.0	*546*	10.9	6.7	*6505*	0.33	7.6	*2660*	7.7	*1448*	7.4	*651*	9.5	*3717*	15.7	*1802*	16.9	*1676*	19.8	*1143*
36LM830/0.45b	43.4	38.7	0.446	835	36.2	*283*	10.3	*247*	10.2	6.6	*3740*	0.18	7.6	*1208*	7.8	*628*	7.5	*262*	10.2	*2996*	19.6	*971*	21.7	*785*	26.8	*515*
36LM900/0.45	39.9	36.3	0.399	898	29.6	*164*	10.7	*146*	9.9	6.6	*3514*	0.21	7.2	*1216*	7.2	*636*	7.2	*228*	9.2	*2155*	17.4	*747*	18.2	*686*	21.5	*400*
36LM950/0.45	42.6	31.6	0.464	949	42.6	*202*	9.9	*151*	8.7	6.5	*2517*	0.13	7.1	*868*	7.3	*409*	6.8	*137*	10.4	*2254*	21.7	*637*	25.3	*484*	30.9	*339*
50LM730/0.45	58.5	52.1	0.435	731	22.0	*607*	7.7	*604*	8.9	6.4	*6825*	0.29	6.9	*2813*	6.8	*1536*	6.5	*739*	9.3	*3873*	13.3	*2315*	14.4	*1940*	16.8	*1319*
50LM780/0.45a	55.6	47.3	0.429	776	34.4	*333*	11.6	*277*	8.0	6.4	*3893*	0.20	7.0	*1368*	6.8	*672*	7.1	*252*	9.8	*3482*	15.9	*1510*	18.9	*1110*	23.2	*666*
50LM780/0.45b	55.6	47.3	0.429	776	36.2	*387*	11.0	*328*	8.1	6.5	*3569*	0.24	7.8	*1024*	7.7	*449*	7.8	*171*	9.5	*2946*	18.2	*1161*	21.9	*894*	26.3	*615*
50LM830/0.45	62.6	53.3	0.438	830	33.3	*318*	11.3	*207*	7.6	6.4	*5082*	0.26	7.0	*1822*	6.9	*958*	6.8	*392*	9.5	*3834*	15.3	*1750*	17.6	*1269*	22.0	*754*
65LM700/0.45	73.5	65	0.431	689	21.6	*720*	7.5	*678*	7.9	6.3	*8416*	0.36	6.7	*3262*	6.6	*1737*	6.4	*852*	9.0	*4420*	11.4	*3189*	14.3	*2290*	16.3	*1563*
85LM730/0.45	88.7	82.1	0.419	735	22.8	*308*	5.8	*419*	6.9	6.0	*5818*	0.21	6.3	*2225*	6.0	*1320*	5.5	*729*	9.1	*3697*	14.1	*1501*	15.0	*1279*	16.8	*878*

Table 6.1: List of samples used in this study with the deformation conditions (stress, (σ); natural strain (ε) and temperature (T) and the average sizes (mean) of the deformed grains (d_g), recrystallised grains (d_x), mantle subgrains (d_m) and core subgrains (d_c). The subgrains are measured for specific misorientation angle ranges. The error on the size measurements is 5%. N is the number of each microstructural element measured for calculating the mean. M is the mantle fraction for specific misorientation intervals. On samples indicated with a and b, two EBSD analyses have been performed in order to compare the variation within one sample. In the sample names the first number stands for the stress, LM for Lorano Marble, the second number is the temperature and the last is the natural strain.

deformed calcite is obtained using EBSD in order to test the applicability of the subgrain size-stress relationship for calcite for specific stress (20-85 MPa) and temperature (700-990°C) conditions. Apart from the influence of stress, the influence of temperature, grain size and misorientation on the subgrain size is investigated. Using EBSD, new insights on the formation of subgrains in deformed calcite can be obtained, providing input for the revision of current models on the relation between stress and subgrain size. The mantle and core subgrains are considered separately and their origin is investigated in order to explain their different behaviour in terms of stress dependency.

6.2 Material and approach

6.2.1 Carrara marble

The material used in this study is a set of cylindrical samples of Carrara marble (Lorano type), experimentally deformed under axial compression at a confining pressure of 300 MPa and strain rates between $3x10^{-6}$ and $3x10^{-4}$ s^{-1} (Ter Heege *et al.*, 2002 and this study). After the experiments, the samples have been rapidly cooled (ca. 70 °C/min) to limit static annealing. Experimental details can be found in Ter Heege et al. (2002). The samples used in this study are all deformed to the same natural strain, i.e., 0.45, but at different stress (20-85 MPa) and temperature (700-990 °C i.e., 0.5-0.7 T_m where T_m is the incongruent melting temperature of calcite in the system $CaO\text{-}CO_2$ at 100 MPa pressure – see Wyllie & Tuttle (1960)). Stress strain curves for selected samples are given in Figure 6.1. The curves show a broad peak stress (σ_{peak}), followed by minor weakening continuing up to the maximum strains reached. For the samples considered in this chapter, the weakening (= $(\sigma_{\phi inal} - \sigma_{peak})/\sigma_{peak})*100\%$) is typically 10-20% for strains up to 0.45. All stresses mentioned in this chapter are final stresses unless specified otherwise. More details on the experiments can be found in Ter Heege *et al.* (2002). The deformed samples were sectioned parallel to the maximum compression direction to make polished blocks for EBSD (Valcke *et al.*, 2006; Chapter 2).

6.2.2 Measuring sizes using EBSD

Electron backscattered diffraction (EBSD) data were collected and analysed using HKL Channel 5 software on a FEI XL30SFEG scanning electron microscope (SEM) with a Nordlys 2 CCD camera. Using automated EBSD, 1000 x 1000 grid maps were made with a step size of

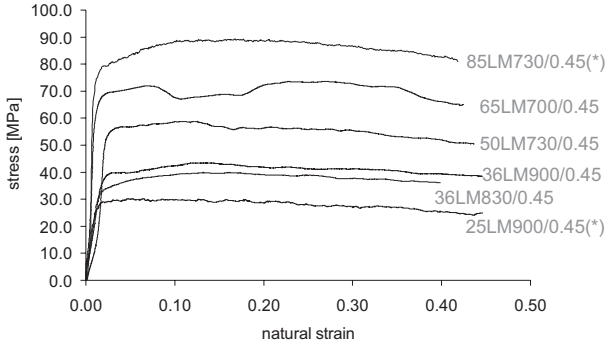

Fig. 6.1: Stress strain curves of a selection of the samples in this study. The samples with an asterisk are from this study and the others are from Ter Heege et al. (2002). The samples are named as in their study: the first number is the stress, LM stands for Lorano Marble, the second number is the temperature and the third number is the natural strain. Ter Heege et al. (2002) have shown that the flow stress at a given strain can be reproduced within ~10%.

1µm. More details on sample preparation, data collection and processing can be found in Chapters 2 (Valcke *et al.*, 2006) & 3 (Valcke *et al.*, 2007). Recrystallised (subgrain free) and deformed (substructured) grains have been separated using the method based on the average internal misorientation within the grain (AMG) (chapter 3 and Valcke *et al.*, 2007). Similarly, core and mantle subgrains are separated based on the average internal misorientation within a subgrain (AMS). This is done for domains with boundaries having misorientation angles within specific intervals: (1°-2°); (2°-3°); (3°-4°) and (>5°) for mantle subgrains and (>1°), (>2°), (>3°) and (>5°) for core subgrains (Chapter 5). The equivalent circular diameter methods for measuring the grain, subgrain and bulge sizes are described in Chapters 3 and 4. Furthermore, we use the parameter 'mantle fraction per grain' (*M*), which is the relative area covered by mantle subgrains adjacent to the grain boundary with respect to the more central parts of the grains, i.e., the total area of the mantle divided by the total area of the deformed grains on a 1000x1000 µm EBSD map (see Chapter 5).

Transmission electron microscopy (TEM) was used as a qualitative and descriptive tool to study the subgrain structure at scales smaller than the EBSD resolution. TEM samples were prepared on copper grids and were thinned using an argon ion beam thinner (beam 5 kV, 4-6°). Because grain boundary zones were preferentially thinned, grains easily dropped out and only narrow areas could be milled. Consequently, the zones that were imaged in TEM were located near grain boundaries rather than grain interiors. For this reason and also because of the limited size of the thinned area, small mantle subgrains were mostly imaged. A Tecnai 20 FEG was used, with a voltage of 200 kV, a current of 4400 µA, a spot size of 5 and a condenser aperture of 4. A double tilt holder was used to visualize the smallest subgrains (~0.5 µm) with misorientations down to 0.1° (Huang & Jensen, 2000; Kumar *et al.*, 2001). Bright field images of subgrains and dislocations were made using two beam conditions (McLaren, 1991). Misorientation angles could be measured by collecting diffraction patterns along the crystal zone axes and recording their accompanying tilt axes α and β of the sample orientation. A few calculations of this type were made and the misorientation between subgrains was often found to be around 1°. However, a systematic study of the misorientation angle distribution was not made as statistics would be too poor to provide complementary data to the large EBSD datasets (cf., Humphreys, 2001). In many of the subgrain boundaries, the individual dislocations could be clearly distinguished and the diffraction patterns on both sides of the boundary did not shift by more than a few degrees, which defines the boundaries as subgrain boundaries and not grain boundaries. The subgrain sizes were measured regardless of their misorientation angle and the average subgrain size is the average of horizontal and vertical line measurements. The maximum subgrain sizes that could be measured were around 15 µm, because the sample areas that were transparent enough for TEM imaging were not more than 15 µm wide. This means that TEM can provide data for the smallest size classes of the subgrain size distribution, but the data cannot be gathered in a statistically meaningful way such that they could complement the EBSD data. In contrast, EBSD provides thousands of subgrain sizes ranging from a few microns to hundred microns such that most part of the subgrain size distribution can be covered. Nevertheless, TEM images were used to check if the main changes of the subgrain size with deformation conditions also occurred in the smallest subgrain size classes. Also, TEM is a useful tool to image the dislocation structure and density within subgrains.

6.3 Qualitative description of the subgrain size evolution with stress and temperature: EBSD and TEM results

6.3.1 General remarks

An EBSD map of the undeformed starting material (not heated) is shown in Figure 6.2. The grains do not show a clear shape preferred orientation and they are fairly equiaxed. Many grains show straight e-twin boundaries. A few grain boundaries show bulges (Fig. 6.2). The isolated, low angle misorientation boundaries (>1°) that have a length of only a few pixels are artificial boundaries not related to real microstructures (see Chapter 3) (Fig. 6.2). There are no clear low angle boundaries that show a subgrain like structure.

In the deformed samples, the qualitative variations

2a	mantle								
	peak stress (σ_{peak})			final stress (σ_{final})			peak stress (σ_{peak})		
θ	$m_{m\ (low\ T)}$	$k_{m\ (low\ T)}$	R^2	$m_{m\ (low\ T)}$	$k_{m\ (low\ T)}$	R^2	$m_{m\ (all)}$	$k_{m\ (all)}$	R^2
(1°-2°)	0.12 ± 0.01	1.01 ± 0.02	0.95	0.11 ± 0.01	0.99 ± 0.02	0.96	0.16 ± 0.03	1.10 ± 0.07	0.77
(2°-3°)	0.24 ± 0.02	1.26 ± 0.03	0.98	0.23 ± 0.01	1.24 ± 0.02	0.98	0.27 ± 0.05	1.33 ± 0.08	0.75
(3°-4°)	0.28 ± 0.03	1.33 ± 0.03	0.96	0.27 ± 0.03	1.30 ± 0.04	0.96	0.33 ± 0.05	1.44 ± 0.09	0.78
(>5°)	0.43 ± 0.04	1.59 ± 0.07	0.97	0.42 ± 0.03	1.54 ± 0.06	0.98	0.42 ± 0.06	1.57 ± 0.10	0.80

2b	core					
	final stress (σ_{final})			final stress (σ_{final})		
θ	$m_{c\ (small)}$	$k_{c\ (small)}$	R^2	$m_{c\ (large)}$	$k_{c\ (large)}$	R^2
(>1°)	0.07 ± 0.02	1.08 ± 0.03	0.79	0.19 ± 0.03	1.31 ± 0.04	0.90
(>2°)	0.29 ± 0.01	1.66 ± 0.18	0.64	0.39 ± 0.09	1.89 ± 0.15	0.78
(>3°)	0.32 ± 0.07	1.75 ± 0.11	0.84	0.39 ± 0.10	1.95 ± 0.16	0.73
(>5°)	0.40 ± 0.07	1.96 ± 0.12	0.89	0.35 ± 0.09	1.98 ± 0.15	0.74

Table 6.2: Parameters m and k of the linear regression in log space to the subgrain size – stress data (Eqn. 6.1) for (a) mantle subgrains and (b) core subgrains per misorientation angle (θ) range. The regressions for mantle subgrains have been made for peak as well as final stress (paragraph 6.4.1), and for the core subgrains for final stress (see paragraph 6.5.2). For the mantle subgrains, the regression has been made (1) based on only the samples deformed at the lowest temperatures of each stress level (indicated by low T) and (2) including all samples (indicated by high T). For the core subgrains, regressions have been done for (1) samples with small average deformed grain sizes (<~35 μm) (indicated by small) and (2) large average deformed grain sizes (> ~35 μm) (indicated by large).

of the microstructure with deformation conditions are investigated using EBSD maps (Figs 6.3 and 6.4). The maps are grouped together such that the influence of each deformation parameter can be seen separately and for the purpose of comparison, some images are shown twice. In general, in all samples, most grains show a heterogeneous microstructure with core and mantle subgrains (Figs. 6.3 & 6.4 - Appendix A). The mantle subgrains are equiaxed and they have a fairly uniform size, while the core subgrains have a more variable size and shape. Mantle subgrains can be associated with a grain boundary in general (Fig. 6.3b-c Appendix A) or with a specific grain boundary bulge (Fig. 6.3e - detail - Appendix A). Henceforth, subgrains associated with bulges, are called bulge subgrains and subgrain boundaries connecting both ends of a bulge are called 'bridging' subgrain boundaries (Fig. 6.3e - detail - Appendix A). These bulge subgrains are distinct from other mantle subgrains that occur near grain boundaries but are not located at the grain boundary. The traces of core subgrain boundaries often form one to two parallel sets (Fig. 6.4h - Appendix A). The traces have a preferred orientation ranging between 45° to 60° to the compression axis, which can vary somewhat from grain to grain (Fig. 6.3a & d - Appendix A). Occasionally the traces of core subgrain boundary are parallel to the traces of grain boundaries (Fig. 6.3d - Appendix A).

6.3.2 Qualitative evolution of the subgrain size with stress from EBSD maps

The influence of stress is considered by comparing samples from four constant temperature series (Fig. 6.3 - Appendix A). In general, the variations in mantle subgrain size with stress appear to be small and are difficult to observe qualitatively. For example, in the first series, there is a decrease in mantle subgrain size going from 65 MPa to 85 MPa (e.g., Fig 6.3b-c).

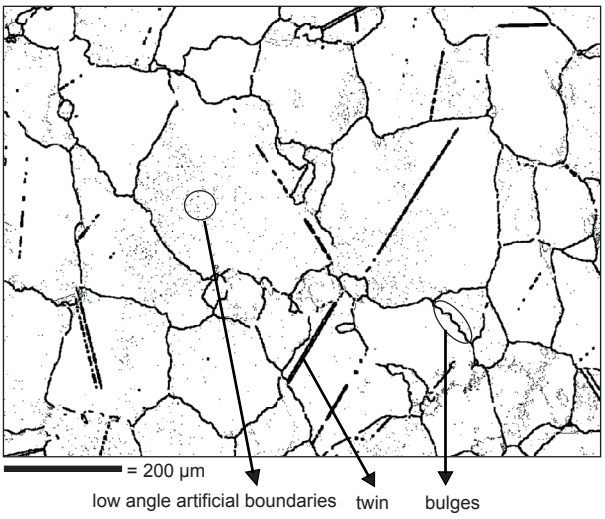

Fig. 6.2: EBSD map of the undeformed starting material. Grain boundaries >10° are indicated in thick black lines and low misorientation angle boundaries >1° are indicated in thin black lines. (Shown also as Fig. 4.4 and 5.3).

The core subgrain size is not related to stress in a systematic way: at low temperatures, it appears to decrease with stress from 50 MPa to 65 MPa, while it clearly increases with stress from 65 MPa to 85 MPa (Fig 6.3a-c). At higher temperatures, the core subgrain size increases with increasing stress (Fig. 6.3f-g and 6.3h-i - Appendix A). Stress does not seem to influence the preferred orientation of the core subgrain boundary traces in a systematic way.

6.3.3 Qualitative evolution of the subgrain size with temperature from EBSD maps

To investigate a possible temperature effect, three constant stress series are considered (Fig. 6.4 - Appendix A). The mantle subgrain size does not obviously vary with temperature although in each stress series, it can be seen that there are some exceptionally large mantle subgrains at higher temperatures. These subgrains are strain free domains, often at the corners of grains and therefore predominantly surrounded by a high angle grain boundary (Fig. 6.4h-i - Appendix A). It is not very obvious how the core subgrain size changes with temperature, although the grain interiors become less subdivided at higher temperatures. Temperature does not seem to influence the preferred orientation of core subgrain boundaries described in paragraph 6.3.1.

6.3.4 Local variations of the mantle and core subgrains

An important observation for all samples is that in the mantle region, the high angle subgrain boundaries occur predominantly at grain boundaries as bridging subgrain boundaries, so the high angle subgrains are often bulge subgrains (Fig. 6.3e - Appendix A). Low angle subgrain boundaries occur at grain boundaries but are predominantly located further away from the grain boundary (Figs. 6.3b-c). Straight core subgrain boundary traces are often either associated with triple junctions, either they depart from grain boundaries and rather subdivide the grain centers. Parallel subgrain boundary traces often occur forming a band (Fig. 6.4c - Appendix A). The most obvious variations in core subgrains are to be seen in deformed grains of different size: smaller grains contain a denser network of core subgrains. Within one grain, the denser core subgrain networks occur near grain corners and in places where the grain boundaries are less widely spaced. Some long core subgrain boundary traces have a wavy geometry (Fig. 6.5).

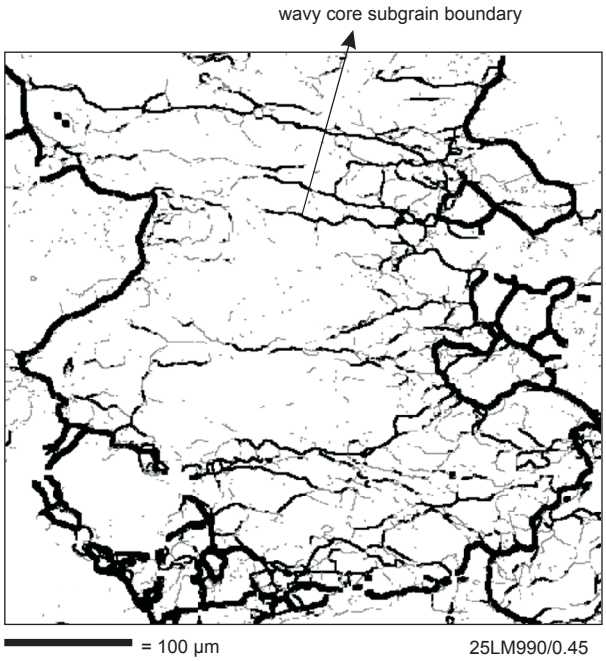

Fig. 6.5: Detail of an EBSD map of sample 25LM990/0.45 showing straight and wavy traces of core subgrain boundaries. Grain boundaries having misorientation angles >10° are indicated by thick black lines; subgrain boundaries >1° in grey; >2° in thin black lines. Compression axis is vertical.

6.4 Quantitative description of the mantle subgrain size variation with stress and temperature

6.4.1 Mantle subgrain size and mantle fraction per grain versus stress and temperature

Table 6.1 summarizes all EBSD subgrain size data. Figure 6.6 shows that the mantle subgrain size for a misorientation interval (1°-2°) decreases with increasing peak as well as final stress. There is some scatter at low stress-high temperature, maybe due to a temperature effect. In Figure 6.7 the mantle subgrain size is plotted versus temperature for a constant misorientation interval (1°-2°). At low stress (25 MPa) the subgrain size increases with increasing temperature, while at the higher stress levels the temperature does not have an effect. Because of this small effect of temperature at low stresses, we consider only the lowest temperature data of each stress series when deducing a quantitative relationship between stress and subgrain size. We do this for each misorientation and for peak (Fig. 6.8 – Table 6.2a) as well as final stress (Table 6.2a). In logarithmic space, the best fit equation is of the form:

$$\log d_m(\theta) = - m_m(\theta) \log \sigma + k_m(\theta) \quad , \qquad (6.1)$$

where $d_m(\theta)$ is the mantle subgrain size for a specific misorientation (θ) range, σ is the peak or final stress, and $m_m(\theta)$ and $k_m(\theta)$ are variable parameters, dependent on θ (Table 6.2a). The best fit for each misorientation range is similar (within error) for peak as well as final stresses and the correlation is very good, with R^2 values above 0.95 (Table 6.2a). The sensitivity to stress of the subgrain size, given by the slope of the linear trend (parameter m_m), increases with increasing misorientation and the values lie between 0.11 and 0.43 (Fig. 6.9). Including the higher temperature data in the dataset results in best fits for each misorientation range with a similar stress sensitivity, m_m, (within error), but the dispersion of the trend is larger at low stress - high temperature (Fig. 6.10) and the R^2 value decreases (Table 6.2a), meaning, the quality of the best fit is poorer.

The mantle fraction per grain for low angle subgrains,

M (1°-2°), decreases with increasing temperature, while at constant temperature, stress does not seem to have an effect on *M* (Fig. 6.11). The scatter in the data is related to the effect of deformed grain size on *M*: with decreasing deformed grain size, *M* becomes larger (Chapter 5) (Fig. 6.11).

6.4.2 Relation between mantle subgrains and grain boundary bulges

The size of the mantle subgrains is linearly related to the size of the bulges (bulge size data from Chapter 4). The mantle subgrains (>5°) are only slightly smaller than the bulges, while the low angle mantle subgrains (1°-2°) are much smaller than the bulges and have a weaker relation with them (Fig. 6.12).

6.5 Quantitative description of the core subgrain size evolution with stress and temperature

6.5.1 Core subgrain size versus deformed grain size and temperature

It was shown in Chapter 5 that the core subgrain size (d_c) is related to the deformed grain size at constant strain ($\varepsilon = 0.45$), which is confirmed here for the samples in this study (Fig. 6.13). The core subgrain size increases linearly with increasing deformed grain size for all misorientation angles, although the core subgrain size changes more rapidly with deformed grain size at higher misorientations (Fig. 6.13).

The deformed grain size is known to increase with increasing temperature (Chapter 4), thus also a relation between the core subgrain size and temperature is expected. Indeed, the average core subgrain size increases with increasing temperature for all misorientation angles, although at higher misorientation angles this increase is stronger (Fig. 6.14).

6.5.2 Average core subgrain size versus stress

Because the core subgrain size considerably decreases with strain (see Chapter 5), it can be related only to the stress at the considered strain increment. As we consider the final microstructure at the end of the deformation, i.e., at $\varepsilon = 0.45$, the core subgrain size is plotted in function of final stress. In general, the core subgrain size decreases with stress, but the data are considerably scattered (Fig. 6.15). Because the core subgrain size is dependent on the grain size (see above), we have separated the smallest grains (≤ ~35μm) (lowest temperatures) from the larger grains (> ~35μm) (higher temperatures) for each stress level. Two linear trends for the small and large grains, can be fitted to the data (Fig. 6.14), with an equation of the following form:

$$\log d_c(\theta, d_g) = m_c(\theta, d_g)\log\sigma + k_c(\theta, d_g), \quad (6.2)$$

in which the stress sensitivity, $m_c(\theta, d_g)$ and parameter $k_c(\theta, d_g)$ are dependent on the subgrain misorientation, θ, and on the deformed grain size, d_g (Table 6.2b). Both m_c as well as k_c increase with increasing misorientation angle. For all misorientations, the deformed grain size has an influence on the core subgrain size (Fig. 6.13), with the core subgrains being larger in large grains than in small grains. For low angle core subgrains (>1°), the deformed grain size also has an influence on the stress sensitivity m_c (Table 6.2b), namely, the low angle (>1°) core subgrain size in the small grains is almost insensitive to stress ($m_c = 0.07$), while in the large grains, the size is more sensitive to stress ($m_c = 0.19$). At higher misorientation angles, the stress sensitivity is not dependent on the grain size.

6.6 Characteristics of subgrains from TEM micrographs

The mantle subgrain sizes and characteristics have been studied by TEM in three samples: 36LM900/0.45, 50LM730/0.45 and 85LM730/0.45, that is, for three different stress levels. In general, the sizes observed are smaller than those obtained from EBSD maps (Table 6.1). The average of the TEM measurements shows no stress dependence, but it should be noted hereby that the measurements are based on a small number of measurements (Fig. 6.16). Systematic measurements for variations in temperature have not been done.

A qualitative observation from the TEM micrographs is that many subgrains have 'wavy' boundaries (Fig. 6.17a-c). Wavy boundaries often separate subgrains that appear to have different dislocation densities (Fig. 6.17a & c).

6.7 Discussion

6.7.1 General

As the starting material does not contain pre-existing subgrains, the subgrain size formation and evolution seen in this study is solely related to the deformation conditions during the experiments. The results show that the subgrain size is not only dependent on stress, but also on temperature and the intrinsic parameters, grain size and misorientation angle. Moreover, the mantle and core subgrains have a different dependency on these parame-

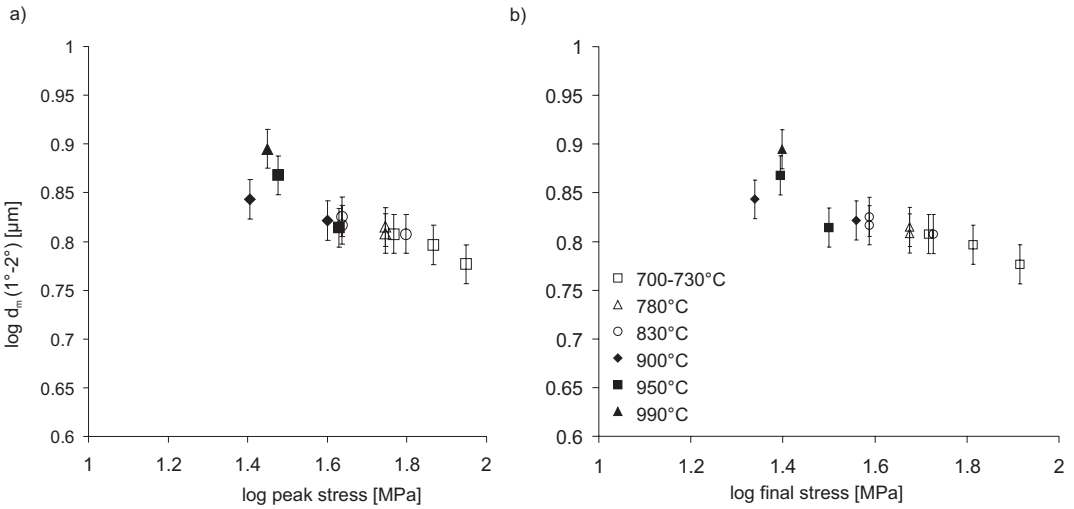

Fig. 6.6: Graph showing the mantle subgrain size (d_m) for misorientation range (1°-2°) as a function of (a) peak stress (σ_{peak}) and (b) final stress (σ_{final}).

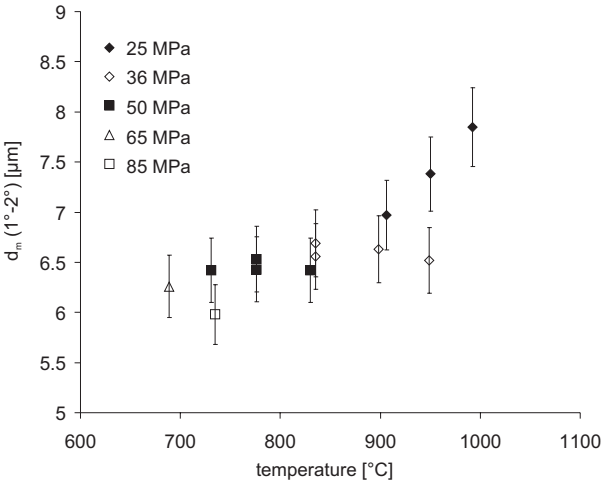

Fig. 6.7: The relation between mantle subgrain size and temperature for nominally constant stress series.

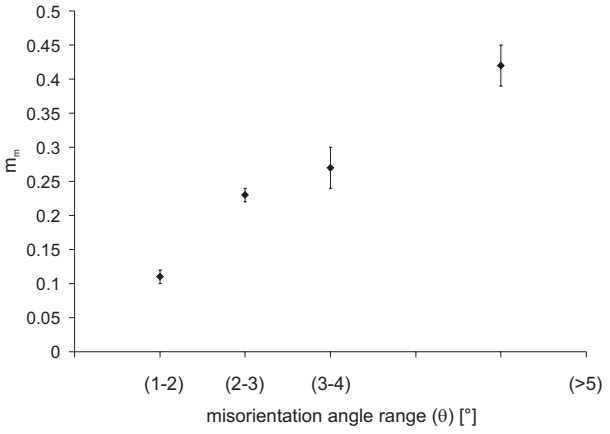

Fig. 6.9: Relation between the stress sensitivity (mm) of the mantle subgrain size and the misorientation angle range of the mantle subgrain boundaries.

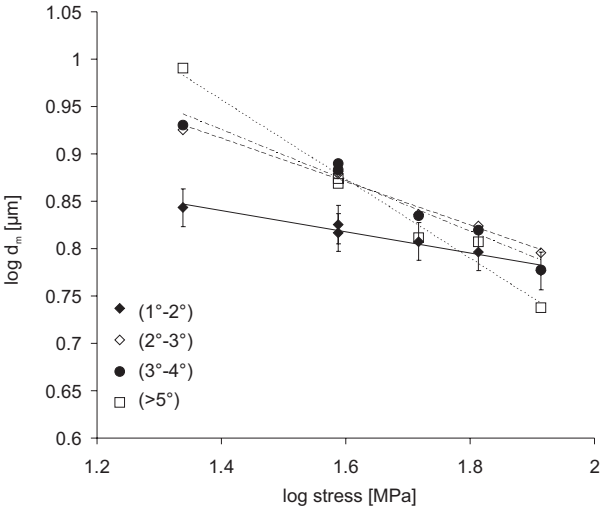

Fig. 6.8: Graph showing the mantle subgrain size as a function of peak stress for various misorientation ranges for only the lowest temperature data (at 25 MPa: 900°C / at 36 MPa: 830°C / at 50 MPa: 730°C / at 65 MPa: 700°C / at 85 MPa: 730°C). Linear best fit lines are shown according to equation 6.1. The parameters km and mm are summarized in Table 2a, for peak as well as final stress.

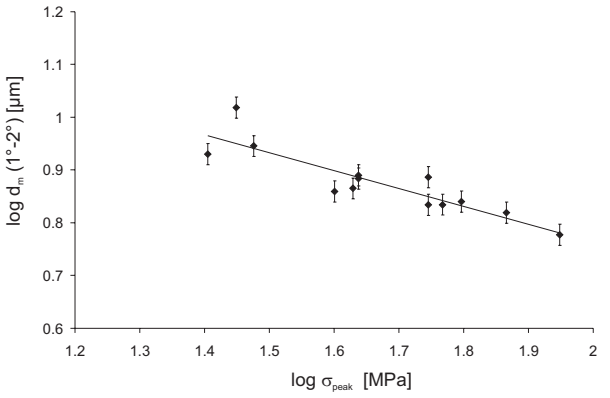

Fig. 6.10: The complete temperature data of the mantle subgrain size (dm) in relation to peak stress. The linear best fit line according to eqn. 6.1 is shown for the misorientation range (1°-2°). The parameters are summarized in Table 6.2a.

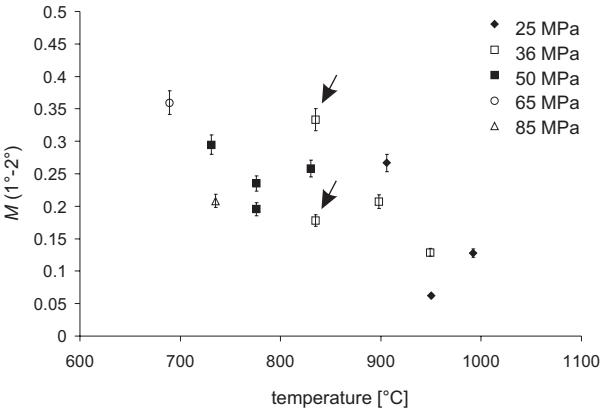

Fig. 6.11: Graph showing the mantle fraction per grain, M, as a function of temperature. The data points indicated with an arrow are measured on two EBSD maps on different areas of the same sample (36LM830/ 0.45a&b) and the difference in the mantle fraction per grain is related to the difference in average deformed grain size (see Chapter 5).

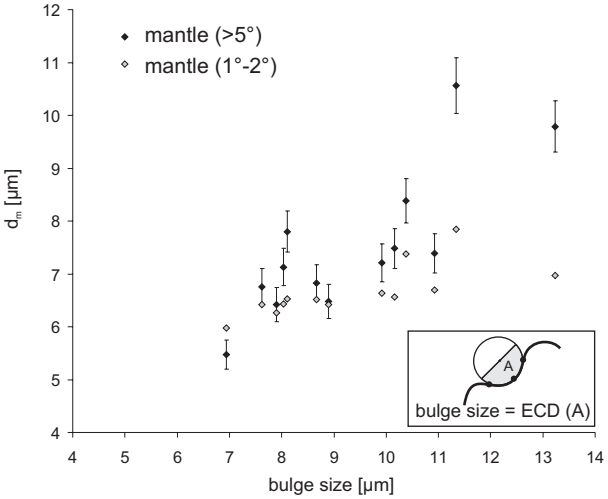

Fig. 6.12: a) Graph showing the relation between the low angle (1°-2°) and high angle (>5°) mantle subgrain size (d_m) and the bulge size. The bulge size data are taken from Chapter 4. (b) measurement of the bulge size:three points are selected on the grain boundary bulge; from these points a circle is constructed and the bulge size is the equivalent circular diameter (ECD) of half the circle. The errors on the size measurements are 5% (see Chapter 3 and 4) and are shown for the high angle mantle subgrains.

ters. In paragraph 6.7.2 we propose a mechanistic model for the development of the mantle and core substructure. In paragraphs 6.7.3 and 6.7.4, the relation between stress and subgrain size is discussed: firstly, reasons for variable stress sensitivities for subgrain size are investigated (paragraph 6.7.3) and secondly, a possible explanation is given for the low stress sensitivity particularly for the low angle subgrains (paragraph 6.7.4). In paragraphs 6.7.5 and 6.7.6 the influence of grain size and temperature on the subgrain size are discussed.

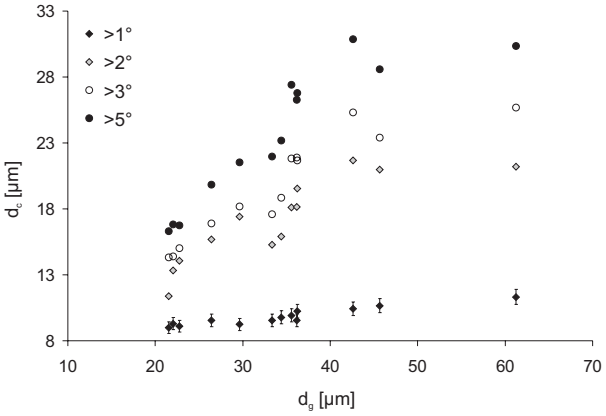

Fig. 6.13: Graph showing the relation between the core subgrain size (dc) and deformed grain size (dg), no distinction is made based on stress or temperature. The errors (5% for all measurements; Chapter 3) for the low angle core subgrains are shown.

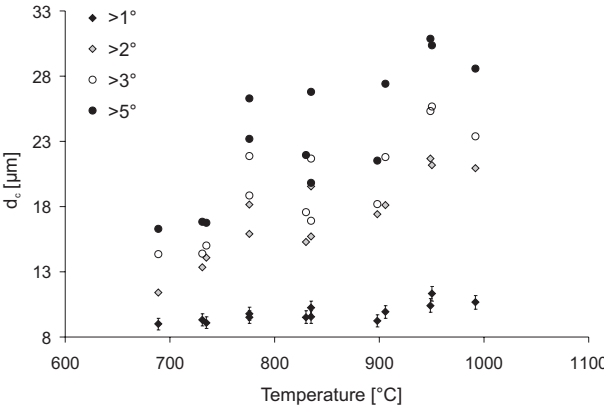

Fig. 6.14: Graph showing the relation between core subgrain size (dc) and temperature, no distinction is made based on stress or grain size.

6.7.2 Model for development of the core-mantle substructure

In a polycrystal deforming by high temperature creep, cross-slip and climb generally act together to enable homogeneous deformation to occur by dislocation motion on multiple independent slip systems (Groves & Kelly, 1969). This requires that the slip systems have similar critical resolved shear stresses (CRSS), i.e., shear stresses necessary to activate the slip system. This is true for many metals, but geological materials are often plastically anisotropic and the CRSS of their independent slip systems can be significantly different. If the applied stress results in (resolved) shear stresses acting on the slip planes at values above the CRSS of several independent slip systems, then slip on multiple systems can occur, but if the resolved shear stresses are lower than the CRSS of most slip systems, then it is possible that only one slip system can be active (single slip). Within a polycrystalline, plastically anisotropic sample, the slip system activation might differ locally due to local stress changes, caused for example by stress intensification at

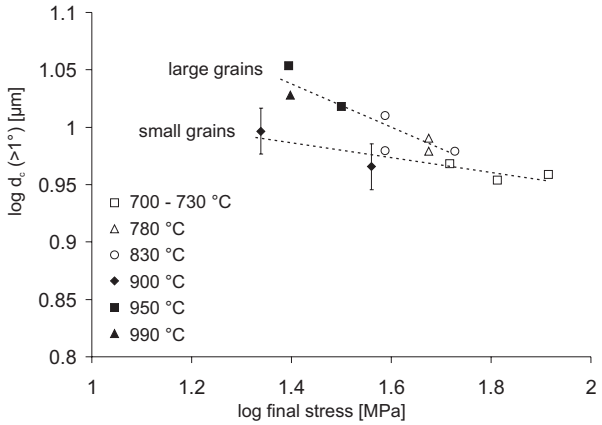

Fig. 6.15: Relation between core subgrain size and stress for different temperatures. Best fit lines are indicated for large grains (> ~35 µm) and for small grains (< ~35 µm). The errors on the measurements are 5% and indicated for two samples.

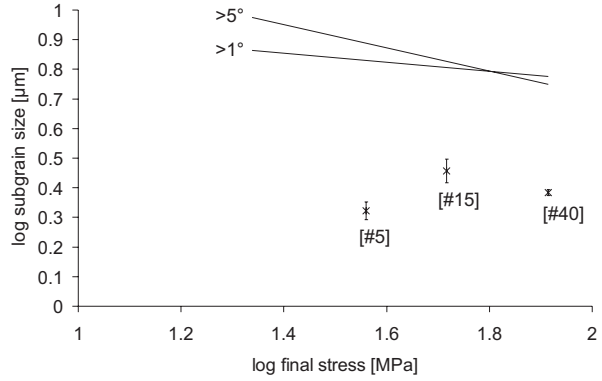

Fig. 6.16: Average subgrain size measured using TEM. The measurements are done in the mantle regions of grains. The standard errors and number of measurements are indicated at the datapoints on the graph. For comparison the trend for the mantle subgrain sizes (>1°) and (>5°) measured using EBSD is shown.

grain boundaries. White (1979) has shown that stress intensification and the activation of different slip systems in quartz can result in a core and mantle substructure, but all current subgrain size stress models assume homogeneous deformation resulting in a homogeneous substructure and ignore the possible effect of inhomogeneous (multiple) slip system activation and core-mantle development. For example, the Edward model (Edward *et al.*, 1982) has a cubic geometry which is based on the activation of only two slip systems, having the same slip plane but opposite signs. Considering the above ideas on slip system activation, we have developed a mechanistic model to explain the heterogeneous core-mantle substructure in calcite in relation to stress, temperature and grain size.

It is shown that in calcite, multiple slip may occur (De Bresser & Spiers, 1990). The classical work of Turner et al. (1954) and Griggs et al. (1960) has shown that there are three important systems in calcite, namely, e-twinning on $e\{\bar{1}018\}\langle 40\bar{4}1\rangle^{+}$ (three systems), slip on $r\{\bar{1}014\}\langle\bar{2}021\rangle^{\pm}$ (three systems) and slip on $f\{\bar{1}012\}\langle 2\bar{2}01\rangle^{\pm}$ (six systems). More recent studies have revealed the existence of additional subsidiary glide systems, such as $f\{\bar{1}012\}\langle 10\bar{1}1\rangle^{\pm}$ and $c\{0001\}\langle\bar{1}2\bar{1}1\rangle$ (cf., De Bresser & Spiers, 1997). The critical resolved shear stress (CRSS), which is the shear stress resolved on the slip plane in the slip direction needed to produce significant plastic deformation, is different for each slip system and is dependent on temperature. For example, for single crystals of calcite, the CRSS of the weak *r*-slip system is one-fourth of the CRSS of the harder *f*-slip system within the temperature range considered in this study (De Bresser & Spiers, 1997). We consider the slip system activation within a grain in a polycrystal in two steps:

(1) Starting from the first increment of strain, stress will raise until the point is reached that the resolved shear stress on the weakest system equals the CRSS, so that this easy slip system is activated to produce macroscopic plastic strain. Note that in calcite easy slip can occur on more than one slip plane. At this point, the stress within a grain is still relatively homogeneously distributed and is probably close to the bulk stress. During this event of easy slip, straight subgrain boundaries are formed, departing from grain corners and grain boundaries and running into the core of the grains (see image of a low strain sample in which the mantle has not significantly developed yet - Fig. 6.18 taken from Chapter 5). The straight core subgrain boundaries are parallel and have a preferred orientation at ~ 40°-60° with the compression axis (Figs. 6.3-6.5). This orientation can slightly change from grain to grain, which suggests that these boundaries are likely linked to parallel sets of crystallographic planes (Fig. 6.3-6.4 - Appendix A). These boundaries may develop by glide polygonization parallel to the slip planes or by recovery of dislocations into walls at high angle to the slip plane. These boundaries do not disappear at higher strains, but develop higher misorientation angles and will form part of both the mantle and core substructure (Fig. 6.5). The straight subgrain boundaries are not evenly spaced throughout the grains (Figs. 6.3 & 6.4) and the spacing is likely to be a complex combination of the deformation conditions and geometry of the grains (see paragraphs 6.7.3-6.7.6).

(2) As the strain further increases, the dislocations continue to glide on the single slip planes and accumulate at the grain boundaries, which results in a local stress increase at the grain boundaries (Humphreys, 1981). Moreover, single slip alone can no longer accommodate the increasing strain imposed by the external conditions, especially at the grain boundaries because grains tend to respond differently to deformation depending on the orientation of their slip planes. This results in a strong strain

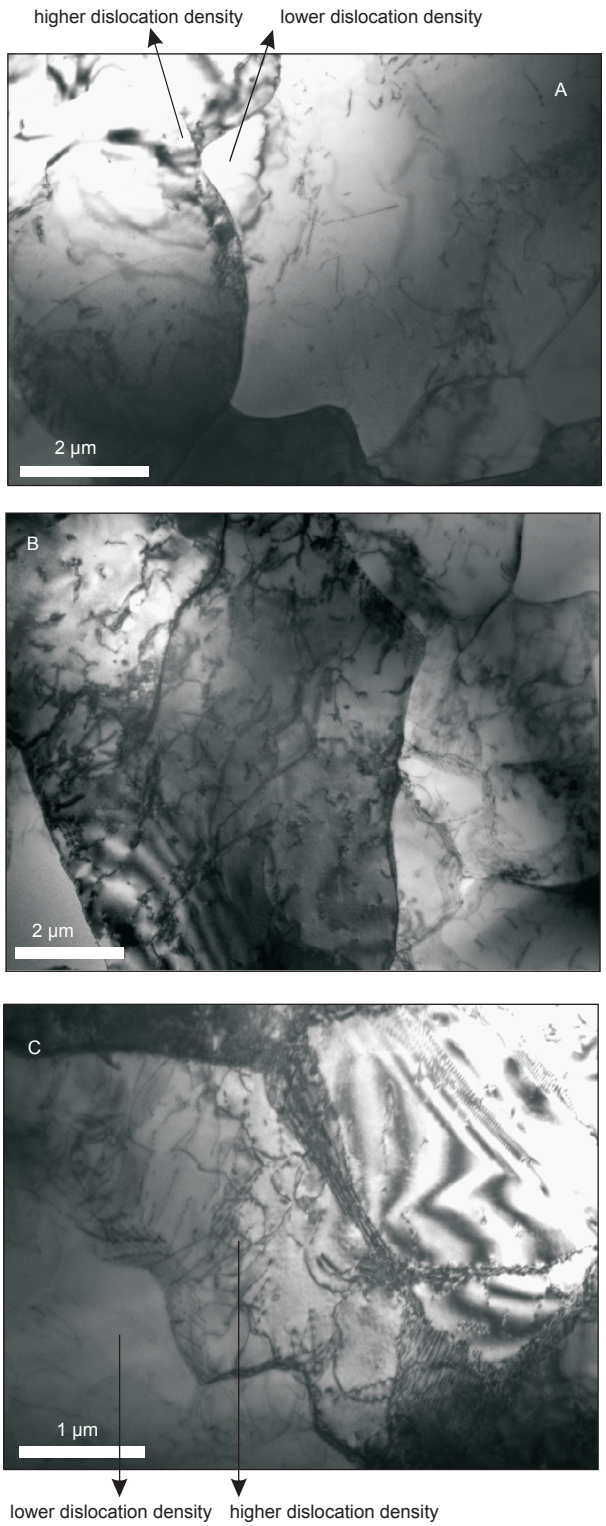

Fig 6.17: Bright field TEM images: a) – c) show heterogeneous distributions of dislocations and wavy subgrain boundaries; a) and b) from sample 50LM730/0.45 and c) is from sample 85LM730/0.45.

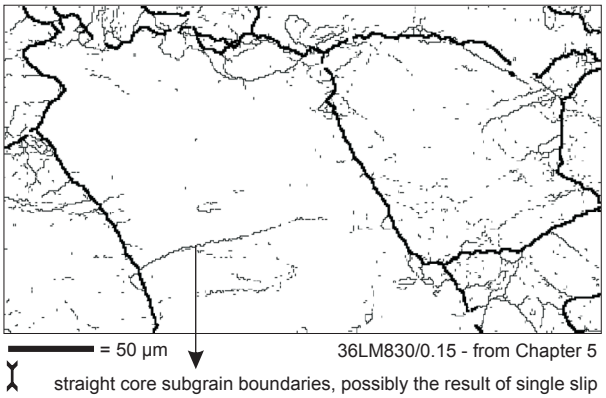

Fig. 6.18: EBSD map of a low strain sample (36LM830/0.15) taken from Chapter 5 to illustrate straight subgrain boundaries dividing a grain that likely result from single slip at low strain (see text). Subgrain boundaries (>1°) are indicated in thin black lines, grain boundaries (>10°) in thick black lines. Compression axis is vertical.

incompatibility, which necessarily induces increased local (shear) stresses at the grain boundaries. Consequently, a stress gradient with an intensified stress at the grain boundaries develops. In this way, the applied stress, now heterogeneously distributed throughout the grain, can result in a resolved shear stress reaching the CRSS for harder slip systems near the grain boundaries. As a result, multiple slip can occur in the boundary regions (Evans & Langdon, 1976; White, 1979; Humphreys, 1981; Ion *et al.*, 1983). The strain accommodation near the grain boundaries will lead to an increased number of geometrically necessary dislocations and subboundaries (Ashby, 1970; Gifkins, 1976).

The width of region in a grain in which multi-slip occurs and in which a dense distribution of small subgrains is formed, i.e., the mantle fraction, is dependent on the character of the stress profile across the grain. This in turn is dependent on external parameters such as bulk stress, strain and temperature as well as internal parameters such as grain size and grain orientation. Given the trigonal system of calcite with multiple slip planes and directions, plus the anisotropic nature of calcite in terms of the CRSS of the various slip systems, it can be expected that in all grains a hard as well as a weak slip system is present. We now consider the effect of grain size, temperature and stress on the core-mantle development and more specifically on the mantle fraction per grain using the two conceptual diagrams shown in Figure 6.19, which represent the same strain and the same grain orientation.

Small grains tend to have a much denser subgrain structure in the core and larger mantle fraction compared to large grains (Figs. 6.3 & 6.4 and Chapter 5). This is probably related to the fact that the stress intensification is more severe in small grains than in large grains, due to higher strain incompatibilities with neighbouring grains and/or to dislocations on single slip planes accumulating faster at the grain boundaries due to the shorter slip distance in smaller grains. Therefore the small grains have a larger proportion of multiple slip than the large grains. The fact that small grains have higher stress levels was also suggested by De Bresser (1996) on the basis of sys-

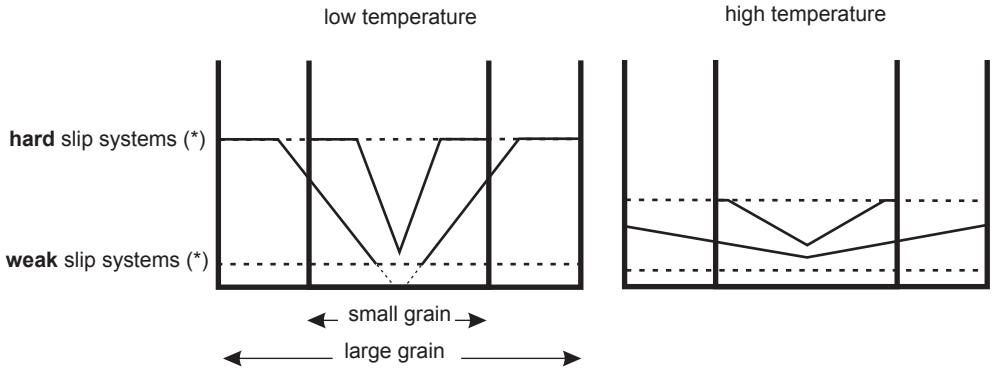

Fig. 6.19: Simplified box diagrams of the stress distribution within grains at a given strain, grain orientation and grain size (two grain sizes are shown per box diagram). The vertical, thick black lines are the axes for the stress level and they represent the grain boundaries. The horizontal black line represents the width of a grain. The dashed lines indicate the critical applied stress needed to activate a given slip system (hard or soft). The level of this critical applied stress is a function of the CRSS and of the orientation of the slip planes with respect to the applied stress direction. The thin, black line indicates the stress gradient that has built up in the grains at a given strain (see text).

tematic variations in dislocation densities between grains of different sizes.

With increasing temperature, the mantle fraction per grain (M) decreases (Fig. 6.11). This is the reflection of the fact that at higher temperature the difference between small versus large grains is more pronounced: small grains contain mainly equiaxed (mantle) subgrains and large grains contain virtually no mantle subgrains and only straight subgrain bands (Fig. 6.4b-c and e-f - Appendix A). The large grains cover a large area of the map in high temperature samples and therefore the average mantle fraction per grain, calculated over the whole map, is low. The fact that the core-mantle development is significantly different in small versus large grains in the high temperature samples is explained by two temperature effects.

(1) The CRSS decreases with increasing temperature for all slip systems, while the ratio between the CRSS of the different slip systems is more or less constant (De Bresser & Spiers, 1997). This means that at high temperatures the CRSS for multiple slip is reached at lower applied stresses than at low temperatures.

(2) A high temperature might prevent or reduce the stress intensification at grain boundaries, resulting in a less steep stress gradient, because the increased mobility and annihilation of dislocations as well as the increased boundary migration at higher temperatures will reduce the build up of geometrically necessary dislocations.

Due to both temperature effects, at high temperature, the CRSS of the hardest system is reached easily in small grains, resulting in multiple slip, and thus the mantle fraction is large. In large grains, the CRSS values required to come to multiple slip might not be reached and no mantle subgrains are formed (Fig. 6.19).

The data show that the mantle fraction per grain, M, does not change significantly, or only decreases slightly, with increasing stress (Fig. 6.11). It is known that for calcite, increasing the strain rate at constant temperature not only results in an increase in flow stress, but also raises the CRSS for all slip systems (De Bresser & Spiers, 1997). As a consequence, the stress gradient in a grain might lay at a higher absolute level, but its effect on the width of the region of the multiple slip activity can be expected to be small (Fig. 6.19), since the critical stresses to activate weak and strong systems increase accordingly.

Strain gradients, stress gradients and stress intensification at grain boundaries as a consequence of incompatibilities between neighbouring grains and rotations of the grains have been demonstrated in the literature both experimentally and theoretically (Berka, 1982; Berka & Růžek, 1984; Mika & Dawson, 1999; Delaire *et al.*, 2000; Raabe *et al.*, 2001; Spolenak *et al.*, 2003). The above model explains the development of the core and mantle subgrains. However, there is a special type of high angle mantle subgrains, namely bulge subgrains, that are formed by (high angle) bridging subgrain boundaries closing off a grain boundary bulge (see Chapter 4 and Fig. 6.2e). These bulge subgrains have a different origin than the rest of the mantle subgrains. They are the direct consequence of a rotating bulge (Chapter 4), in contrast to the rest of the mantle subgrains that can be explained by polygonization of dislocations produced by multiple slip.

6.7.3 Variable stress sensitivity of the subgrain size: why?

Previous experimental studies

In order to compare the subgrain size – stress relations in this study with previous studies, we rewrite 6.1

and normalize the equation by the Burgers vector, b, (6.37 x 10^{-10} m for calcite (De Bresser, 1996) and shear modulus, μ, (25000 MPa for calcite at 700°C (De Bresser, 1996)):

$$\frac{d}{b} = K\left(\frac{\mu}{\sigma}\right)^{m} \quad , \tag{6.3}$$

in which d is the subgrain size; K, a parameter; m, the subgrain size – stress sensitivity and σ, the stress. Takeuchi and Argon (1976), Twiss (1977) and Raj and Pharr (1986) have made compilations of the subgrain size stress sensitivities, reported for several materials, mainly metals and ceramics, and some minerals (olivine and quartz). In Figure 6.20 all data collected by Raj and Pharr (1986) are plotted versus the normalized stress (σ/μ). It appears that at low normalized stresses, m approaches 1, while at higher normalized stresses above m varies substantially between 0 and 2 (Fig. 6.20). The low stress sensitivity as observed in our calcite samples for mantle subgrains (m_m) has also been reported for other materials such as aluminium and iron (α-Fe and Fe-3Si) (Raj & Pharr, 1986) (Fig. 6.19a). Raj and Pharr (1986) and Orlova (1996) consider the variations in m as well as K (see Eq. 6.4). Strikingly, the parameters m and K are related to each other, small m values correlate with large K values (Fig. 6.20) (Twiss, 1977; Raj & Pharr, 1986; Orlova, 1996). Our data on mantle subgrains in calcite fit the relationship between m and K, given by Orlova (1996) for TEM observations (Fig. 6.21):

$$\log K = -\,3m + 4 \quad , \tag{6.4}$$

The data for light microscopy have slightly higher m and K values (Fig. 6.21), so the parameters are somewhat technique dependent (Orlova, 1996). The variations in m have been attributed to different causes such as experimental errors (Raj & Pharr, 1986), stress (Raj and Pharr, 1986), a dependency of temperature (Streb & Reppich, 1973; Orlova & Podstranská, 1998), material characteristics (Edward *et al.*, 1982), type of subgrains (Raj & Pharr, 1989) or geometrically necessary boundaries (Hughes, 1992). Models for subgrain – size stress relations generally have $m = 1$. The review of actual data (Fig. 6.20) clearly shows significant deviations of $m = 1$. In what follows we will suggest two possible reasons for the variations in stress sensitivity in accordance with our observations and the literature.

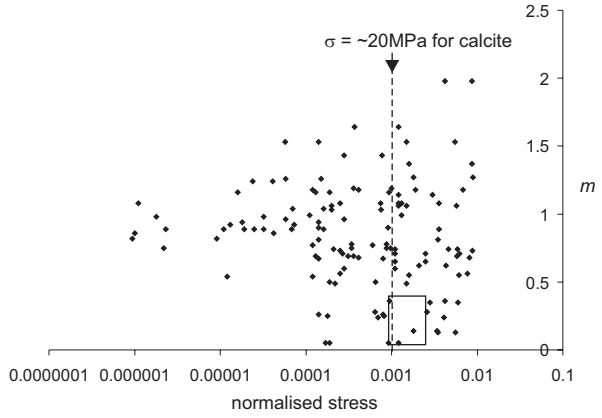

Fig. 6.20: Compilation of literature data of stress sensitivity, m, versus normalized stress (σ/μ) (Raj & Pharr, 1986). The range of stresses and m_m values obtained in this study are indicated in the rectangle. The dotted line indicates the normalized stress level at which a transition from power law creep behaviour to exponential-type creep behaviour (due to cross-slip) is observed for calcite (De Bresser, 1996) (see text, 6.7.3).

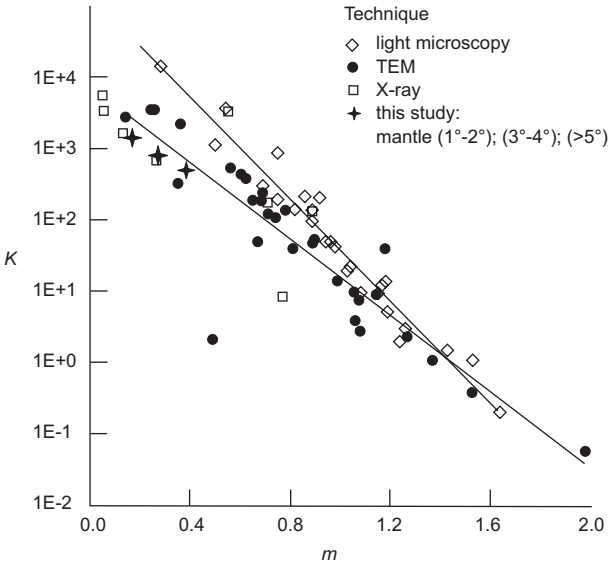

Fig. 6.21: Relation between m and K (parameters of equation 6.3), compilation of our data and literature data (Orlova 1996).

Flow behaviour

Raj and Pharr (1986) have explained the variations in stress sensitivity, m, by experimental errors. Namely, most subgrain size data lay in the stress range, 10^{-4} - 10^{-2}, and at lower and higher stresses, fewer datapoints exist such that correlations with those are prone to errors in the slope. Alternatively, we propose that the observed range in stress sensitivities could be caused by the occurrence of different stress regimes in which different deformation mechanisms dominate, resulting in different flow behaviour and possibly also in different stress – subgrain size relationships. The relations between subgrain size and stress and therefore also m, are linked to deformation mechanisms, because subgrain formation is dependent on the mechanism of dislocation motion (Edward *et al.*, 1982). At the stress levels where the m values deviate significantly from 1, that is, normalized stresses above 10^{-4}, a transition from power law to exponential behaviour occurs in many materials (e.g., Nix *et al.*, 1985; Raj, 2002). For some materials in the exponential regime, steady-state flow is not achieved so the stress and micro-

structure could be more strongly strain dependent. This could explain some variation of m. More specifically, in calcite a change from power law behaviour to a more exponential-type behaviour still resulting in near steady state behaviour, occurs around 20 MPa (normalized stress ~10^{-3}, taking μ = 25000 MPa at 700°C (cf., De Bresser, 1996)) (Fig. 6.20). This transition can be explained for Carrara marble by deformation by cross-slip rather than dislocation climb (De Bresser, 1996). This may result in a different (lower) stress sensitivity of the subgrain size compared to materials predominantly deformed by climb (see also paragraph 6.7.4). In this cross-slip controlled regime, grain size plays a role and finer grained materials tend to be stronger (Renner & Evans, 2002).

Misorientation angle and subgrain type

Raj and Pharr (1989) suggest that the stress sensitivity of the subgrain size can vary depending on the type of substructure, such as cells (subgrains with diffuse, very low angle (~0.1°) boundaries) or primary and secondary subgrains (higher angle subgrains, primary subgrains are subdivided by secondary subboundaries). Raj and Pharr (1989) have shown a variable stress sensitivity of these different subgrain types for salt. The microstructures in calcite are quite different to the structures in salt. In calcite, there is no obvious evidence, not even using TEM, of a clear hierarchy of very low angle misorientation (<0.1°) cells inside larger higher angle subgrains, nor a clear difference between secondary and primary subgrains. Nevertheless, although salt and calcite show a different development of substructures, in both materials the lower misorientation subgrains have a lower stress sensitivity than the higher misorientation subgrains. Below, we speculate why this is the case in calcite.

In calcite having heterogeneous core – mantle substructures, the stress sensitivity of the mantle subgrains increases with increasing misorientation angle (Fig. 6.9). This could be explained by the existence of two types of mantle subgrains, each having a different stress sensitivity: (1) 'normal' mantle subgrains, which have low to medium misorientation angles and (2) high angle mantle subgrains that mainly consist of bulge subgrains. The first type are the mantle subgrains that form as a consequence of stress intensification and their size is not very (bulk) stress sensitive (see paragraph 6.7.4). The second type, the high angle mantle subgrains are mostly bulge subgrains. Therefore, the size of high angle mantle subgrains is very similar to that of the bulges (Fig. 6.12) and consequently their sensitivity to stress is similar. The bulge size and its stress dependency are suggested to be related to the subgrain boundary spacing, where the bulges are pinned, and/or the amount of migration of the bulges (Chapter 4). The change in stress sensitivity from low to high angle subgrains happens gradually because

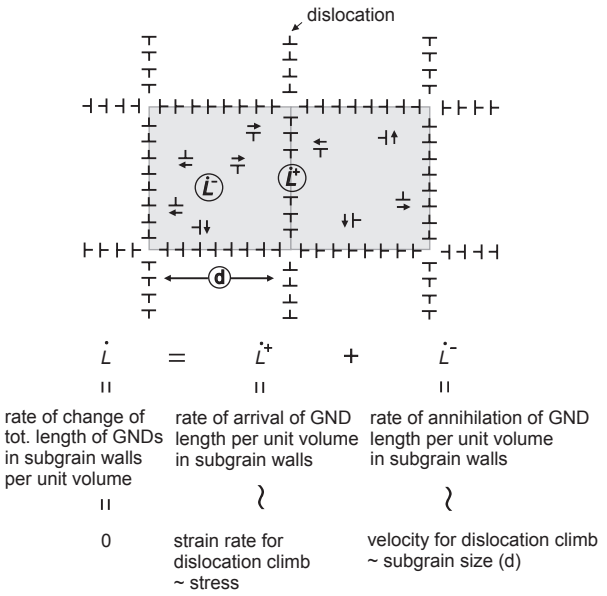

Fig. 6.22: Simplified figure to illustrate the Edward model; modified after Edward et al. (1982). The two grey squares are two subgrains, having subgrain boundaries consisting of parallel sets of dislocations; within the subgrains, free dislocations are shown that move towards the subgrain boundaries.

the medium angle mantle subgrains will be a mixture of bulge subgrains and 'normal' mantle subgrains, while the highest angle subgrains almost exclusively are bulge subgrains.

Furthermore, the mantle and core subgrains of heterogeneous microstructures can have a different stress sensitivity with respect to each other (White, 1979; Schmid et al., 1980 and this study) and with respect to other subgrain types from more spatially uniform microstructures. For example, mantle subgrains are suggested to result from stress intensification (paragraph 6.7.2), and therefore they may be related differently to the bulk stress than subgrains formed in grains that have no stress intensification and contain more homogeneously distributed subgrains. Because the heterogeneous core – mantle substructure has been suggested to evolve with increasing strain to a more spatially homogeneous subgrain structure (Chapter 5), it is possible that for the same material, the subgrains have different stress sensitivities at low versus high strains.

6.7.4 Origin of the low stress sensitivity of the low angle subgrain size

Low angle mantle subgrains

Within the mantle, the low angle mantle subgrains are equiaxed and homogeneously distributed (Figs. 6.3 & 6.4) and their average size does not change significantly with strain, so it is dynamically stable (Chapter 5). Existing microphysical models that link the subgrain size to

stress are all based on a dynamically stable substructure. Therefore we can use these models to a first approximation to investigate what the cause could be of the low stress sensitivity particularly of the mantle subgrains.

In contrast to the Twiss model, the model of Edward (1982) is dynamic, where subgrains can form and annihilate within a dynamic balance, directly related to the creep process. The model is based on the fact that the total change in geometrically necessary dislocation length ($\dot{L}$) equals the rate of arrival of geometrically necessary dislocation length at subgrain walls ($\dot{L}^+$) minus the rate of annihilation of geometrically necessary dislocation length in subgrain walls ($\dot{L}^-$) (Fig. 6.22). If there is no subgrain rotation, there is no change in total dislocation length, so that $\dot{L}= 0$. In this case, there is a dynamic balance between $\dot{L}^+$ and $\dot{L}^-$. The influence of stress comes in through $\dot{L}^+$, which is dependent on the creep rate, chosen by Edward et al. (1982) to be controlled by the dislocation climb rate. The subgrain size factor comes in through $\dot{L}^-$: the dislocation climb distance is determined by the subgrain size because the dislocations can climb at maximum over the length of the subgrain walls to the nodes of the subgrain walls where they may annihilate by meeting dislocations of opposite sign. The resultant stress sensitivity of the subgrain size is:

$$m = \frac{n}{4} \quad , \tag{6.5}$$

with n being the stress exponent of the power creep law in which the strain rate, $\dot{\varepsilon}$, is related to stress, σ, as follows:

$$\dot{\varepsilon} = R\sigma^n \quad , \tag{6.6}$$

with R being dependent on temperature and material properties (Weertman, 1955; Poirier, 1985).

Because the stress exponent, n, in our calcite experiments is very high, ≥ 7 (De Bresser, 2002), the Edward model predicts a high stress sensitivity for calcite, $m \geq 1.75$. This is in contrast with the stress sensitivities (0.1-0.5) observed in this study. Still, the Edward model leaves some options for coming to a lower stress sensitivity:

1) In the Edward model, the controlling creep mechanism for the motion of dislocations within the subgrains and in the walls is dislocation climb (Fig. 6.22). If another creep mechanism depending on dislocation motion, such as cross-slip, is considered, the stress dependency in the model is likely to change (see also paragraph 6.7.3). De Bresser (1991; 2002) and Barber et al. (2007) have shown evidence for the occurrence of cross-slip in calcite, both in single and polycrystalline samples, based on mechanical and microstructural observations. In consequence, the low stress sensitivity of the mantle subgrains in calcite may be related to the occurrence of cross-slip in the mantle region.

2) There are data and models that show evidence for a clear relation between subgrain size and misorientation (Trimby *et al.*, 1998; Pennock *et al.*, 2005). In this case, the subgrain size factor (d) can enter the model when allowing subgrain rotation (~θ) to play a role, i.e., $\dot{L} \neq 0$ (Fig. 6.22). This will likely change the subgrain size – stress relation. However, the mantle subgrains in calcite are not related in a straightforward manner to misorientation (see Chapter 5), so this option has to be rejected for calcite.

Considering the above, the Edward model can be used as a framework to model the stress – subgrain size relation for the mantle subgrains in calcite, on the condition it is modified to obtain lower stress sensitivities. However, it should be noted that the basic geometry of the model, comprising a cubic arrangement of edge dislocations of opposite signs (Fig. 6.22) is quite unrealistic for calcite and most minerals because quadrupole junctions of the subgrain boundaries are not observed, instead subgrain boundaries are mostly joining at triple junctions. So a challenge for future work is to include new deformation mechanisms such as cross slip in the Edward model, as well as to adjust the geometry of the model towards a more polygonal structure.

Orlová (2001), Raj (2002) and Orlová and Dobes (2004) modeled the subgrain size versus stress relation using a composite model of dislocation structure. This means that hard and soft regions are considered, consisting of the subgrain boundaries and subgrain interiors respectively. These regions both have internal stresses and the sum of these stresses, when volume averaged for the relative fraction of hard and soft regions, equals the total stress. The model of Raj (2002) makes similar assumptions as Twiss (1977) and combines the same basic equations to come to a subgrain size – stress dependency. However, the model of Raj (2002) is linked with a model for creep and therefore does not separate the subgrain forming processes from the deformation processes. The two basic equations of the model link (1) subgrain size (d) to dislocation density (ρ) (Holt, 1970):

$$d = P\rho^{-\frac{1}{2}} \quad , \tag{6.7}$$

with P being a geometrical constant and (2) dislocation density (ρ) with stress (σ) (Honeycombe, 1968; Kohlstedt & Weathers, 1980; Weertman & Weertman, 1983; Poirier, 1985):

$$\sigma = \alpha\mu b\rho^q \quad , \tag{6.8}$$

where α is a constant, μ is the shear modulus, b, the Burgers vector and q, the stress sensitivity of the disloca-

tion density. In most studies, q equals 0.5, a value which is also used in the model of Raj, such that combining Eqn. 6.7 and 6.8 results in a subgrain size – stress sensitivity, m, that is linked to the sensitivity of dislocation density to stress, with the value of m being 1. A possible way to adjust the Raj model and obtain a lower value for m is by inserting a lower dislocation density – stress sensitivity, q, in equation 6.8. Raj (2002) mentioned this possibility, because they observe a lower stress sensitivity than 1 for salt, but they do not give a theory why the dislocation density sensitivity to stress, q, could be lower. Schmid et al. (1980) and De Bresser (1996) have observed abnormally high dislocation densities in Carrara marble. Schmid et al. (1980) have ascribed this to post deformational annealing, but De Bresser (1996) has suggested that this is most likely related to the presence of geometrically necessary dislocations (GNDs). GNDs accommodate strain gradients within grains and strain variations between adjacent grains in contrast to incidental dislocations (INDs) (Ashby, 1970). Our mechanistic model (paragraph 6.7.2) on the core-mantle development, proposes the generation of GNDs especially at grain boundaries. The geometrically necessary dislocation density is less sensitive to stress than the density of incidental dislocations because of the following: the density of free GNDs is primarily controlled by strain gradients and grain size (Hughes, 1992; Pennock *et al.*, 2005) and when the density of geometrically necessary dislocations is larger than that of incidental dislocations, the total dislocation density will be mainly grain size, and only weakly stress dependent (De Bresser, 1996).

Even though the model of Raj (2002) could be adjusted for the presence of GNDs and possibly explain a low stress sensitivity, its disadvantage is that the final equation of subgrain size versus stress actually links the subgrain size with the internal stress of the subgrain interiors, which is not equal to the bulk stress and therefore this equation is hard to verify, particularly in materials with heterogeneous stress distributions. Orlova and Dobes (2004) modified the Raj model in order to overcome this problem, but still, their model and the modified Raj model both contain parameters that have to be defined empirically or are material dependent and difficult to measure, such as the volume fractions and internal stresses of the subgrain boundaries (Orlová & Dobes, 2004).

In summary, existing theoretical models leave some options for modification and obtaining a lower stress sensitivity of mantle subgrains, provided another deformation mechanism than climb is considered (Edward model) or there is evidence for a lower stress sensitivity of the dislocation density (Raj and Orlova and Dobes models).

Low angle core subgrains

So far we have only considered the mantle subgrain size versus stress, although the core subgrain size also shows a stress sensitivity that is low. However, for the core subgrains it is much harder to separate the effect of stress from other effects such as grain size, strain and temperature. For example, in paragraph 6.5.2 it has been shown that the small grains have low angle core subgrains that are hardly sensitive to stress (m=0.07), while the large grains have low angle core subgrains that are relatively more sensitive to stress (m>0.2). The core subgrains are at a transient stage and they are continuously evolving in size and shape with increasing strain (Chapter 5), and therefore microphysical models, which assume steady state, cannot be applied in a straightforward way to explain the core subgrain size – stress relation. Because of the complexity of the factors influencing the core subgrain size, we feel that we do not have enough basis to discuss the reasons of their stress sensitivity in a meaningful way.

6.7.5 Influence of grain size

In paragraph 6.7.2, the proposed mechanistic model implies that the grain size influences the core-mantle development and more specifically the mantle fraction per grain. However, grain size also influences the core subgrain size directly, which we will discuss here. The core subgrain size clearly decreases with decreasing deformed grain size (Fig. 6.13), but it is unclear if this is a direct effect, where the grains influence the core subgrains, or if it is rather an indirect consequence of the fact that both core subgrain size and grain size are dependent in the same way on external parameters such as stress, strain and temperature (see also Chapter 4). Below we will discuss qualitatively how in fact both microstructural entities might influence each other. In the samples studied here, recrystallisation and resulting grain size reduction of original, deformed grains is mainly related to an increase in misorientation angle of subgrain boundaries, whether they are in the mantle or in the core (Chapter 4). For example, in the sample 85LM730/0.45 (Fig. 6.3c - Appendix A) it can be seen that core subgrain boundaries can have high misorientations and many grain boundaries effectively have similar orientations as the core subgrain boundaries, which indicates that these grain boundaries might have formed by rotation of core subgrains. Consequently, on the one hand core subgrains can determine the deformed grain size, but on the other hand, the grain size appears to influence the core subgrain development. Observations show that core subgrain boundaries initiate at grain boundaries and sometimes at triple junctions, so their development is effectively constrained by the grain geometry. Thus, it appears that there is a mutual influence of core subgrains and deformed grains on each

other. The development of core subgrains enhances grain size reduction, but the grain size itself has an influence on the nucleation, location and frequency of core subgrain boundaries.

6.7.6 Influence of temperature

We have considered the effect of temperature on the mantle fraction per grain (paragraph 6.7.2), but not yet the effect of temperature on the size of mantle or core subgrains (Figs. 6.7 & 6.14). In Chapter 5, it was proposed that at lower stresses and higher temperatures, subgrain boundary migration occurs (rather than coalescence) in the mantle and this can lead to more scatter in the average mantle subgrain size, because boundary migration leads to more variable sizes than subgrain coalescence. Evidence for subgrain boundary migration can also be seen on Figure 6.17. Therefore, the small deviation at higher temperatures from the mantle subgrain size – stress relation (Fig. 6.10), is possibly related to the fact that at higher temperatures more subgrain boundary migration occurs.

The temperature effect for the core subgrain size is more pronounced: the size of the core subgrains systematically increases with temperature at constant stress, even though there is quite some scatter. This could be an indirect consequence of the fact that the deformed grain size is larger at high temperatures (Chapter 4) and the core subgrain size is directly related to the grain size (paragraph 6.7.5). However, temperature could also have a direct influence on the core subgrain size by enhancing the mobility of the core subgrain boundaries. These appear to sometimes have a wavy character (Fig. 6.5), indicating that boundary migration of the core subgrain boundaries occurs. Migrating subgrain boundaries can consume dislocations and moving subgrain boundaries can annihilate by meeting at boundaries with opposite rotation. We speculate that an increased rate of subgrain boundary migration with increased temperature may result in more homogeneous deformation and a lower frequency of core subgrain boundaries, such that the core subgrain size is larger.

6.7.7 The use of subgrain palaeopiezometers

One of the aims of this study was to investigate the applicability of palaeopiezometers in materials having heterogeneous core-mantle substructures, in particular in calcite. It is found that the stress sensitivity can vary, depending on deformation mechanism and subgrain type (paragraph 6.7.3). Here we investigate which subgrain type is the most useful for palaeopiezometry, considering their stress sensitivity.

White (1979) has suggested that the core subgrain size is directly related to the bulk stress, in contrast to the mantle subgrains, which more likely are related to local intensified stresses at the grain boundaries (paragraph 6.7.2). Therefore the core subgrains potentially are more useful for palaeopiezometry than the mantle subgrains. However, as noted in Chapter 5, under the stress – temperature conditions tested in calcite, the core subgrain size continues to decrease even at high strain, because the deformed grain size decreases, and consequently the core subgrain size is the result of a complex combination of grain size, stress, temperature and strain influences. So core subgrains are not straightforward indicators of palaeostress.

The mantle subgrains appear to be dynamically stable at low strains (0.15), and they appear to be related to local, intensified stresses at grain boundaries, which in turn may be related to the bulk stress. Subsequently, the mantle subgrain size may also be a function of the bulk stress. Indeed, the mantle subgrains size decreases systematically with stress (Fig. 6.8 & 6.10). It was found that using peak or final stresses to calibrate a mantle subgrain size stress relation does not result in significantly different equations. The changes in parameters m and k of equation 6.1 are within the errors of the best fits. For applications to natural samples this means that, if some weakening or hardening has occurred during deformation, this cannot be resolved by mantle subgrains as they do not quickly re-establish their size during small stress changes. Consequently, mantle subgrains may represent the stresses when they were first formed and not stresses related to exhumation. However, this should be confirmed by new experiments in which samples, already deformed, are consequently re-deformed at a different stress level.

The stress sensitivity of the low angle mantle subgrains is very low (m=0.1), which means that small errors in the size measurements can cause large errors in the stress estimations. The maximum error on the predicted stress due to the 5% error on the measurements, is up to ~50%. Therefore, it is recommended to use low angle mantle subgrains only for a first order estimate of stresses. Alternatively, when using the equation for high angle mantle subgrains, which are more stress sensitive (m=0.4), the maximum error is ~25%. Consequently, high angle mantle subgrains are more accurate indicators of palaeostress than low angle mantle subgrains. It has been shown that high angle mantle subgrains are often associated with the rotation of bulges (bulge subgrains) (paragraph 6.7.2 and Chapter 4), and therefore new microphysical models, which include a mechanism for bulge subgrain formation, are needed to support this type of palaeopiezometer (Chapter 4).

6.8 Conclusions

Using EBSD, the size of core and mantle subgrains in experimentally deformed Carrara marble has been quantified as a function of misorientation angle. On the basis of a hypothesis on the origin of core - mantle subgrain microstructures, we have evaluated the use of the subgrain size as an indicator of palaeostress for a range of deformation conditions (stress 20-85 MPa; temperature 700-990°C).

We have proposed a mechanistic model in which core subgrains result from single slip activity at the onset of deformation, while mantle subgrains develop later due to stress intensification at grain boundaries and multiple slip activity during continued deformation.

The core subgrains are dependent on stress, but they are also significantly dependent on grain size and temperature. Moreover, the average core subgrain size is not yet dynamically stable below strains of 0.90. Therefore, the core subgrains are not useful for palaeopiezometry, at least not for calcite.

The average mantle subgrain size is dynamically stable at natural strains above 0.15. The mantle subgrain size is mainly dependent on stress, and only slightly on temperature. The latter might be due to the effect of temperature on subgrain boundary migration. The mantle subgrain size (d_m) - stress (σ) sensitivity, m (in $d \sim \sigma^{-m}$), of the low angle mantle subgrains (1°-2°) is much lower (m = 0.11) than expected from theoretical models (m ~ 1). We suggest that this might be the result of (1) the motion of dislocations predominantly by cross-slip rather than by a climb process as assumed in the model of Edward et al. (1982) and/or (2) the presence of geometrically necessary dislocations which may be less sensitive to stress than incidental dislocations. We suggest that these effects are included in future theoretical models on the subgrain size – stress relationship.

Due to its low stress sensitivity, the mantle subgrain size is not very accurate as a palaeostress indicator, because small errors in size measurements can lead to large errors in stress estimations. In contrast, high angle mantle subgrains are more sensitive to stress (m = 0.4), which is likely related to the fact that many high angle mantle subgrains are bulge subgrains. The stress dependency of bulge subgrains is similar to the stress dependency of their nucleation sites, namely, grain boundary bulges. Due to their higher stress dependency, high angle mantle subgrains are relatively accurate palaeostress indicators. However, before high angle mantle subgrains can be applied in palaeopiezometry to its full extent, theoretical models should be established that include the formation of bulge subgrains from grain boundary bulges.

7

Conclusions and suggestions for future research

7.1 Conclusions

In this study, novel methods have been established using electron backscattered diffraction (EBSD) to allow a quantitative description of heterogeneous microstructures. These new methods allow objective separation of various elements of the microstructure and measurement of their sizes in relation to misorientation angle. The methods have been applied to Carrara marble, deformed in axial compression at flow stresses between 15 and 85 MPa, temperatures between 700-990 °C and to natural strains up to 0.90. The samples show a slight weakening, such that after a peak stress at natural strains of ~0.15, the stress decreases slightly (~15%) up to strains of ~0.90. Within the deformation conditions studied, the microstructure is heterogeneous on the grain and subgrain scale, with the typical microstructural elements being recrystallised grains, grain boundary bulges, deformed grains and core and mantle subgrains. On the basis of the EBSD measurements made in this study, deformation and recrystallisation mechanisms in Carrara marble have been reconsidered in order to understand better the relationship between the individual microstructural elements and the deformation conditions. Below, the major conclusions are given for specific research questions in this study.

1. How to measure the subgrain size in relation to misorientation angle for the whole microstructure?

Two methods have been compared: the linear intercept hierarchy (LI-MH), which measures domain sizes based on linear intercepts between boundaries larger than a given misorientation angle and the domain hierarchy (DH) method, which measures domain sizes based on the area of domains surrounded by boundaries larger than a given misorientation angle. The LI-MH method appears to be better than the DH method to measure (sub)grain sizes as a function of their misorientation angle when no separation is made between recrystallised and deformed grains nor between core and mantle subgrains. The main advantages of the linear intercept hierarchy method compared to the domain hierarchy method are: (i) the LI-MH method successfully measures subgrains that are not fully closed owing to the angular resolution limit of EBSD in our samples, whereas the DH method ignores these subgrains ; (ii) the LI-MH method provides a reasonable sampling of domain sizes for analyses in which the mapped area is small with respect to the grain size (for practical EBSD mapping times).

The domain size for all subgrain and grain types taken together increases with increasing misorientation angle, such that the microstructure shows a domain hierarchy. The characteristics of this hierarchy are related to the relative amount of subgrain rotation, grain boundary migration and recrystallisation. The disadvantage of the LI-MH method is that the single size values are averages of the sizes of various microstructural elements taken together: recrystallised grains, core and mantle subgrains. This average is biased towards the mantle subgrain size because of the high frequency of these mantle subgrains in our material. Therefore, in order to allow assessment of for example, core subgrains, new methods are needed that separate recrystallised from deformed grains and core from mantle subgrains.

2. How to separate the various microstructural elements in heterogeneous Carrara marble?

To measure different microstructural elements separately, the domain hierarchy method is needed because the separation is made based on the average misorientation within a domain. Recrystallised grains are defined as grains that are free of subgrains. As a practical criterion for separating deformed from recrystallised grains, the average internal misorientation within a grain (AMG) is used: if this is below 1°, the grain is considered as a recrystallised grain. Mantle subgrains are defined as small subgrains near the grain boundary that are free of internal lower angle subgrains. Hence, the average internal misorientation of a subgrain (AMS) in the mantle is below 1°. Based on this, mantle subgrains can be separated from core subgrains that have their AMS above 1°.

3. How and why do the sizes of grain boundary bulges, recrystallised grains and deformed grains depend on strain and deformation conditions?

It has been found that both the grain boundary bulge and recrystallised grain sizes are independent of strain (at least up to 0.90) and decrease in a similar way with increasing stress. The bulge size decreases slightly with increasing temperature. In contrast, the recrystallised grain size does not vary with temperature at relatively low stresses (below 50 MPa), while it increases with temperature at high stress (≥ 50 MPa).

The bulges are interpreted as being formed by limited migration of an existing grain boundary. Subsequently the bulges start rotating and subgrains are formed associated with the bulges. If rotation of the ‘bulge subgrains’ continues, this results in nucleation of recrystallised grains (bulging recrystallisation). As recrystallisation proceeds, a necklace of recrystallised grains forms around deformed grains. Once the necklace is complete, subsequent new recrystallised grains nucleate by the formation and subsequent rotation of subgrains at the grain boundary irregularities in between the previously formed

recrystallised grains. This is a process of subgrain rotation recrystallisation rather than bulging recrystallisation.

The stress dependency of the first generation of recrystallised grains is directly related to the size of the grain boundary bulges. The bulge size and its stress dependency in turn are related to the subgrain boundary spacing where the bulges are pinned, and in case of no pinning, the bulge size is solely dependent on the amount of local grain boundary migration at the bulges. The local migration at the bulge is likely to be driven by differences in subgrain boundary density on the opposite sides of a grain boundary and, to a minor extent, by the surface energy of a bulged grain boundary. Because the latter is dependent on temperature, this might explain the slight temperature dependency of the bulge size. The temperature dependency of the recrystallised grain size at high stresses is proposed to be related to enhanced pervasive migration at high temperatures of recrystallised grains after their nucleation.

With increasing strain, the deformed grain size reduces with respect to the starting grain size because of progressive replacement by recrystallised grains, including rotation of core subgrains, which increases the misorientation angle of the core subgrain boundary until it becomes a grain boundary. High temperatures delay this process (see (5)) and therefore the deformed grain size reduces less quickly at high temperatures.

4. How and why are the mantle and core subgrain sizes related to strain and misorientation angle?

- **Mantle subgrains**

At the same strain, the average mantle subgrain size shows a weak hierarchy of sizes with misorientation angle at low stress (~36 MPa) and shows no hierarchy at high stress (~85 MPa). At strains of 0.15 to 0.90, the mantle subgrain size does not change significantly. The maintenance of the dynamically stable size is attained by a balance between subgrain formation and growth processes (such as subgrain coalescence and subgrain boundary migration).

- **Core subgrains**

At the same strain, the average core subgrain size increases with increasing misorientation until it reaches an upper limit at misorientation angles used to define a grain boundary (angles >10°). The core subgrain size continues to decrease with strain at least up to strains of 0.90, which is likely the consequence of a simultaneous reduction in the deformed grain size with strain.

5. How does a heterogeneous microstructure evolve during post peak, minor weakening?

The microstructural changes that accompany minor weakening towards a steady state flow behaviour are an increasing amount of recrystallised grains, the increase in mantle fraction per grain and the simultaneous reduction of deformed grains and core subgrains until the sizes of the grains and subgrains have become similar. By comparison of the new results to previous data of Carrara marble deformed to high strains, it is inferred that when recrystallised grains are similar in size to deformed grains and in the latter the subgrains no longer show a core mantle substructure, a true mechanical steady state will be reached where the stress no longer changes with increasing strain.

6. How and why are the core and mantle subgrains related to stress and temperature?

The size of the core subgrains decreases with increasing stress, but also with decreasing deformed grain size. Moreover, the core subgrains are not dynamically stable at natural strains below 0.9, which hampers straightforward interpretation of the stress dependency of the core subgrain size. The core subgrain size increases with increasing temperature. This may be due to the fact that an increase in temperature may enhance subgrain boundary mobility and annihilation, which will slow down the development of core subgrains.

The mantle subgrain size decreases with increasing stress and is slightly dependent on temperature. The latter may be due to the fact that temperature enhances subgrain boundary migration. The mantle subgrain size - stress sensitivity, m (in $d \sim \sigma^{-m}$), of the low angle mantle subgrains (1°-2°) is much lower ($m = 0.11 \pm 0.01$) than expected on the basis of theoretical models ($m \sim 1$). We infer that this might be the result of (1) the motion of dislocations predominantly by cross-slip rather than by a climb process as assumed in the model of Edward et al. (1982) and/or (2) the presence of geometrically necessary dislocations, which may be less sensitive to stress than incidental dislocations.

In contrast to the low angle mantle subgrains, high angle mantle subgrains (>5°) are more sensitive to stress ($m = 0.42 \pm 0.03$). Many high angle mantle subgrains are in fact 'bulge subgrains', which are subgrains that nucleated at grain boundary bulges. Therefore the stress sensitivity of the high angle mantle subgrains is similar to that of the bulges.

7. Which elements of the microstructure are the most useful for palaeopiezometry?

The recrystallised grains and subgrains decrease with increasing stress according to the general equation:

$$\frac{d}{b} = K\left(\frac{\mu}{\sigma}\right)^{c} ,$$

in which d is the size of recrystallised grains or subgrains, b, is the length of the Burgers vector, μ, the shear modulus, σ, the flow stress, and K and C are parameters that are related to the type of microstructure measured, i.e., recrystallised grain size ($C = p$) or subgrain size ($C = m$). The evaluation of the microstructural elements that are the most useful as indicators of (palaeo-)stress, has been done by critically assessing their stress sensitivity (p and m) and considering if parameters other than stress are of relevance.

The relation between recrystallised grains and stress has been calibrated in this study for a specific type of microstructure, namely, a heterogeneous microstructure of calcite in which deformed grains have grain boundary bulges and contain core and mantle subgrains. In this type of microstructure the recrystallised grains were mainly formed by grain boundary bulging and subgrain rotation, and they are located at old grain boundaries. The stress sensitivity of recrystallised grains, $p = 0.6$, is lower than in recrystallised grain size piezometers from previous studies on Carrara marble ($p \sim 1$). This may be related to the different way in which the microstructures are treated: for example, whether or not rotation and migration recrystallised grains were separated or whether or not heterogeneous microstructures were combined with homogeneous microstructures. This suggests that recrystallised grains can have different stress sensitivities, depending on the details of the recrystallisation mechanism in relation to the microstructure. In the case of bulging recrystallisation as the main mechanism, the bulge size plays an important role in determining the recrystallised grain size rather than, for example, the subgrain size in subgrain rotation dominated recrystallisation.

The bulge size is a potential palaeostress indicator that can serve as an alternative to the recrystallised grain size. The bulge size is not dependent on strain and its temperature dependency is small and more clearly defined than that of the recrystallised grain size. While a grain boundary migration component can affect the average recrystallised grain size such that it significantly deviates from the general subgrain size – stress relation, the bulge size appears not to be affected by pervasive migration.

Due to its low stress sensitivity ($m = 0.11$), the low angle mantle subgrain size is not very useful as a palaeostress indicator, because small errors in size measurements can lead to large errors in stress estimations. In contrast, high angle mantle subgrains are more sensitive to stress ($m = 0.43$), so they are more accurate as palaeostress indicators.

Because core subgrains are not only dependent on stress, but also on deformed grain size, temperature and strain, they are not straightforward to use as an indicator of (palaeo-)stress.

7.2 Suggestions for future research

The EBSD processing methods established in this study to quantify microstructures as a function of their misorientation angle and to separate recrystallised from deformed grains and core from mantle subgrains, have been tested for calcite but are likely to be applicable to other materials as well. However, the cut off average internal misorientation (AMG and AMS, see above) used to distinguish recrystallised from deformed grains and core from mantle subgrains, is not only related to internal microstructure but also to a limited extend to artificial low angle misorientations (noise), which are characteristic for the material and the microscope conditions. Therefore it should be established which values have to be used to apply the method reliably to other materials.

Using the new EBSD separation technique, materials with heterogeneous core - mantle microstructures can now be investigated quantitatively in order to determine in an objective way if the complex relationships between microstructure and external conditions found for calcite rock also apply to other materials, for which thus far more simple relations have been assumed to apply. This concerns for example, the low stress sensitivity of low angle mantle subgrains and the higher stress sensitivity of higher angle ‘bulge subgrains’.

In compression tests at high confining pressures the maximum strain that can be easily attained is about 1. Higher strains are possible in torsion and simple shear tests. A series of low to high strain tests, preferably in the same experimental set up, are interesting to determine how the core mantle microstructure develops towards a more spatially homogeneous microstructure on the grain and subgrain scale. It is suggested to determine how the deformation and recrystallisation mechanisms change during progressive deformation when core – mantle microstructures no longer may develop due to the lack of stress intensification at grain boundaries. It should be verified if this results in a different relationship between recrystallised grain/subgrain size and stress. It is essential to investigate this option in order to be able to reliably apply experimentally calibrated relationships to

naturally deformed rocks.

For understanding the various stress dependencies of recrystallised grains, grain boundary bulges and mantle subgrains as observed in our experimental samples, renewed work on microphysical models is needed:

(1) Models for the stress dependency of recrystallised grains should take into account the different types of microstructure, making a distinction between homogeneous microstructures and heterogeneous core – mantle microstructures. In case of core – mantle microstructures, the mechanism for development of recrystallised grains from grain boundary bulges should be included.

(2) The sizes of grain boundary bulges appears to be a potentially useful indicator of (palaeo-)stress, because they are less affected by grain boundary migration than the recrystallised grain size at the same conditions. Before a bulge size piezometer can be reliably applied to nature, a detailed microphysical model is needed to underpin the empirically observed relation between stress and bulge size. In this model, the small temperature dependence of the bulges, probably related to surface energy, should be accounted for. The high angle mantle subgrains are often associated with grain boundary bulges and therefore a model that explains the bulge size – stress relation can also serve as a foundation for palaeopiezometry using high angle mantle subgrains.

(3) Low misorientation angle mantle subgrains are less useful for palaeopiezometry than high misorientation angle mantle subgrains, at least for calcite. However, modeling the relation between the low angle mantle subgrains and stress can help to understand the formation of mantle subgrains. Existing theoretical models leave some options for modification and obtaining a lower stress sensitivity of mantle subgrains. It is suggested that at least for mantle subgrains, another deformation mechanism than climb is considered and the possibly lower stress sensitivity of geometrically necessary dislocations is included in the existing models of the subgrain size – stress relation.

References

Ashby, M. F. 1970. The deformation of plastically non-homogeneous materials. *Philosophical Magazine* **21**, 399-424.

Atkinson, H. V. 1988. Overview no. 65 : Theories of normal grain growth in pure single phase systems. *Acta Metallurgica* **36**(3), 469-491.

Austin, N. J. & Evans, B. 2007. Paleowattmeters: A scaling relation for dynamically recrystallised grain size. *Geology* **35**, 343-346.

Avé Lallement, H. 1985. Subgrain rotation and dynamic recrystallisation of olivine, upper-mantle diapirism, and extension of the basin-and-range province. *Tectonophysics* **119**, 89-117.

Bailey, J. E. & Hirsch, P. B. 1962. The recrystallisation process in some polycrystalline metals. *Proceedings of the Royal Society London A* **267**, 11-30.

Barber, D., Wenk, H. R., Gomez-Barreiro, J., Rybacki, E. & Dresen, G. 2007. Basal slip and texture development in calcite: new results from torsion experiments. *Physics and Chemistry of Minerals* **34**(2), 73-84.

Barnhoorn, A., Bystricky, M., Burlini, L. & Kunze, K. 2004. The role of recrystallization on the deformation behaviour of calcite rocks: large strain torsion experiments on Carrara marble. *Journal of Structural Geology* **26**, 885-903.

Bate, P. & Hutchinson, B. 1997. A re-evaluation of the mechanism of SIBM. *Scripta Materialia* **36**(2), 195-198.

Beck, P. A. 1954. Annealing of cold worked metals. *Advances in Physics* **3**, 245.

Berger, A., Wilbrandt, P. J. & Haasen, P. 1983. Development of the recrystallization texture in tensile deformed aluminium single crystals--I. HVEM observations. *Acta Metallurgica* **31**, 1433-1443.

Berka, L. 1982. On stress distribution in a structure of polycrystals. *Journal of Materials Science* **17**, 1508-1512.

Berka, L. & Růžek, M. 1984. Analysis of microdeformations in a structure of polycrystals. *Journal of Materials Science* **19**(5), 1486-1495.

Bestmann, M., Kunze, K. & Matthews, A. 2000. Evolution of a calcite marble shear zone complex on Thassos Island, Greece: microstructural and textural fabric and their kinematic significance. *Journal of Structural Geology* **22**, 1789-1807.

Bestmann, M. & Prior, D. J. 2003. Intragranular dynamic recrystallisation in naturally deformed calcite marble: diffusion accommodated grain boundary sliding as a result of subgrain rotation recrystallisation. *Journal of Structural Geology* **25**, 1597-1613.

Bird, J. M., Mukherjee, A. K. & Dorn, J. F. 1966. Correlations between high temperature creep behaviour and structure. In: *Quantitative Relation Between Properties and Microstructure* (edited by Brandon, D. G. & Rosen, R.). *Proceedings of the Third International Conference on the Strength of Metals and Alloys*, 380-385.

Busch, J. P. & van der Pluijm, B. A. 1995. Calcite textures, microstructures and rheological properties of marble mylonites in the Bancroft shear zone, Ontario, Canada. *Journal of Structural Geology* **17**(5), 677-688.

Cao, W. Q., Godfrey, A. & Liu, Q. 2003. Determining dislocation cell sizes for high-strain deformation microstructures using the EBSP technique. *Journal of Microscopy* **211**, 219-229.

Carreras, J., Estrada, A. & White, S. 1977. The effects of folding on the C-axis fabrics of a quartz mylonite. *Tectonophysics* **39**(1-3), 3-24.

Christie, J. M., Ord, A. & Koch, P. S. 1980. Relationship between recrystallised grain size and flow stress in experimentally deformed quartzite. *EOS Transactions of the American Geophysical Union* **61**, 377.

Covey-Crump, S. J. 1998. Evolution of mechanical state in Carrara marble during deformation at 400°C to 700°C. *Journal of Geophysical Research* **103**, 29781-29794.

De Bresser, J. H. P. 1989. Calcite c-axis textures along the Gavarnie thrust zone, central Pyrenees. *Geologie en Mijnbouw* **68**, 367-375.

De Bresser, J. H. P. 1991. Intracrystalline Deformation of Calcite. Unpublished Ph.D. thesis, Utrecht University, 191p.

De Bresser, J. H. P. 1996. Steady state dislocation densities in experimentally deformed calcite materials: Single crystals versus polycrystals. *Journal of Geophysical Research* **101**(B10), 22189-22201.

De Bresser, J. H. P. 2002. On the mechanism of dislocation creep of calcite at high temperature: Inferences from experimentally measured pressure sensitivity and strain rate sensitivity of flow stress. *Journal of Geophysical Research* **107**, doi:10.1029/2002JB001812.

De Bresser, J. H. P., Peach, C. J., Reijs, J. P. J. & Spiers, C. J. 1998. On dynamic recrystallization during solid state flow: Effects of stress and temperature. *Geophysical Research Letters* **25**, 3457-3460.

De Bresser, J. H. P. & Spiers, C. J. 1990. High temperature deformation of calcite single crystals by r^+ and f^+ slip. In: *Deformation mechanisms, Rheology and Tectonics* (edited by Knipe, R. J. & Rutter, E. H.). *Special Publications* **54**. Geological Society, London, 285-298.

De Bresser, J. H. P. & Spiers, C. J. 1997. Strength characteristics of the r, f, and c slip systems in calcite. *Tectonophysics* **272**, 1-23.

De Bresser, J. H. P., Ter Heege, J. H. & Spiers, C. J. 2001. Grain size reduction by dynamic recrystallization: can it result in major rheological

weakening? *International Journal of Earth Sciences* **90**, 28-45.

De Bresser, J. H. P., Urai, J. L. & Olgaard, D. L. 2005. Effect of water on the strength and microstructure of Carrara marble axially compressed at high temperature. *Journal of Structural Geology* **27**, 265-281.

de Meer, S., Drury, M. R., de Bresser, J. H. P. & Pennock, G. M. 2002. Current issues and new developments in deformation mechanisms, rheology and tectonics. In: *Deformation Mechanisms, Rheology and Tectonics: Current Status and Future Perspectives* (edited by de Meer, S., Drury, M. R., de Bresser, J. H. P. & Pennock, G. M.). *Special Publications* **200**. Geological Society, London, 1-27.

Deer, W. A., Howie, R. A. & Zussman, J. 1962. *Rock-Forming minerals - Vol. 5: non-silicates*. Longmans, Green and co, London, 301p.

Delaire, F., Raphanel, J. L. & Rey, C. 2000. Plastic heterogeneities of a copper multicrystal deformed in uniaxial tension: experimental study and finite element simulations. *Acta Materialia* **48**, 1075-1087.

Derby, B. 1990. Dynamic recrystallization and grain size. In: *Deformation Processes in Minerals, Ceramics and Rocks* (edited by Barber, D. J. & Meredith, P. G.). Unwin Hyman, London, 354-364.

Derby, B. & Ashby, M. F. 1987. On dynamic recrystallisation. *Scripta Metallurgica* **21**, 879-884.

Doherty, R. D., Hughes, D. A., Humphreys, F. J., Jonas, J. J., Juul Jensen, D., Kassner, M. E., King, W. E., McNelley, T. R., McQueen, H. J. & Rollett, A. D. 1997. Current issues in recrystallisation: a review. *Materials Science and Engineering* **A238**, 219-274.

Drury, M. R., Humphreys, F. J. & White, S. H. 1985. Large strain deformation studies using polycrystalline magnesium as a rock analogue. Part II: dynamic recrystallisation mechanisms at high temperatures. *Physics of The Earth and Planetary Interiors* **40**, 208-222.

Drury, M. R. & Urai, J. L. 1990. Deformation-related recrystallization processes. *Tectonophysics* **172**, 235-253.

Duyster, J. & Stöckhert, B. 2001. Grain boundary energies in olivine derived from natural microstructures. *Contributions to Mineralogy and Petrology* **140**, 567-576.

Ebert, A., Herwegh, M. & Pfiffner, A. 2007. Cooling induced strain localization in carbonate mylonites within a large-scale shear zone (Glarus thrust, Switzerland). *Journal of Structural Geology* **29**(7), 1164-1184.

Edward, G. H., Etheridge, M. A. & Hobbs, B. E. 1982. On the stress dependence of subgrain size. *Textures and Microstructures* **5**, 127-152.

Etheridge, M. A. & Wilkie, J. C. 1981. An assessment of dynamically recrystallised grainsize as a palaeopiezometer in quartz-bearing mylonite zones. *Tectonophysics* **78**, 475-508.

Evans, A. G. & Langdon, T. E. 1976. Structural Ceramics. *Progress in Materials Science* **21**, 171-441.

Evans, K. R., Bailey, D. J. & Flanagan, W. F. 1967. An interpretation of the dislocation velocity-stress exponent *Physica Status Solidi* **22**, 607-161.

Exell, S. F. & Warrington, D. H. 1972. Subgrain boundary migration in aluminium. *Philosophical Magazine* **26**, 1121-1136.

Exner, H. E. 1972. Analysis of grain- and particle-size distributions in metallic materials. *International Metallurgical Reviews* **17**, 25-42.

Fliervoet, T. F., Drury, M. R. & Chopra, P. N. 1999. Crystallographic preferred orientations and misorientations in some olivine rocks deformed by diffusion or dislocation creep. *Tectonophysics* **303**, 1-27.

Fynn, G. W. & Powell, W. J. A. 1979. *The cutting and polishing of electro-optic materials*. Adams Hilger, London, 216p.

Gifkins, R. C. 1970. *Optical microscopy of metals*. Elsevier, New York, 208p.

Gifkins, R. C. 1976. Grain boundary sliding and its accommodation during creep and superplasticity. *Metallurgical Transactions A* **72**, 1225 - 1252.

Godfrey, A. & Hughes, D. A. 2000. Scaling of the spacing of deformation induced dislocation boundaries. *Acta Materialia* **48**, 1897-1905.

Griggs, D. T. 1936. Deformation of rocks under high confining pressures - I. Experiments at room temperature. *Journal of Geology* **44**, 541-577.

Griggs, D. T., Turner, F. J. & Heard, H. C. 1960. Deformation of rocks at 500 to 800°. *Geological Society of America Memoir* **79**, 39-105.

Groves, G. W. & Kelly, A. 1969. Change of shape due to dislocation motion. *Philosophical Magazine* **19**, 977-986.

Guillopé, M. & Poirier, J. P. 1979. Dynamic recrystallisation during creep of single-crystalline halite: an experimental study. *Journal of Geophysical Research* **84**, 5557-5567.

Hacker, B.R., Yin, A., Christie, J. M. & Snoke, A. W. 1990. Differential stress, strain rate, and temperature of mylonitization ini the Ruby Mountains, Nevada: Implications for the rate and duration of uplift. *Journal of Geophysical Research* **95**, 8569-8580.

Haessner, F. & Hoffmann, S. 1978. Migration of high angle grain boundaries. In: *Recrystallisation of Metallic Materials* (edited by Haessner, F.). Rieder Verlag, Stuttgart, 63-95.

Han, J.-H. & Kim, D.-Y. 1995. Analysis of the proportionality constant correlating the mean intercept length to the average grain size. *Acta Metallurgica et Materialia* **43**, 3185-3188.

Heard, H. C. & Raleigh, C. B. 1972. Steady state flow in marble at 500 to 800 °C. *Geological Society of America Bulletin* **83**, 935-956.

Heidelbach, F., Kunze, K. & Wenk, H. R. 2000. Texture analysis of a recrystallised quartzite using electron backscattered diffraction in the scanning electron microscope. *Journal of Structural Geology* **2000**, 91-104.

Heinemann, S., Wirth, R., Gottschalk, M. & Dresen, G. 2005. Synthetic [100] tilt grain boundaries in forsterite: 9.9 to 21.5°. *Physics and Chemistry of Minerals* **32**, 229-240.

Hirth, G. & Tullis, J. 1992. Dislocation creep regimes in quartz aggregates. *Journal of Structural Geology* **14**, 145-159.

Hobbs, B. E. 1968. Recrystallisation of single crystal of quartz. *Tectonophysics* **6**, 353-401.

Holt, D. L. 1970. Dislocation cell formation in metals. *Journal of Applied Physics* **41**, 3197-3201.

Honeycombe, R. W. K. 1968. *The plastic deformation of metals*. Edward Arnold, London, 477p.

Hu, H. 1962. Direct observations on the annealing of Si-Fe crystals in the electron microscope. *Transactions of the Metallurgical Society AIME* **224**, 75-84.

Huang, X. & Jensen, D. J. 2000. EBSD contra TEM characterization of a deformed aluminium single crystal. In: *Electron Backscatter Diffraction in Materials Science* (edited by Schwartz, A. J., Kumar, M. & Adams, B. L.). Kluwer Academic/ Plenum, New York, 265-276.

Huang, Y., Humphreys, F. J. & Ferry, M. 2000. The annealing behaviour of deformed cube-oriented aluminium single crystals. *Acta Materialia* **48**, 2543-2556.

Hughes, D. A. 1992. Microstructure and flow stress of deformed polycrystalline metals. *Scripta Metallurgica et Materialia* **27**, 969-974.

Humphreys, F. J. 1981. Dynamic recrystallisation - the influence of crystal structure. In: *Deformation of Polycrystals: Mechanisms and Microstructures* (edited by Hansen, N., Horsewell, A., Leffers, T. & Lilholt, H.). *Proceedings on the 2nd International Symposium on Metals and Materials Sciences*, Riso, 305-311.

Humphreys, F. J. 1999. Quantitative metallography by electron backscattered diffraction. *Journal of Microscopy* **195**, 170-185.

Humphreys, F. J. 2001. Review: Grain and subgrain characterization by electron backscattered diffraction. *Journal of Materials Science* **36**, 3833-3854.

Humphreys, F. J., Bate, P. S. & Hurley, P. J. 2001. Orientation averaging of electron backscattered diffraction data. *Journal of Microscopy* **201**, 50-58.

Humphreys, F. J. & Hatherly, M. 1995. *Recrystallisation and Related Annealing Phenomena*. Pergamon Press, Oxford, 520p.

Humphreys, F. J. & Hatherly, M. 2004. *Recrystallisation and Related Annealing Phenomena*. Elsevier, Oxford, 628p.

Ion, S. E., Humphreys, F. J. & White, S. H. 1983. Dynamic recrystallisation and the development of microstructure during the high temperture deformation of magnesium. *Acta Metallica* **30**, 1909-1919.

Jessel, M. W. 1987. Grain-boundary migration microstructures in a naturally deformed quartzite. *Journal of Structural Geology* **9**, 1007-1014.

Karato, S. & Ogawa, M. 1982. High-pressure recovery of olivine: implications for creep mechanisms and creep activation volume. *Physics of The Earth and Planetary Interiors* **28**(2), 102-117.

Kellermann Slotemaker, A. 2006. Dynamic recrystallization and grain growth in olivine rocks. In: *Geologica Ultraiectina* **268**. Utrecht University, Utrecht, 187p.

Kenkmann, T. & Dresen, G. 2002. Dislocation microstructure and phase distribution in a lower crustal shear zone: an example from the Ivrea-Zone, Italy. *International Journal of Earth Sciences (Geologische Rundschau)* **91**, 445-458.

Kohlstedt, D. L. & Weathers, M. S. 1980. Deformation induced microstructures, paleo-piezometers, and differential stresses in deeply eroded fault zones. *Journal of Geophysical Research* **85**, 6269-6285.

Kuhlmann-Wilsdorf, D. 1989. Theory of plastic deformation: properties of low energy dislocation structures. *Materials Science and Engineering A* **113**, 1-41.

Kumar, M., Schwartz, A. J. & Wayne, E. K. 2001. Correlating observations of deformation microstructures by TEM and automated EBSD techniques. *Materials Science and Engineering* **309-310**, 78-81.

Kunze, K., Heidelbach, F., Wenk, H.-R. & Adams, B. L. 1994. Orientation imaging microscopy of calcite rocks. In: *Textures of Geological Materials* (edited by Bunge, H. J., Siegesmund, S., Skrotzki, W. & Weber, K.). DGM Informationsgesellschaft, Oberursel, 127-143.

Kuwahara, M. & Eiho, S. 1976. Processing of radio-isotope angiocardiographic images. In: *Digital processing of biomedical images* (edited by Preston, K. & Onoe, M.). Plenum Press, New York, 187-203.

Li, J. C. M. 1962. Possibility of Subgrain Rotation during Recrystallization. *Journal of Applied Physics* **33**(10), 2958-2965.

Lloyd, G. E. 2004. Microstructural evolution in a mylonitic quartz simple shear zone: the significant roles of dauphine twinning and misorientation. In: *Flow processes in faults and shear zones* (edited by Alsop, G. I., Holdsworth, R. E., McCaffrey, K. J. W. & Hand, M.). *Special Publications* **224**. Geological

Society, London, 39-61.
Lloyd, G. E. & Ferguson, C. C. 1986. A spherical electron channelling pattern map for use in quartz petrofabric analysis. *Journal of Structural Geology* **8**, 517-526.
Lloyd, G. E. & Freeman, B. 1994. Dynamic recrystallisation of quartz under greenshist conditions. *Journal of Structural Geology* **16**, 867-881.
McCabe, R. J. & Teter, D. F. 2006. Analysis of recrystallised volume fractions in uranium using electron backscatter diffraction. *Journal of Microscopy* **223**, 33-39.
McCaig, A., Covey-Crump, S., Ben Ismaïl, W. & Lloyd, G. 2007. Fast diffusion along mobile grain boundaries in calcite. *Contributions to Mineralogy and Petrology* **153**(2), 159-175.
McLaren, A. C. 1991. *Transmission electron microscopy of minerals and rocks*. Cambridge University Press, Cambridge, 387p.
Means, W. D. 1981. The concept of steady-state foliation. *Tectonophysics* **78**, 179-199.
Means, W. D. 1983. Microstructure and micronotion in recrystallization flow of octachloropropane, a first look. *Geologische Rundschau* **72**, 511-528.
Means, W. D. 1989. Synkinematic microscopy of transparent polycrystals. *Journal of Structural Geology* **11**, 163-174.
Means, W. D. & Ree, J. H. 1988. Seven types of subgrain boundaries in octachloropropane. *Journal of Structural Geology* **10**(7), 765-770.
Mercier, J.-C. C., Anderson, D. A. & Carter, N. L. 1977. Stress in the lithosphere: inferences from steady state flow of rocks. *Pure and Applied Geophysics* **115**, 199-226.
Mika, D. P. & Dawson, P. R. 1999. Polycrystal plasticity modeling of intracrystalline boundary textures. *Acta Materialia* **47**, 1355-1369.
Molli, G., Conti, P., Giorgetti, G., Meccheri, M. & Oesterling, N. 2000. Microfabric study on the deformational and thermal history of the Alpi Apuane marbles (Carrara marbles), Italy. *Journal of Structural Geology* **22**, 1808-1825.
Nabarro, F. R. N. 2006. Creep in commercially pure metals. *Acta Materialia* **54**(2), 263-295.
Nix, W., Gibeling, J. & Hughes, D. 1985. Time-dependent deformation of metals. *Metallurgical and Materials Transactions A* **16**(12), 2215-2226.
Oesterling, N. 2004. Dynamic recrysatllisation and deformation mechanisms of naturally deformed Carrara Marble - a study on one- and two-phase carbonate rocks. Unpublished Ph.D. thesis, Basel, 292p.
Orlova, A. 1996. On the applied stress dependence of subgrain size. *Materials Science and Engineering* **220**, 117-122.
Orlova, A. 2001. Subgrain size in the view of the composite model of dislocation structure. *Materials Science and Engineering* **A297**, 281-285.
Orlová, A. & Dobes, F. 2004. On the stress-subgrain size relationships derived from the composite model of dislocation structure. *Materials Science and Engineering* **A381**, 171-174.
Orlova, A. & Podstranská, I. 1998. On the influence of temperature on the subgrain size. *Materials Science and Engineering* **A248**, 56-64.
Pennock, G. M. & Drury, M. R. 2005. Low-angle subgrain misorientations in deformed NaCl. *Journal of Microscopy* **217**, 130-137.
Pennock, G. M., Drury, M. R. & Spiers, C. J. 2005. The development of subgrain misorientations with strain in dry synthetic NaCl using EBSD. *Journal of Structural Geology* **27**, 2159-2170.
Pfiffner, O. A. & Ramsay, J. G. 1982. Constraints on geological strain rates: arguments from finite strain states of naturally deformed rocks. *Journal of Geophysical Research* **87**, 311-321.
Phillips, F. C. 1962. *An introduction to crystallography*. Longmans, Green and co, London, 340p.
Pieri, M., Burlini, L., Kunze, K., Olgaard, D. L. & Stretton, I. C. 2001. Rheological and microstructural evolution of Carrara marble with high shear strain: results from high temperature torsion experiments. *Journal of Structural Geology* **23**, 1393-1413.
Poirier, J. P. 1974. Quelques remarques sur la sous-structure de fluage. Analogies hydrodynamiques. *Materials Science and Engineering* **13**, 191-193.
Poirier, J. P. 1985. *Creep of crystals. High temperature deformation processes in metals, ceramics and minerals.* Cambridge University Press, Cambridge, 260p.
Poirier, J. P. & Nicolas, A. 1975. Deformation induced recrystallisation due to progressive misorientation of subgrains, with special reference to mantle peridotites. *Journal of Geology* **83**, 707-720.
Ponge, D. & Gottstein, G. 1998. Necklace formation during dynamic recrystallization: mechanisms and impact on flow behavior. *Acta Materialia* **46**(1), 69-80.
Post Jr., R. L. 1977. High-temperature creep of Mt. Burnet Dunite. *Tectonophysics* **42**, 75-110.
Prior, D. J. 1999. Problems in determining the misorientation axes for small angular misorientations, using electron backscatter diffraction in the SEM. *Journal of Microscopy* **1995**, 217-225.
Raabe, D., Sachtleber, M., Zhao, Z., Roters, F. & Zaefferer, S. 2001. Micromechanical and macromechanical effects in grain scale polycrystal plasticity experimentation and simulation. *Acta Materialia* **49**(17), 3433-3441.
Raj, S. V. 2002. Power-law and exponential creep in class M materials: discrepancies in experimental observations and implications for creep modelling.

Materials Science and Engineering **A322**, 132-147.
Raj, S. V. & Pharr, G. M. 1986. A compilation and analysis of data for the stress dependence of subgrain size. *Materials Science and Engineering* **81**, 217.
Raj, S. V. & Pharr, G. M. 1989. Creep substructure formation in sodium chloride single crystals in the power law and exponential creep regimes. *Materials Science and Engineering A* **122**(2), 233-242.
Ray, R. K., Hutchinson, W. B. & Duggan, B. J. 1975. A study of the nucleation of recrystallization using HVEM. *Acta Metallurgica* **23**, 831-840.
Read, W. T. 1953. *Dislocations in Crystals*. McGraw-Hill, New York, 228p.
Renner, J. & Evans, B. 2002. Do calcite rocks obey the power-law creep equation? In: *Deformation Mechanisms, Rheology and Tectonics: Current Status and Future Perspectives* (edited by de Meer, S., Drury, M.R., de Bresser, J.H.P. & Pennock, G.M.). *Geological Society Special Publications* **200**. Geological Society, London, 293-307.
Ross, J. V., Ave Lallemant, H. G. & Carter, N. L. 1980. Stress dependence of recrystallised grain and subgrain size in olivine. *Tectonophysics* **70**, 39-61.
Rossi, P. L. O. & Sellars, C. M. 1997. Quantitative metallography of recrystallization. *Acta Materialia* **45**, 137-148.
Russ, J. C. & Dehoff, R. T. 1999. *Practical Stereology*. Plenum Press, New York, 312p.
Rutter, E. H. 1974. The influence of temperature, strain rate and interstitial water in the experimental deformation of calcite rocks. *Tectonophysics* **22**, 311-334.
Rutter, E. H. 1995. Experimental study of the influence of stress, temperature and strain on the dynamic recrystallisation of Carrara marble. *Journal of Geophysical Research* **100**, 24651-24663.
Schmid, S. M., Boland, J. N. & Paterson, M. S. 1977. Superplastic flow in fine grained limestone. *Tectonophysics* **43**(257-291).
Schmid, S. M., Paterson, M. S. & Boland, J. N. 1980. High temperature flow and dynamic recrystallisation in Carrara marble. *Tectonophysics* **65**, 245-280.
Schwartz, A. J., Kumar, M. & Adams, B. L. 2000. *Electron Backscatter Diffraction in Materials Science*. Kluwer Academic / Plenum Publishers, New York, 339p.
Sellars, C. M. 1978. Recrystallisation of metals during hot deformation. *Philosophical Transactions of the Royal Society of London* **288**, 147-158.
Shimizu, I. 1998. Stress and temperature dependence of recrystallised grain size: A subgrain misorientation model. *Geophysical Research Letters* **25**, 4237-4240.
Smallman, R. 1985. *Modern Physical Metallurgy*. Butterworths, London, 530p.
Smith, C. S. 1948. Grains, phases, and interactions: An interpretation of microstructure. *Transactions of the Metallurgical Society AIME* **175**, 15-51.
Spolenak, R., Brown, W. L., Tamura, N., MacDowell, A. A., Celestre, R. S., Padmore, H. A., Valek, B., Bravman, J. C., Marieb, T., Fujimoto, H., Batterman, B. W. & Patel, J. R. 2003. Local plasticity of Al thin films as revealed by X-ray microdiffraction. *Physical Review Letters* **90**(9), 1-4.
Stipp, M., Stunitz, H., Heilbronner, R. & Schmid, S. M. 2002. The eastern Tonale fault zone: a `natural laboratory' for crystal plastic deformation of quartz over a temperature range from 250 to 700 [degree sign]C. *Journal of Structural Geology* **24**(12), 1861-1884.
Stipp, M. & Tullis, J. 2003. The recrystallised grain size piezometer for quartz. *Geophysical Research Letters* **30**, doi: 10.1029/2003GL018444.
Streb, G. & Reppich, B. 1973. Steady state deformation and dislocation structure of pure and Mg-doped LiF single crystals. *Physica Status Solidi (a)* **16**, 493-505.
Takeuchi, S. & Argon, A. S. 1976. Review: Steady-state creep of single phase crystalline matter at high temperature. *Journal of Materials Science* **11**, 1542-1566.
Ter Heege, J. H., de Bresser, J. H. P. & Spiers, C. J. 2002. The influence of dynamic recrystallization on the grain size distribution and rheological behaviour of Carrara Marble deformed in axial compression. In: *Deformation mechanisms, Rheology and Tectonics: Current Status and Future Perspectives* (edited by de Meer, S., Drury, M. R., de Bresser, J. H. P. & Pennock, G. M.). *Special Publications* **200**. Geological Society, London, 331-353.
Trimby, P., Day, A., Mehnert, K. & Schmidt, N.-H. 2002. Is fast mapping good mapping? A review of the benefits of high-speed orientation mapping using electron backscatter diffraction. *Journal of Microscopy* **205**, 259-269.
Trimby, P. W., Drury, M. R. & Spiers, C. J. 2000. Misorientations across etched boundaries in deformed rocksalt: a study using electron backscatter diffraction. *Journal of Structural Geology* **22**, 81-89.
Trimby, P. W., Prior, D. J. & Wheeler, J. 1998. Grain boundary hierarchy development in a quartz mylonite. *Journal of Structural Geology* **20**, 917-935.
Tullis, J. & Yund, R. A. 1985. Dynamic recrystallisation of a feldspar - a mechanism for ductile shear zone formation. *Geology* **13**, 238-241.
Tungatt, P. D. & Humphreys, F. J. 1981. An in-situ optical investigation of the deformation behaviour of sodium nitrate - an analogue for calcite. *Tectonophysics* **78**, 661-674.
Tungatt, P. D. & Humphreys, F. J. 1984. The plastic

deformation and dynamic recrystallisation of polycrystalline sodium nitrate. *Acta Metallica* **32**, 1625-1635.

Turner, F. J., Griggs, D. T. & Heard, H. C. 1954. Experimental deformation of calcite crystals. *Geological Society of America Bulletin* **65**, 883-934.

Turner, M. S. 2001. The textural and microstructural evolution of Carrara Marble samples experimentally deformed at high temperature. Unpublished MSc thesis, University of Manchester, 158p.

Twiss, R. J. 1977. Theory and applicability of a recrystallised grain size paleopiezometer. *Pure and Applied Geophysics* **115**, 227-244.

Twiss, R. J. 1986. Variable sensitivity piezometric equations for dislocation density and subgrain diameter and their relevance to olivine and quartz. *Geophysical Monograph* **36**, 247-261.

Ulrich, S., Schulmann, K. & Casey, M. 2002. Microstructural evolution and rheological behaviour of marbles deformed at different crustal levels. *Journal of Structural Geology* **24**(5), 979-995.

Ulrich, S., Thompson, A. B., Schulmann, K. & Casey, M. 2006. Microstructure mechanism map of dynamically recrystallized marble. *Tectonophysics* **412**(3-4), 173-182.

Underwood, E. E. 1970. *Quantitative Stereology*. Addison-Wesley, Reading, Massachusetts, 274p.

Urai, J. L., Means, W. D. & Lister, G. S. 1986. Dynamic recrystallisation of minerals. *Geophysical Monograph* **36**, 161-199.

Valcke, S. L. A., Drury, M. R., De Bresser, J. H. P. & Pennock, G. M. 2007. Quantifying heterogeneous microstructures: core and mantle subgrains in deformed calcite. *Materials Science Forum* **550**, 307-312.

Valcke, S. L. A., Pennock, G. M., Drury, M. R. & De Bresser, J. H. P. 2006. Electron backscattered diffraction as a tool to quantify subgrains in deformed calcite. *Journal of Microscopy* **224**, 264-276.

Van der Pluijm, B. A. 1991. Marble mylonites in a Bancroft shear zone, Ontario, Canada: microstructures and deformation mechanisms. *Journal of Structural Geology* **13**, 1125-1135.

Van der Wal, D. 1993. Deformation processes in mantle peridotites - with emphasis on the Ronda peridotite of SW Spain. Unpublished Geologica Ultraiectina **102**, PhD thesis, Utrecht University, 180p.

Van der Wal, D., Chopra, P. N., Drury, M. R. & Fitz Gerald, J. D. 1993. Relationships between dynamically recrystallized grain size and deformation conditions in experimentally deformed olivine rocks. *Geophysical Journal International* **20**, 1479-1482.

Vernon, R. H. 1981. Optical microstructure of partly recrystallized calcite in some naturally deformed marbles. *Tectonophysics* **78**, 601-612.

Weathers, M. S., Bird, J. M., Cooper, R. F. & Kohlstedt, D. L. 1979. Differential stress determined from deformation-induced microstructures of the Moine thrust zone. *Journal of Geophysical Research* **84**(B13), 7495-7509.

Weertman, J. 1955. Theory of steady-state creep based on dislocation climb. *Journal of Applied Physics* **26**, 1213-1217.

Weertman, J. 1968. Dislocation climb theory for steady state creep. *Transactions of the American Society for Metals* **61**, 681-694.

Weertman, J. & Weertman, J. R. 1983. Mechanical properties, mildly temperature-dependent. In: *Physical Metallurgy: Third, Revised and Enlarged Edition* (edited by Cahn, R. W. & Haasen, P.). North-Holland Physics, New York, 1259-1307.

Wheeler, J., Jiang, Z., Prior, D. J., Tullis, J., Drury, M. R. & Trimby, P. W. 2003. From geometry to dynamics of microstructure: using boundary lengths to quantify boundary misorientations and anisotropy. *Tectonophysics* **376**, 19-35.

Wheeler, J., Prior, D. J., Jiang, Z., Spiess, R. & Trimby, P. 2001. The petrological significance of misorientations between grains. *Contributions to Mineralogy and Petrology* **141**, 109-124.

White, S. 1975. Estimation of strain rates from microstructural features. *Quarterly Journal of the Geological Society of London* **131**, 577-583.

White, S. 1979a. Difficulties associated with paleo-stress estimates. *Bulletin de Minéralogie* **102**, 210-215.

White, S., Drury, M. R., Ion, S. E. & Humphreys, F. J. 1985. Large strain deformation studies using polycrystalline magnesium as a rock analogue. Part I: grain size paleopiezometry in mylonite zones. *Physics of The Earth and Planetary Interiors* **40**, 201-207.

White, S. H. 1973. Syntectonic recrystallization and texture development in quartz. *Nature* **244**, 276-278.

White, S. H. 1976. The effects of strain on microstructures, fabrics and deformation mechanisms in quartzites. *Philosophical Transactions of the Royal Society of London* **A283**, 69-86.

White, S. H. 1977. Geological significance of recovery and recrystallisation processes in quartz. *Tectonophysics* **39**, 143-170.

White, S. H. 1979b. Grain and subgrain size variations across a mylonite zone. *Contributions to Mineralogy and Petrology* **70**, 193-202.

Wyllie, P. J. & Tuttle, O. F. 1960. The system CaO-CO_2-H_2O and the origin of carbonatites. *Journal of Petrology* **1**, 1-17.

Young, C. M. & Sherby, O. D. 1973. Subgrain formation and subgrain boundary strengthening in iron based materials. *Journal of Iron and Steel Institute* **211**, 640-647.

Acknowledgements

Here I am at the end, writing the part of which I thought it would be the most fun to do, and it is of course, but it is at the same time the end of four years working in a pleasant place and so I m not only saying thank you, but unfortunately also saying goodbye to many persons I enjoyed working with…

First of all, a big thanks to my supervisors!

Martyn, already when we met at the DRT conference, I had the idea it would be nice working with you, and this definitely was the right idea! Even though you are very busy with teaching and research, you remain calm and I always felt questions and discussions were welcome. These chats could be very encouraging for me because often when I thought new data were not helping us at all, you somehow knew how to turn them into a useful outcome and I gained new inspiration and motivation...

Hans, I enjoyed our collaboration very much, which was always a good mix between brain cracking science and a relaxing good laugh! You thought me how to be more direct in scientific communication and how to use google, how to manipulate data (in a scientific way of course) and how to dance the foxtrot, or was it the jive... I easily forgave you your endless, unreadable pencil marks, because they were always very useful comments ;-) Your energy and enthousiasm (especially when it concerns marble) is really contagious!

Gill, it's great to have the encouragement of a female collegue! I guess together we gave the female touch to the science in this work. I was lucky to learn the EBSD skills from you, you taught me to be thorough and critical and to find my way in the vast forest of data that come out of EBSD analyses. I especially also want to thank you for the healthy and tasty vegetables you brought us from your garden. I hope in future you will find more time to enjoy this beautiful garden.

Stan, many thanks for critically reading the whole manuscript in a short period of time, your suggestions improved this work still in the very last stage. I was very happy to be able to stay at your house the first half a year when I arrived in Utrecht. This gave me the opportunity to take the time to find a nice place to live.

Chris, with my glasses on I tell you, even though we didn't have so many discussions, they always were very inspiring and great ideas came out of them. It was encouraging to have the interest and scientific input of someone who was less closely involved in the project...

The members of my reading committee: K. Kunze, J. White, J. Tullis, E. Rutter and J. Wheeler are thanked for carefully reading my thesis and giving useful comments. Martin Casey, I would like to thank you for your continued interest in my research after leaving Leeds and for the interesting discussions on marble. Pim Van Maurik, Hans Meeldijk and John Geus, thanks a lot for your invaluable help in the complex world of electron microscopy. Especially thanks for reassuring me and giving me the confidence when things had gone seriously wrong with the microscope... Also the people from the HKL company are thanked for their assistance with software problems. Austin Day, many thanks for writing a subroutine specifically designed for analyzing subgrains, it was very useful! Otto Stiekema, thank you for patiently dealing with my high demands for sample preparation. To all my collegues and ex-collegues from the STG group, Dirk, Bart, Reinoud (thanks for the summary!), Herman and Auke, with you guys around it was always a pleasure to come to work: coffee breaks, little chats and 'borrels' in the corridor cheered up the long working days! Magda, thank you for arranging the many administrative things, and especially, for finding my unconsciously lost passport just when I was about to go crossing the border with Switserland!

To my new collegues at TNO: I am very grateful for the understanding and freedom I got during the last thesis rush. This allowed the time needed to finsih the layout... I am happy to work with you guys!

Thanks to so many inspiring artists and the guys from the Deezer site: music has appeared to be indispensible in writing my thesis!

Laurie, you became a very good friend after four years sharing the same office. While we were obviously seriously working, you introduced me into a lot of good music, I got to know all the juicy actualities and you were always prepared to listen to my little stories. And I guess in mean time, our explosive giggling has become famous in the STG group...even beyond...when paper aeroplanes started flying out of the window ;-)

Fenny, Judith, Roberta, Ueli, Christian, Simona, Thomas, Alex, Dirk, Nadine, Cornelia, Pasha, Otto, Nerminka, Joost, Celine…and also Suzan and my friends from dance: it's not always easy to build up a new social life in a new city, but thanks to you guys I very much enjoy living in Utrecht. I hope we will continue to have these evenings out and even though some of you have moved by now, this just makes me visit other cities!

Babs, Sari, Charlotte, Boris, Goele, Dafke, Romain, Luisma, Vicky… and all my friends far away: I am very happy we managed to sustain our friendship so well from a distance, thanks for coming over here, for the endless phone calls and always making it a little feast whenever I visit.

Derya, Marielle, Marjan, Mieke, Milena and my ex-housemates: thanks to you girls I really felt comfortably at home in Utrecht, with your friendship and all the tasty meals, it's like having a family here. I am especially grateful for your care and support during the last stages of writing up!

Steeve, I have seen you finishing your thesis from nearby and sometimes I didn't quite understand how it could be so stressful... but suprise surprise, I ve now clearly experienced everything myself, and indeed! ;-) Thank you for always being understanding and ready to listen, you are my invaluable wise friend!

Mariene, Côme and Xavier, you guys came into the picture at the very last stage of my thesis, but exactly at the right moment to make these hard working days light with much laughter and fun. Your close friendship has become very precious to me. Il y a pas le feu au lac, mais j' ai quand même envie d'applaudir!

To my grand parents and family: thanks for caring and remaining interested in what I do up there in the north! Mama, papa and Lisa: your unconditional, loving support was the omnipresent pilar throughout these four years. Great you have found your way in the world of 'SMS-ing', 'MSN' and 'Skype' ;-) Jullie zijn onmisbaar in alles wat ik onderneem, dankjewel!

Curriculum Vitae

28 March 1979	Born in Kortrijk, Belgium
1997-2001	Study of Geology, University of Ghent, Belgium
2001	Junior project leader in geological studies, Envico, Mechelen, Belgium
2002-2003	MSc. by Research in Microstructural Geology, University of Leeds, United Kingdom
2003	Junior project leader in geological studies, Royal Haskoning, Mechelen, Belgium
2003-2008	Ph.D. Student in the Structural Geology and Tectonics Group and the Experimental Rock Deformation Lab, University of Utrecht, The Netherlands
from March 2008	Scientist in construction materials at TNO (Toegepast Natuurwetenschappelijk Onderzoek) Delft, the Netherlands

A

Appendix A - Colour figures

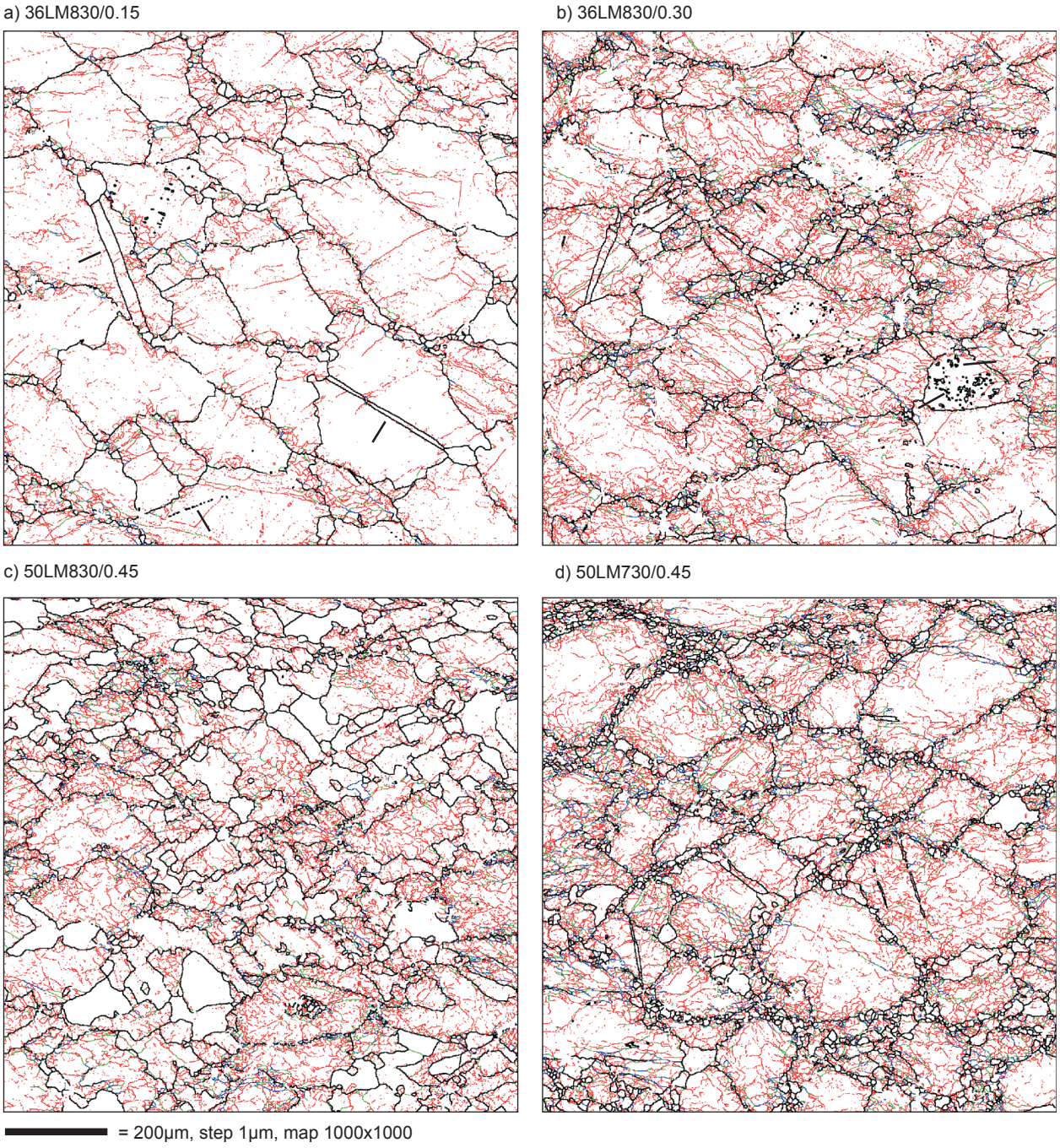

Figure 2.1: EBSD maps (a-d) showing boundaries of selected calcite samples used in this paper. The red boundaries have misorientations >1°, the green boundaries >3°, the blue boundaries >5° and the black boundaries representing boundaries >15° (~grain boundaries). Noise has been reduced although some isolated open noise boundaries remain (see >1° red boundaries). On (a) twin boundaries are indicated by arrows, on (b) misindexing is indicated by two arrows. Both types of misindexing are ignored in the size measurements.

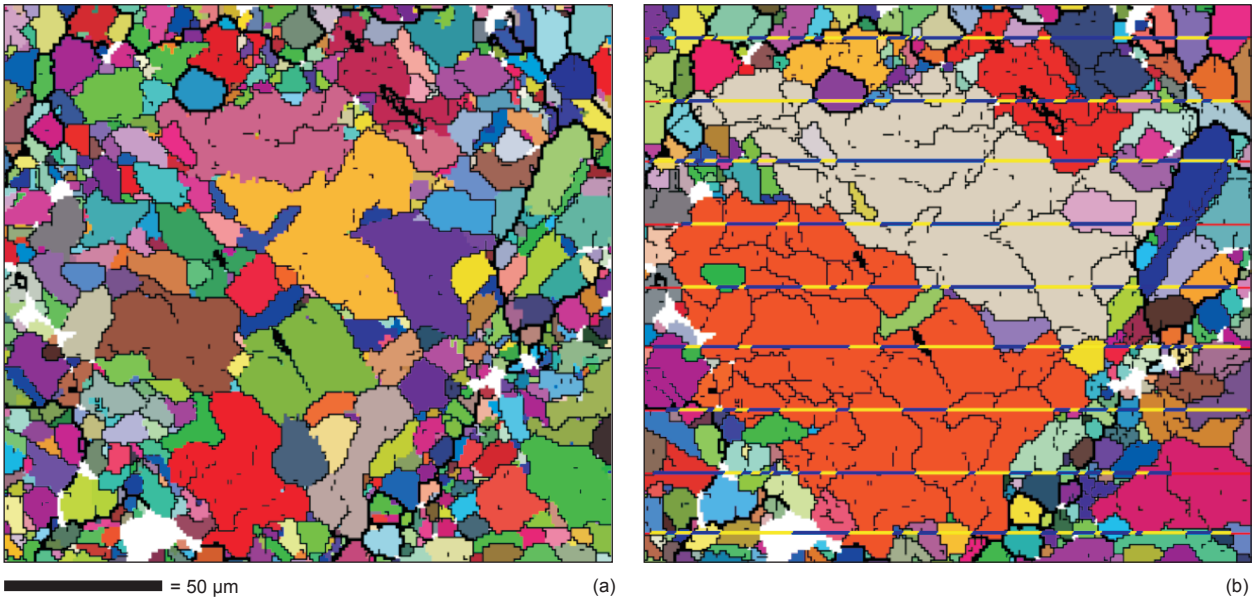

Figure 2.3: EBSD map of sample 36LM830/0.45, illustrating the *DH* and *LI-MH* methods for determining subgrain size (after noise reduction). White pixels are non-indexed solutions. Thick black boundaries show grain boundaries (>15°) and thin black lines show subgrain boundaries (>1°). Fully enclosed domains (*DH* method) are shown in random colours for $\theta > 0.5°$ in (a) and for $\theta > 1°$ in (b). In (b) the linear intercept lengths (*LI-MH* method) are shown for $\theta > 1°$.

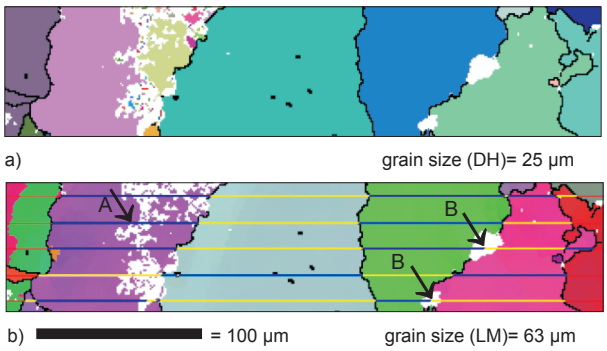

Figure 2.4: Part of a noise reduced EBSD map of sample 36LM830/0.30 to illustrate the influence of non-indexing on a) the DH method and b) the LI-MH method. Both maps cover the same area, thick black lines are boundaries > 15°. White pixels are non-indexed solutions. a) Grains detected on the basis of enclosed area, with misorientations >15° are shown in random colours. Within the purple grain, many small detected regions are recognized as small domains within the larger grain. b) Grains with different orientations are shown in colours related to the crystal Euler angles. Alternating yellow and blue linear intercept lines (LI-MH method) locate boundaries. The red intercept lines are at map borders and not included in the measurements. At (A) the intercept line runs through a non-indexed patch within a grain (the purple colour, related to orientation, shows that small parts between the non-indexed patches belong to the same grain). At (B) the intercept line in the non-indexed patch at the grain boundary is divided in two and each half is added to the neighbouring grains. The grain size detected on this map with the DH method is 25µm and with the LI-MH method is 63 µm.

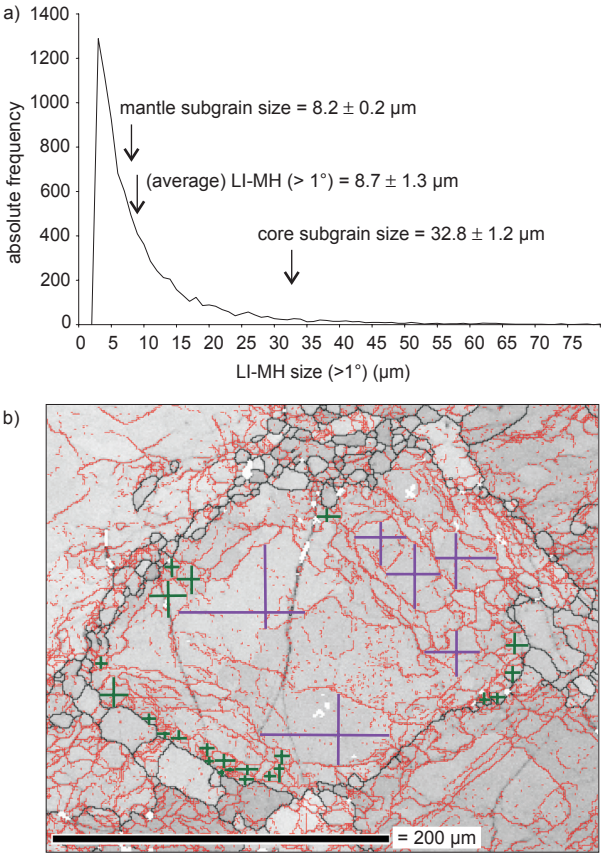

Figure 2.9: a) Intercept distribution for sizes of subgrains with boundaries having misorientations >1° for sample 50LM730/0.45. On the graph the LI-MH (>1°) average and the LI-MH (>1°) distribution are compared with manual measurements of mantle subgrain size and core subgrain size. b) EBSD-pattern quality image of part of the analysed area of sample 50LM730/0.45, showing an example of manual measurements of mantle subgrain size (green lines) and core subgrain size (purple lines).

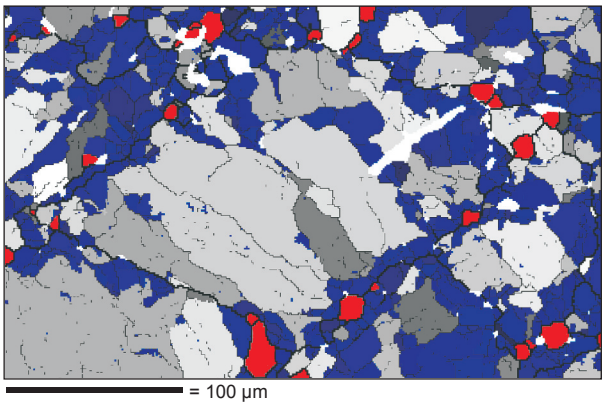

Fig. 3.11: Detail of EBSD map in sample 36LM830/0.45 showing a core mantle microstructure. The map has been processed using the Cao method and subsequently recrystallised grains (red) have been distinguished from the deformed grains in which core (grey) and mantle (blue) subgrains have been separated. Boundaries > 10° are drawn in the thick black lines and boundaries >1° in the thin black lines. Domains (subgrains) have been detected for θ_{min} = 1° and θ_c = 0.5°. Individual core subgrains are indicated in different grey shades, while individual mantle subgrains are indicated in different blue shades. Non-indexed pixels are indicated in white.

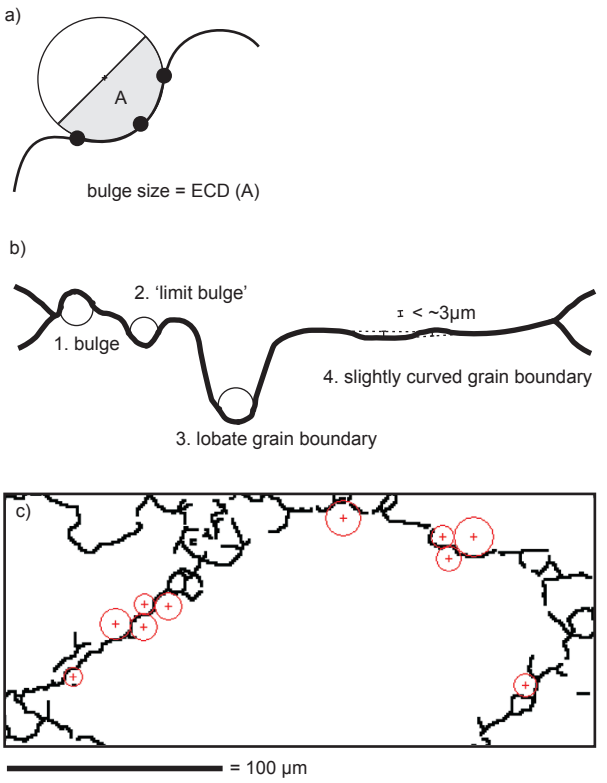

Fig. 3.12: a) schematic diagram to illustrate how a bulge size is measured: a circle is fitted to three points lying on the bulge, this circle is divided by two and the equivalent circular diameter (ECD) of its area (A) is the 'bulge size'. b) schematic diagram of a grain boundary to illustrate the distinction between grain boundary bulges, lobate grain boundaries and slightly curved, wavy boundaries. c) Example of circles that are fitted to the bulges using the commercial program Scandium (Soft Imaging System, Germany).

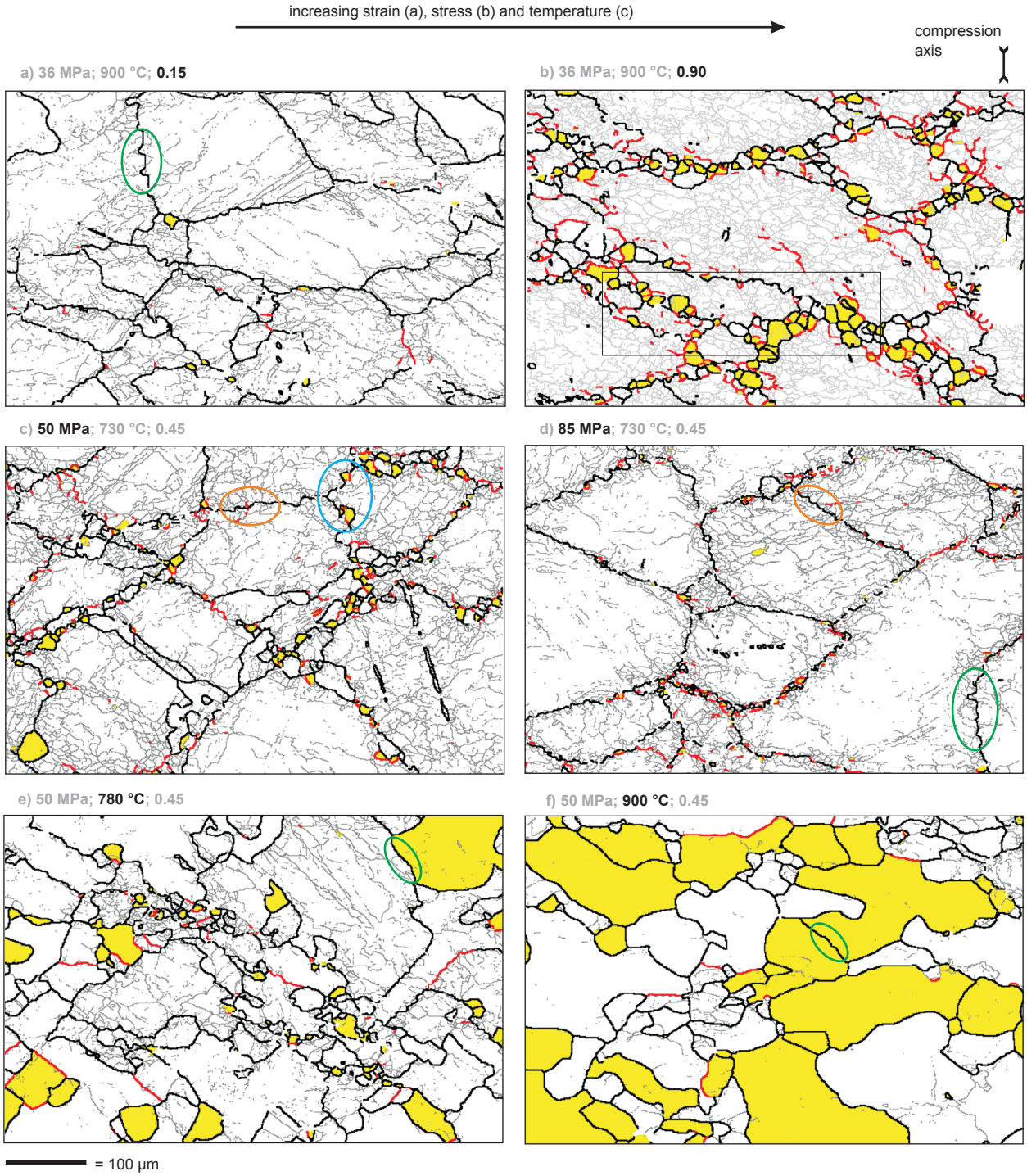

Fig. 4.5: EBSD maps of representative samples to illustrate the microstructural changes with stress, temperature and strain. From left to right, the considered deformation condition increases, while the other two are constant. The black lines are grain boundaries >30°; the red lines, grain boundaries >10° and the grey lines are subgrain boundaries >1°. The recrystallised grains are coloured yellow. The deformation conditions (final stress, temperature and natural strain) are indicated with each figure. The scale is the same for all maps. The coloured circles and the frame are indicating specific features mentioned in the text (paragraph 4.3.1). The compression axis is vertical.

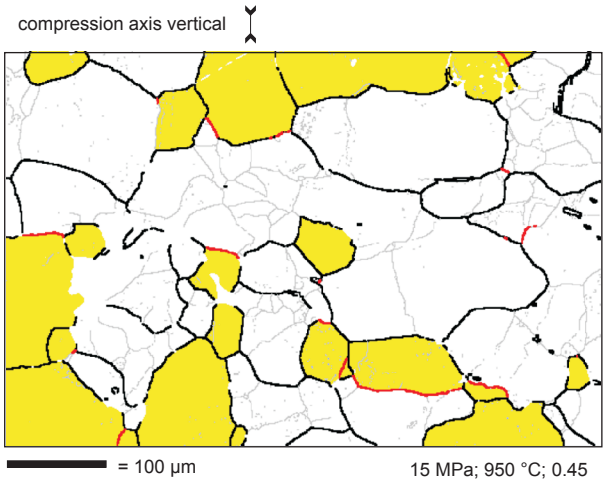

Fig. 4.6: EBSD map of sample 15LM950/0.45 to illustrate the homogeneous microstructure. The black lines are grain boundaries >10°, the grey lines, subgrain boundaries >1°. The recrystallised grains are coloured yellow. The compression axis is vertical.

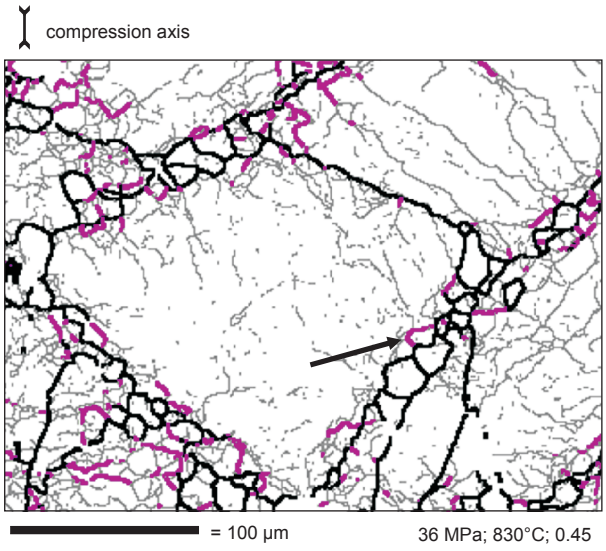

Fig. 4.8: EBSD map of sample 36LM830/0.45 illustrating the occurrence of high angle bridging subgrain boundaries. Black lines are grain boundaries >10°, pink lines, subgrain boundaries >5° and grey lines, subgrain boundaries >1°. The arrow indicates an example of a subgrain bulge with a 'bridging' subgrain boundary. The compression axis is vertical.

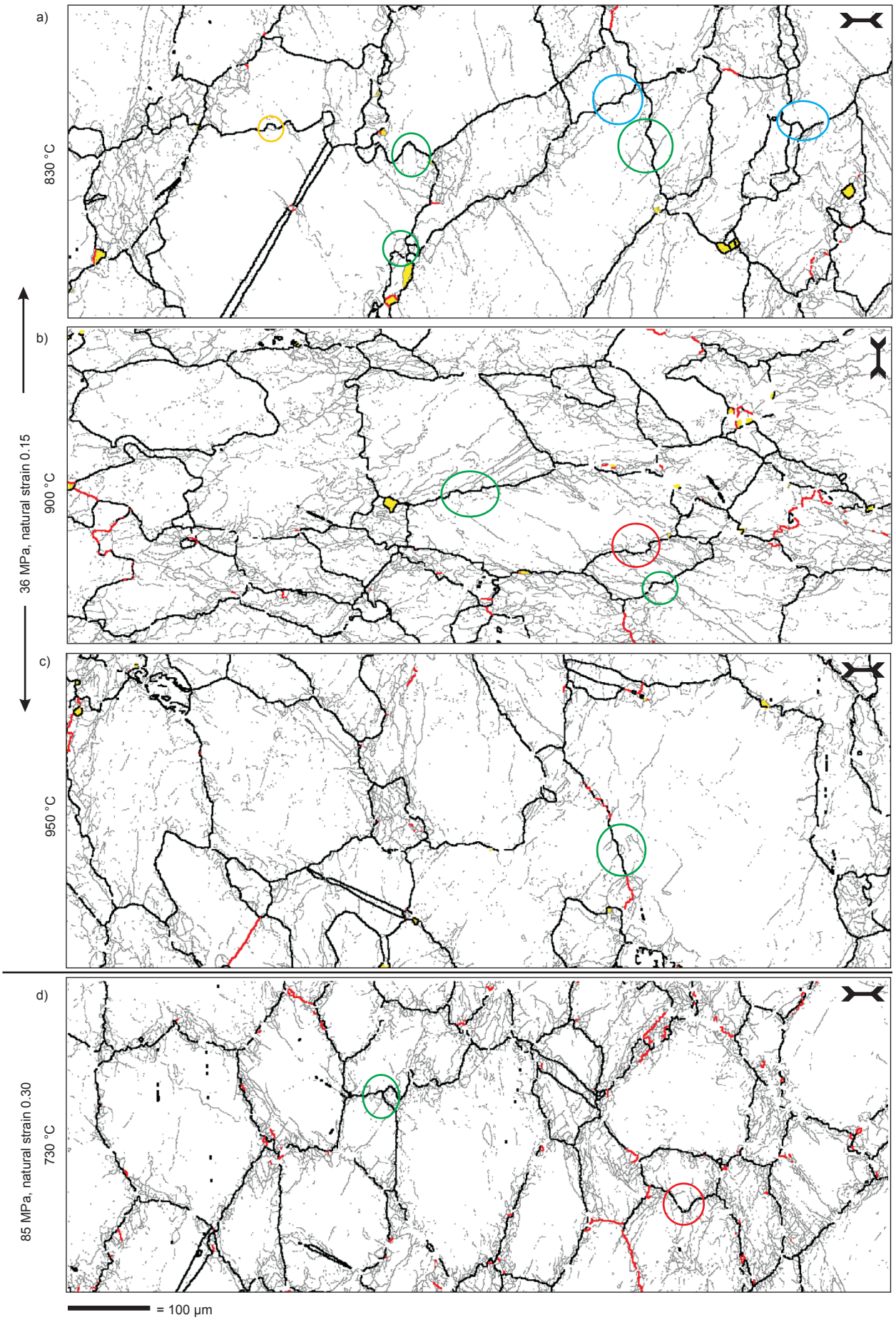
a)
830 °C
b)
900 °C
36 MPa, natural strain 0.15
c)
950 °C
d)
730 °C
85 MPa, natural strain 0.30
= 100 µm

Fig. 4.7 (previous page): Selected areas of EBSD maps of representative samples at low strain to illustrate the grain boundary bulges. The black lines are grain boundaries >30°; the red lines, grain boundaries >10° and the grey lines are subgrain boundaries >1°. The recrystallised grains are coloured yellow. The deformation conditions are indicated on the figure. The scale is the same for all maps. The coloured circles highlight specific microstructures that are discussed in the text (paragraph 4.3.1). The compression axis is indicated by the double black arrow in the upper right corner of each map.

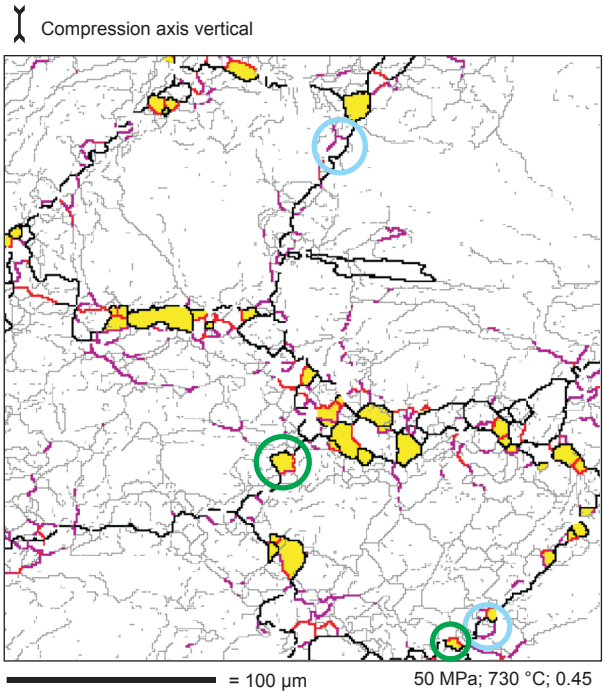

Fig. 4.12 (left): EBSD map of 50LM730/0.45 to illustrate microstructures that can be interpreted in terms of grain boundary bulges. The black lines are grain boundaries >30°, the red lines, grain boundaries >10°, the pink lines, subgrain boundaries >5° and grey lines, subgrain boundaries >1°. The recrystallised grains are indicated in yellow. Bulges can be associated with high angle subgrain boundaries (>5°) (blue circles) or with grain boundaries (>10°), the latter forming recrystallised grains (green circles).

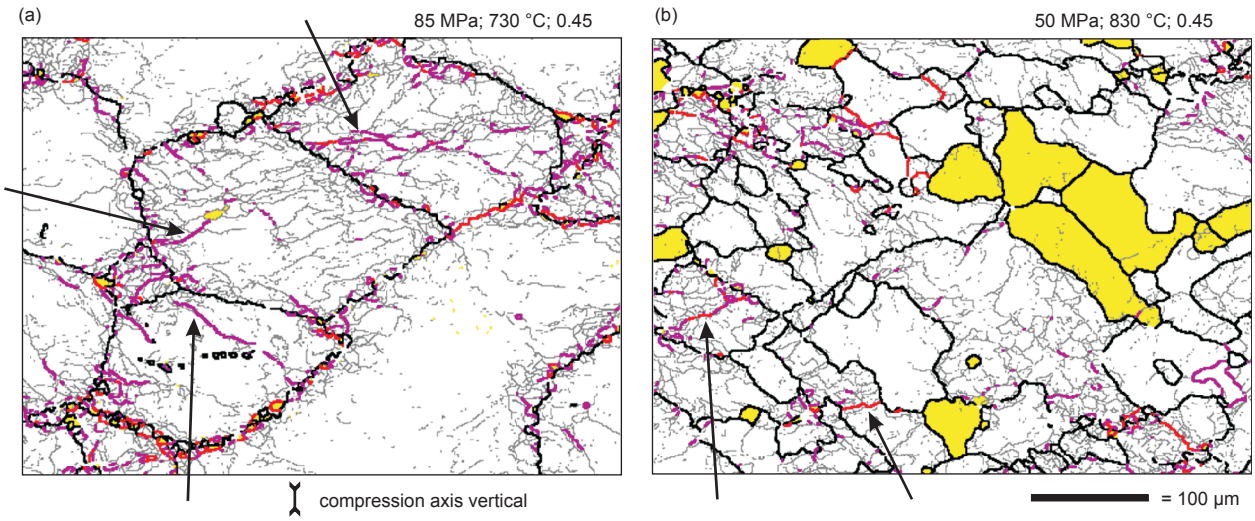

Fig. 4.14: EBSD maps on 85LM730/0.45 (a) and 50LM830/0.45 (b) to illustrate the relation between core subgrain boundaries and deformed grain boundaries. The thick black lines are grain boundaries >30°; the red lines, grain boundaries > 10°; the pink lines, subgrain boundaries >5°; the grey lines, subgrain boundaries >1° and the recrystallised grains are indicated in yellow. (a) shows high angle core subgrain boundaries starting from triple junctions and grain boundaries (arrows). (b) additionally shows high angle segments of boundaries with misorientations >10° and an example of a grain boundary that is parallel to straight core subgrain boundaries. The compression axis is vertical.

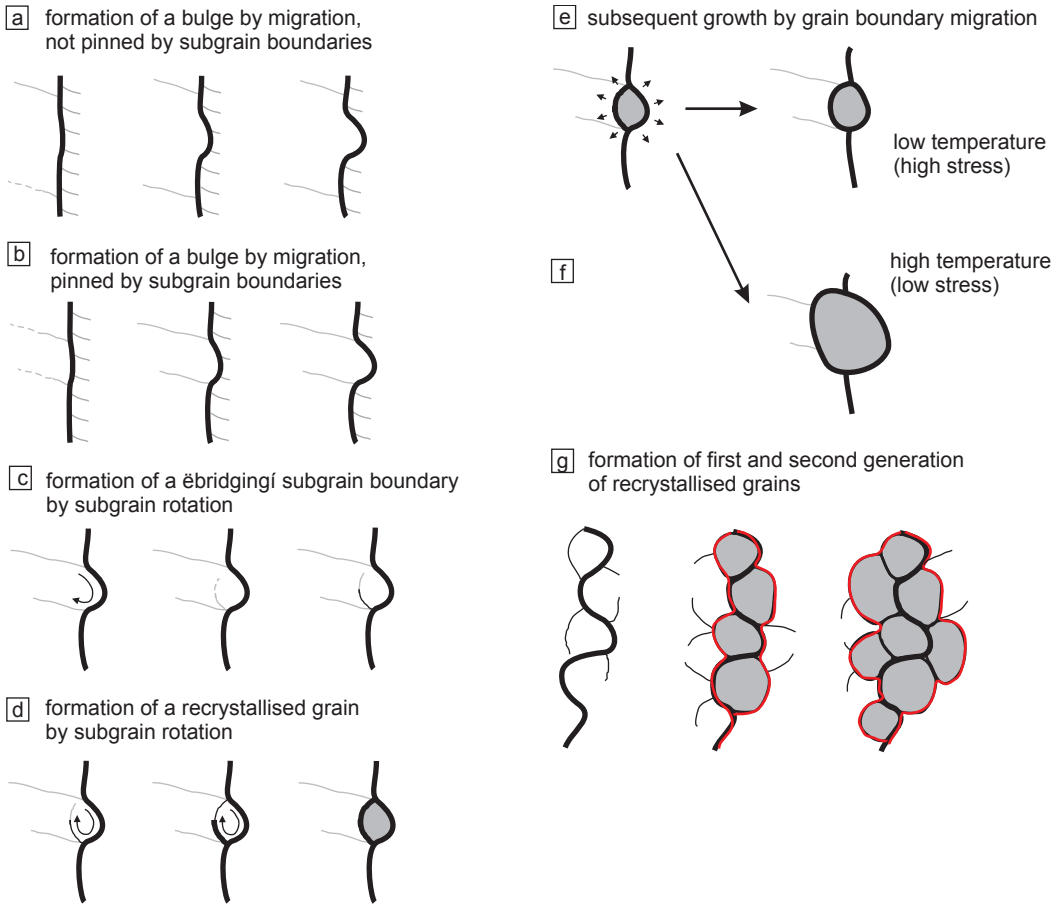

Fig. 4.15: Conceptual model of the formation of bulges, 'bridging' subgrain boundaries and recrystallised grains. Thick black lines: grain boundaries; thin grey lines: low angle subgrain boundaries; thin black lines: high angle subgrain boundaries; curved arrows: indicate rotation; small, straight arrows: indicate grain growth. Recrystallised grains are coloured grey. Red lines in (g) indicate the 'new' grain boundary of the deformed grains related to the geometry of recrystallised grains that form a necklace around the old grain.

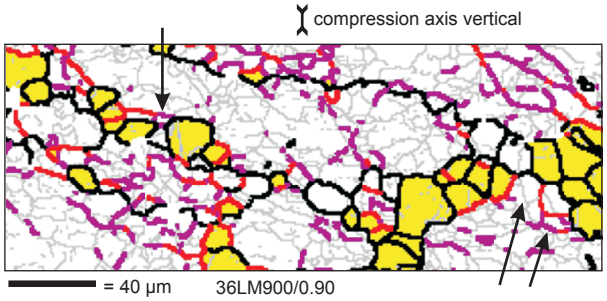

Fig. 4.16: Detail of Fig. 4b, illustrating the formation of a second generation of recrystallised grains (see text, 4.4.3). The thick black lines are grain boundaries >30°; the red lines, grain boundaries > 10°; the pink lines, subgrain boundaries >5°; the grey lines, subgrain boundaries >1° and the recrystallised grains are indicated in yellow. The arrows show where a recrystallised grain might nucleate between existing recrystallised grains. The compression axis is vertical.

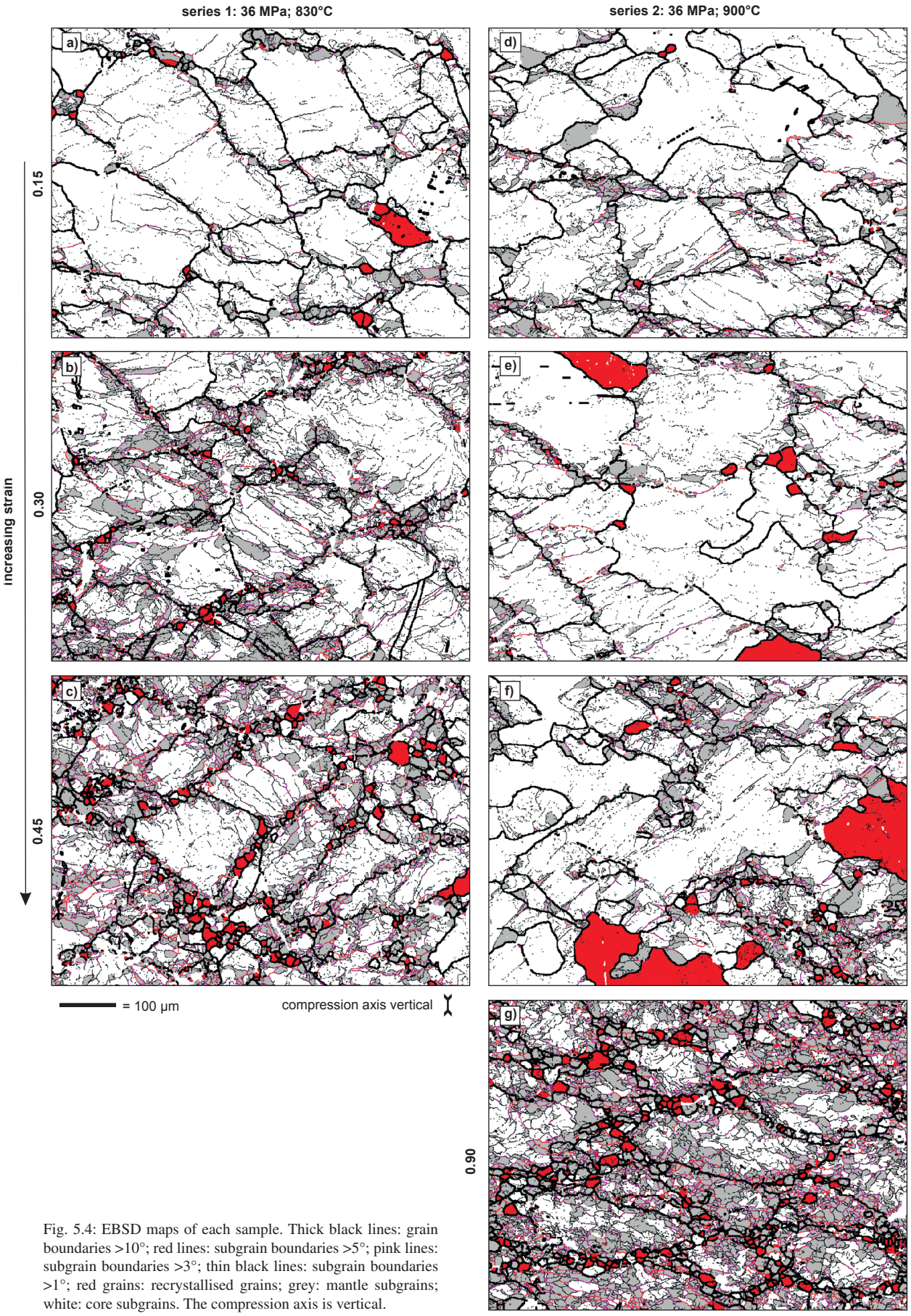

Fig. 5.4: EBSD maps of each sample. Thick black lines: grain boundaries >10°; red lines: subgrain boundaries >5°; pink lines: subgrain boundaries >3°; thin black lines: subgrain boundaries >1°; red grains: recrystallised grains; grey: mantle subgrains; white: core subgrains. The compression axis is vertical.

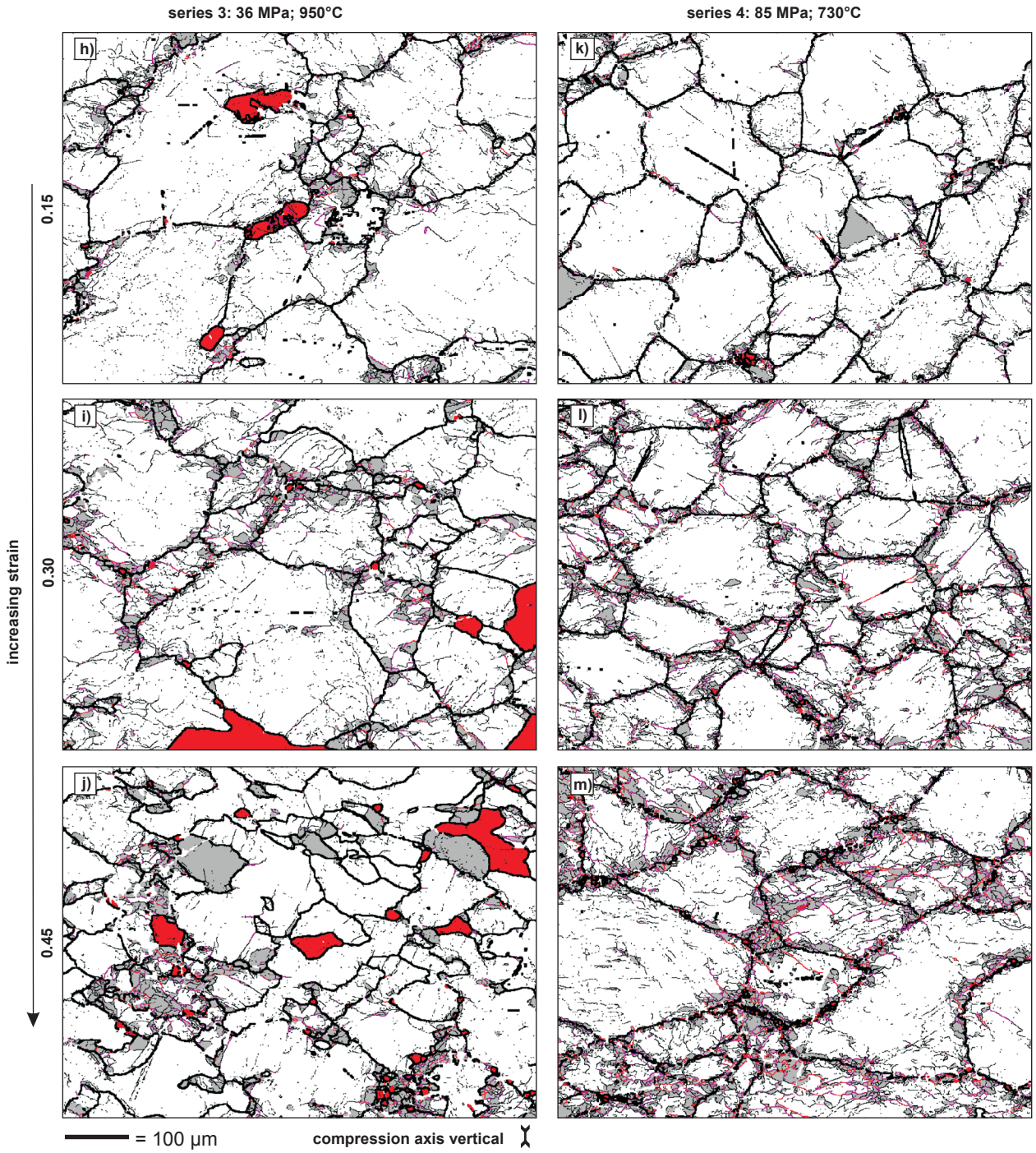

Fig. 5.4(h-m): for caption see Fig. 5.4(a-g)

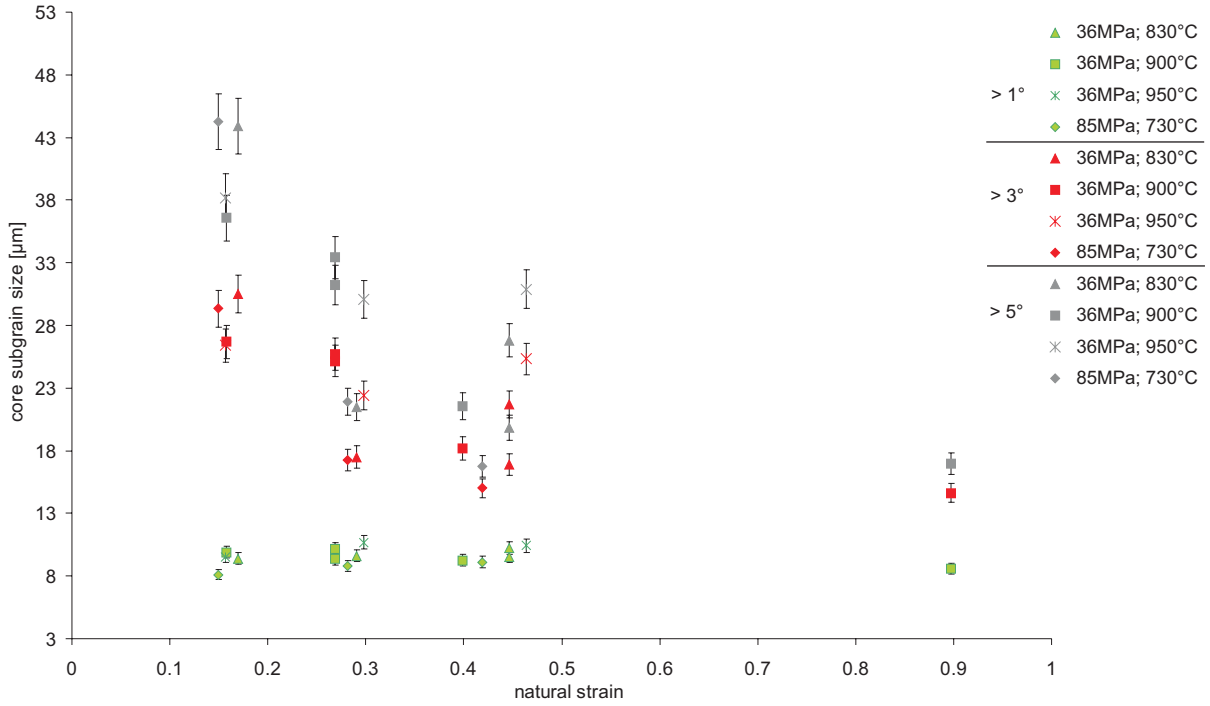

Fig. 5.10: Graph of the core subgrain size versus strain for different misorientation angles at the same strain (0.45) (see legend).

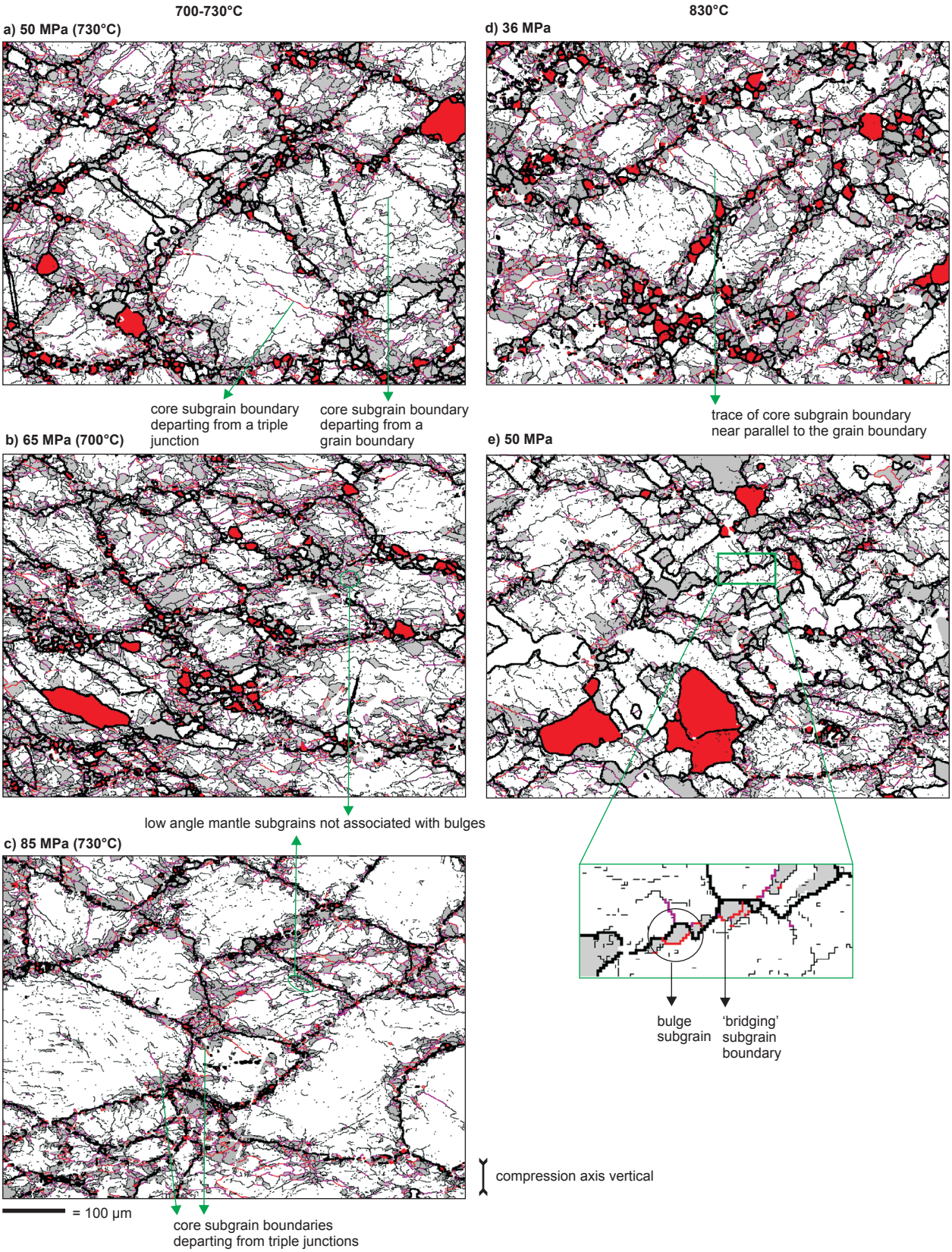

Fig. 6.3: EBSD maps of all samples, arranged in series to see the effect of stress. The compression axis is vertical. Subgrain boundaries having misorientation angles >1° are indicated in thin black lines, >3° in pink, >5° in red; grain boundaries having boundaries with misorientation angles >10° in thick black lines. Recrystallised grains are coloured red and the mantle subgrains >1° in grey. On Fig. 6.3e, a detail is shown of grain boundary bulges and subgrains. Compression axis is vertical.

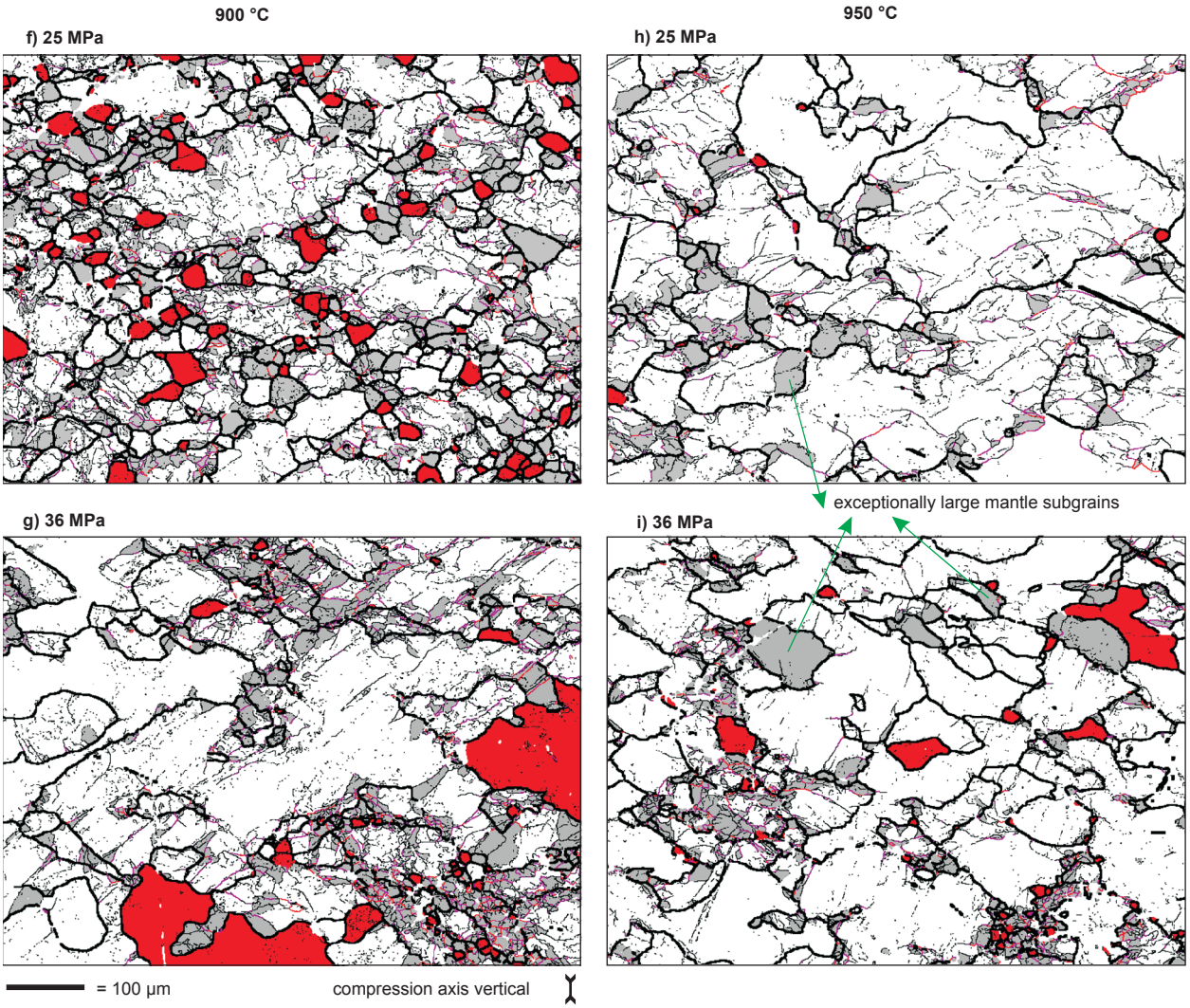

Fig. 6.3(f-i): for caption see Fig. 6.3(a-e)

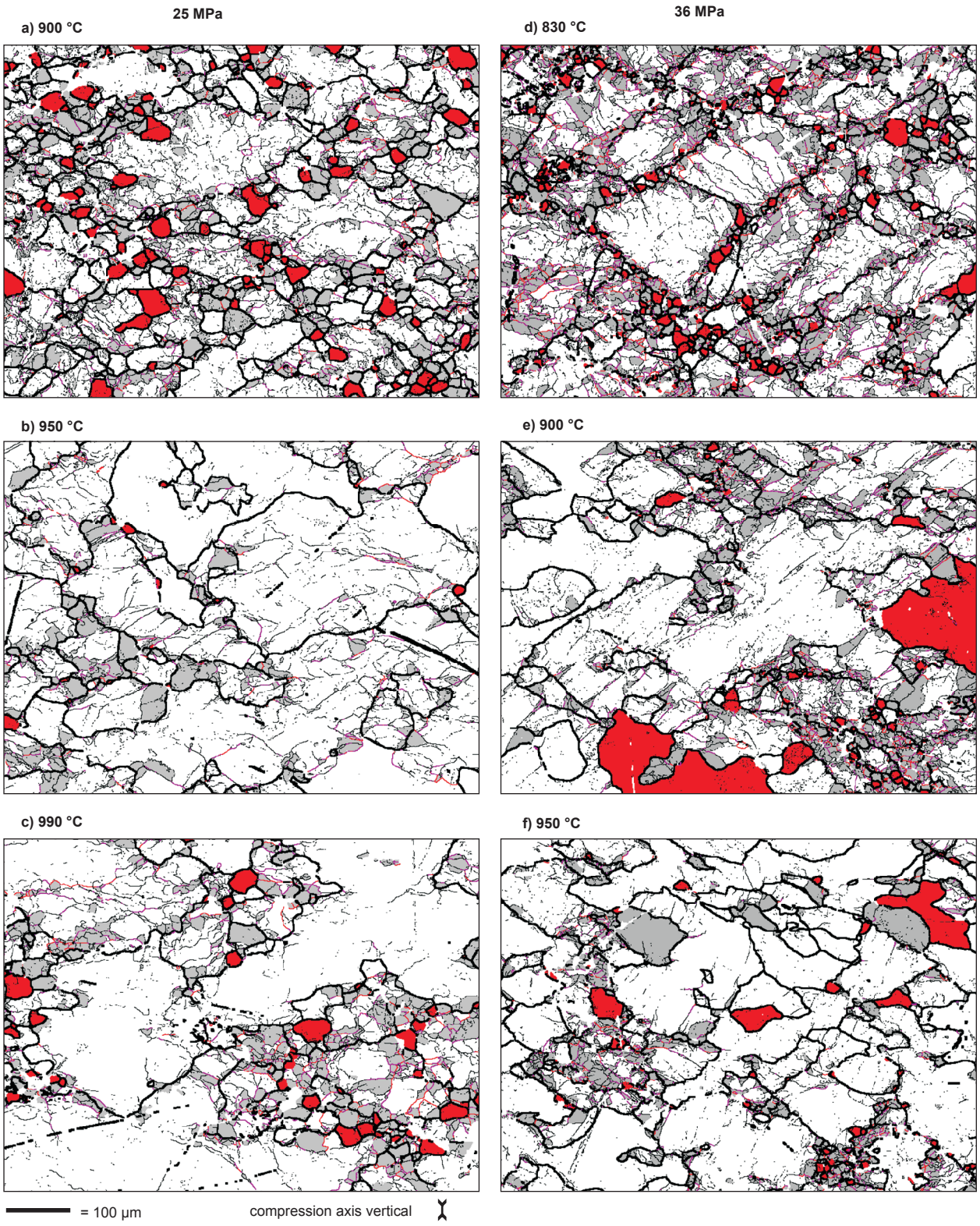

Fig. 6.4(a-f): EBSD maps of all samples, arranged in series to see the effect of temperature. The compression axis is vertical. Subgrain boundaries having misorientation angles >1° are indicated in thin black lines, >3° in pink, >5° in red; grain boundaries having boundaries with misorientation angles >10° in thick black lines. Recrystallised grains are coloured red and the mantle subgrains >1° in grey. Compression axis is vertical.

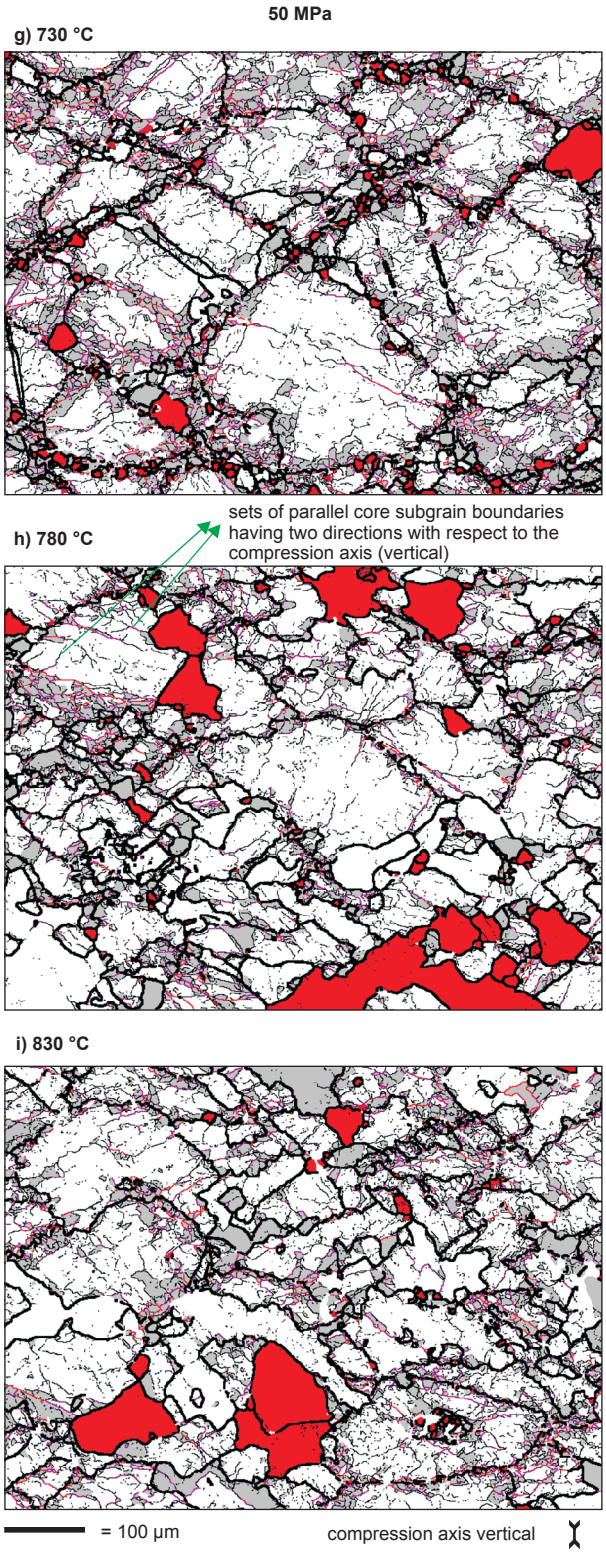

Fig. 6.4(g-i): for caption see Fig. 6.4(a-f)